Group 2 and Group 12 Metal-Metal Bonded Complexes

Ross Green MChem AMRSC



Thesis submitted to the University of Oxford for the degree of Doctor of Philosophy, September 2018.

The work described in this Thesis was carried out in the Chemistry Research Laboratory, University of Oxford from October 2013 to September 2018 under the supervision of Professor Philip Mountford. All work is my own unless stated to the contrary, and has not previously been submitted for any degree at this or any other university.

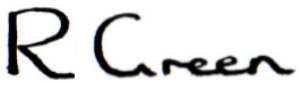

Ross Green

September 2018

Abstract

Ross Green Trinity 2018

St Edmund Hall D.Phil. Thesis

This Thesis describes the synthesis and characterisation of new alkaline earth-transition metal complexes and the synthesis and characterisation of group 12 complexes featuring metal-metal bonds. Experimental and computational studies were performed to investigate the structure and bonding in these complexes.

Chapter 1 introduces metal-metal bonded complexes and discusses alkaline earth-transition metal and group 12-group 12 bonded complexes.

Chapter 2 describes the synthesis of characterisation of new amidinate and guanidinate supported alkaline earth-transition metal bonded compounds.

Chapter 3 describes the attempted synthesis and computational studies of new Zn–Hg–Zn bonded compounds and the isolation of a new Zn–Zn bonded compound.

Chapter 4 describes the reactivity study of $\{(^{Dipp}NacNac)Zn\}_2Hg$ with several unsaturated small molecules.

Chapter 5 presents full experimental procedures and characterising data for the new compounds reported.

CD Appendix contains .cif files for all new crystallographically characterised complexes described.

Contents

	Declaration	i
	Abstract	ii
	Contents	iii
	Acknowledgements	vi
	Abbreviations	vii
	Notes	xi
Chapter One – Introduction		1
1.1	General Introduction	2
1.2	Criteria	3
1.3	Transition metal-transition metal complexes	4
1.4	Alkaline earth-alkaline earth complexes	8
1.5	Alkaline earth-transition metal complexes	11
1.6	Group 12 metal-metal bonding	24
1.7	Group 12-metal heterometallic complexes	25
1.8	Group 12 homobimetallic complexes	35
1.9	Summary and objectives	43
1.10	References	44
Chapter Two – Synthesis and study of amidinate and guanidinate supported Ae–TM bonded complexes		52
2.1	Overview	53
2.2	Introduction	53
2.2.1	Privileged anions in metal-metal bonding	53
2.2.2	β-diketiminate supported Ae–TM bonded complexes	61
2.2.3	Effects of the supporting ligand on structure and reactivity of Ae–TM bonded complexes	63
2.3	Synthesis of Mg–TM bonded complexes supported by the N,N'-diisopropylamidinate ligand	65
2.4	Synthesis of bulky aryl carbodiimides	71
2.5	Synthesis of Mg–TM bonded complexes supported by the N,N'-bis(diisopropylphenyl)amidinate ligand	72

2.6	Synthesis of Mg–TM bonded complexes supported by the N,N'-bis(trimethylphenyl)amidinate	76
2.7	Reactivity studies of amidinate-supported Mg–TM bonded compounds	80
2.8	Synthesis of a Mg–Fe bonded complex supported by the N,N'-bis(diisopropylphenyl)guanidinate ligand	87
2.9	Reactivity of a guanidinate supported Mg–TM bonded compound	97
2.10	Diffusion measurements by NMR spectroscopy	97
2.11	Conclusions	101
2.12	References	102
Chapter Three – Synthetic study of Zn–Hg–Zn and Zn–Zn bonded complexes		109
3.1	Overview	110
3.2	Introduction	110
3.3	Attempted syntheses of new β-diketiminate supported Zn–Hg–Zn Compounds	117
3.4	DFT study of the relative stabilities of β-diketiminate supported Zn–Hg–Zn compounds	124
3.5	Attempted synthesis of a guanidinate supported Zn–Hg–Zn compound	128
3.6	Conclusions	133
3.7	References	134
Chapter Four – Reactivity study of $\{(^{Dipp}NacNac)Zn\}_2Hg$		137
4.1	Overview	138
4.2	Introduction	138
4.3	Reactions of $\{(^{Dipp}NacNac)Zn\}_2Hg$ with silyl halides	149
4.4	Reaction of $\{(^{Dipp}NacNac)Zn\}_2Hg$ with phenyl azide	150
4.5	Reaction of $\{(^{Dipp}NacNac)Zn\}_2Hg$ with carbon disulfide	151
4.6	Reactions of $\{(^{Dipp}NacNac)Zn\}_2Hg$ with isocyanates	156
4.7	Reaction of $\{(^{Dipp}NacNac)Zn\}_2Hg$ with peroxides	162
4.8	Reaction of $\{(^{Dipp}NacNac)Zn\}_2Hg$ with azobenzene	162
4.9	Conclusions	166
4.10	References	168

Chapter Five – Experimental details and characterising data 172

5.1 General methods and instrumentation 173
5.2 X-ray data collection and processing parameters 173
5.3 Computational details 174
5.4 Diffusion NMR details 174
5.5 Literature preparations 176
5.6 Experimental details and characterising data for Chapter Two 176
5.7 Experimental details and characterising data for Chapter Three 186
5.8 Experimental details and characterising data for Chapter Four 191
5.9 References 195

CD Appendix

Acknowledgements

Firstly, I would like to express my gratitude to Professor Philip Mountford. The guidance and advice (and occasional cup of coffee) received throughout my studies have been invaluable. It has been a great privilege to work under his supervision.

Special thanks go to Dr Matthew Blake, who has been a supervisor, a confidant, occasional travel companion and friend. The commitment he displayed during his time in the lab was inspirational and I am grateful for his all hard work. I would also like to thank the other members of the Mountford group, past and present, for making the lab such a great place to work.

I am grateful to Prof. Philip Mountford, Dr Matthew Blake, Dr Benjamin Clough, Dr Bowen Xie and Dr Amber Thompson for their contribution to the collection and solving of X-ray crystallographic data. I am grateful to Prof. Philip Mountford and Dr Matthew Blake for their help with DFT calculations and also to Prof. Nikolas Kaltsoyannis at University of Manchester and Prof. Eric Clot at Université de Montpellier for their helpful contributions to the computational efforts of the Mountford group. I would also like to thank Dr Nick Rees for his assistance with all things NMR.

Special thanks go to my family who have supported me throughout my studies. I am incredibly grateful for everything that they have done for me throughout my life. Special thanks also go to Kim Green who, during the course of my studies has been my friend, partner, fiancée and wife.

Finally, I would like to thank all those people in my life have supported and encouraged me, including the members of the SDKA (Derby) and KSMBDA (Swindon) and especially my friends who have always helped me to keep things in perspective.

Abbreviations

General

Å	Ångstrom
Ar_{cent}	computed aryl ring carbon centroid
atm	atmosphere(s)
avg.	average
au	atomic units
ca.	*circa*, about
calcd.	calculated
cf.	*confer*, compared to
Cp_{cent}	computed cyclopentadienyl ring carbon centroid
CSD	Cambridge Structural Database
°	degrees
°C	degrees Celsius
d	day(s)
eV	electron volt
e.s.d.	estimated standard deviation
equiv.	equivalents
g	gram(s)
h	hour(s)
K	Kelvin
mbar	millibar(s)
min	minute(s)
mL	millilitre(s)
mmol	millimole(s)
RT	room temperature
s	second(s)
vs.	versus

Chemical

Ae	alkaline earth metal
An	actinide
Ar	aryl group

BIAN	bis[(2,6-diisopropylphenyl)imino]acenaphthene
$BAr^F{}_4^-$	tetrakis[3,5-bis(trifluoromethyl)phenyl]borate
Bu	*n*-butyl
COD	cyclooctadiene
COT	cyclooctatetraene
Cp	C_5H_5
Cp'	C_5H_4Me
Cp*	C_5Me_5
Cy	cyclohexyl
DABCO	1,4-diazobicyclooctane
Dipp	2,6-diisopropylphenyl
DME	1,2-dimethoxyethane
DPPE	$Ph_2PCH_2CH_2PPh_2$
DPPM	$Ph_2PCH_2PPh_2$
en	ethylenediamine
Et	ethyl
Fp^-	$[CpFe(CO)_2]^-$
HMPA	$P(O)(NMe_2)_3$
^iPr	*iso*-propyl
IPr	$C\{N(Dipp)CH\}_2$
L	a supporting ligand (set)
Ln	lanthanide
M	metal
Me	methyl
Mes	$2,4,6\text{-}Me_3C_6H_2$
^{R}NacNac	$[\{(R)NC(Me)\}_2CH]^-$
OTf^-	$CF_3SO_3^-$
Ph	phenyl
Pr	*n*-propyl
py	pyridine
pz	pyrazolyl
R	generic aryl or alkyl
Rp^-	$[CpRu(CO)_2]^-$
^tBu	*tert*-butyl
THF	tetrahydrofuran

TM	transition metal
TMEDA	tetramethylethylenediamine
Tol	4-MeC_6H_4
Tp	tris(pyrazolyl)hydroborate
tren	$N(CH_2CH_2NSiMe_3)_3$
Trityl	triphenylmethyl
Ts^{Xy}	$HC\{SiMe_2N(3,5\text{-}Me_2C_6H_3)\}_3$
X	Generic halide
Xy	3,5-$Me_2C_6H_3$
Xyl	2,6-$Me_2C_6H_3$

Calculations

AO	atomic orbital
(QT)AIM	(quantum theory of) atoms-in-molecules
BCP	bond critical point
DFT	density functional theory
EBO	effective bond order
H	energy density
HOMO	highest occupied molecular orbital
LUMO	lowest unoccupied molecular orbital
MO	molecular orbital
NBO	natural bond orbital
ρ	electron density
$\nabla^2\rho$	Laplacian of the electron density

Mass Spectrometry

EI	electron impact
m/z	mass to charge ratio
MS	mass spectrometry

Nuclear Magnetic Resonance Spectroscopy

$^{13}C\{^1H\}$	proton-decoupled ^{13}C
$^{31}P\{^1H\}$	proton-decoupled ^{31}P
app.	apparent
br	broad

COSY	correlation spectroscopy
d	doublet
DOSY	diffusion ordered spectroscopy
HMBC	heteronuclear multiple bond correlation
HMQC	heteronuclear single quantum correlation
Hz	Hertz
i	*ipso*
J	coupling constant
m	*meta*
m	multiplet
MHz	Megahertz
NMR	nuclear magnetic resonance
o	*ortho*
p	*para*
PGSE	pulsed gradient spin echo
ppm	parts per million
q	quartet
s	singlet
sept	septet
t	triplet
VT	variable temperature
δ	chemical shift in ppm

Infrared Spectroscopy

br	broad
FT-IR	fourier transform infrared red
IR	infrared
cm^{-1}	wavenumber
m	medium
s	strong
sh	sharp
w	weak
ν	frequency
ν(CO)	carbonyl absorption band

Notes

Literature compounds described in this Thesis are numbered **1.x**, **2.x**, **3.x**, **4.x** according to the Chapter in which they first occur. The new compounds described in this Thesis are numbered **1** – **31**.

X-ray crystallography data was solved and refined by the author with help and guidance from Prof. Philip Mountford. Data for compounds **1**, **4**, **10**, **11**, **18** and **25** were collected by Dr Matthew Blake. Data for compound **27** was collected by Dr Bowen Xie. Data for compounds **28**, **29** and **31** were collected by Dr Benjamin Clough. All other crystallography data was collected by the author. Molecular drawings were produced by Prof. Philip Mountford.

DFT calculations were performed by the author, Prof. Philip Mountford and Dr Matthew Blake.

Chapter One

Introduction

1.1 General introduction

Molecular compounds with bonds between two or more metal atoms have been of interest in inorganic chemistry for many years and have helped to advance our understanding of structure and bonding, reactivity and catalysis.[1–3] Of the structurally authenticated complexes containing metal-metal bonds, those containing bonds between group 2 (Gp2; also known as alkaline earth, Ae) and transition metal (TM) elements are comparatively rare.[4] In the vast majority of these complexes Mg is the Ae element. The group 12 (Gp12) elements, especially Zn, share (in general terms) many characteristics with the Ae elements; they are typically divalent and are typically characterised as electropositive elements, although they are much less electropositive than the Ae elements. These similarities make the group 12 elements notable candidates for study in this area. In the area of group 2 and group 12 metal-metal bonding there is also significant interest surrounding metal-metal bonded complexes (typically homometallics) which feature the metal elements in unusual formal oxidation states as a necessary result of the synthesis.[5–7] The utility of metal-metal bonded complexes for chemical transformations has developed considerably over the past decade but is still a relatively sparse area of study.[8–10]

This Thesis describes complexes which feature metal-metal bonding as their core motif. The first part describes the synthesis of heterobimetallic Mg–TM complexes. The use of X-ray diffraction allowed the structural authentication of compounds for which single crystals could be grown. Comparison with known structures allowed for a description of the metal-metal interaction to be developed. Diffusion NMR studies allow for the elucidation of the behaviour of these complexes in several solvents. This work has been published.[11] The second part describes the synthesis of homometallic and heterometallic group 12 complexes. DFT calculations have been carried out to give insights into aspects of the synthesis of these complexes.

This Chapter introduces the milestone complexes in transition metal-transition metal bonding, followed by complexes with Mg–Mg bonding. Complexes with Ae–TM bonding are introduced and discussed. Complexes containing Gp12–metal bonds are then examined. This discussion is broken down into sub-categories which examine Gp12–main group metal bonded complexes followed by Gp12–Gp12 homobimetallics.

Gp12–TM bonded complexes are omitted from this discussion as examples of this type of bonding constitute an entire topic in themselves and have been present in the scientific literature for over 40 years.[4] The majority of these complexes feature Zn as the group 12 metal and were reviewed by Fischer *et al.* in 2012.[9]

1.2 Criteria

When considering metal-metal bonding interactions this Thesis places significance on single crystal X-ray diffraction data. A complex which contains two metals does not necessarily contain a metal-metal bond. Analysis of X-ray diffraction data can infer the presence of a bonding interaction between two metal atoms and can allow for the direct comparison of structural properties between two complexes. Where X-ray diffraction data are not available the structure of the complex and the nature of the metal-metal interaction is uncertain and must be investigated *via* indirect techniques.

To ensure that the description of what constitutes a metal-metal bond is consistent the M–M' interaction will be considered to be a bonding interaction if the M–M' distance is within the sum of the covalent radii of M and M'. In reality, an apparently close M–M' contact by itself does not confirm direct interaction of the metal atoms. This is usually the case with compounds containing bridging ligands between two metal centres. $Fe_2(CO)_9$ possesses a short Fe···Fe distance of 2.523(1) Å[12] as a result of Fe{μ-C(O)}Fe interactions. While the Fe···Fe separation is shorter than the sum of covalent radii (2.64(4) Å), $Fe_2(CO)_9$ has been shown by Green and Parkin to not possess a direct Fe–Fe bond.[13] In practice, an unbridged M···M' interaction will usually be present in a complex as a result of the M–M' bond. If bridging ligands are present further consideration might be required to infer the presence of a bonding interaction.

The covalent radii are obtained from a reports by Alvarez *et al.*[14] and Pyykkö *et al.*[15] Alvarez and co-workers calculate covalent radii by measuring the distances between a given element and the reference elements C, N or O are compiled from structures reported in the Cambridge Structural Database (CSD).[16] The criteria and derivation of the radii are detailed in the publication. The radii were benchmarked by comparing 172,000 predicted element-element distances which did not contain C, N or O against experimentally derived values with 96% accuracy within 3 standard deviations. Pyykkö *et al*. employ a similar method; incorporating data from complexes containing E–E, E–H and E–CH_3 bonds in order to derive atomic radii. The atomic radii defined by Pyykkö

et al. are derived from species which generally possess lower coordination numbers than those defined by Alvarez *et al*. and so tend to give a slightly smaller value for each element.[15] Pyykkö *et al*. state in their paper that the radii defined by Alvarez *et al*. are "presumably better" for complexes with higher coordination numbers, which is applicable to many compounds discussed hereafter. Therefore, if a compound possesses a non-bridged M–M' interaction that is shorter than the longer of the two calculated sums of atomic radii (either Alvarez or Pyykkö), it will be considered a metal-metal bond for the purpose of this Thesis.

The e.s.d. (estimated standard deviation) of the difference of two values having e.s.d.s x and y is given by $\sqrt{(x^2+y^2)}$. The e.s.d. of the difference of two averaged values having e.s.d.s x and y is given by $\sqrt{\{(x^2+y^2)/2^2\}}$.[17]

1.3 Transition metal-transition metal complexes

The first structurally authenticated complex containing a metal-metal quadruple bond was $K_2[Re_2Cl_8]\cdot 2H_2O$ (**1.1**) reported by Cotton *et al*. in 1965.[18–21] This complex demonstrated that bond orders of higher than three (the limit for compounds of the p-block elements) were accessible *via* δ bonding. It was not until 2005, however, that the first structurally authenticated example of a quintuple bond was published. Power *et al*. reported $[CrAr]_2$ (**1.2**, Equation 1.1, Ar = C_6H_3-2,6-$(Dipp)_2$, Dipp = 2,6-diisopropylphenyl), obtained from the reduction of $[Cr(\mu\text{-}Cl)Ar]_2$ with KC_8, which contains a Cr–Cr bond of 1.8351(1) Å.[22] DFT analysis and the temperature-independent weak paramagnetism support the electronic description of strongly coupled $3d^5$-$3d^5$ bonding electrons in the molecular orbitals of the quintuple bond. The ground state electron configuration of $\sigma^2\pi^4\delta^4$ confers a formal Cr–Cr bond order of 5.0. There is a weak interaction between the ipso carbons of a neighbouring ring in the terphenyl group and the Cr atoms (indicated by a dashed line). Fe and Co homobimetallic analogues have been synthesised which feature considerably longer M–M distances.

Quantum chemical calculations of $[CrPh]_2$ (a simplified model of **1.2**) show an effective bond order (EBO) of between 3.69 and 3.52 (for the linear and *trans*-bent structures, respectively).[23] The same calculations performed for **1.2** itself showed an EBO of 3.43.[24] These EBOs are less than the formal bond order due to the mixing of excited states into the ground state. These excited states involve promotion of electrons from δ

bonding orbitals into δ* antibonding orbitals, reducing the overall bond order of the Cr–Cr interaction.

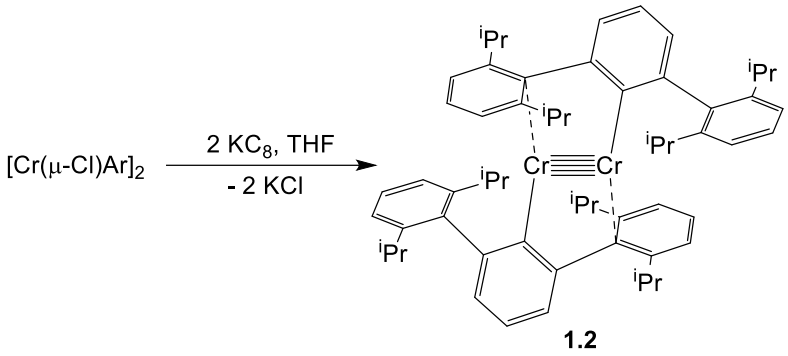

Equation 1.1[22]

Power *et al*. also synthesised Fe and Co homobimetallic analogues of **1.2** which feature considerably longer M–M distances (Fe–Fe 2.5151(9) Å, Co–Co 2.8033(5) Å).[25] The longer M–M distances are to be expected in these compounds as the number of valence electrons necessitates population of antibonding orbitals. However, the authors note that the M–M distances are both much longer than expected for multiply bonded species. The calculated EBOs for $[FePh]_2$ and and $[CoPh]_2$ are 1.47 and 1.38, respectively.[24] The calculated EBO for $[CoAr]_2$ was found to be 0, consistent with a non-bonding interaction. Consistent with this finding the Co···Co separation was found to be significantly longer than the sum of covalent radii for low spin Co (2.52(4) Å).

In each $[MAr]_2$ compound an interaction is present between a metal centre and a flanking aryl group. The Cr···Ar_{cent} distance in **1.2** is 2.203(6) Å. The Fe···Ar_{cent} distances of 1.733(2) and 1.763(2) Å and the Co···Ar_{cent} distance of 1.764(2) Å represent much stronger interactions. Hence with decreasing bond order in the M–M interaction the M···Ar interaction becomes more significant. In the extreme case of Co, due to the essentially non-bonding interaction between the metal centres the dimer is held together by interaction of the metal atoms with the flanking aryl group of the second fragment.

Shortly following on from the report of **1.2**, the synthesis of $[Cr(\mu\text{-}\kappa^2\text{-DAB})]_2$ (**1.3**, Equation 1.2, DAB = N,N'-bis-(Dipp)-1,4-diazadiene)) was reported by Theopold *et al*. from the reduction of $[Cr(\mu\text{-Cl})(DAB)]_2$ with KC_8.[26] Complex **1.3** contains an extremely short Cr–Cr bonding interaction (1.8028(9) Å) which, coupled with the low formal oxidation state of the metals, indicates a high degree of Cr–Cr multiple bonding. The formal oxidation state of the metals suggests the presence of a quadruple bond

however a formal bond order is difficult to assign due to extensive delocalisation of electron density over the ligands. DFT and natural resonance theory (NRT) analysis shows five occupied molecular orbitals with Cr–Cr bonding character and a calculated Cr–Cr EBO of 4.28. The authors suggest that this Cr–Cr interaction involves some degree of quintuple bonding.

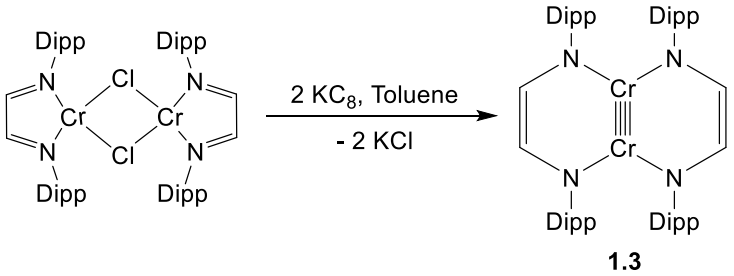

1.3

Equation 1.2[26]

Only one year later Tsai *et al*. reported a set of structurally authenticated, quintuply bonded Cr complexes.[27] The reduction of $[Cr(\mu\text{-}Cl)\{\mu\text{-}\kappa^2\text{-}HC(NXyl)_2\}(THF)]_2$ (**1.4**, Xyl = 2,6-dimethylphenyl) with KC_8 gave $Cr_2\{\mu\text{-}\kappa^2\text{-}HC(NXyl)_2\}_3$ (**1.5**, Scheme 1.1). Complex **1.5** contains a $[Cr_2]^{3+}$ core with a Cr–Cr bond length of 1.8169(7) Å. DFT analysis in conjunction with EPR spectroscopy identified that the SOMO possesses primarily $d_{x2\text{-}y2}$ character. The electronic configuration was therefore determined to be $\sigma^2\pi^4\delta^3$ which results in a formal Cr–Cr bond order of 4.5. Despite this the Cr–Cr bond is shorter than that found in **1.2**. Further reduction of **1.5** with KC_8 in the presence of 2.2.2-crypt gives $[K(2.2.2\text{-crypt})][Cr_2\{\mu\text{-}\kappa^2\text{-}HC(NXyl)_2\}_3]$ (**1.6**, Scheme 1.1, 2.2.2-crypt = $N\{(CH_2)_2O(CH_2)_2O(CH_2)_2\}_3N$), which possesses an electron configuration of $\sigma^2\pi^4\delta^4$ and hence a formal Cr–Cr bond order of 5.0. The Cr–Cr bond length is shortened to 1.7397(9) Å as a result of the higher bond order. Tsai *et al*. have synthesised several more amidinate supported quintuply bonded Cr–Cr which all possess bond lengths of approx. 1.74 Å.[28]

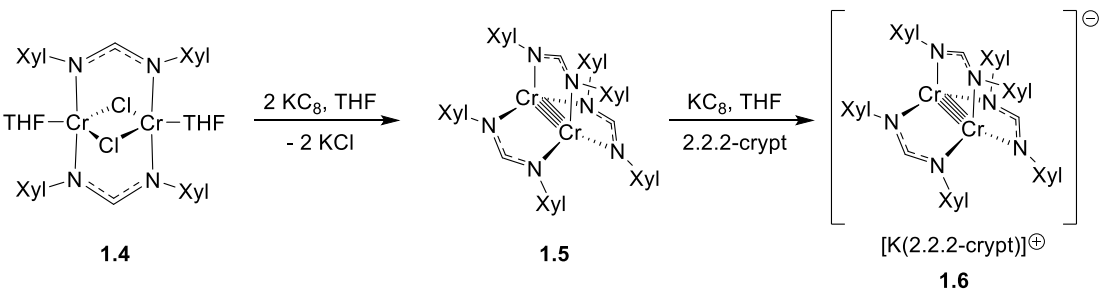

1.4 **1.5** **1.6**

Scheme 1.1 Synthesis of Cr dimers **1.5** and **1.6** *via* reduction.

The extremely short Cr–Cr bond lengths detailed above are likely influenced by constraining ligand geometries which are able to compress the Cr–Cr bond. To examine this effect Kempe *et al*. reported their studies with similarly constraining ligands.[29] The reduction of {(DMP)C(NDipp)$_2$}Cr(μ-Cl)$_2$Li(THF)$_2$ (DMP = 2,6-dimethylpipiridinide) with KC_8 in THF gave a mixture of [Cr{(DMP)C(NDipp)$_2$}]$_2$ (**1.7**) and [Cr{μ-κ^2-(DMP)C(NDipp)$_2$} (**1.8**) (Equation 1.3), which were separated by fractional crystallisation and analysed by X-ray diffraction studies.

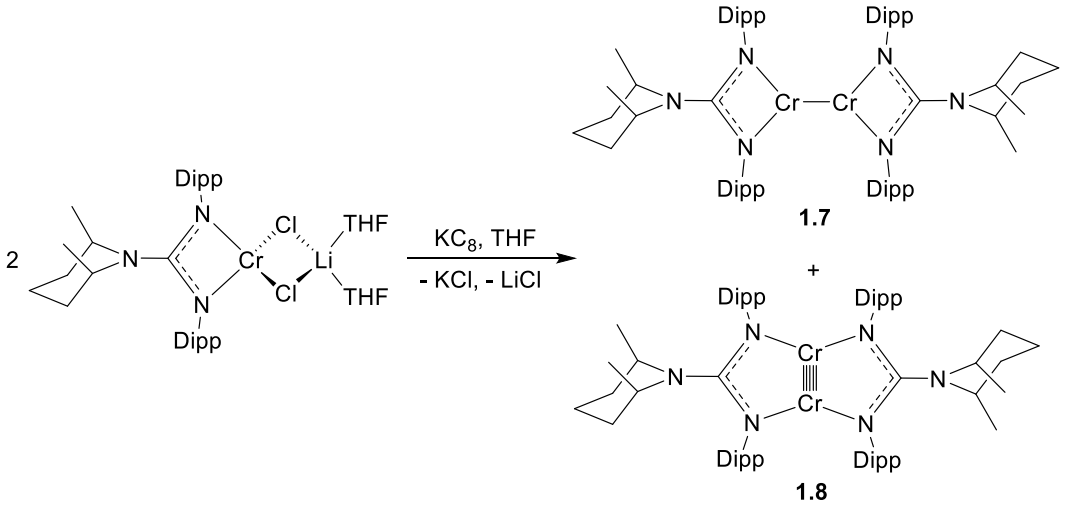

Equation 1.3[29]

Complex **1.7** is a rare example of an unsupported Cr–Cr single bond with a metal-metal bond length of 2.652(2) Å and a calculated Cr–Cr EBO of 1.25. More pertinent to this discussion, however, is the quintuply bonded **1.8** which features a Cr–Cr bond length of 1.7056(12) Å, the shortest metal-metal bond of this type. The calculated EBO for the Cr–Cr bond is 3.93. Amidinates and guanidinates are favoured ligands in coordination chemistry due to the 'tuneability' of their steric and electronic properties, which can have a strong influence on their coordination properties.[30–32] In this case the presence of the bulky DMP substituent in the distal position of the guanidinate ligand has the effect of displacing the aryl substituents and pushing them forward. In **1.8** the aryl substituents of the opposing guanidinate ligands are pushed towards each other which creates a repulsive effect not only between the opposing aryl substituents but also with the Cr atoms. This effect effectively compresses the Cr–Cr bond accounting for the extremely short bond length. Increased steric repulsion between distal substituent and the N-bound substituents generally results in a more acute N–C–N angle and causes the lone pairs of the coordinating N atoms to point towards each other. Consequently, as

the steric repulsion from a bulky distal substituent increases, these ligands become less effective at bridging between two metal atoms and more effective at chelating to only one metal atom due to the directionality of the lone pairs. This effect may explain why a mixture of **1.7** (where the guanidinate acts as a bidentate chelating ligand) and **1.8** (where the guanidinate acts as a bridging ligand) is obtained.

In addition to their work with Cr–Cr multiple bonds, Tsai *et al*. also reported the first synthesis of a complex containing a Mo–Mo quintuple bond. The reduction of the quadruply bonded complex $Mo_2(\mu\text{-}Cl)\{Cl_2Li(OEt_2)\}\{\mu\text{-}\kappa^2\text{-}PhC(NDipp)_2\}_2$ with KC_8 gave the quintuply bonded complex $[Mo\{\mu\text{-}\kappa^2\text{-}PhC(NDipp)_2\}]_2$ (**1.9**, Equation 1.4). This increased bond order results in a decreased Mo–Mo distance from 2.0756(8) (in the parent complex) to 2.0157(4) Å (**1.9**).

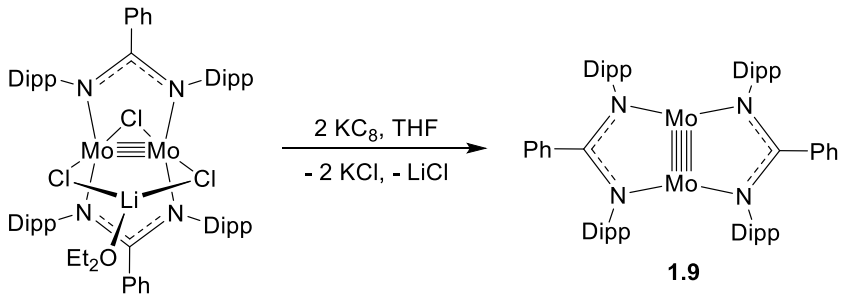

Equation 1.4[33]

Since the discovery of the first Zn–Zn bonded complex[5] by Carmona in 2004 the study of Zn(I) chemistry has flourished. This field, although relevant to this Section, is of particular interest with respect to the focus of this Thesis and will therefore be discussed later in this Chapter.

1.4 Alkaline earth-alkaline earth complexes

The study of metal-metal bonding has pursued not only increased bond order in bimetallic complexes but has also sought to access previously unknown oxidation states for metals. A good example of this endeavour are the Mg(I) dimers reported by Jones *et al*.[6,34,35] The first example of an isolable and structurally authenticated Mg(I) dimer possessing a Mg–Mg bond was reported in 2007.[6] The reduction of 2 equivs. of (^{Dipp}NacNac)MgI(OEt_2) (^{R}NacNac = $HC\{C(Me)NR\}_2$) in toluene in the presence of excess K metal gave $[(^{Dipp}NacNac)Mg]_2$ (**1.10**, Equation 1.5) with a Mg–Mg bond length of 2.8457(8) Å. The analogous reduction of $\{^{i}Pr_2NC(NDipp)_2\}Mg(\mu\text{-}I)_2Mg(OEt_2)\{(NDipp)_2CN^{i}Pr_2\}$ gave $[\{^{i}Pr_2NC(NDipp)_2\}Mg]_2$ (**1.11**, Equation 1.6)

with a Mg–Mg bond length of 2.8508(12) Å. These complexes were not only the first reported examples of Mg(I) complexes but the first reported examples of an alkaline earth metal in the +1 oxidation state.

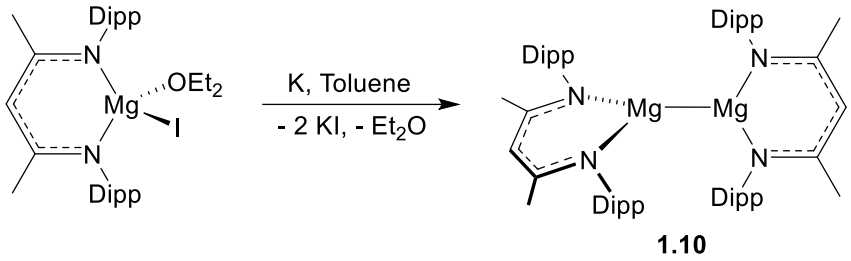

1.10

Equation 1.5[6]

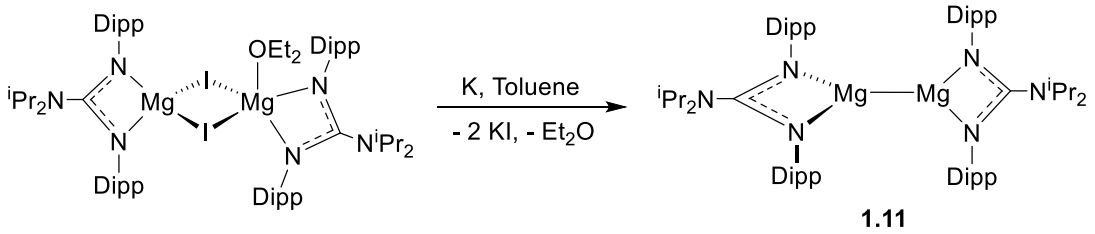

1.11

Equation 1.6[6]

Following on from this first generation, Jones *et al*. have reported several more Mg(I) dimers based on a chelating NacNac architecture. Discoveries of note are $[Mg(HC\{C(^tBu)NDipp\}_2)]_2$ (**1.12**, Scheme 1.2, Mg–Mg = 2.847(2) Å),[34] which employs the so called "super-bulky" *tert*-butyl substituted NacNac ligand, and $[(^{Mes}NacNac)Mg]_2$ (**1.13**, Scheme 1.2, Mg–Mg = 2.808(1) Å),[34] which appears to have become the reagent of choice for chemists wishing to utilise the reductive properties of Mg(I) in synthetic procedures. The preparation of **1.12** was achieved *via* same synthetic procedure which produced **1.10** and **1.11**. K reduction of $(^{Mes}NacNac)MgI(OEt_2)$ gave **1.13** in very low yield (ca. 2 – 5%). Instead, reduction with Na was required to produce the complex in satisfactory yields. As expected the Mg–Mg distance is shortest for the least sterically hindered complex, **1.13**.

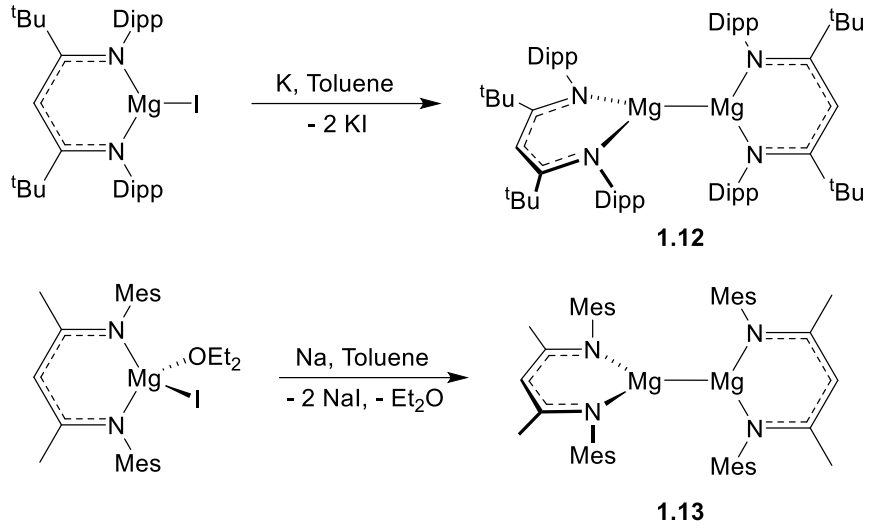

Scheme 1.2 Preparation of Mg(I) dimers.[34]

Recently Jones *et al*. have developed an extremely bulky amide ligand[36] which they have employed to synthesis a new class of Mg(I) dimers.[35] The reduction of $[LMg(\mu\text{-}I)]_2$ (L = $N(Ar^{R'})(SiR_3)$, $Ar^{R'}$ = $C_6H_2\{C(H)Ph_2\}_2R'$), R = Me or ^{i}Pr, R' = ^{i}Pr or Me) with KC_8 in toluene gave $[LMg]_2$ (R = Me, R' = ^{i}Pr (**1.14**); R = ^{i}Pr, R' = Me (**1.15**)). These complexes are among the first two-coordinate, non-chelated Mg(I) dimers reported. The Mg–Mg bond length is shorter for the less sterically hindered **1.14** (2.8223(11) Å) and slightly longer for **1.15** (2.8504(13) Å).

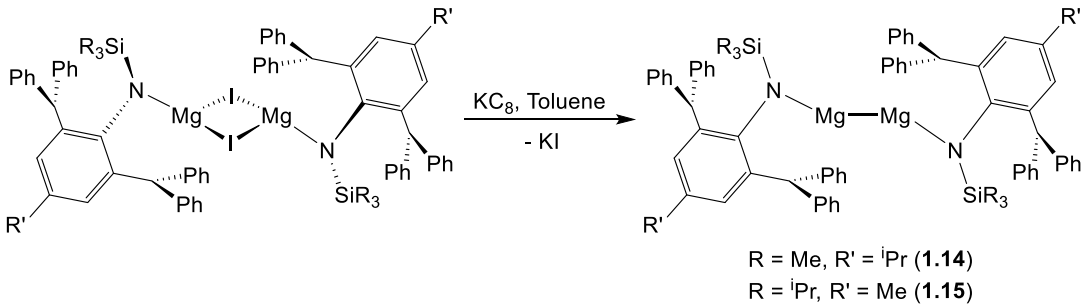

Scheme 1.3 Preparation of two-coordinate Mg(I) dimers.[35]

The reactivity of these Mg(I) dimers with organic substrates has been developed in the years following their discovery.[6,34,37] Indeed these complexes have found their niche as soft, two-centre/two-electron reductants. A good illustration of this feature is the reduction of $GeCl_2$(IPr) (**1.16**, Equation 1.7, IPr = $C\{N(Dipp)CH\}_2$).[38] When **1.16** was treated with either Na or KC_8 only decomposition products (*e.g*. elemental Ge and free IPr) could be obtained from the reaction mixture, however the use of either **1.10** or **1.13**

as the reductant afforded [Ge(IPr)] (**1.17**), albeit in low yields. Other stable, structurally authenticated Ae(I) complexes have yet to be reported.[4,16]

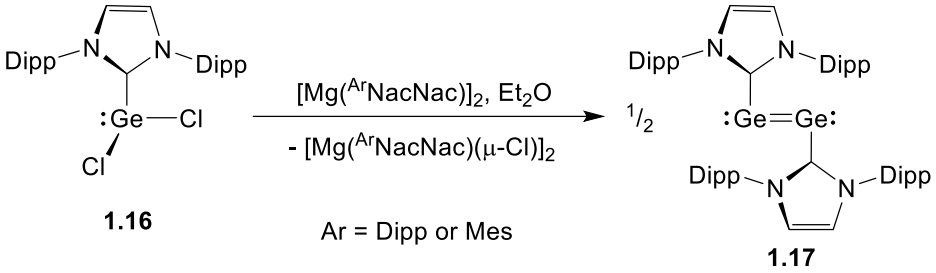

Equation 1.7[38]

1.5 Alkaline earth-transition metal complexes

Although considerable attention has been paid to the study of TM–TM and TM–main group bonds, complexes with bonds between Ae and TM elements are comparatively rare.[4,16] The first of these complexes was reported by Felkin in 1974.[39] CpFe(DPPE)Mg(Br)$(THF)_2$ (**1.18**, Equation 1.8) was synthesised from the reaction of CpFeBr(DPPE) with excess magnesium, activated by $BrCH_2CH_2Br$, in THF. The formation of the FeMgBr moiety is analogous to the formation of organic Grignard complexes, in which a Mg atom inserts into a C–X bond (where X = halide, commonly Cl, Br, I).[40] The Mg centre of **1.18** is four-coordinate, bonding to Fe, Br and two molecules of THF, with an approximately tetrahedral geometry. The Mg–Fe bond distance (2.593(7) Å) is shorter than the sum of covalent radii defined by Alvarez (2.73(8) Å),[14] but not those defined by Pyykkö (2.55 Å).[15]

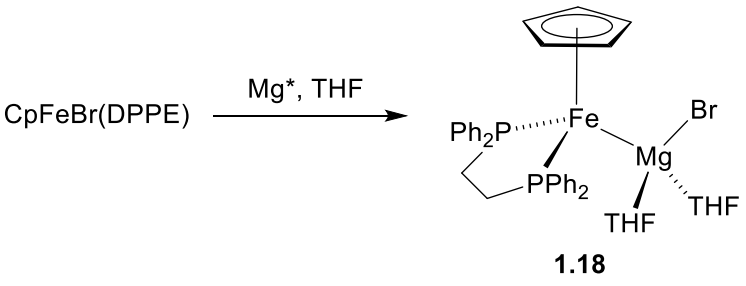

Equation 1.8[39]

In 1986, Jonas *et al*. reported a set of Mg–Co bonded compounds.[41] The reaction of $CpCo(C_2H_4)_2$ with Grignard compounds RMgBr (R = C_3H_5 or Ph) gave $CpCo(\eta^3\text{-}C_3H_5)MgBr(THF)_2$ (**1.19**) and $CpCo(C_2H_4)(Ph)MgBr(TMEDA)$ (**1.20**), respectively (Scheme 1.4). Upon reaction the R group of the Grignard reagent is transferred to the Co centre, a Mg–Co bond is formed and ethene is eliminated. The

Mg–Co bonds within **1.19** and **1.20** measure 2.480(4) and 2.565(3) Å, respectively. Jonas *et al*. describe **1.20** as a Lewis acid/base adduct between the 18-eletron $[CpCoPh]^-$ anion and a $[Mg(TMEDA)Br]^+$ cation. The Mg–Co bond of **1.19** is shorter than the sum of covalent radii defined by Pyykkö (2.50 Å),[15] although its counterpart in **1.20** is longer than this value. Nevertheless, both values are shorter than the sum of covalent radii define by Alvarez (2.67(8) Å).[14] The Mg–Co distance for **1.20** is substantially greater than that of **1.19**, likely as a result of the Ph–Mg interaction.

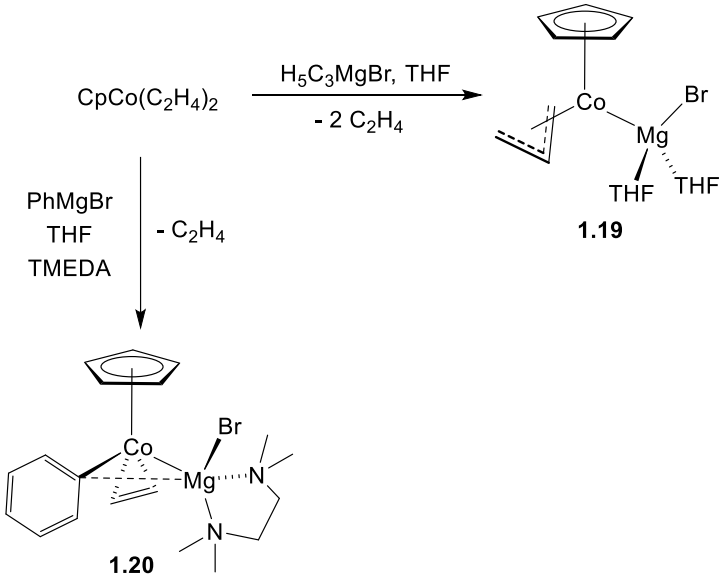

Scheme 1.4 Reaction of $CpCo(C_2H_4)_2$ with Grignard reagents.[41]

Green *et al.* synthesised the complexes $[\{Cp_2Mo(H)\}\{\mu\text{-}Mg_2Br_2(R)(OEt_2)\}]_2$ (R = Cy (**1.21**) or ^{i}Pr (**1.22**), Scheme 1.5) *via* the alkane elimination reaction between Cp_2MoH_2 and corresponding Grignard reagent in Et_2O.[42–44] The crystals grown from these reactions were quite unstable in the presence of air and moisture and in the case of the ^{i}Pr derivative **1.22** had undergone extensive decomposition during data collection resulting in high background scatter. Nonetheless the Mo–Mg–Br skeleton was apparent. The Mg–Mo distances of 2.853(7) and 2.737(6) Å in **1.21**, and 2.76(3) and 2.81(3) Å in **1.22** indicate metal-metal bonds, falling within the sum of the respective covalent radii defined by Alvarez (2.95(9) Å).[14] The hydrides were not located in the Fourier difference map but were placed tentatively within the ring in the Mg–Mo–Mg plane.[43] Recrystallisation of **1.22** from hot THF afforded the monomeric $Cp_2Mo(H)MgBr(THF)_2$ (**1.23**) with an unsupported Mg–Mo bond of 2.732 Å.[45,46] Complexes **1.21**, **1.22** and **1.23** were reactive towards CO_2 producing $Cp_2Mo(CO)$ in all cases. The authors propose that that the reactivity of these compounds towards CO_2

indicates the presence of covalent interactions between the transition metal (Mo) and the electropositive metal (Mg) but also concede that reactions such as these are not limited to these systems.[44]

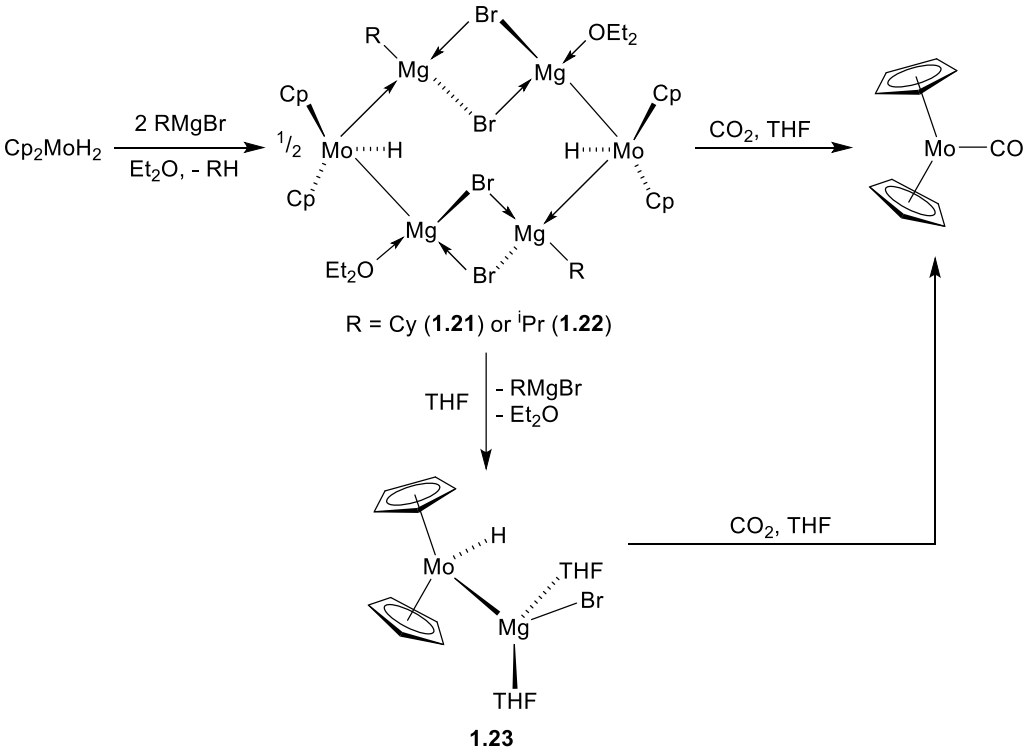

Scheme 1.5 The synthesis of $[\{Cp_2Mo(H)\}\{\mu\text{-}Mg_2Br_2(R)(OEt_2)\}]_2$ (R = Cy (**1.21**) or ^{i}Pr (**1.22**)) and $Cp_2Mo(H)\{MgBr(THF)_2\}$(**1.23**) and their reactions with CO_2.[42–44,46]

Another hydride-containing complex, $[Cp^*Ir(PMe_3)(H)MgPh]_2$ (**1.24**), was reported by Bergman *et al*. in 1998.[47] The dimeric complex was synthesised from the reaction of $Cp^*IrH_2(PMe_3)$ and $MgPh_2(THF)_2$, which eliminates benzene affording **1.24** over the course of 24 h (Equation 1.9). The Mg–Ir distances (2.660(2) and 2.750(2) Å) are within the sum of the respective covalent radii defined by Alvarez (2.82(9) Å).[14] This complex was the first reported example of a bonding interaction between an alkaline earth metal and a 3rd row transition metal.[16]

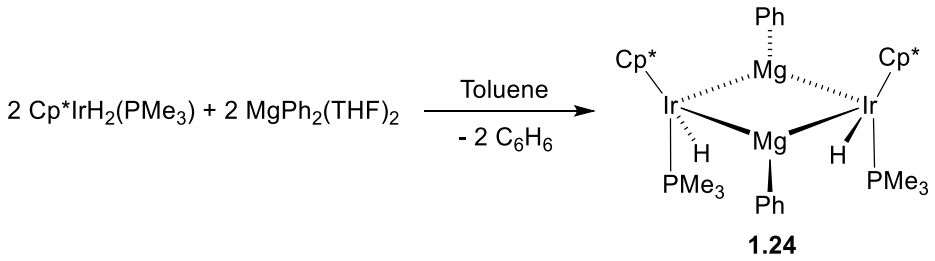

Equation 1.9[47]

Braunschweig *et al*. reported $Pt(PCy_3)_2BeCl_2$ (**1.25**), the first structurally authenticated example of a Be–TM bonded complex, in 2009.[48] Compound **1.25** is a Lewis acid/base adduct resulting from the reaction of $Pt(PCy_3)_2$ with excess $BeCl_2$. The Be–Pt bond distance is 2.168(4) Å. This is the shortest Ae-TM bonded reported to date,[16] which is expected due to the small radius of Be. Compound **1.25** was shown to react with MeLi to form $Pt(PCy_3)_2Be(Me)Cl$ (**1.26**), with preservation of the Be–Pt bond, which increases to 2.195(3) Å upon conversion to **1.26**. Both of these Be–Pt bonds are within the sum of the respective covalent radii defined by Alvarez (2.32(6) Å)[14] and Pyykkö (2.25 Å).[15] Hypothesising that a shorter Be–Pt bond results from a stronger bond, the authors performed DFT calculations for the model compounds $Pt(PH_3)_2BeCl(X)$ (X = Cl or Me). The calculated Be–Pt bond dissociation energies of 77.6 and 47.8 kJ mol^{-1} (X = Cl and Me, respectively) support this proposal and reflect the reduced Lewis acidity of Be in **1.26**.

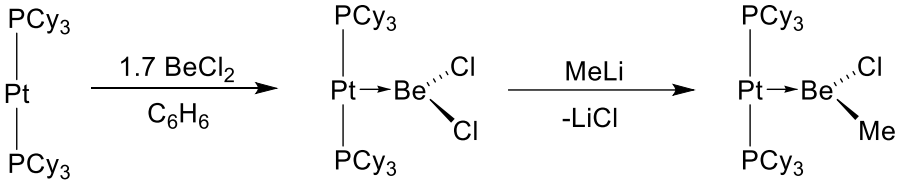

1.25 **1.26**

Scheme 1.6 The synthesis of $Pt^0 \rightarrow Be^{II}$ adduct $[(Cy_3P)_2Pt(BeCl_2)]$ (**1.25**) and its conversion to $[(Cy_3P)_2Pt(BeClMe)]$ (**1.26**).[48]

In 2014, Jones *et al*. reported $L^{\dagger}MnMg(^{Mes}NacNac)$ (**1.27**, $L^{\dagger}$ = $N(Ar^{\dagger})(Si^iPr_3)$, $Ar^{\dagger}$ = 2,6-$\{C(H)Ph_2\}_2$-4-^{i}Pr-C_6H_2), obtained from the reaction of $[L^{\dagger}Mn(\mu\text{-}Br)(THF)]_2$ with 2 equivs. of $[Mg(^{Mes}NacNac)]_2$.[49] Compound **1.27**, which contains the first reported Mg–Mn bond, uses the same extremely bulky monodentate amide ligand architecture utilised in **1.14** and **1.15** to stabilise the M–M' interaction. Besides being an unusual example of two-coordinate Mn in the zero oxidation state, **1.27** was also the first reported example of a three-coordinate Mg complex which possessed a Mg–TM bond. The Mg–Mn bond length is 2.8244(13) Å. This distance is significantly longer than other Mg–TM bonds reported.[4] However, the authors identify that it is still within the sum of Alvarez covalent radii for Mg and high-spin Mn (3.02(11) Å).[14] Compound **1.27** was shown to react with the less bulky $[L^*Mn(\mu\text{-}Br)(THF)]_2$ (L^* = $N(Ar^*)(SiMe_3)$, Ar^* = 2,6-$\{C(H)Ph_2\}_2$-4-Me-C_6H_2) to afford $L^{\dagger}MnMnL^*$ (**1.28**). It is notable that **1.28** is synthetically accessible, while the bulkier analogue $L^{\dagger}MnMnL^{\dagger}$, which might be

expected to form from the dimerisation of transient L†Mn(I) species formed *in situ*, is not. It is likely that the "L†Mn" fragments are incapable of dimerisation due to their extreme steric bulk and so are further reduced and trapped by the Mg(I) reagent, allowing the isolation of **1.27**. To test this hypothesis, Jones *et al*. performed the analogous reaction between [L*Mn(μ-Br)(THF)]$_2$ and 1 equiv. of [Mg(^{Mes}NacNac)]$_2$. The sole product of this reaction was the dimeric Mn(I) compound, L*MnMnL* (**1.29**). The Mn–Mn bond lengths are 2.7431(7) and 2.7224(6) Å, for **1.28** and **1.29**, respectively. As expected **1.28** possesses a slightly longer Mn–Mn bond due to the greater steric bulk of the L† ligand.

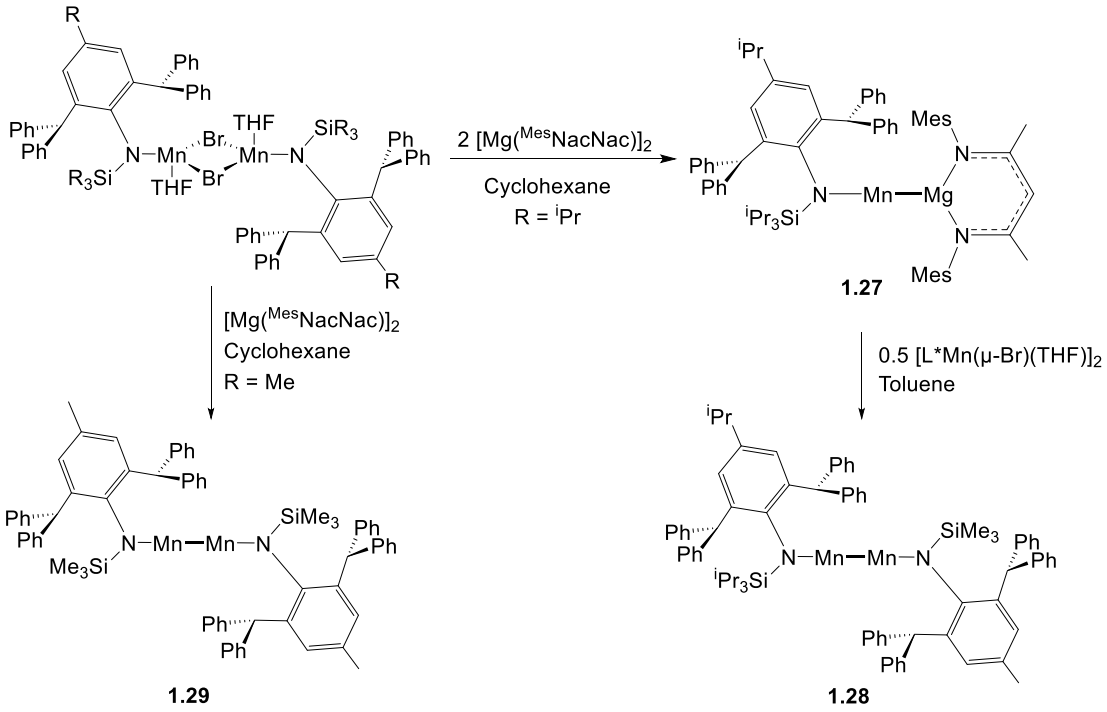

Scheme 1.7 Synthesis of L†MnMg(^{Mes}NacNac) (**1.27**) and the synthesis of the Mn–Mn dimers **1.28** and **1.29**.[49]

Compound **1.27** was also shown to react with {L*Cr(THF)(μ-Cl)}$_2$ to afford the mixed valence Mn^{II}/Cr^0 compound, Mn(μ-L†)(μ-L*)Cr (**1.30**).[49] Although the Mn···Cr distance (3.0443(6) Å) is close to the sum of covalent radii (3.00(9) Å),[14] computational studies revealed that metal–metal bonding between the two atoms was negligible. Based on the reactivity of the preceding compounds, Jones *et al*. believe that it is feasible that **1.30** forms *via* a metal-metal bonded Mn^I/Cr^I intermediate, L†Mn–CrL*, which undergoes a further internal redox process to afford the final Mn^{II}/Cr^0 product.

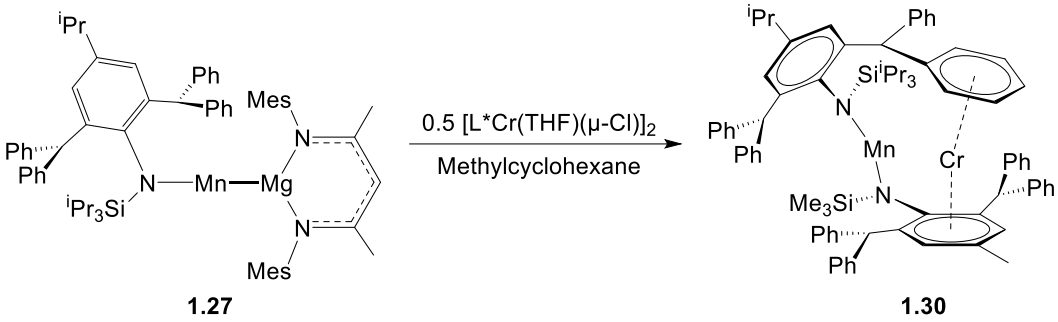

Equation 1.10[49]

Using the synthetic rationale described above, Jones *et al*. reported the isolation of the first Mg–Zn bonded complexes in 2015.[10] The reduction of {(Ar^{R})(^{i}Pr$_3$Si)N}ZnBr (Ar^{R} = C$_6$H$_2${C(H)Ph$_2$}$_2$R, R = Me or ^{i}Pr) by [Mg(^{Mes}NacNac)]$_2$ gave {(Ar^{R})(^{i}Pr$_3$Si)N}ZnMg(^{Mes}NacNac) (R = Me (**1.31**) or ^{i}Pr (**1.32**), Equation 1.11). The Zn–Mg distances of 2.5775(9) and 2.6082(14) Å for complexes **1.31** and **1.32**, respectively, were less than the sum of covalent radii compiled by Alvarez (2.63(8) Å)[14] but not less than those compiled by Pyykkö (2.57 Å).[15] This is possibly the result of steric repulsion between the extremely bulky amide ligand and the relatively sterically shielding NacNac ligand, which may result in a lengthening of the Mg–Zn bond. These Mg–Zn complexes are important precursors in the formation of Zn–Zn and Zn–Gp12 bonded complexes,[10] which will be discussed in detail in Chapter 3.

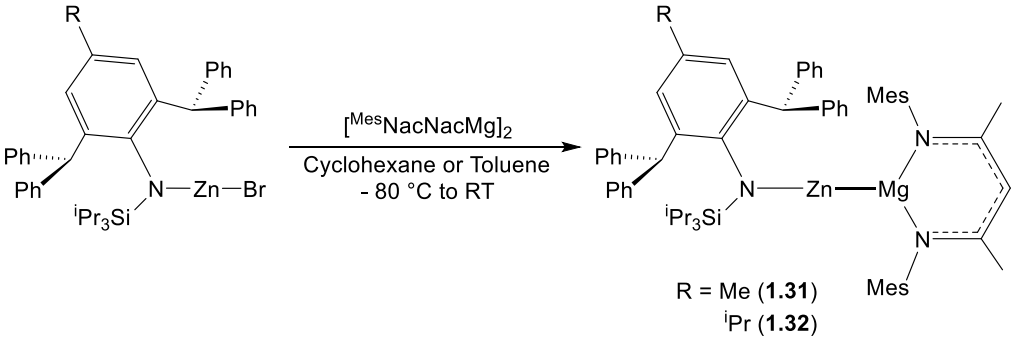

Equation 1.11[10]

Crimmin *et al*. reported another set of Mg–Zn compounds more recently, in 2018.[50] The reaction of **1.13** with (^{Dipp}NacNac)ZnI gave (^{Mes}NacNac)MgZn(^{Dipp}NacNac) (**1.33**, Scheme 1.8). Structural authentication revealed a Mg–Zn bond length of 2.5993(8) Å, comparable to those reported for **1.31** and **1.32**. Compound **1.33** was shown to be unstable in non-donor solvents, degrading to [Mg(^{Mes}NacNac)(^{Dipp}NacNac)] and a black precipitate, said to be Zn(0). A small quantity of a second product was crystallised

alongside **1.33**, which crystallographic analysis revealed to be a Zn–Zn–Zn complex. This complex will be discussed in detail in Chapter Three. Addition of THF to **1.33** gave the THF adduct (^{Mes}NacNac)(THF)MgZn(^{Dipp}NacNac) (**1.34**), with a Mg–Zn bond length of 2.6816(8) Å, significantly longer than that of **1.33**.

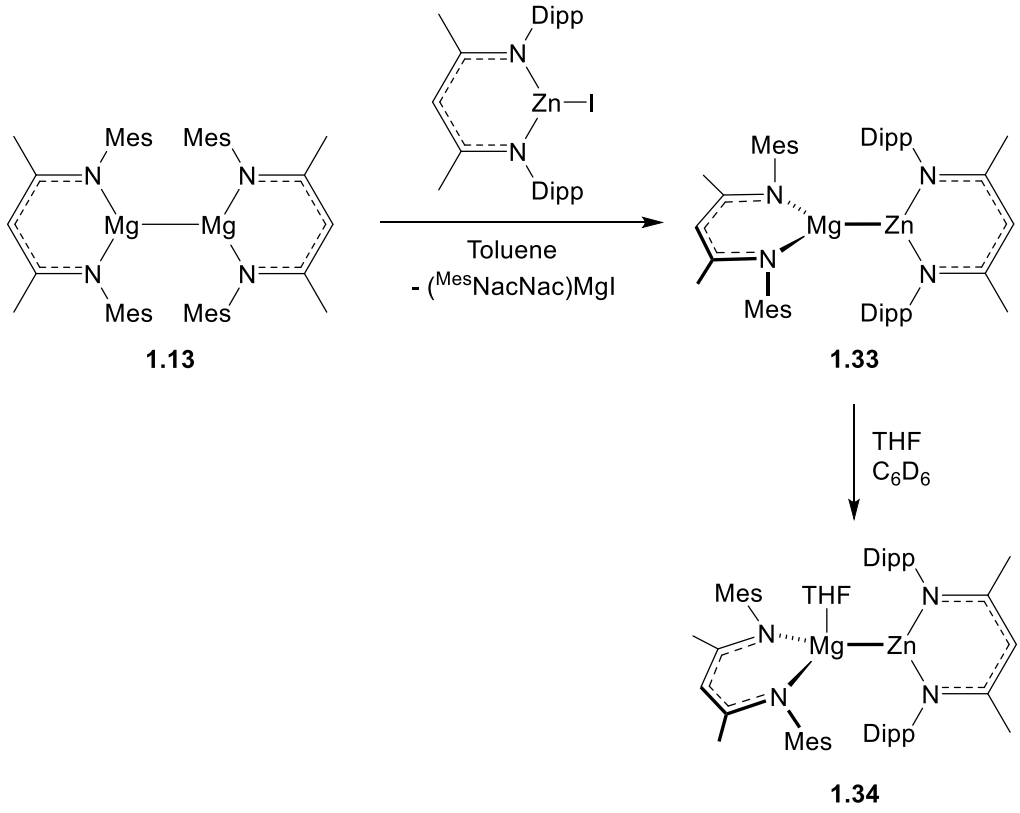

Scheme 1.8 The synthesis of Mg–Zn bonded **1.33** and its THF adduct **1.34**.[50]

In 2015, Crimmin and co-workers reported the first Mg–Rh bonded compound.[51] The thermolysis of Cp*Rh(H)$_2$(SiEt$_3$)$_2$ in the presence of [(^{Dipp}NacNac)Mg(μ-H)]$_2$ gave Cp*Rh(H)$_2$(SiEt$_3$)Mg(^{Dipp}NacNac) (**1.35**, Equation 1.12), which possesses a Mg–Rh bond length of 2.5049(8) Å. This distance is shorter than the sum of respective covalent radii reported by Alvarez (2.83(10) Å)[14] and Pyykkö (2.64 Å).[15] Since hydride ligands are difficult to locate using X-ray diffraction it can be troublesome to prove definitively that a complex such as **1.35** contains an unsupported metal-metal interaction which is not being stabilised by bridging hydrides. In the case of **1.35**, the Rh–H bonds are relatively short (1.42(3) – 1.56(3) Å) and the Mg···H distances are relatively long (2.06(3) − 2.17(3) Å), suggesting that the hydrides have limited interaction with the Mg centre. QTAIM (Quantum Theory of Atoms-in-Molecules) calculations found bond paths between Rh and H, Rh and Mg but not between Mg and H. The authors point out

that the efficacy of QTAIM is questionable in detecting very weak bonding interactions. Indeed, NBO calculations found a minor Mg–H bonding interaction. Nevertheless, it appears as though the Mg···H interaction is fairly weak and is not likely to account for the formation of the Rh–Mg bond.

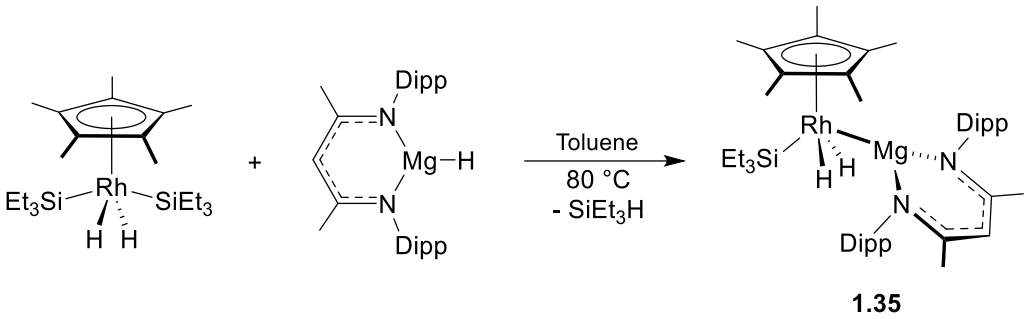

1.35

Equation 1.12[51]

Recently, Kays *et al*. reported the reaction of {CH($Ph_2PNSiMe_3$)$_2$}MgI(THF) (**1.36**) with NaFp to give {CH($Ph_2PNSiMe_3$)$_2$}MgFp (**1.37**, Fp = [$CpFe(CO)_2$], Equation 1.13).[52] Compound **1.37** was found to contain a Mg−Fe bond of 2.530(3) Å, within the sum of the respective covalent radii compiled by Alvarez and Pyykkö (2.73(8) and 2.55 Å, respectively).[14,15] Compound **1.37** is an unusual example of a Mg−TM bonded complex that has been isolated without coordinated donor solvent and is the first example of a three coordinate Mg species with a Mg–Fe bond.[4] The methine carbon of bis(iminophosphorano)methanide ligands often demonstrates carbene-like behaviour.[53] Indeed, both **1.36** and **1.37** exhibit close Mg···C interactions and consequently the ligand adopts a pseudo-boat conformation. The Mg···C distance of 2.573(6) Å in **1.36**[54] decreases to 2.471(8) Å upon conversion to **1.37**;[52] an observation consistent with an increasingly electropositive Mg centre, suggesting a largely ionic interaction between Mg and Fe centres.

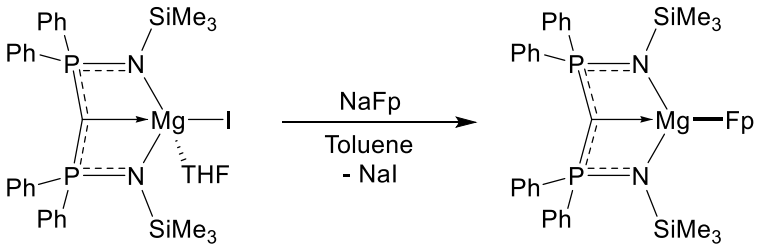

1.36 **1.37**

Equation 1.13[52]

An early report by McVicker (1974) detailed the reduction of Fp_2 with Mg/Hg amalgam in THF.[55] Although no crystal structure determination was reported, NMR, IR and elemental analyses of the product were consistent with the formation of "$MgFp_2(THF)_2$" (**1.38**, Equation 1.14).

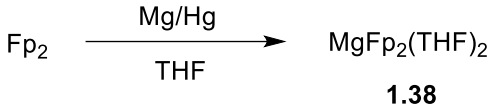

Equation 1.14[55]

Reproducing McVicker's synthesis and recrystallising the crude product from benzene, Blake and Mountford obtained and structurally authenticated $[MgFp_2(THF)]_2$ (**1.39**, Equation 1.15).[56] Compound **1.39** is a dimeric compound consisting of two $MgFp_2(THF)$ units joined by Mg(μ-OC)Fe isocarbonyl linkages. There are two independent Mg–Fe bonds in **1.39**, one within the ring and one external to the ring, measuring 2.6112(5) and 2.5629(5) Å, respectively. Both of these Mg–Fe distances are within the sum of covalent radii (2.73(8) Å).[14] The longer Mg–Fe bond results from the poorer donor property of the Fe which itself is a consequence of extensive backbonding to the bridging isocarbonyl group. The IR spectrum (Nujol mull) gave ν(CO) = 1912, 1855, and 1775 cm^{-1}, consistent with both terminal and isocarbonyl bridging CO groups.

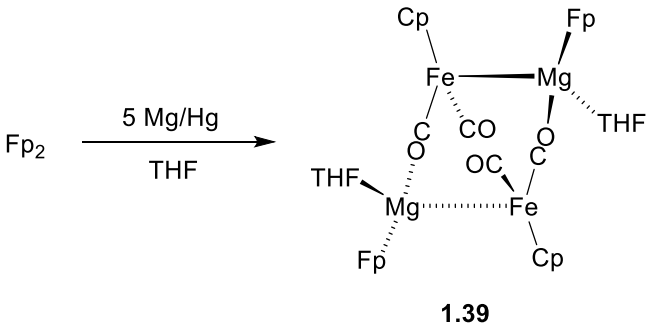

Equation 1.15[56]

Recrystallising **1.39** from THF gave $MgFp_2(THF)_4$ (**1.40**, Equation 1.16)[56,57] which contained no metal-metal bonds. The Mg centre exists in an octahedral coordination environment with two *trans*-axial isocarbonyl bridging interactions and four molecules of THF occupying the equatorial plane. Solution phase IR studies in THF were consistent with an isocarbonyl bridged species with ν(CO) = 1875 cm^{-1} for the terminal carbonyl ligands and ν(CO) = 1703 cm^{-1} for the bridging ones.[56] Recrystallising **1.40**

from benzene reformed **1.39**. This result represents a tuneable metal-metal bonding interaction which can be activated or deactivated depending on the donor properties of the solvent.

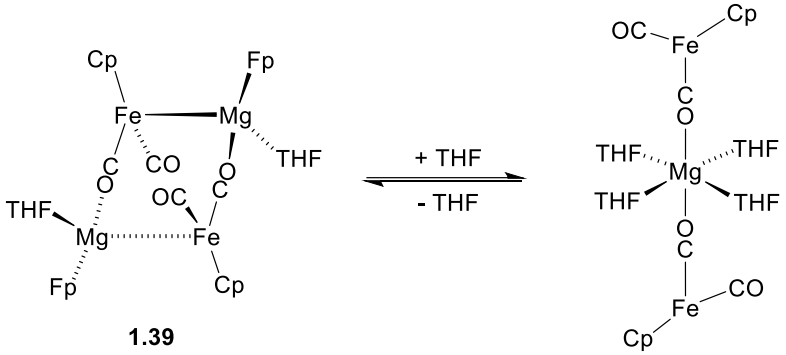

1.39 **1.40**

Equation 1.16[56,57]

Blake and Mountford reported the synthesis of $[MFp_2(THF)_3]_2$ (M = Ca (**1.41**) or Yb (**1.42**)) from the reduction of Fp_2 with M/Hg amalgams followed by recrystallisation from THF.[57] The similarities in the covalent radii (Ca = 1.76(10) and Yb = 1.87(8) Å),[14] and six-coordinate divalent ionic radii (Ca = 1.00, Yb = 1.02 Å)[58] of calcium and ytterbium are such that the solid state structures of **1.41** and **1.42** are isostructural and isomorphous in the solid state. Complex **1.41** contains one unique Ca–Fe bond distance of 3.0185(6) Å, within the sum of the respective covalent radii (3.08(10) Å).[14] The Yb–Fe bond distance in **1.42** (2.9892(4) Å, within the sum of the respective covalent radii (3.19(9) Å),[14] is shorter than its Ca counterpart, despite the slightly larger radius of Yb. This finding was reproduced using DFT, which found a stronger interaction between Yb and Fe than between Ca and Fe. In addition to being the first report of a Ca–TM bond, this was the first direct comparison between alkaline earth- and rare earth-transition metal bonding. The centrosymmetric eight-membered ring structure of **1.41** is analogous to **1.39**. However, the external Ae–Fe interaction has switched from the direct bond seen in **1.39** to an isocarbonyl interaction in **1.41**.

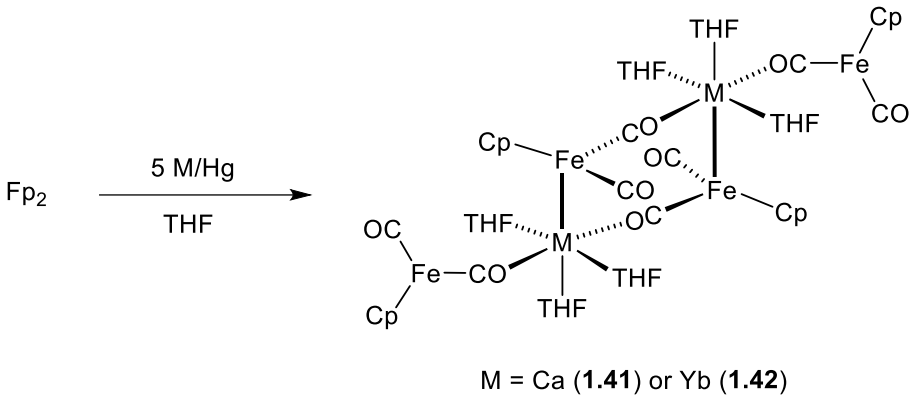

Scheme 1.9 Synthesis of $[CaFp_2(THF)_3]_2$ (**1.41**) and $[YbFp_2(THF)_3]_2$ (**1.42**).[57]

Finding success with the cleavage of Fp_2 with various metal amalgams, Blake and Mountford turned their investigation towards similar carbonyl-containing metal dimers, $[Co(CO)_3L]_2$ (L = CO (**1.43**), PPh_3 (**1.44**), or PCy_3 (**1.45**)).[56] Alteration of the ancillary ligand, L, allowed the solubility of the final products in non-donor solvents to be varied, as well as the σ-donor ability of the $[Co(CO)_3L]^-$ anion. The reduction of **1.43** in THF gave only insoluble material, no further studies were conducted with this species. The reduction of **1.44** with Ca/Hg, Sr/Hg, or Ba/Hg gave products soluble only in THF. The recrystallised products of these reactions, $Ca\{Co(CO)_3(PPh_3)\}_2(THF)_4$, $[Sr\{Co(CO)_3(PPh_3)\}_2(THF)_5]_2$, and $[Ba\{Co(CO)_3(PPh_3)\}_2(THF)_6]_2$, contained only isocarbonyl interactions and no metal-metal bonds.

The reduction of **1.45** with an excess of Mg/Hg amalgam in THF gave $[Mg\{Co(CO)_3(PCy_3)\}_2(THF)]_2$ (**1.46**, Equation 1.17), which could be recrystallised from toluene. Similar to **1.39**, compound **1.46** is a centrosymmetric dimer, with two $Mg\{Co(CO)_3(PCy_3)\}_2(THF)$ units connected by isocarbonyl bridging interactions. The structure possesses two independent Mg–Co bonds, one within the ring (2.6163(6) Å) and one external to the ring (2.5427(6) Å). Both of these distances are within the sum of the Alvarez covalent radii (2.67(8) Å)[14] and are comparable to the Mg–Co distances reported previously by Jonas, **1.19** (2.480(4) Å) and **1.20** (2.565(3) Å).[41]

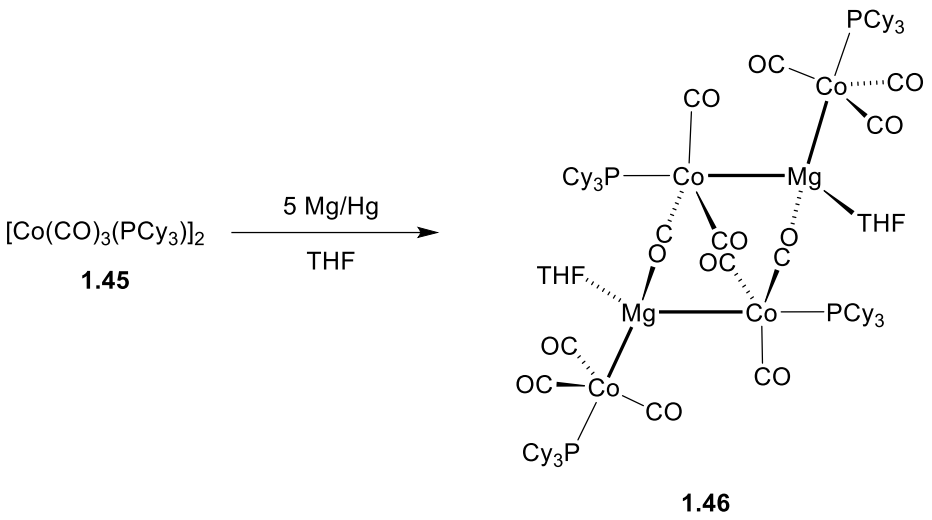

Equation 1.17[56]

Reduction of **1.45** with an excess of Ca/Hg in THF gave a toluene soluble material consistent with the formula, "Ca{$Co(CO)_3(PCy_3)$}$_2(THF)_2$".[56] Crystallisation from toluene afforded [Ca{$Co(CO)_3(PCy_3)$}$_2(THF)_2$]$_\infty$ (**1.47**, Equation 1.18). The solid state structure was revealed to contain alternating eight- and twelve-membered rings connected at vertices consisting of six-coordinate Ca atoms, forming an infinite polymeric chain (Figure 1.1). The eight-membered ring is analogous to that found in **1.46** and, indeed, in **1.39**. The direct Ca–Co interaction contained within the eight-membered ring has a distance of 3.0450(9) Å, similar within error to the sum of the respective Alvarez covalent radii (3.02(10) Å).[14] The twelve-membered ring contains no direct metal-metal bonds and consists of two Co centres joined to two Ca centres entirely by isocarbonyl bridging interactions.

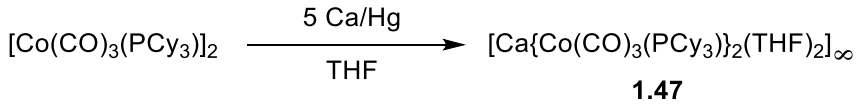

Equation 1.18[56]

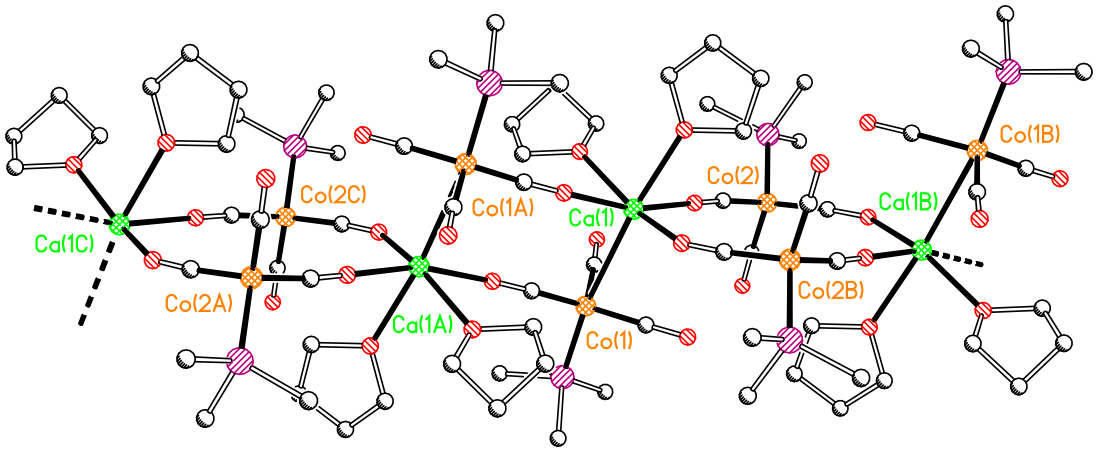

Figure 1.1 A portion of the $[Ca\{Co(CO)_3(PCy_3)\}_2(THF)_2]_\infty$ (**1.47**) chain. H atoms and cyclohexyl methylene carbons are omitted for clarity.[56,59]

Reduction of **1.45** with an excess of Sr/Hg amalgam in THF afforded a toluene-soluble material consistent with the formula, "$Sr\{Co(CO)_3(PCy_3)\}_2(THF)_3$".[56] Recrystallisation from pentane afforded $[Sr\{Co(CO)_3(PCy_3)\}_2(THF)_3]_\infty$ (**1.48**, Equation 1.19). Compound **1.48** crystallises in infinite polymeric chains (Figure 1.2) in a similar fashion to **1.47**. The polymer contains two distinct, alternating ring structures which connect at vertices consisting of seven- and eight-coordinate Sr atoms. The twelve-membered ring structure seen in **1.47** is present in **1.48**, containing analogous Sr(μ-OC)Co interactions. The second ring structure contains two Sr(μ-OC)Co interactions of the type observed in previous structures and two side-on Sr(μ-η^2-OC)Co interactions. The distance between the metal atoms in the Sr(μ-η^2-OC)Co bond (3.6263(4) Å) is longer than the sum of respective Alvarez radii (3.21(10) Å), though some residual metal-metal interaction may be present.

$$[Co(CO)_3(PCy_3)]_2 \xrightarrow[THF]{5\ Sr/Hg} \underset{\textbf{1.48}}{[Sr\{Co(CO)_3(PCy_3)\}_2(THF)_3]_\infty}$$

Equation 1.19[56]

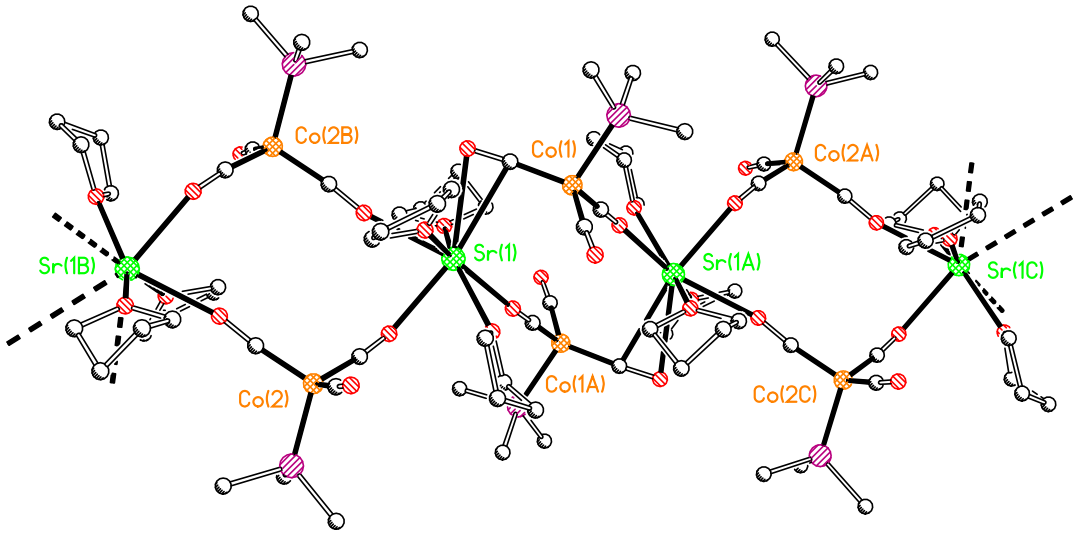

Figure 1.2 A portion of the $[Sr\{Co(CO)_3(PCy_3)\}_2(THF)_3]_\infty$ (**1.48**) chain. H atoms and cyclohexyl methylene carbons are omitted for clarity.[56,59]

This method has also been employed for the synthesis of several lanthanide–transition metal (Ln–TM) bonded complexes, including $[YbFp_2(THF)_3]_2$,[57] $[Yb\{Co(CO)_3(PCy_3)\}_2(THF)_3]_2$,[56] and $Sm\{Co(CO)_3(PCy_3)\}_3(THF)_3$,[56] the latter of which forms from the disproportionation of $Sm\{Co(CO)_3(PCy_3)\}_2(THF)_3$.

1.6 Group 12 metal-metal bonding

The group 12 elements (Gp12, herein used to refer to the congeners zinc, cadmium and mercury) occupy a unique position in the periodic table. Although they possess d-electrons in their valence shell, these orbitals are completely filled. It is not therefore suitable to treat them as transition metals. The nd^{10} valence electron configuration is so stable that oxidation of a group 12 element will remove electrons preferentially from the $(n+1)$s orbitals. The chemistry of the group 12 metals is therefore dominated by the +2 oxidation state, and hence is more comparable to that of the main group metals than the transition metals.

In the context of metal-metal bonding, group 12 complexes can be divided into two categories: homometallics, in which a bond exists between two (or more) of the same group 12 element, and heterometallics, in which a bond exists between a group 12 element and any other metallic element(s). The heterometallics can be further divided into two sub-categories: heterometallic complexes with a bond between a group 12 element and any other metallic element of a different group, and heterometallic complexes with a bond between two different group 12 elements. The latter sub-

category is a recently emerging field of study and will be omitted in this Chapter in favour of a detailed discussion in Chapter Three of this Thesis.

1.7 Group 12-metal heterometallic complexes

The heterobimetallic chemistry of the group 12 elements is diverse and expansive. This is primarily due to the wide variety of Gp12–TM bonded complexes which have been prepared. These examples are too numerous to describe in detail and are beyond the scope of this work; recent reviews, however, describe this area in detail.[9,60]

Metal-metal bonds between group 12 elements and the main group metals have been less frequently reported. The first compounds containing unsupported bonds between a group 12 element and an s-block metal (Zn–Mg) were prepared by Jones *et al*. in 2015, (**1.31** and **1.32**, *vide supra*).[4,10] Crimmin *et al*. have also recently reported a Zn–Mg bonded structure and its THF adduct (**1.33** and **1.34**, *vide supra*).[50] All other Gp12-main group bonded complexes feature bonds between the group 12 metal and a metal of the p-block.

The first structurally authenticated Zn–Al bonded complex was reported by Fischer *et al*. in 2017.[61] The reaction of $Zn\{N(SiMe_3)_2\}_2$ with 2 equivs. of AlCp* at 60 °C gave $Zn\{Al(\eta^2\text{-}Cp^*)(N\{SiMe_3\}_2)\}_2$ (**1.49**, Equation 1.20). Crystallographic analysis revealed a centrosymmetric structure containing one unique Zn–Al distance of 2.448(2) Å, consistent with the sum of Alvarez covalent radii (2.43(6) Å),[14] within experimental error. Compound **1.49** was found to be unstable under reaction conditions, marked by rapid decomposition and deposition of a metallic precipitate.

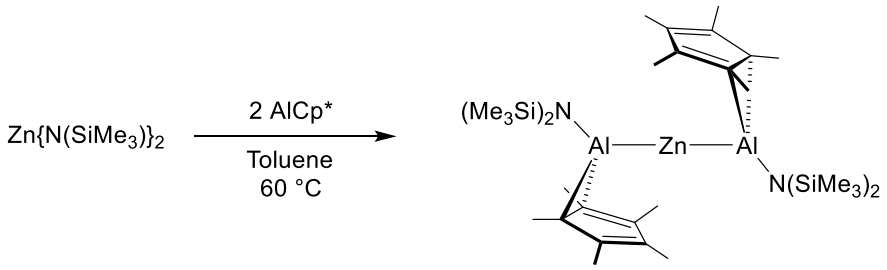

1.49

Equation 1.20[61]

A more recent Zn–Al bond was reported by Crimmin *et al*.[50] The reaction of (^{Mes}NacNac)Zn(Et)(OEt_2) with (^{Dipp}NacNac)Al gave (^{Mes}NacNac)ZnAl(Et)(^{Dipp}NacNac) (**1.50**, Equation 1.21) *via* an alkyl transfer reaction

and subsequent formation of the metal-metal bond. The solid state structure of **1.50** shows a Zn–Al bond length of 2.488(1) Å, consistent with the sum of covalent radii (2.43(6) Å),[14] within experimental error. Compound **1.50** was found to be thermally robust up to 80 °C, contrasting with **1.49** which decomposed under its reaction conditions (60 °C).

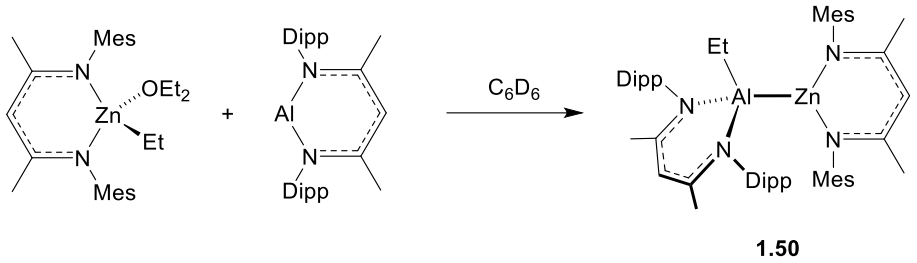

1.50

Equation 1.21[50]

The first structurally characterised Zn–Ga bonded complexes were reported by Jones *et al*. in 2007.[62] Reaction of [(DAB)Ga][K(TMEDA)] (**1.51**, DAB = {N(Dipp)CH}$_2$) with {^{i}Pr$_2$NC(NDipp)$_2$}ZnCl gave {^{i}Pr$_2$NC(NDipp)$_2$}ZnGa(DAB) (**1.52**) with a Zn–Ga distance of 2.3230(7) Å. Reaction of **1.51** with 0.5 equivs. of ZnCl$_2$(TMEDA) gave (TMEDA)Zn{Ga(DAB)}$_2$ (**1.53**) with Zn–Ga distances of 2.4491(17) and 2.4307(17) Å. Each of these Zn–Ga distances are within the sum of the respective Alvarez covalent radii (2.44(5) Å).[14] In 2010, Jones *et al*. employed the same methodology to produce (^{Dipp}NacNac)ZnGa(DAB) (**1.54**) and ZnBr(TMEDA){Ga(DAB)} (**1.55**) from the reaction of **1.51** with (^{Dipp}NacNac)Zn(μ-Br)$_2$Li(OEt$_2$)$_2$ and ZnBr$_2$(TMEDA), respectively.[63] The Zn–Ga distances for **1.54** and **1.55** are 2.3841(6) and 2.3829(8) Å, respectively. These distances are, again, within the sum of the respective covalent radii (*vide supra*).

The 1:1 reaction of **1.51** with ZnCl$_2$(TMEDA) produced no other clean products instead giving an intractable mixture of species. The heteroleptic complex **1.55**, however, forms cleanly from the 1:1 reaction of **1.51** with ZnBr$_2$(TMEDA). The authors sought **1.55** as a heteroleptic precursor from which to access a dimeric (LGa)ZnZn(GaL) species. Reduction with K metal, KC$_8$, KH and LiH all failed to furnish the desired dimeric product, however, resulting instead in decomposition of the complex indicated by the deposition of metallic Zn.

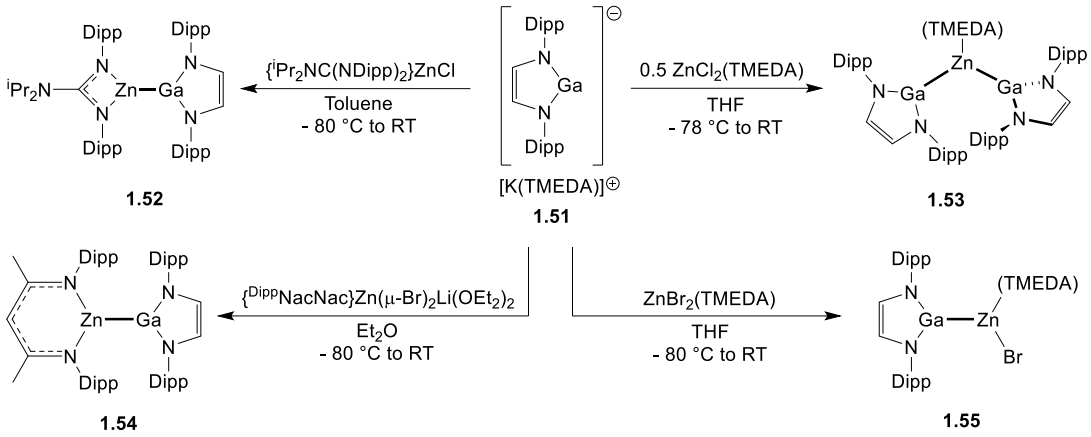

Scheme 1.10 Preparation of Zn–Ga bonded complexes **1.52** - **1.55**.[62,63]

During their investigations into Gp12–Ga bonded complexes, Jones *et al*. also prepared the Cd–Ga bonded species CdI(TMEDA){Ga(DAB)} (**1.56**, Equation 1.22) using the same methodology that produced the Zn analogue **1.55**.[63] Compound **1.56** is the first structurally authenticated complex containing a Cd–Ga bond. The unit cell contained two independent molecules of **1.56** with Cd–Ga distances of 2.509(1) and 2.5479(9) Å, both of which are less than the sum of the covalent radii (2.66(10)/2.60 Å).[14,15] Attempts to prepare the Cd analogue of **1.54** from the reaction of **1.51** and (^{Dipp}NacNac)Cd(μ-I)$_2$Li(OEt$_2$)$_2$ gave only **1.56**. The authors suggested that **1.51** reacts instead with CdI_2 which is formed *in situ* from the Schlenk equilibrium between (^{Dipp}NacNac)Cd(μ-I)$_2$Li(OEt$_2$)$_2$ and its products.

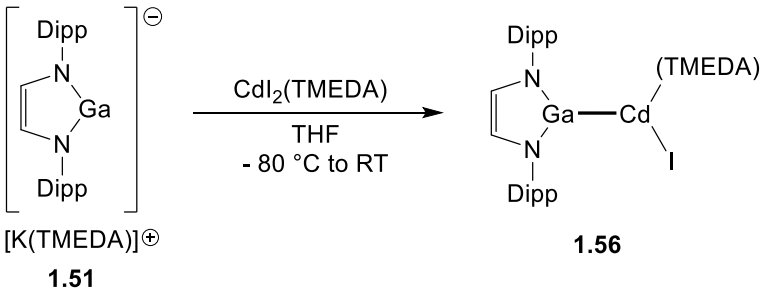

Equation 1.22[63]

Fischer *et al*. reported the reactions of (^{Dipp}NacNac)Ga (**1.57**, Scheme 1.11) with either $ZnMe_2$ or $ZnCl_2$ to give {(^{Dipp}NacNac)Ga(Me)}$_2$Zn (**1.58**, Zn–Ga 2.4631(7) and 2.4609(7) Å) and (^{Dipp}NacNac)Ga(Cl)Zn(Cl)(THF)$_2$ (**1.59**, Zn–Ga 2.3920(6) Å), respectively.[64] Complex **1.59** reacted with Na[BAr^F_4] to produce the dimeric species [(^{Dipp}NacNac)Ga(THF)Zn(THF)(μ-Cl)]$_2$ (**1.60**, Zn–Ga 2.3960(11) Å).

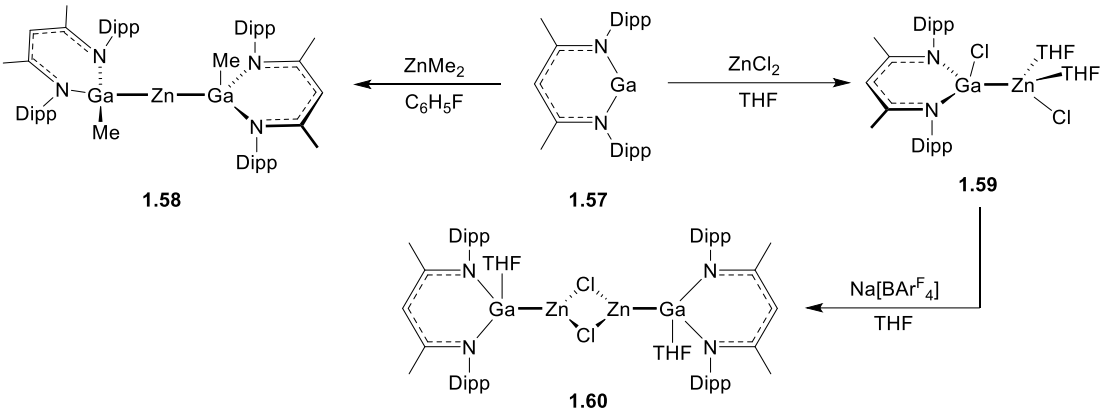

Scheme 1.11 Preparation of Zn–Ga bonded complexes **1.58** - **1.60**.[64]

In the same article the authors describe the synthesis of $[Zn(GaCp^*)_4][BAr^F{}_4]_2$ (**1.61**, Equation 1.23) which contains four Zn–Ga bonds.[64] The complex is prepared by treating a mixture of $ZnMe_2$ and Brookhart's acid, $[H(OEt_2)_2][BAr^F{}_4]$, with GaCp*. The coordination environment around the Zn centre has a distorted tetrahedral geometry giving two unique Zn–Ga distances of 2.4036(6) and 2.4111(6) Å.

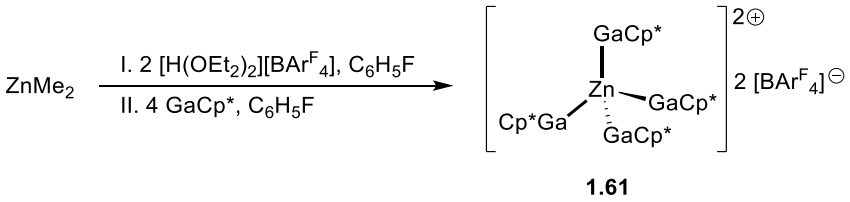

Equation 1.23[64]

Using the methodology described previously for **1.58**, Fischer *et al*. were also successful in isolating a Hg–Ga bonded complex. $\{(^{Dipp}NacNac)(C_6F_5S)Ga\}_2Hg$ (**1.62**) was prepared by treating **1.57** with $Hg(SC_6F_5)_2$ (Scheme 1.12).[65] As a result of the coordination environment at Ga, **1.62** exhibits conformational isomerism. When crystallised directly from the reaction mixture **1.62** is isolated as the *anti* conformer. However, heating a toluene solution of the complex to reflux before crystallisation results in the isolation of the *gauche* conformer (**1.62a**). The Hg–Ga distances for **1.62** and **1.62a** are 2.5339(6) and 2.5332(5) Å, respectively. The Hg–Ga bonds within each complex are crystallographically equivalent and both are less than the sum of the covalent radii (2.54(6) or 2.57 Å).[14,15]

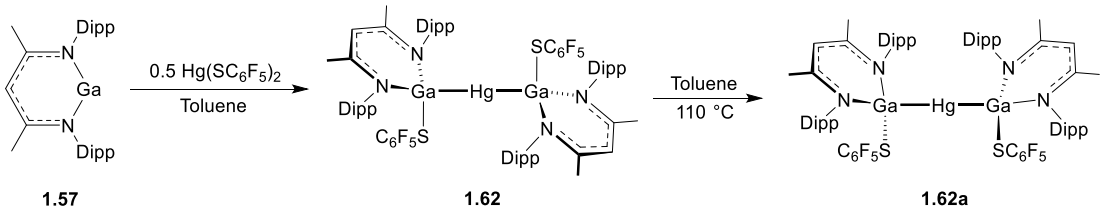

1.57 **1.62** **1.62a**

Scheme 1.12 Preparation of Hg–Ga bonded complex **1.62** and the transformation to its *gauche* conformer, **1.62a**.[65]

Fedushkin and Schumann reported the preparation of the paramagnetic Zn–Ga complex (Dipp-BIAN)ZnGa(Dipp-BIAN) (**1.63**, Dipp-BIAN = 1,2-bis[(2,6-diisopropylphenyl)imino]-acenaphthene, Equation 1.24).[66] The radical compound was prepared by first treating $[(\text{Dipp-BIAN})\text{ZnI}]_2$ with $GaCl_3$ followed by K_4[Dipp-BIAN]. The Zn–Ga distance was determined to be 2.3531(8) Å from single crystal X-ray diffraction data. Zn and Ga occupy adjacent positions in the periodic table and thus have very similar X-ray scattering properties. Due to the similarity of the coordination environments, it was not trivial to distinguish these atoms from one another during refinement of X-ray diffraction data. The ESR spectrum of **1.63**, however, showed clear coupling between the unpaired electron and ^{69}Ga and ^{71}Ga nuclei, supporting the presence of a Zn–Ga bond.

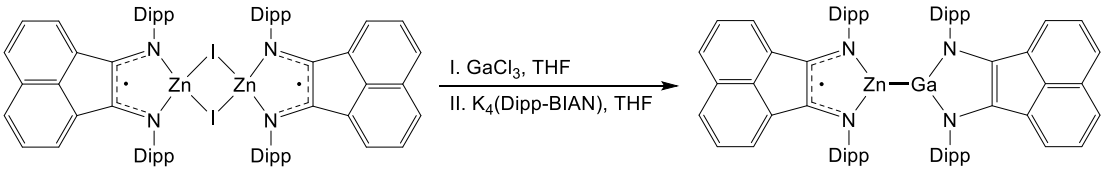

1.63

Equation 1.24[66]

The first structurally authenticated example of a Gp12–Gp14 bonded complex was reported by Boersma *et al*. in 1990.[67] The reaction of bis[3-(dimethylamino)propyl]zinc with bis(dibenzoylmethonato)tin(II) gave $(HC\{C(Ph)O\}_2)_2ZnSn\{(CH_2)_3NMe_2\}_2$ (**1.64**, Equation 1.25). Compound **1.64** results from the transmetallation of the two reactants, followed by trapping of the stannylene unit by the electrophilic zinc moiety. The product is therefore considered to be a donor-acceptor interaction which results in a dative Sn→Zn bond. The Zn–Sn distance was determined to be 2.634(6) Å. This value is within the sum of covalent radii complied Alvarez (2.61(6) Å),[14] within experimental

error. Repulsion between the bulky ligands, coupled with the weak donor-acceptor nature of the bonding electrons, are the likely cause of the lengthened Zn–Sn bond.

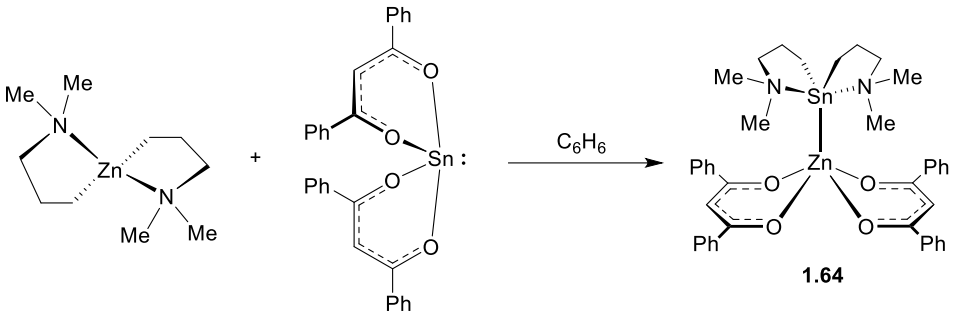

Equation 1.25[67]

The first comparative structural study of a set of Gp12–Sn complexes was reported by Gade *et al*. in 2002.[68] Reaction of $MeSi\{SiMe_2NTol\}_3SnLi(OEt_2)$ ($L^{Sn}Li(OEt_2)$) with the series of group 12 chlorides gave $(MeSi\{SiMe_2NTol\}_3Sn)_2M$ (M = Zn (**1.65**), Cd (**1.66**), Hg (**1.67**)). Complexes **1.66** and **1.67** were isolated as isomorphous single crystals. Their solid state structures show that the metal atoms adopt a linear Sn–M–Sn motif with the group 12 metal occupying a crystallographic inversion centre. The two unsupported M–Sn bonds are therefore equivalent within each complex. The Hg–Sn distance found in **1.67** (2.6492(2) Å) is shorter than the Cd–Sn distance found in **1.66** (2.6758(1) Å). The authors attribute this observation to the effects of the lanthanide contraction, citing a similar effect observed in analogous isostructural Ag(I)/Au(I) chemistry.[69] Both of the M–Sn distances are shorter than the sum of their respective covalent radii (Cd–Sn: 2.83(10) or 2.76 Å; Hg–Sn: 2.71(6) or 2.73 Å).[14,15]

The coordination environment of **1.65** is significantly different from that of its heavier group 12 analogues. It contains one unsupported Zn–Sn bond (2.5782(4) Å) which is shorter than the sum of the covalent radii (2.61(6)/2.58 Å).[14,15] However, one ligand acts in a bridging fashion, complexing both the Sn and Zn atoms. The resultant Zn–Sn distance (2.9930(4) Å) is significantly lengthened compared to its unbridged counterpart and is significantly greater than the sum of the covalent radii. As such, this Zn–Sn interaction cannot be considered a metal-metal bond, though some metal-metal interaction may be present.

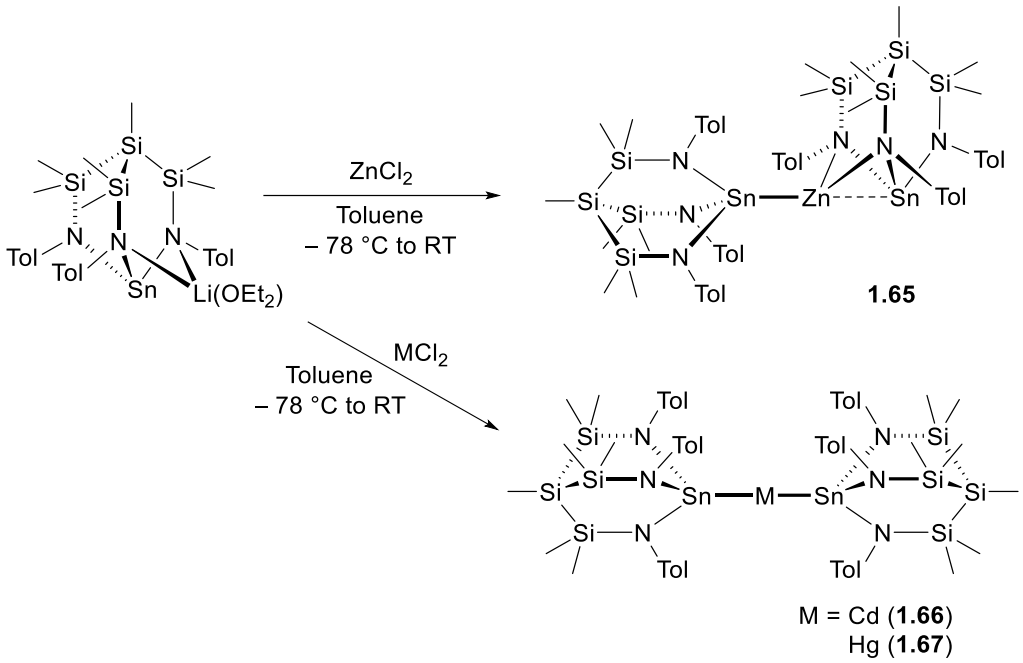

Scheme 1.13 Synthesis of Gp12–Sn bonded complexes **1.65 - 1.67**.[68]

More recently Power *et al*. reported the synthesis of $(Ar^{Me6})_2Sn(Me)ZnMe$ (**1.68**, Ar^{Me6} = 2,6-$C_6H_3(Mes)_2$, Scheme 1.14) from the reaction of $(Ar^{Me6})_2Sn$ with $ZnMe_2$.[70] Crystals of **1.68** gave a solid state structure which contained two independent molecules in the asymmetric unit. The Zn–Sn distances were 2.5524(7) and 2.5529(7) Å, both of which are significantly shorter than the sum of covalent radii (2.61(6) or 2.58 Å).[14,15] Dissolution of crystals of **1.68** in hydrocarbon solvents was accompanied by the appearance of the characteristic violet colour of the $(Ar^{Me6})_2Sn$ precursor, suggesting an equilibrium between reactants and product. Cooling the solution below RT resulted in complete conversion to **1.68**.

Similarly, the reaction of $ZnMe_2$ with $(Ar^{Me6})_2Ge$ afforded $(Ar^{Me6})_2Ge(Me)ZnMe$ (**1.69**), however diffraction quality crystals of this complex could not be grown. Instead, the reaction of $(Ar^{Me6})_2Ge$ with $ZnEt_2$ produced $(Ar^{Me6})_2Ge(Et)ZnEt$ (**1.70**) from which a single crystal structure could be obtained with a Zn–Ge distance of 2.3839(11) Å. This value is shorter than the sum of the covalent radii (2.42(6) or 2.39 Å),[14,15] indicating a clear bonding interaction.

Attempts were made to apply this methodology to the synthesis of a Zn–Pb bonded complex. The reaction of $(Ar^{Me6})_2Pb$ with $ZnMe_2$ instead gave $(Ar^{Me6})_2ZnMe$ *via* a ligand exchange reaction. To date, Zn–Pb bonds have only been observed[4] in Zintl clusters.[71–73]

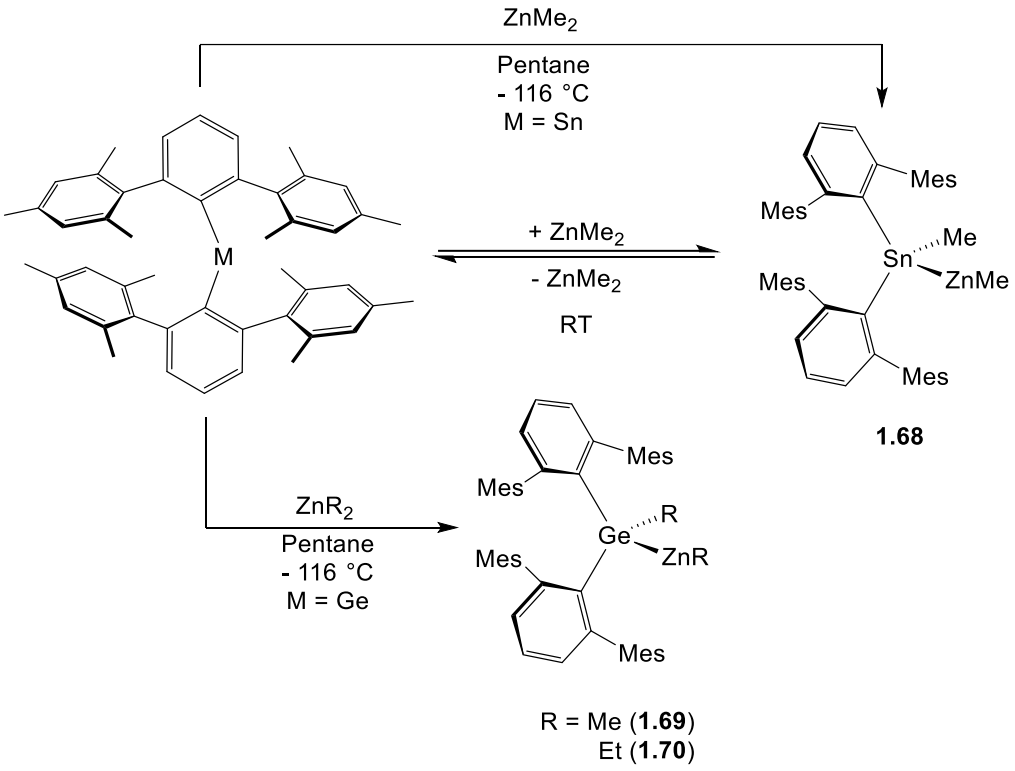

Scheme 1.14 Preparation of Zn–Sn and Zn–Ge bonded complexes **1.68** - **1.70**.[70]

There are considerably fewer reports of complexes which possess Gp12–Gp15 metal-metal bonds. In 1993 Dickson *et al.* reported the synthesis of $[Sb_2Et_4{\cdot}2CdI_2]_\infty$ (**1.71**, Equation 1.26);[74] an adduct formed from the reaction of Sb_2Et_4 and CdI_2 in THF. Upon removal of the solvent a coordination polymer is formed with a bridging iodide interaction between the $Sb_2Et_4{\cdot}2CdI_2$ monomers. The two Cd–Sb distances were determined to be 2.822(2) and 2.821(2) Å. These are shorter than the sum of covalent radii compiled by Alvarez (2.83(10) Å)[14], but are slightly longer than those compiled by Pyykkö (2.76 Å).[15] These data suggest that the solid possesses a weak Cd–Sb metal-metal bond in the solid state. A possible explanation for this is that the donation of electron density from bridging iodides between monomer units results in a less electrophilic Cd atom which is subsequently less attracted to the lone pair of the distibine moiety, resulting in a weaker Cd–Sb bond.

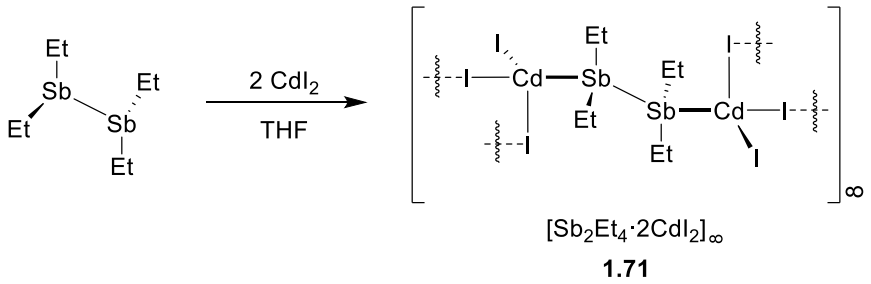

$[Sb_2Et_4{\cdot}2CdI_2]_\infty$

1.71

Equation 1.26[74]

The first structurally authenticated compound with Zn–Sb bonds was reported by Schulz *et al.* in 2005.[75] The metal cluster has the formula $[\{(MeZn)\{Sb(SiMe_3)_2\}_3Zn_2(SbSiMe_3)\}_2(ZnMe)Cl]$ (**1.72**) and is formed from the reaction of $[(DMAP)AlMe_2Sb(SiMe_3)_2]$ with $[(DMAP)_2ZnMe_2]$. The origin of the Cl atom is attributed to impurities in the $ZnMe_2$ precursor solution. The cluster consists of three annulated Zn_3Sb_3 rings with the outer rings bridged by a $Sb(SiMe_3)_2$ unit and a Cl atom (a simplified representation of the metallic core of the cluster is presented in Figure 1.3). The nine Zn–Sb distances within the cyclic Zn_3Sb_3 units range between 2.604(1) to 2.656(1) Å. All of these distances are within the sum of the respective Alvarez covalent radii (2.61(6) Å),[14] within experimental error. The Zn–Sb distances from the bridging $Sb(SiMe_3)_2$ unit are 2.604(1) and 2.686(1) Å, to Zn(2A) and Zn(3), respectively. The Zn(3)–Sb(4A) bond length is significantly lengthened compared to all others and is significantly longer than the sum of covalent radii. Additionally, the geometry at the Sb(4A) atom displays distinct pyramidalisation, suggesting that the Zn(3)–Sb(4A) bond has pronounced dative character.

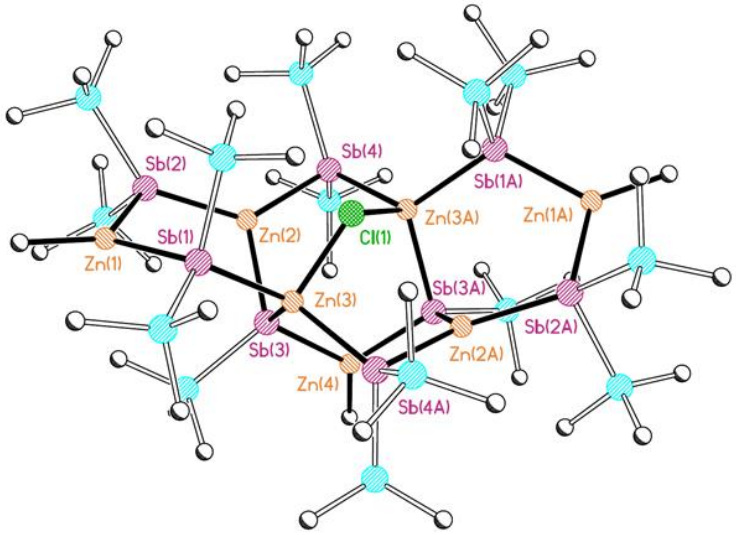

Figure 1.3 Representation of the metallic core of **1.72**.[75]

The only other successful synthesis of structurally authenticated Zn–Sb bonds comes from the work of Dehnen and co-workers. They reported the preparation of $[K(2.2.2\text{-crypt})]_3[Sn_2Sb_5(ZnPh_2)_2]$ (**1.73**) from the reaction of K_8SnSb_4, 2.2.2-crypt and $ZnPh_2$ in ethylenediamine (Equation 1.27).[76] The Zintl ion has four unique Zn–Sb bonds which measure 2.6557(13), 2.6564(12), 2.6620(14) and 2.6767(14) Å in length. Similar to **1.72**, these distances are longer than the sum of the Alvarez covalent radii (2.61(6) Å),[14] however they are within the range of experimental error.

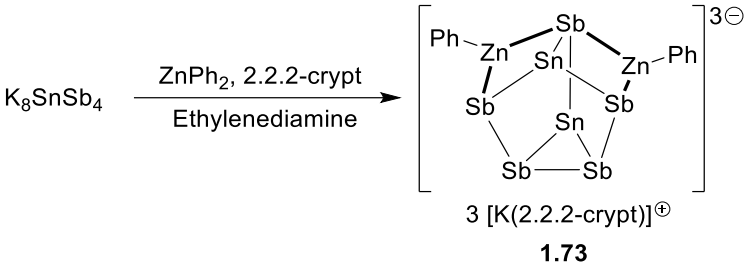

1.73

Equation 1.27[76]

Gabbaï and co-workers have reported a series of compounds which possess Hg–Sb interactions. Sequential reaction of 1,8-dilithionaphthalene with Ph_3SbBr_2 followed by $HgBr_2$ gave the dimeric complex $[Ph_2Sb(\mu\text{-}C_{10}H_6)_2Hg(\mu\text{-}Br)]_2$ (**1.74**, Hg–Sb 3.0879(5) Å, Scheme 1.15). Treatment of **1.74** with $TlPF_6$ gave the monomeric hexafluorophosphate salt $[Ph_2Sb((\mu\text{-}C_{10}H_6)_2Hg][PF_6]$ (**1.75**, Hg–Sb 3.0601(7) Å). Alternatively, a one-pot reaction between **1.74**, $TlPF_6$ and $[^nBu_4N]I$ gave the monomeric iodide complex $Ph_2Sb(\mu\text{-}C_{10}H_6)_2HgI$ (**1.76**, Hg–Sb 3.073(1) Å). Each of

the Hg–Sb distances in complexes **1.74 - 1.76** are significantly longer than the sum of covalent radii (2.71(7) or 2.73 Å).[14,15] In order to assess the degree of bonding between the two metals DFT analysis was performed for complexes **1.75** and **1.76**, in addition to two reference compounds, $Hg_2(\mu\text{-}C_{10}H_6)_2$ and $Hg(\mu\text{-}C_{10}H_6)_2InBr(THF)_2$. These two reference compounds showed no evidence of bonding between metal atoms. Complex **1.75** showed a small degree of polarisation of electron density in a Hg 5d orbital towards the Sb atom. This polarisation effect was observed to a greater degree in **1.76**, suggesting that there may be a small interaction from Hg→Sb in both complexes despite their distance from each other. Overall, it is difficult to separate the effect of the ligand geometry from the effects of bonding when considering the final Hg–Sb distances. These interactions cannot be considered full metal-metal bonds due to their separation. However, the evidence presented by the authors may suggest a weak metal-metal interaction.

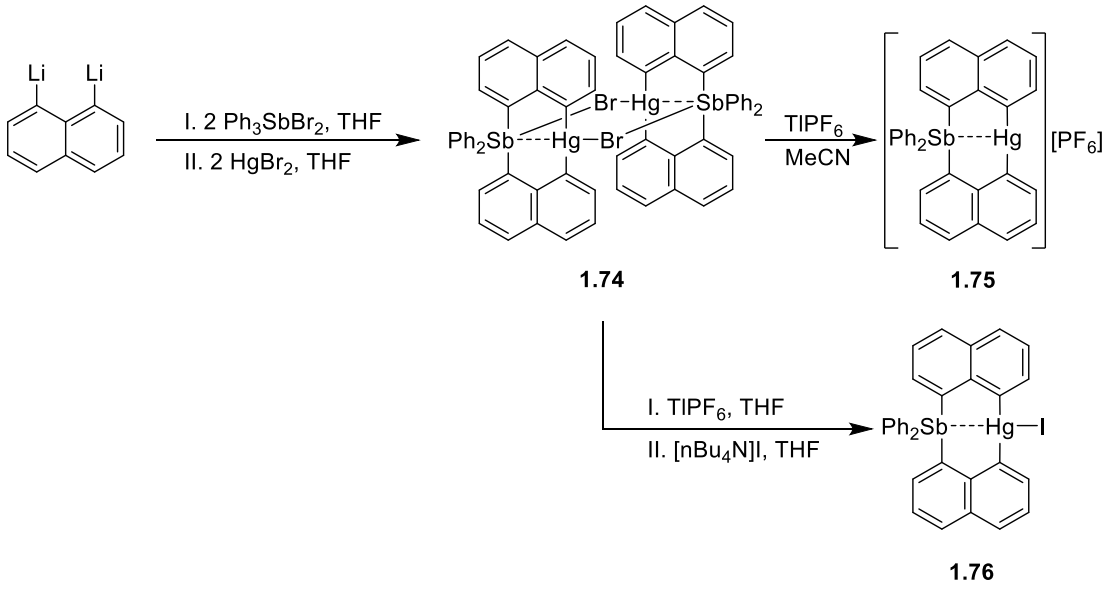

Scheme 1.15 Preparation of complexes **1.74 - 1.76**, which possess Hg–Sb interactions.[77]

1.8 Group 12 homobimetallic complexes

Renewed interest in metal-metal bonded complexes and their chemical properties may be a relatively recent occurrence. However, homometallic Gp12–Gp12 bonded complexes have been known since antiquity. The oldest synthetic formulation for calomel (Hg_2Cl_2) can be found in a Chinese alchemy manuscript written between 25 – 220 A.D.[60] An analysis of the single crystal X-ray structures of the homobimetallic

Hg(I) halides, Hg_2X_2 (X = F, Cl, Br) was published in 1971.[78] Dimercury(I) salts have also been studied as their oxo-acids,[79–86] pseudo-halides,[87–90] metallates,[91,92] and even as bridging ligands between other metal centres.[93]

Dicadmium(I) and dizinc(I) salts are considerably rarer than dimercury(I) compounds. The first dicadmium(I) salt was prepared in 1956 by dissolving Cd metal in molten $CdCl_2$.[94] Performing the same reaction in the presence of Lewis-acidic $AlCl_3$ gave $Cd_2(AlCl_4)_2$. Crystal structures were obtained of this compound, some thirty years later.[95,96] The Cd–Cd distance was shown to be 2.576 Å, shorter than the sum of covalent radii (2.88(13) or 2.72 Å).[14,15]

The first dizinc(I) salt was similarly formed in 1967; by dissolving Zn metal in molten $ZnCl_2$.[97] UV-vis, Raman, ESR spectroscopy, magnetic susceptibility and chemical assays were all used to test for the presence of Zn_2Cl_2 within the glass. However, no crystal structure was determined.

The first molecular complex containing a Gp12–Gp12 bond was synthesised in 1993 by Reger *et al.*[98] $[(Tp^{Me2})Cd]_2$ (**1.77**) was synthesised by first treating $CdCl_2$ with $LiBHEt_3$, followed by reaction with $Tp^{Me2}Tl$ (Equation 1.28). No crystal structure of **1.77** was obtained, however the existence of the Cd–Cd bonding interaction was demonstrated through the observation of the particularly large ^{111}Cd–^{113}Cd coupling constant (20,646 Hz) in the ^{113}Cd NMR spectrum.

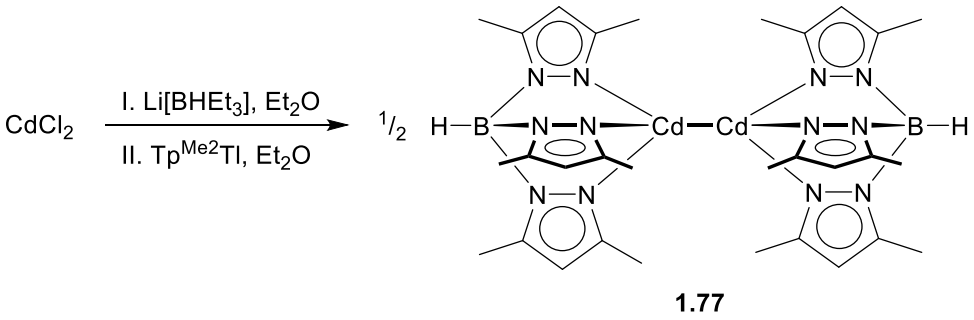

1.77

Equation 1.28[98]

The first molecular Hg–Hg bonded complex was reported in 1999 by Apeloig *et al.*[99] Reaction of $^tBu_2Hg$ with 2 equivs. of $HSi(SiMe_2SiMe_3)_3$ gave $[HgSi(SiMe_2SiMe_3)_3]_2$ (**1.78**). The X-ray crystal structure shows a Hg–Hg bond length of 2.6569(8) Å. This distance is equivalent within error to the sum of covalent radii compiled by Alvarez (2.64(7) Å). The bond length is, however, within the sum of covalent radii compiled by

Pyykkö (2.66 Å). These observations suggest that although there is a bonding interaction between the Hg centres, the Hg–Hg bond is likely lengthened due to repulsion between the sterically demanding silane ligands.

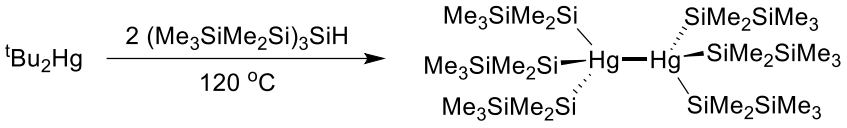

1.78

Equation 1.29[99]

It was not until 2004 that the first Zn–Zn bonded complex was reported by Carmona *et al*. $Zn_2Cp^*_2$ (**1.79**) was first synthesised *via* the reaction of Cp^*_2Zn and $ZnEt_2$ (Scheme 1.16),[5] although the reaction was fairly low-yielding (rarely greater than 30%).[100] Several improved synthetic preparations have been reported in the years since.[100,101] These preparations employ alkali metal hydrides as reductants and provide much greater yields of the dizincocene. X-ray crystal structure analysis shows the Zn–Zn distance in **1.79** to be 2.305(3) Å, shorter than the sum of covalent radii (2.44(6) or 2.36 Å).[14,15]

In addition to its reactivity with a number of small molecules, **1.79** undergoes a variety of ligand exchange reactions which preserve the formal $[Zn_2]^{2+}$ core.[9,102] Compound **1.79** has therefore allowed access to a diverse set of new Zn–Zn complexes. These reactions will be discussed in Chapter Three.

Carmona *et al*. have demonstrated that the optimised synthesis of **1.79** can also be applied to the synthesis of similar dizincocene analogues.[100] The reaction of $(C_5Me_4Et)_2Zn$ with $ZnCl_2$ and 2 equivs. of KH gave $Zn_2(C_5Me_4Et)_2$ (**1.80**, Scheme 1.16). The crystallographically determined Zn–Zn bond distance of 2.295(2) Å is equivalent to that found in **1.79**, within experimental error.

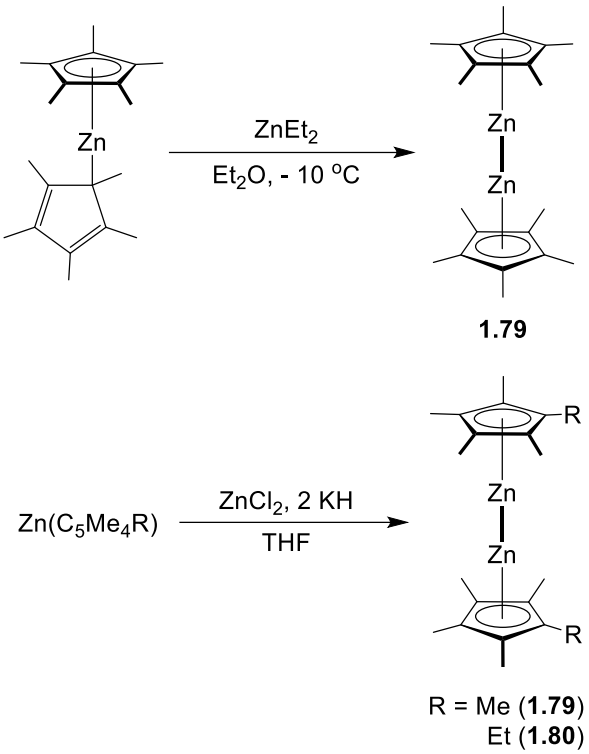

Scheme 1.16 Synthetic routes to cyclopentadienyl Zn(I) dimers.[5,100]

The discovery of **1.79** was followed up relatively quickly with the discovery of (^{Dipp}NacNac)$_2$Zn$_2$ (**1.81**, Equation 1.30) by Robinson *et al*. in 2005.[103] This complex was synthesised by the reduction of (^{Dipp}NacNac)Zn(μ-I)$_2$Li(OEt$_2$)$_2$ with potassium metal. The crystal structure revealed a Zn–Zn bond of 2.3586(7) Å. The Zn–Zn distance is longer than that of **1.79** by 0.054(8) Å; potentially a result of repulsion between the sterically demanding Dipp groups of the NacNac ligand.

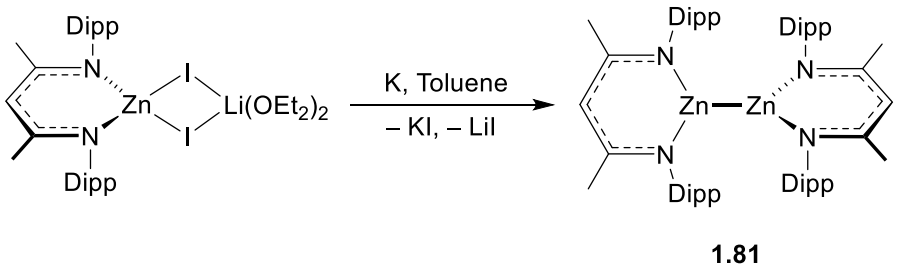

Equation 1.30[103]

The first homologous series of Gp12–Gp12 bonded complexes was reported by Power *et al*. in 2007 (Scheme 1.17).[104] Bulky terphenyl ligands were employed to protect the $[M_2]^{2+}$ cores, producing complexes of the form Ar'$_2$M$_2$ (Ar' = C$_6$H$_3$-2,6-Dipp$_2$) for M = Zn (**1.82**), Cd (**1.83**) and Hg (**1.84**). Each of the three complexes is synthesised *via* the

reduction of an iodide precursor, however the reducing agent employed is different in each case. Compound **1.82** is obtained from the reduction of $[Ar'Zn(\mu\text{-}I)]_2$ with metallic sodium,[105] while **1.83** is produced through the reaction of $[Ar'Cd(\mu\text{-}I)]_2$ with NaH.[106] Attempts were made to obtain **1.84** from the salt metathesis reaction of Ar'MgBr with Hg_2I_2, installing the sterically protecting terphenyl ligands around the pre-existing $[Hg_2]^{2+}$core. This approach resulted in a disproportionation reaction, giving the corresponding arylmercury(II) iodide and elemental mercury among the products. Compound **1.84** was eventually obtained *via* the reduction of Ar'HgI with KC_8.[104] The M–M bond distances are 2.3591(9) Å for **1.82**, 2.6257(5) Å for **1.83** and 2.5738(3) Å for **1.84**. Each distance is shorter than the sum of the respective covalent radii defined by both Alvarez[14] and Pyykkö,[15] indicating a considerable metal-metal bonding interaction in each complex.

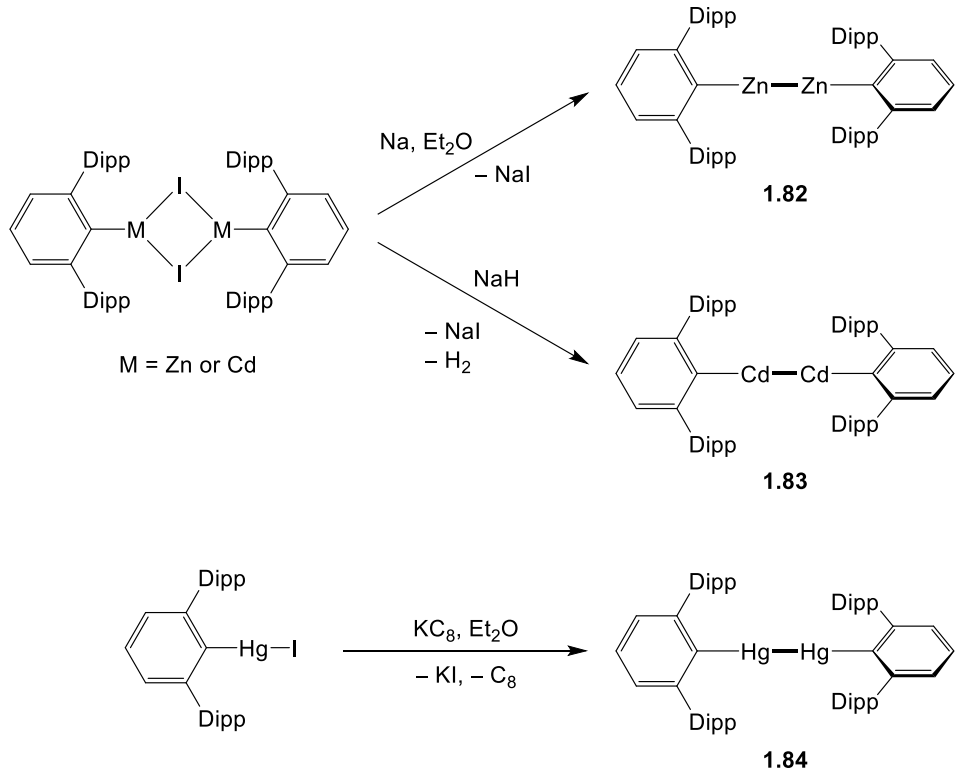

Scheme 1.17 Preparation of the homologous series of Gp12 homobimetallic dimers **1.82** – **1.84**.[104]

Several other Zn homobimetallic dimers have been synthesised in the years following the initial report by Carmona. In 2007 Tsai *et al*. attempted to prepare a Zn–Zn bonded complex in which the metal-metal bond lay perpendicular to the principal axis of the molecule. Reduction of the dinuclear complex $Zn_2\{\mu\text{-}Me_2Si(NDipp)_2\}_2$ with KC_8

instead gave $K_2[Zn_2\{Me_2Si(NDipp)_2\}_2]$ (**1.85**), where the newly formed Zn–Zn bond (2.3695(17) Å) adopts a co-axial orientation with each Zn atom ligated by one bidentate ligand (Scheme 1.18).[107] $[K(2.2.2\text{-crypt})]_2[Zn_2\{Me_2Si(NDipp)_2\}_2]$ (**1.86**) was obtained by carrying out the reduction in the presence of 2.2.2-crypt. The compound possessed a slightly shorter Zn–Zn bond of 2.3634(11) Å.

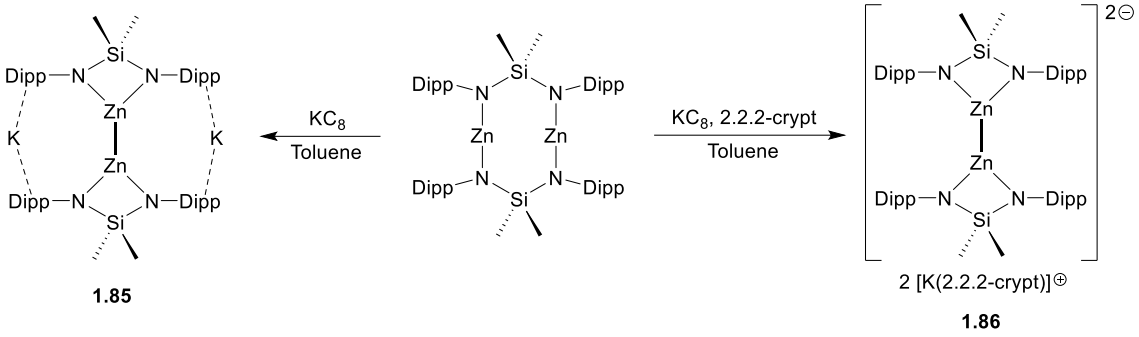

1.85 **1.86**

Scheme 1.18 Synthesis of two Zn–Zn bonded species from a dinuclear Zn complex.[107]

In 2012, Stasch *et al*. reported the synthesis of $[Zn\{Ph_2P(NDipp)_2\}]_2$ (**1.87**, Equation 1.31) *via* the reduction of $\{Ph_2P(NDipp)_2\}Zn(\mu\text{-}Br)_2Zn\{Ph_2P(NDipp)_2\}_2$ with the Mg(I) complex **1.13**[108] Single crystals were obtained from recrystallisation from benzene or hexane. X-ray structural analysis revealed Zn–Zn bond lengths of 2.3132(9) and 2.3147(6) Å, respectively.

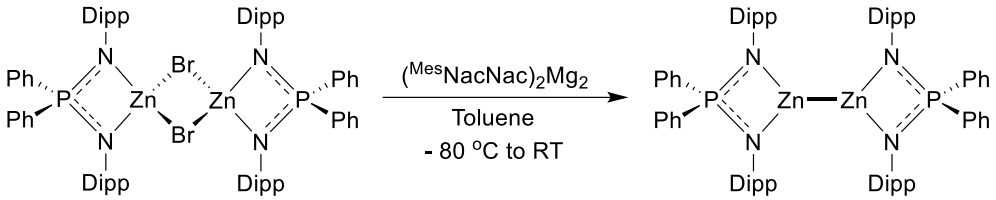

1.87

Equation 1.31[108]

In 2007, Fedushkin and co-workers reported the synthesis of a Zn–Zn bonded complex bound by the radical anionic Dipp-BIAN ligand.[109] $[Zn(Dipp\text{-}BIAN)]_2$ (**1.88**) was produced by the reaction of Dipp-BIAN with $ZnCl_2$ in the presence of Na metal (Equation 1.32). The X-ray structural analysis showed Zn–Zn bond distances of 2.3321(2) and 2.3386(6) Å for crystals of **1.88** grown from diethyl ether or toluene, respectively. Performing an ESR analysis of the diradical complex **1.88** allowed the authors to estimate the unpaired electron separation at 7.57 Å, a value in agreement

with the distance between the imino-carbon atoms (7.78 Å). This observation confirms that the Zn–Zn bond is retained in solution.

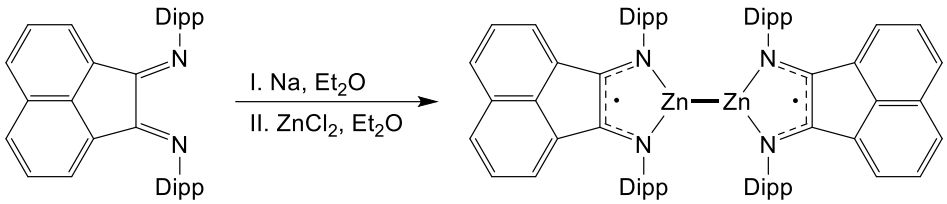

1.88

Equation 1.32[109]

Several Zn–Zn homobimetallic complexes featuring α-diimine ligands have been reported by Wu *et al*. The first of these, reported in 2007, was $[Na(THF)_2]_2{\cdot}[^{Me}LZnZn^{Me}L]$ (**1.89**, ^{Me}L = {DippN(Me)C}$_2$) which is formed by the reduction of $^{Me}LZnCl_2$ with Na metal in THF.[110] X-ray crystal analysis shows a Zn–Zn bond distance of 2.3994(6) Å. Reduction of $^{Me}LZnCl_2$ with K in THF produces $[K(THF)_2]_2{\cdot}[^{Me}LZnZn^{Me}L]$ (**1.90**).[111] X-ray crystal analysis reveals crystals of **1.90** to be isomorphous with **1.89,** containing a Zn–Zn bond length of 2.3934(8) Å.

Wu *et al*. have since showed that the alkali metal countercations of the previous two compounds can be encapsulated within various crown ethers.[112] Treatment of **1.89** with 15-crown-5 gives $[^{Me}LZnZn^{Me}L][Na(15\text{-Crown-}5)(THF)_2]_2$ (**1.91**, Zn–Zn 2.4247(8) Å). Treatment of **1.90** with either 15-crown-5 or 18-crown-6 gives the complexes $[^{Me}LZnZn^{Me}L][K(15\text{-Crown-}5)_2]_2$ (**1.92**, Zn–Zn 2.4447(12) Å) and $[^{Me}LZnZn^{Me}L][K(18\text{-Crown-}6)(THF)_2]_2$ (**1.93**, Zn–Zn 2.4208(6) Å), respectively. Each Zn–Zn bond distance is slightly longer than that found in the parent compound, in the range 0.025 – 0.051 Å.

The initial approach adopted by Wu *et al*. for the synthesis of α-diimine supported Zn–Zn dimers involved the reaction of a pre-ligated zinc complex with an excess of alkali metal acting as the reducing agent. Accordingly, the complexes produced (*e.g*. **1.89** and **1.90**) were in a highly reduced state, featuring not only reduced Zn centres (from the point of view of the group oxidation state) but also doubly reduced (dianionic) ligands, with the corresponding alkali metals acting as countercations. Wu *et al*. found that when the reduced ligand was reacted directly with $ZnCl_2$, the neutral complex $^{Me}LZnZn^{Me}L$ (**1.94**) was produced.[113] This complex possessed a Zn–Zn distance of 2.3403(18) Å; the shortest for Zn–Zn bonded complexes featuring α-diimine ligands. Reaction of **1.94**

with Na or K afforded the highly reduced species **1.89** and **1.90**, as expected. The syntheses of all Zn–Zn bonded complexes stabilised by the α-diimine ligand ^{Me}L are presented in Scheme 1.19.

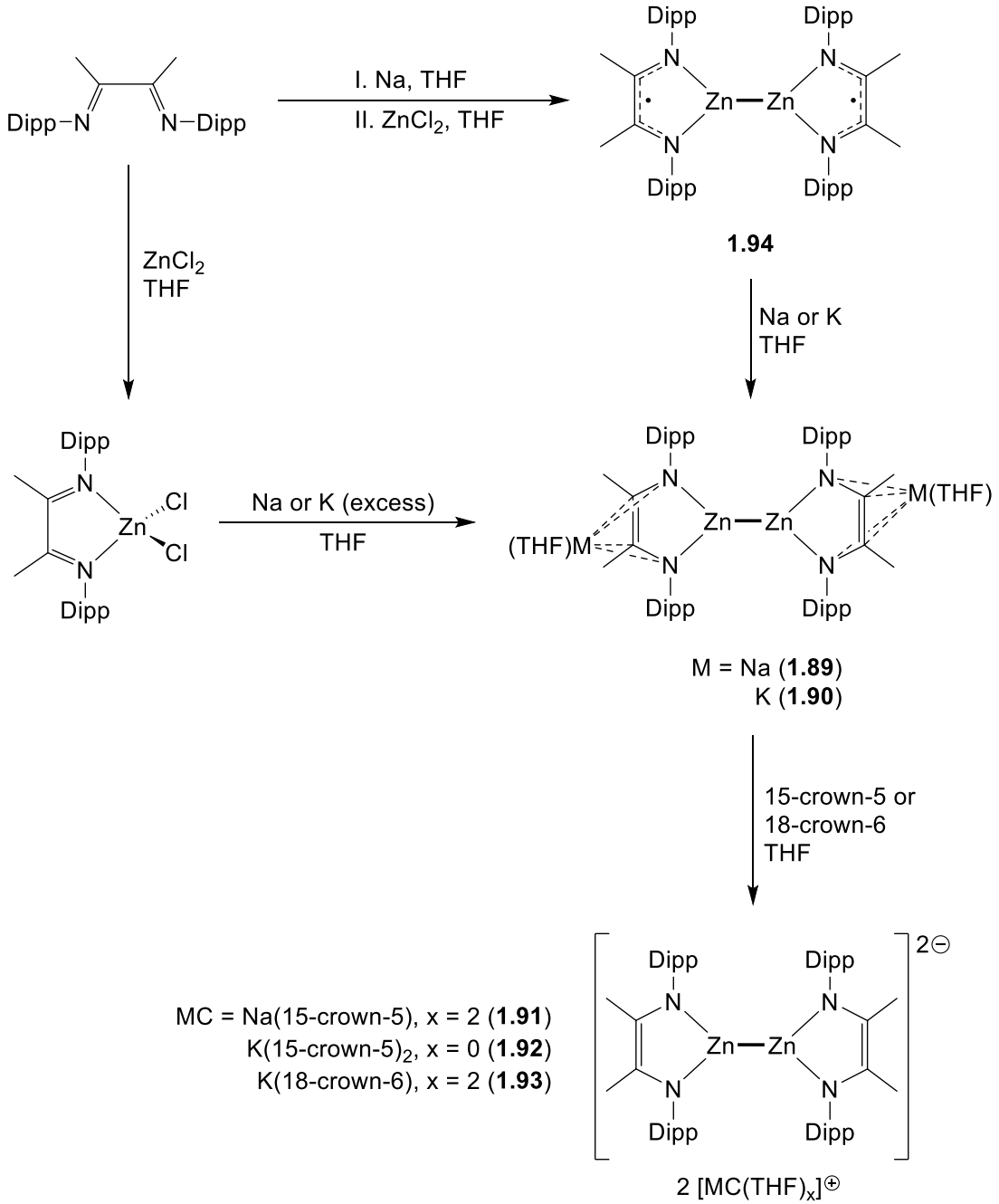

Scheme 1.19 Synthesis of various Zn–Zn bonded complexes supported by α-diimine ligands.[110–113]

During their investigations into the synthesis of Zn–Zn bonded complexes, Wu and co-workers also had limited success with a sterically reduced ligand, {DippN(H)C}$_2$ (^{H}L). Reduction of ^{H}LZnCl$_2$ with Na in diethyl ether gave [Na$_2$(Et$_2$O)$_2$][^{H}LZnZn^{H}L]·(Et$_2$O)

(**1.95**),[114] in a similar fashion to the synthesis of **1.89**. X-ray crystal analysis showed the Zn–Zn bond length to be 2.3673(6) Å; 0.03 Å shorter than that found in **1.89**. Reduction of $^{H}LZnCl_2$ with K did not lead to the isolation of the potassium analogue of **1.95** but instead gave several products including Zn(0). Recrystallisation of the residue from diethyl ether gave $[(^{H}L)Zn(\mu\text{-}^{H}L)Zn(^{H}L)K_2(Et_2O)_2]_n$ (**1.96**), a polymeric material which consists of two ^{H}LZn units, another ^{H}L unit acting as a bridge between the two Zn centres and two solvated potassium ions. Recrystallisation of the same residue from THF allowed isolation of $[K_4{}^{H}L_2(THF)_2]_n$ (**1.97**), which results from the fully reduced ^{H}L crystallising as a coordination polymer with the corresponding countercations. The authors suggest that **1.96**, **1.97** and Zn(0) are formed following the *in situ* formation and disproportionation of $[K_2(Et_2O)_2][^{H}LZnZn^{H}L]$, the potassium analogue of **1.95**, which is the expected product of the reduction of $^{H}LZnCl_2$ with K metal.

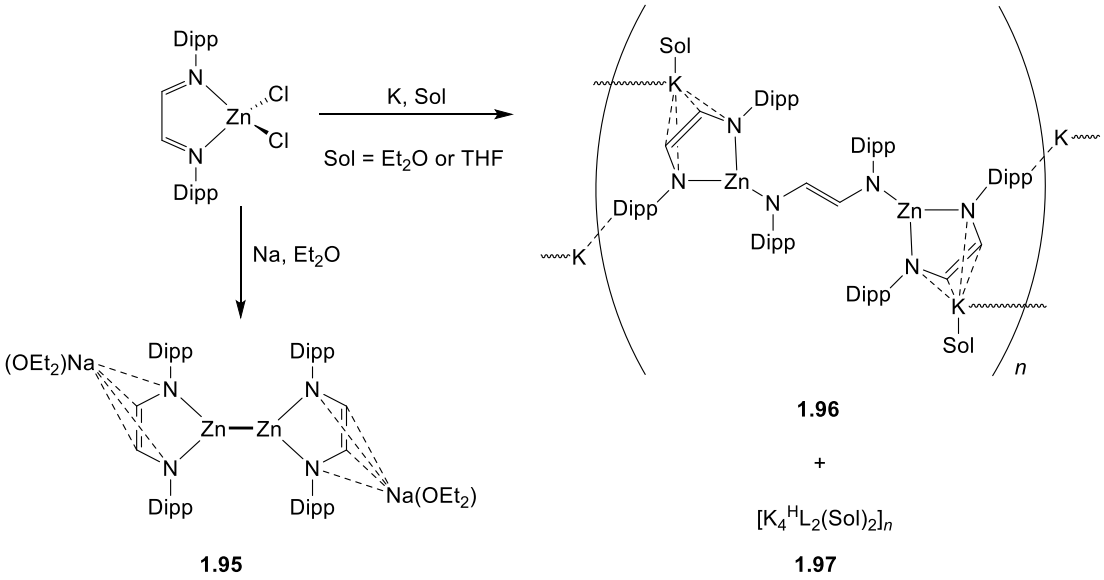

Scheme 1.20 Preparation of Zn–Zn bonded complex **1.95** and complexes **1.96** and **1.97** from the reduction of $^{H}LZnCl_2$ with Na and K, respectively.[114]

1.9 Summary and objectives

This Chapter has presented landmark transition metal homobimetallic complexes with multiple metal-metal bonds. Mg–Mg bonded complexes were introduced and the recent developments in their chemistry was detailed. The few examples of Ae–TM bonded complexes were presented which demonstrate the potential for expansion in this limited (albeit expanding) field of research.

Similarities might be expected between Ae–TM bonded complexes and polar "early-late" TM–TM bonded complexes. The latter are known for unusual cooperative reactivity between the metal centres arising from the polarity of the M–M' bond.[2,3] Given the sparse reports of Ae–TM bonded compounds in the literature it is currently difficult to ascertain whether the concept of cooperative reactivity extends to these compounds. The work detailed in this Thesis therefore seeks to expand the number of compounds with Ae–TM bonds and to explore their reactivity with simple heterocumulene substrates.

Also presented are examples in the field of unusual Gp12–M bonding. Although Gp12–TM bonds are prevalent in the literature, the group 12 elements have recently been demonstrated to bond to s-block, p-block and even other group 12 elements forming complexes with unusual properties. Reports of heterometallic Gp12–Gp12 bonded compounds are still very recent.[7,10] These compounds present a unique opportunity to study the fundamental properties of M–M' bonds. Work in this Thesis therefore seeks to explore the synthesis and reactivity of these unusual compounds.

1.10 References

1. F. A. Cotton, C. A. Murillo, and R. A. Walton, *Multiple Bonds Between Metal Atoms*, Springer, Berlin, 3rd Edition, 2005.
2. S. T. Liddle, Ed., *Molecular Metal–Metal Bonds. Compounds, Synthesis, Properties*, Wiley-VCH, Weinheim, 2015.
3. L. H. Gade, *Angew. Chem. Int. Ed.*, 2000, **39**, 2658–2678.
4. D. A. Fletcher, R. F. McMeeking, and D. Parkin, *J. Chem. Inf. Comput. Sci.*, 1996, **36**, 746–749.
5. I. Resa, E. Carmona, E. Gutierrez-Puebla, and A. Monge, *Science*, 2004, **305**, 1136–1138.
6. S. P. Green, C. Jones, and A. Stasch, *Science*, 2007, **318**, 1754–1757.
7. M. P. Blake, N. Kaltsoyannis, and P. Mountford, *Chem. Commun.*, 2015, **51**, 5743–5746.
8. S. Schulz, D. Schuchmann, U. Westphal, and M. Bolte, *Organometallics*, 2009, **28**, 1590–1592.

9. T. Bollermann, C. Gemel, and R. A. Fischer, *Coord. Chem. Rev.*, 2012, **256**, 537–555.

10. J. Hicks, E. J. Underhill, C. E. Kefalidis, L. Maron, and C. Jones, *Angew. Chem. Int. Ed.*, 2015, **54**, 10000–10004.

11. R. Green, A. C. Walker, M. P. Blake, and P. Mountford, *Polyhedron*, 2016, **116**, 64–75.

12. F. A. Cotton and J. M. Troup, *J. Chem. Soc., Dalton Trans.*, 1974, 800.

13. J. C. Green, M. L. H. Green, and G. Parkin, *Chem. Commun.*, 2012, **48**, 11481.

14. B. Cordero, V. Gómez, A. E. Platero-Prats, M. Revés, J. Echeverría, E. Cremades, F. Barragán, and S. Alvarez, *Dalton Trans.*, 2008, 2832–2838.

15. P. Pyykkö and M. Atsumi, *Chem. Eur. J.*, 2009, **15**, 186–197.

16. C. R. Groom, I. J. Bruno, M. P. Lightfoot, and S. C. Ward, *Acta Cryst. B*, 2016, **72**, 171–179.

17. G. H. Stout and L. H. Jensen, *X-Ray Structure Determination: A Practical Guide*, John Wiley & Sons, New York, 2nd Edition, 1989.

18. F. A. Cotton, N. F. Curtis, C. B. Harris, B. F. G. Johnson, S. J. Lippard, J. T. Mague, W. R. Robinson, and J. S. Wood, *Science*, 1964, **145**, 1305–1307.

19. F. A. Cotton, N. F. Curtis, B. F. G. Johnson, W. R. Robinson, and W. R. Robinson, *Inorg. Chem.*, 1965, **4**, 326–330.

20. F. A. Cotton and C. B. Harris, *Inorg. Chem.*, 1965, **4**, 330–333.

21. F. A. Cotton, *Inorg. Chem.*, 1965, **4**, 334–336.

22. T. Nguyen, A. D. Sutton, M. Brynda, J. C. Fettinger, G. J. Long, and P. P. Power, *Science*, 2005, **310**, 844–847.

23. M. Brynda, L. Gagliardi, P.-O. Widmark, P. P. Power, and B. O. Roos, *Angew. Chem. Int. Ed.*, 2006, **45**, 3804–3807.

24. G. La Macchia, L. Gagliardi, P. P. Power, and M. Brynda, *J. Am. Chem. Soc.*, 2008, **130**, 5104–5114.

25. T. Nguyen, W. A. Merrill, C. Ni, H. Lei, J. C. Fettinger, B. D. Ellis, G. J. Long, M. Brynda, and P. P. Power, *Angew. Chem. Int. Ed.*, 2008, **47**, 9115–9117.

26. K. A. Kreisel, G. P. A. Yap, O. Dmitrenko, C. R. Landis, and K. H. Theopold, *J. Am. Chem. Soc.*, 2007, **129**, 14162–14163.

27. Y.-C. Tsai, C.-W. Hsu, J.-S. K. Yu, G.-H. Lee, Y. Wang, and T.-S. Kuo, *Angew. Chem. Int. Ed.*, 2008, **47**, 7250–7253.

28. C.-W. Hsu, J.-S. K. Yu, C.-H. Yen, G.-H. Lee, Y. Wang, and Y.-C. Tsai, *Angew. Chem. Int. Ed.*, 2008, **47**, 9933–9936.

29. A. Noor, T. Bauer, T. K. Todorova, B. Weber, L. Gagliardi, and R. Kempe, *Chem. Eur. J.*, 2013, **19**, 9825–9832.

30. S. Dagorne, I. A. Guzei, M. P. Coles, and R. F. Jordan, *J. Am. Chem. Soc.*, 2000, **122**, 274–289.

31. M. P. Coles, D. C. Swenson, R. F. Jordan, and V. G. Young, *Organometallics*, 1997, **16**, 5183–5194.

32. F. T. Edelmann, *Chem. Soc. Rev.*, 2009, **38**, 2253–68.

33. Y.-C. Tsai, H.-Z. Chen, C.-C. Chang, J.-S. K. Yu, G.-H. Lee, Y. Wang, and T.-S. Kuo, *J. Am. Chem. Soc.*, 2009, **131**, 12534–12535.

34. S. J. Bonyhady, C. Jones, S. Nembenna, A. Stasch, A. J. Edwards, and G. J. McIntyre, *Chem. Eur. J.*, 2010, **16**, 938–955.

35. A. J. Boutland, D. Dange, A. Stasch, L. Maron, and C. Jones, *Angew. Chem. Int. Ed.*, 2016, **55**, 9239–9243.

36. T. J. Hadlington, B. Schwarze, E. I. Izgorodina, and C. Jones, *Chem. Commun.*, 2015, **51**, 6854–6857.

37. A. Stasch and C. Jones, *Dalton Trans.*, 2011, **40**, 5659.

38. A. Sidiropoulos, C. Jones, A. Stasch, S. Klein, and G. Frenking, *Angew. Chem. Int. Ed.*, 2009, **48**, 9701–9704.

39. H. Felkin, P. J. Knowles, B. Meunier, A. Mitschler, L. Ricard, and R. Weiss, *J. Chem. Soc., Chem. Commun.*, 1974, 44.

40. H. R. Rogers, C. L. Hill, Y. Fujiwara, R. J. Rogers, H. L. Mitchell, and G. M. Whitesides, *J. Am. Chem. Soc.*, 1980, **102**, 217–226.

41. K. Jonas, G. Koepe, and C. Krüger, *Angew. Chem. Int. Ed.*, 1986, **25**, 923–925.

42. M. L. H. Green, G. A. Moser, I. Packer, F. Petit, R. A. Forder, and K. Prout, *J. Chem. Soc., Chem. Commun.*, 1974, 839b.

43. K. Prout and R. A. Forder, *Acta Cryst. B*, 1975, 31, 852–856.

44. M. L. H. Green, T. Luong-Thi, G. A. Moser, I. Packer, F. Petit, D. M. Roe, F. Pettit, and D. M. Roe, *J. Chem. Soc., Dalton Trans.*, 1976, 1988–1992.

45. S. G. Davies, M. L. H. Green, K. Prout, A. Coda, and V. Tazzoli, *J. Chem. Soc., Chem. Commun.*, 1977, 135.

46. S. G. Davies and M. L. H. Green, *J. Chem. Soc., Dalton Trans.*, 1978, 1510.

47. J. T. Golden, T. H. Peterson, P. L. Holland, R. G. Bergman, and R. A. Andersen, *J. Am. Chem. Soc.*, 1998, **120**, 223–224.

48. H. Braunschweig, K. Gruss, and K. Radacki, *Angew. Chem. Int. Ed.*, 2009, **48**, 4239–4241.

49. J. Hicks, C. E. Hoyer, B. Moubaraki, G. L. Manni, E. Carter, D. M. Murphy, K. S. Murray, L. Gagliardi, and C. Jones, *J. Am. Chem. Soc.*, 2014, **136**, 5283–5286.

50. C. Bakewell, B. J. Ward, A. J. P. White, and M. R. Crimmin, *Chem. Sci.*, 2018, **9**, 2348–2356.

51. O. Ekkert, A. J. P. White, H. Toms, and M. R. Crimmin, *Chem. Sci.*, 2015, **6**, 5617–5622.

52. C. Birchall, G. J. Moxey, J. McMaster, A. J. Blake, W. Lewis, and D. L. Kays, *Inorg. Chim. Acta*, 2017, **458**, 97–100.

53. S. T. Liddle, D. P. Mills, and A. J. Wooles, *Chem. Soc. Rev.*, 2011, **40**, 2164.

54. P. Wei and D. W. Stephan, *Organometallics*, 2003, **22**, 601–604.

55. G. B. McVicker, *Inorg. Chem.*, 1975, **14**, 2087–2092.

56. M. P. Blake, N. Kaltsoyannis, and P. Mountford, *J. Am. Chem. Soc.*, 2015, **137**, 12352–12368.

57. M. P. Blake, N. Kaltsoyannis, and P. Mountford, *J. Am. Chem. Soc.*, 2011, **133**, 15358–61.

58. R. D. Shannon, *Acta Cryst. A*, 1976, 32, 751–767.

59. M. P. Blake, Alkaline Earth- and Rare Earth-Transition Metal Complexes, D.

Phil. Thesis, University of Oxford, 2013.

60. X. Wu and S. Harder, in *Molecular Metal-Metal Bonds: Compounds Synthesis, Properties*, ed. S. T. Liddle, Wiley-VCH Verlag GmbH & Co. KGaA, Weinheim, Germany, 1st Edition, 2015.

61. J. Weßing, C. Göbel, B. Weber, C. Gemel, and R. A. Fischer, *Inorg. Chem.*, 2017, **56**, 3517–3525.

62. C. Jones, R. P. Rose, and A. Stasch, *Dalton Trans.*, 2007, 2997–2999.

63. O. Bonello, C. Jones, A. Stasch, and W. D. Woodul, *Organometallics*, 2010, **29**, 4914–4922.

64. A. Kempter, C. Gemel, T. Cadenbach, and R. A. Fischer, *Inorg. Chem.*, 2007, **46**, 9481–9487.

65. G. Prabusankar, C. Gemel, M. Winter, R. W. Seidel, and R. A. Fischer, *Chem. Eur. J.*, 2010, **16**, 6041–6047.

66. I. L. Fedushkin, A. N. Lukoyanov, S. Y. Ketkov, M. Hummert, and H. Schumann, *Chem. Eur. J.*, 2007, **13**, 7050–7056.

67. J. T. B. H. Jastrzebski, H. A. J. Sypkens, F. J. A. des Tombe, P. A. van der Schaaf, J. Boersma, G. van Koten, A. L. Spek, and A. J. M. Duisenberg, *J. Organomet. Chem.*, 1990, **396**, 25–31.

68. M. Lutz, B. Findeis, M. Haukka, R. Graff, T. A. Pakkanen, and L. H. Gade, *Chem. Eur. J.*, 2002, **8**, 3269.

69. A. Bayler, A. Schier, G. A. Bowmaker, and H. Schmidbaur, *J. Am. Chem. Soc.*, 1996, **118**, 7006–7007.

70. J. D. Erickson, R. D. Riparetti, J. C. Fettinger, and P. P. Power, *Organometallics*, 2016, **35**, 2124–2128.

71. J. M. Goicoechea and S. C. Sevov, *Organometallics*, 2006, **25**, 4530–4536.

72. B. Zhou, M. S. Denning, C. Jones, and J. M. Goicoechea, *Dalton Trans.*, 2009, 1571.

73. R. Ababei, J. Heine, M. Hołyńska, G. Thiele, B. Weinert, X. Xie, F. Weigend, and S. Dehnen, *Chem. Commun.*, 2012, **48**, 11295.

74. R. S. Dickson, K. D. Heazle, G. N. Pain, G. B. Deacon, B. O. West, G. D. Fallon, R. S. Rowe, P. W. Leech, and M. Faith, *J. Organomet. Chem.*, 1993, **449**, 131–139.

75. F. Thomas, S. Schulz, and M. Nieger, *Angew. Chem. Int. Ed.*, 2005, **44**, 5668–5670.

76. F. Lips, I. Schellenberg, R. Pöttgen, and S. Dehnen, *Chem. Eur. J.*, 2009, **15**, 12968–12973.

77. T.-P. Lin, C. R. Wade, L. M. Pérez, and F. P. Gabbaï, *Angew. Chem. Int. Ed.*, 2010, **49**, 6357–6360.

78. E. Dorm, *J. Chem. Soc. D: Chem. Commun.*, 1971, **0**, 466.

79. E. Dorm, B. Lindh, P. Fischer, E. Stoll, G. Eriksson, R. Blinc, S. Paušak, L. Ehrenberg, and J. Dumanović, *Acta Chem. Scand.*, 1967, **21**, 1661–1662.

80. R. B. English, D. Röhm, and C. J. H. Schutte, *Acta Cryst. C*, 1985, **41**, 997–998.

81. M. Weil and R. Glaum, *Z. Anorg. Allg. Chem.*, 1999, **625**, 1752–1761.

82. M. Weil, *Z. Naturforsch.*, 2000, **55b**, 699–706.

83. A. Stiewe, E. Kemnitz, and S. Troyanov, *Z. Anorg. Allg. Chem.*, 1999, **625**, 329–335.

84. M. Sikirica and D. Grdenić, *Acta Cryst. B*, 1974, **30**.

85. K. Brodersen and J. Hofmann, *Z. Anorg. Allg. Chem.*, 1992, **609**, 29–34.

86. M. S. Wickleder, *Z. Anorg. Allg. Chem.*, 2002, **628**, 1848.

87. T. Curtius, *Chem. Ber.*, 1890, **23**, 3023–3033.

88. D. Seybold and K. Dehnicke, *Z. Anorg. Allg. Chem.*, 1968, **361**, 277–283.

89. P. Nockemann, U. Cremer, U. Ruschewitz, and G. Meyer, *Z. Anorg. Allg. Chem.*, 2003, **629**, 2079–2082.

90. H. Lund, O. Oeckler, T. Schröder, A. Schulz, and A. Villinger, *Angew. Chem. Int. Ed.*, 2013, **52**, 10900–10904.

91. T. J. Mormann and W. Jeitschko, *Inorg. Chem.*, 2000, **39**, 4219–4223.

92. M. S. Schriewer-Pöttgen and W. Jeitschko, *Z. Anorg. Allg. Chem.*, 1994, **620**,

1855–1860.

93. F. Cecconi, C. A. Ghilardi, S. Midollini, and S. Moneti, *J. Chem. Soc., Dalton Trans.*, 1983, 349–352.

94. J. D. Corbett and R. K. McMullan, *J. Am. Chem. Soc.*, 1956, **78**, 2906–2907.

95. R. Faggiani, R. J. Gillespie, and J. E. Vekris, *J. Chem. Soc., Chem. Commun.*, 1986, 517.

96. T. Staffel and G. Meyer, *Z. Anorg. Allg. Chem.*, 1987, **548**, 45–54.

97. D. H. Kerridge and S. A. Tariq, *J. Chem. Soc. A: Inorganic, Physical, Theoretical*, 1967, 1122.

98. D. L. Reger, S. S. Mason, and A. L. Rheingold, *J. Am. Chem. Soc.*, 1993, **115**, 10406–10407.

99. D. Bravo-Zhivotovskii, M. Yuzefovich, M. Bendikov, K. Klinkhammer, and Y. Apeloig, *Angew. Chem. Int. Ed.*, 1999, **38**, 1100–1102.

100. A. Grirrane, I. Resa, A. Rodriguez, E. Carmona, E. Alvarez, E. Gutierrez-Puebla, A. Monge, A. Galindo, D. del Río, and R. A. Andersen, *J. Am. Chem. Soc.*, 2007, **129**, 693–703.

101. D. del Río, A. Galindo, I. Resa, and E. Carmona, *Angew. Chem. Int. Ed.*, 2005, **44**, 1244–1247.

102. T. Li, S. Schulz, and P. W. Roesky, *Chem. Soc. Rev.*, 2012, **41**, 3759.

103. Y. Wang, B. Quillian, P. Wei, H. Wang, X. Yang, Y. Xie, R. B. King, P. v. R. Schleyer, H. F. Schaefer, and G. H. Robinson, *J. Am. Chem. Soc.*, 2005, **127**, 11944–11945.

104. Z. Zhu, M. Brynda, R. J. Wright, R. C. Fischer, W. A. Merrill, E. Rivard, R. Wolf, J. C. Fettinger, M. M. Olmstead, and P. P. Power, *J. Am. Chem. Soc.*, 2007, **129**, 10847–10857.

105. Z. Zhu, R. J. Wright, M. M. Olmstead, E. Rivard, M. Brynda, and P. P. Power, *Angew. Chem. Int. Ed.*, 2006, **45**, 5807–5810.

106. Z. Zhu, R. C. Fischer, J. C. Fettinger, E. Rivard, M. Brynda, and P. P. Power, *J. Am. Chem. Soc.*, 2006, **128**, 15068–15069.

107. Y.-C. Tsai, D.-Y. Lu, Y.-M. Lin, J.-K. Hwang, and J.-S. K. Yu, *Chem. Commun.*, 2007, 4125.

108. A. Stasch, *Chem. Eur. J.*, 2012, **18**, 15105–15112.

109. I. L. Fedushkin, A. A. Skatova, S. Y. Ketkov, O. V. Eremenko, A. V. Piskunov, and G. K. Fukin, *Angew. Chem. Int. Ed.*, 2007, **46**, 4302–4305.

110. X.-J. Yang, J. Yu, Y. Liu, Y. Xie, H. F. Schaefer, Y. Liang, B. Wu, J. M. Basset, S. Cadars, A. Lesage, C. Coperet, and L. Emsley, *Chem. Commun.*, 2007, **37**, 2363–2365.

111. J. Yu, X.-J. Yang, Y. Liu, Z. Pu, Q.-S. Li, Y. Xie, H. F. Schaefer, and B. Wu, *Organometallics*, 2008, **27**, 5800–5805.

112. J. Gao, S. Li, Y. Zhao, B. Wu, and X.-J. Yang, *Organometallics*, 2012, **31**, 2978–2985.

113. Y. Liu, S. Li, X.-J. Yang, P. Yang, J. Gao, Y. Xia, and B. Wu, *Organometallics*, 2009, **28**, 5270–5272.

114. P. Yang, X.-J. Yang, J. Yu, Y. Liu, C. Zhang, Y.-H. Deng, and B. Wu, *Dalton Trans.*, 2009, **42**, 5773.

Chapter Two

Synthesis and study of amidinate and guanidinate supported Ae–TM bonded complexes

2.1 Overview

This Chapter describes the synthesis of amidinate ligated Mg–TM bonded complexes, where TM = Fe, Ru or Co. The synthesis of a guanidinate ligated Mg–Fe bonded complex is also described. Where available, the structures of these complexes are authenticated by single crystal X-ray diffraction data, supported with IR studies. The solution phase behaviour of selected complexes is interrogated by diffusion NMR studies.

2.2 Introduction

Many complexes which feature bonding between the alkaline earth and transition metal elements have been discussed in Chapter One. The role of the transition metal anion will be discussed with regards to its role in metal-metal bonding. Several heterobimetallic complexes will be discussed which provide the precedent for the so-called 'privileged anions' in metal-metal bonding. Complexes synthesised in the Mountford group which provide the direct precedent for this research will be then discussed in detail.

2.2.1 Privileged anions in metal-metal bonding

Although the field of Ae–TM bonding is rather limited, there is a relative abundance of structurally authenticated compounds which feature bonds between the TM elements and either main group, lanthanide or actinide elements.[1,2] In addition, there are many examples of polar 'early-late' TM–TM bonded complexes. The study of these compounds reveals several TM anions which feature frequently in such systems and which therefore are good candidates for the synthesis of Ae–TM complexes.[3]

One of the most prevalent transition metal anions in the field of metal-metal bonding is the $[CpFe(CO)_2]^-$ (Fp^-) anion. Use of Fp^- has facilitated the formation of bonds between Fe and many metal elements. Examples include Mg,[4–7] Al,[8] Ca,[9] Ga,[8,10,11] Ge,[12,13] In,[8,14] Sn,[15,16] Sb,[17] Nd,[18] Tl[19] and Bi.[20,21]

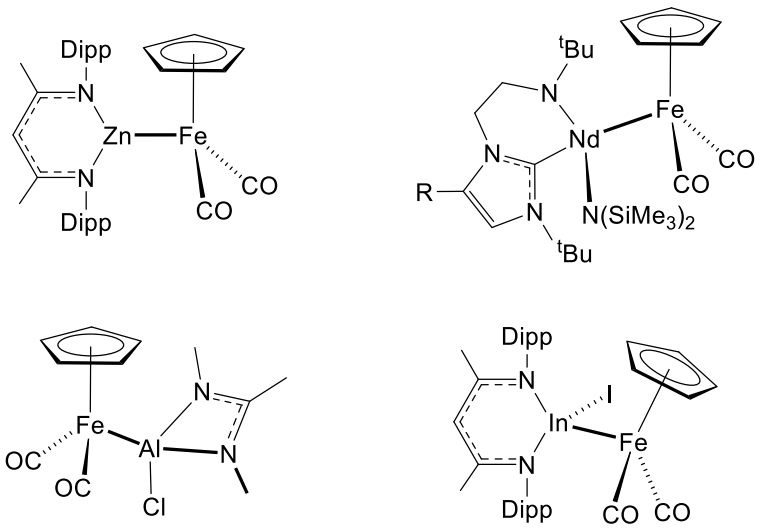

Figure 2.1 Selected examples of M–Fe bonded complexes with the Fp^- anion.[8,14,18,22]

Fp_2 is commercially available at low cost and provides a convenient starting point from which to access Fp^-. As detailed in Chapter One, metal-metal bonded complexes can be accessed directly from Fp_2 *via* reductive cleavage of the Fe–Fe bond. The reaction of Fp_2 with an Ae (or Ln) amalgam gives M–Fe bonded complexes *via* a reductive insertion process.[5,9] More commonly, Fp_2 is reduced with a range of alkali metals to give MFp (where M is typically Na or K). This reduction is commonly achieved by reaction with an alkali metal amalgam,[23,24] although it has been reported that this approach may result in contamination of the product with $HgFp_2$.[25,26] The reduction may also be achieved by reaction of Fp_2 with KH,[27] $NaK_{2.8}$ alloy,[28] K-benzophenone,[29] KC_8,[30] or the direct reaction of the alkali metal with Fp_2 *via* sonication.[31,32] The very poor solubility of MFp in non-donor solvents means that all of the above reactions are performed in THF.

Although less commonly reported, several complexes have been synthesised which feature the $[CpRu(CO)_2]^-$ (Rp^-) anion with bonds between Ru and other metal elements. Examples include Al,[33] In,[34] Sn,[35,36] Sb,[37] Tl,[38] Yb,[39] Lu,[40] Th,[41] and U.[42] The major disadvantage of the Rp^- anion is the high cost associated with the use of ruthenium.

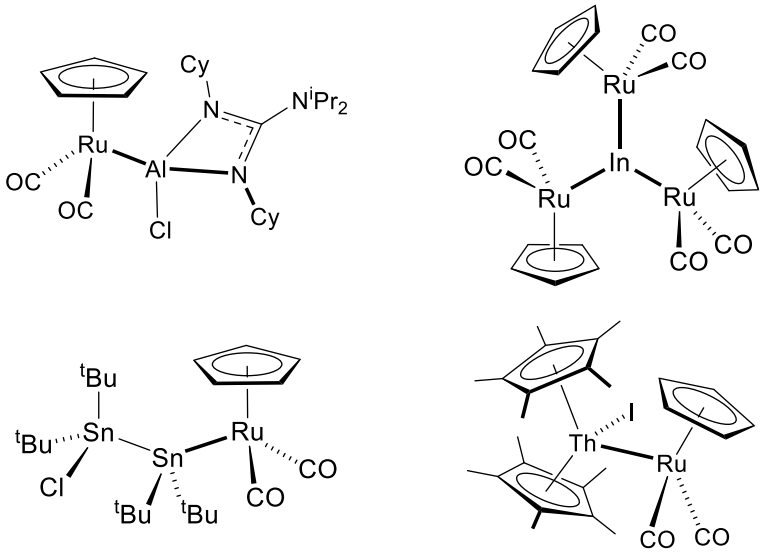

Figure 2.2 Selected examples of M–Ru bonded complexes with the Rp^- anion.[33,34,36,41]

Ru is the heavier Group 8 analogue of Fe and hence the reactive properties of the Rp^- anion are very similar to its Fp^- counterpart. The more diffuse nature of the Ru 4*d* orbitals *vs* Fe 3*d* orbitals make Rp^- slightly less nucleophilic than Fp^-, although it is expected to form stronger metal-metal bonds due to greater orbital overlap. An illustrative example is Liddle's synthesis of ($Tren^{TMS}$)URp (**2.1**, $Tren^{TMS}$ = $N(CH_2CH_2NTMS)_3$), ($Tren^{TBDMS}$)URp (**2.2**), Ts^{Tol}URp(THF) (**2.3**) and Ts^{Xy}URp(THF) (**2.4**), which were prepared from the reaction of the uranium halides with KRp.[42] The attempted syntheses of the Fp analogues *via* the same synthetic rationale were unsuccessful, giving Fp_2 as the only identifiable decomposition product. The authors reason that either the Fp^- ion is too powerful a reducing agent or that the highly contracted nature of the Fe 3*d* valence orbitals disfavours U–Fe bond formation.

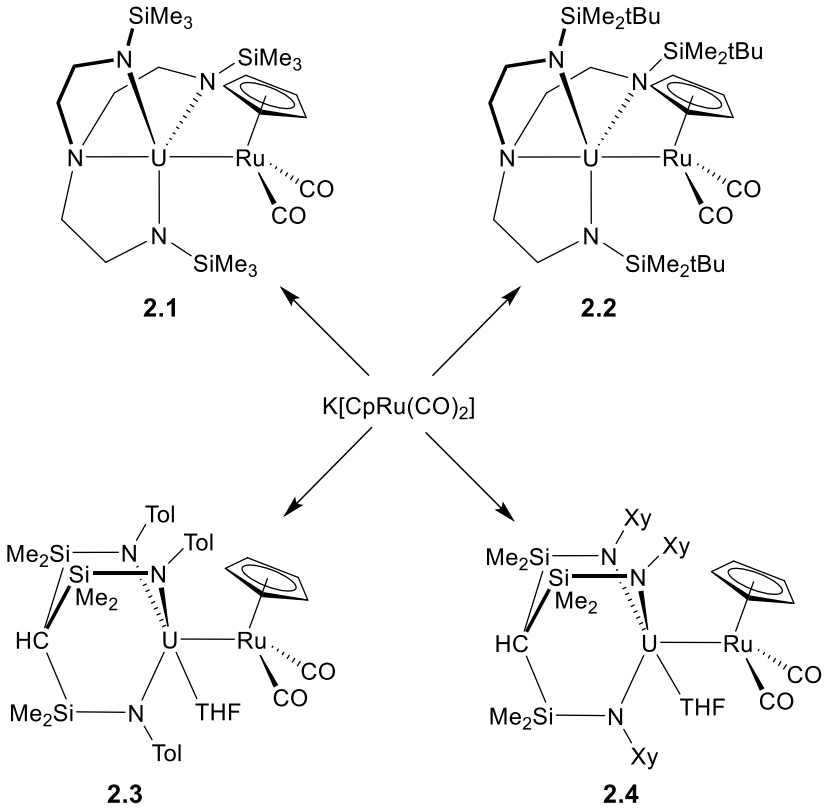

Scheme 2.1 Synthesis of various U–Ru bonded complexes *via* reaction of KRp with the corresponding uranium halide precursors in THF.[42]

Another commonly used set of anions employed in metal-metal bonding studies are species of the form $[Co(CO)_3(L)]^-$ (L = CO, PPh_3, $PTol_3$, PCy_3). Variation of the L group allows for modification of the physical or electronic properties of the anion and therefore of the final complex *e.g.* substitution of CO for a phosphine will result in a product with a greater solubility in organic solvents, while the substitution of an aryl phosphine for an alkyl phosphine will give a more nucleophilic anion. Gade and Jensen have made use of these anions in their studies of early-late TM–TM bonded complexes.[43] Reaction of $MeSi\{SiMe_2N(p\text{-}Tol)\}_3MX$ (M = Ti, X = Br; M = Zr, X = Cl) with $Na[Co(CO)_3(L)]$ (L = CO, PPh_3, $PTol_3$) in toluene gave $MeSi\{SiMe_2N(p\text{-}Tol)\}_3M\{Co(CO)_3(L)\}$ (M = Ti, L = CO (**2.5**), PPh_3 (**2.6**), $PTol_3$ (**2.7**); M = Zr, L = CO (**2.8**), PPh_3 (**2.9**), $PTol_3$ (**2.10**), Scheme 2.2). The solid state structures of **2.5** and **2.7** revealed unsupported metal-metal bonds with Ti–Co distances of 2.5542(10) and 2.471(4) Å, respectively. The solid state structures of **2.8** and **2.9** also revealed unsupported metal-metal bonds with Zr–Co distances of 2.7051(11) and 2.6175(14) Å, respectively. In both cases the substitution of a CO ligand for an arylphosphine ligand results in a shorter M–Co bond. This is a predictable consequence of the stronger

electron donating properties of the phosphine ligand increasing the nucleophilicity of the Co centre. This results in a stronger attraction between the metal centres and therefore a shorter M–M' bond.

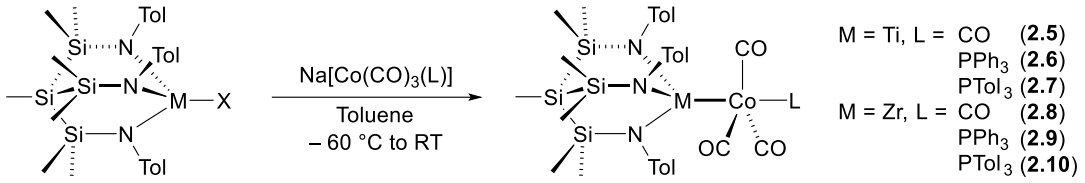

Scheme 2.2 Synthesis of Ti–Co and Zr–Co bonded complexes.[43]

The cobalt anion can also be found in actinide-TM bonded complexes. In 2011, Liddle *et al*. reported the reduction of (MeSi{SiMe$_2$N(Xyl)}$_3$UCl(THF) (**2.11**) with KC_8 in toluene to give (MeSi{SiMe$_2$N(Xyl)}$_3$U)$_2$(μ-η^6:η^6-C$_6$H$_5$Me) (**2.12**, Scheme 2.3);[44] a U^{II} species obtained from the reduction of the U^{III} precursor. The reaction of **2.12** with [Co(CO)$_3$(PPh$_3$)]$_2$ gave (MeSi{SiMe$_2$N(Xyl)}$_3$U{Co(CO)$_3$(PPh$_3$)} (**2.13**, Scheme 2.3), with a U–Co bond length of 2.9450(9) Å. Interestingly, the salt metathesis reaction between **2.11** and Na[Co(CO)$_3$(PPh$_3$)] was unsuccessful in a variety of solvents. This contrasts with **2.5 - 2.10**, which were all prepared *via* facile salt metathesis reactions[43] (*vide supra*).

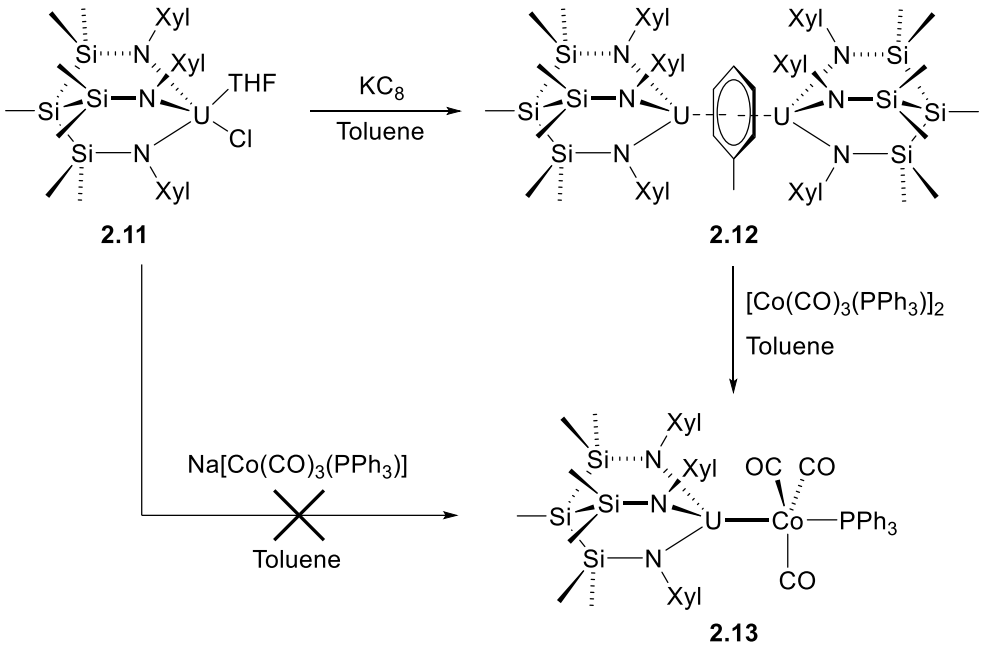

Scheme 2.3 Synthesis of a reduced diuranium(II) compound (**2.12**) and its reductive cleavage of a cobalt dimer to give a U–Co bonded compound (**2.13**).[44]

In addition to the cases discussed above, the use of $[Co(CO)_3(L)]^-$ anions has enabled the synthesis of many structurally authenticated compounds which feature bonds between Co and main group metals. Examples include Mg,[5,6] Ca,[5] Ga,[45] In,[45,46] Tl,[19,47] Ge,[48] Sn,[49–51] Pb,[51] Sb[52,53] and Bi.[54,55]

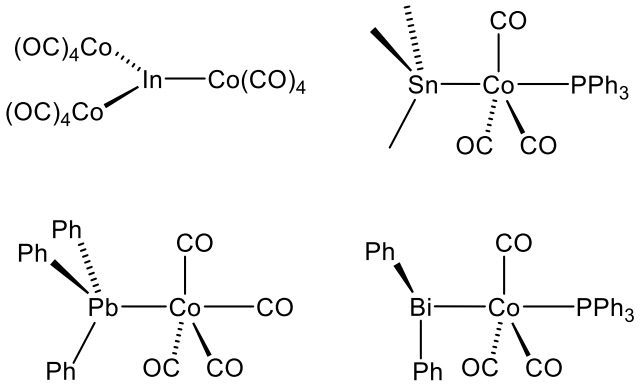

Figure 2.3 Selected examples of M–Co bonded complexes with the $[Co(CO)_3(L)]^-$ anion.[46,50,51,54]

Brammer *et al*. have investigated the extent to which interaction of the $[Co(CO)_3(L)]^-$ anion with cationic species affects the geometry at the Co centre.[56] The hydrogen bonded complexes [(DABCO)H][$Co(CO)_3(L)$] (L = CO (**2.14**) or PPh_3 (**2.15**), Figure 2.4, DABCO = 1,4-diazabicyclooctane) were prepared and structurally authenticated. The Co···N distance in **2.15** was found to be substantially shorter (3.294(6) Å) than that found in **2.14** (3.437(3) Å). The geometry of the Co anion was also found to change considerably between the two complexes. The sum of the angles between the axial ligand and the equatorial ligands in **2.14** ($\Sigma(CO_{ax}–Co–CO)$) was found to be 323.2(3)° and 319.0(2)° (two crystallographically independent molecules in the asymmetric unit). The sum of analogous angles in **2.15** (Σ(P–Co–CO)) was found to be 307.0(3)°. The steric effects of introducing a phosphine ligand would serve to repel the CO ligands and increase the P–Co–CO angles. The fact that the L_{ax}–Co–CO angles actually decrease upon substitution of CO for PPh_3 suggests that the electronic effects of the phosphine ligand are the prevalent influence and serve to increase the nucleophilicity of the Co anion; increasing the strength of its interaction with the cation and bringing about the observed change in geometry.

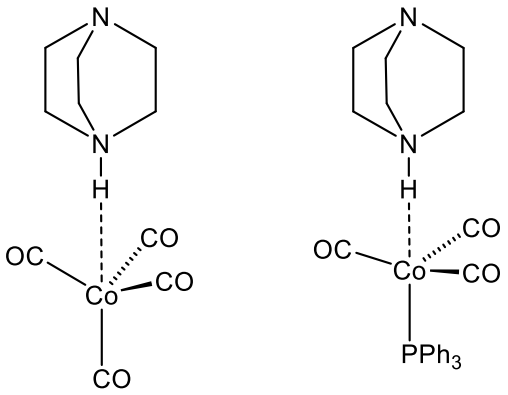

Figure 2.4 Hydrogen bonded complexes [(DABCO)H][$Co(CO)_4$] (**2.14**) and [(DABCO)H][$Co(CO)_3(PPh_3)$] (**2.15**).[56]

The work by Brammer *et al*. demonstrates that the strength of interaction of the $[Co(CO)_3(L)]^-$ with a cationic acceptor can significantly affect the geometry at the Co centre. The sum of angles between the axial ligand and the equatorial ligands (L_{ax}–Co–CO) represents a convenient way to measure this effect. A greater strength of interaction is likely to cause a decrease in this value as the structure of the anion deviates towards a trigonal bipyramidal geometry and away from the ideal tetrahedral geometry of the free anion (Figure 2.5). In the example above, a stronger interaction is observed in **2.15** between the cation and anion (quantified by a shorter Co···N distance) which results in a lesser Σ(L_{ax}–Co–CO) value (307.0(3)°) than that observed in **2.14** (323.2(3)°).

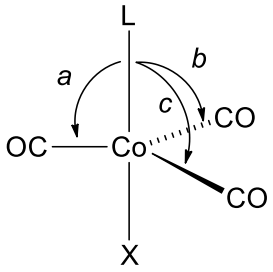

Figure 2.5 Variation of the sum of the L–Co–CO angles (*a*, *b* and *c*) Σ(L–Co–CO) with strength of interaction with a cationic centre (X). L = CO or a phosphine such as PPh_3.

All of the anions considered thus far have featured carbonyl ligands as a core structural component. From a historical perspective, carbonyl containing anions were rational choices for strongly nucleophilic metalates. The ability of carbonyl ligands to accept electron density from an electron-dense metal centre *via* back-donation make them an ideal choice to stabilise low oxidation states. However, the presence of carbonyl ligands

in these anions presents an unfortunate obstacle to metal-metal bonding. Many cationic metal complexes which may be of interest for metal-metal bonding studies (*e.g.* the alkaline earth and rare earth elements) are highly Lewis acidic, 'hard' acceptors. The potential bond between the cationic metal fragment and the relatively 'soft' anionic metal centre may be weaker than the bond between the cationic metal and the much harder oxygen donor of the carbonyl ligand. In this case an isocarbonyl bond (M(μ-OC)M') will form, in which the metals are bridged by a carbonyl group and no direct metal-metal bond is present. Kempe has dubbed this effect the "isocarbonyl problem".[1]

In the years before crystallisation and X-ray diffraction analysis were routine for structural elucidation, some compounds were erroneously classified as containing metal-metal bonds. As discussed in Chapter One, McVicker published the synthesis of **1.40** which was proposed to contain a direct metal-metal bond, based primarily on IR studies in the solid and solution phases (benzene and THF).[57] Blake and Mountford demonstrated that when **1.40** was crystallised from THF only the isocarbonyl bonded structure was obtained.[9] Crystallising **1.40** from a benzene solution, however, gave the dimeric complex **1.39** which contained direct Mg–Fe bonds in addition to isocarbonyl interactions.[5]

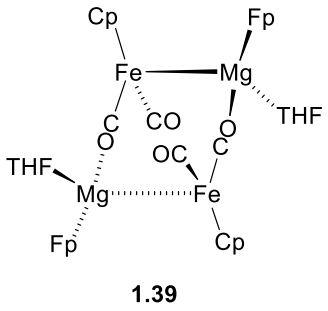

1.39

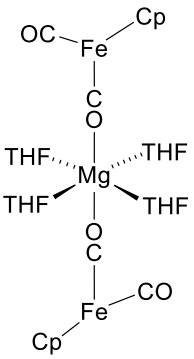

1.40

Figure 2.6 Solid state structures of $[MgFp_2(THF)_x]_y$ crystallised from benzene (**1.39**, $x = 1$, $y = 2$) and THF ((**1.40**, $x = 4$, $y = 1$).[5,9,57]

Other metal anions exist which do not possess carbonyl ligands. $[Cp_2Re]^-$, pioneered by the work of Kempe *et al.* for the synthesis of rare earth-transition metal bonds, has facilitated the formation of bonds between Re and several metal elements. Examples include Sn,[58] Y,[59] Bi,[21,60,61] La,[62,63] Sm,[62] Yb,[39,59] Lu,[62,63] and U.[64,65] Compounds which feature the Cp_2Re ligand tend to be prone to decomposition and C–H activation

processes.[62,66] An additional drawback of this anion is the expense associated with the use of rhenium. Indeed, the original preparation of Cp_2ReH (the precursor for the Cp_2Re^- anion), published by Wilkinson *et al*., only achieves a maximum yield of 40% based on the $ReCl_5$ starting material.[67]

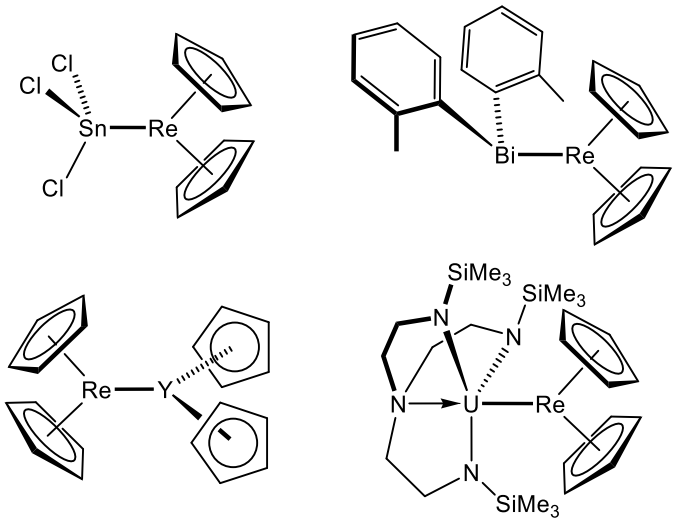

Figure 2.7 Selected examples of M–Re bonded complexes with the $[Cp_2Re]^-$ anion.[58–60,65]

2.2.2 β-diketiminate supported Ae–TM bonded complexes

As discussed in Chapter One, Mountford *et al*. have reported the synthesis of several Ae–TM complexes (in addition to analogous Ln–TM bonded complexes) from the reaction of transition metal dimers with the corresponding Ae or Ln amalgams.[5,9] The products of these reactions exhibited structural changes dependent on the donor properties of the solvent. For example, **1.40**, originally reported by McVicker, was shown to convert from its monomeric, isocarbonyl-bridged form to the dimeric species **1.39** when crystallised from a non-donor solvent. This structural dependence on solvent environment can be problematic during the pursuit of metal-metal bonding. Mountford and co-workers therefore sought to modify the coordination environment of the electropositive metal in order to preserve the molecular structure of the product in a wide range of solvents. The introduction of organic ligands was identified as a way to modify the stability of the metal-metal bond in the final product.

The reaction of (^{Dipp}NacNac)MgI(THF) with KFp in THF gave (^{Dipp}NacNac)MgFp(THF) (**2.16**, Equation 2.1).[4] A benzene solution of **2.16** afforded crystals suitable for X-ray diffraction. The solid state structure revealed a monomeric

complex with a Mg–Fe bond length of 2.6326(4) Å. The IR spectrum revealed two *ν*(CO) bands in Nujol (1926, 1857 cm^{-1}) and THF (1926, 1871 cm^{-1}) which are indicative of a single coordinated Fp^- anion with no isocarbonyl bonding. Compound **2.16** was indefinitely stable in THF, benzene and toluene solutions.

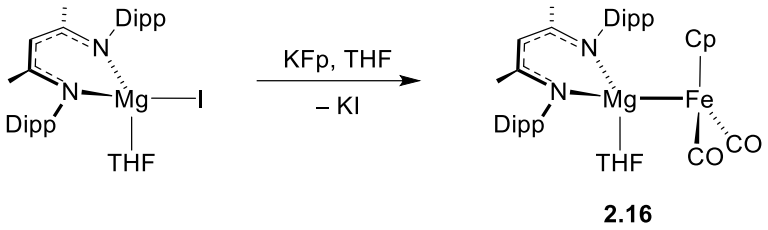

Equation 2.1[4]

Compound **2.16** was shown to undergo a 1:1 reaction with MeI, effecting a cleavage of the Mg–Fe bond to afford the precursor compound (^{Dipp}NacNac)MgI(THF) and MeFp.[4] Somewhat more interestingly **2.16** reacts quantitatively with TolNCNTol at RT to give (^{Dipp}NacNac)Mg{$(NTol)_2$CFp} (**2.17**),[4] which results from the insertion of the carbodiimide into the Mg–Fe bond. Compound **2.17** is the first example of an insertion of an unsaturated substrate into an Ae–TM bond.

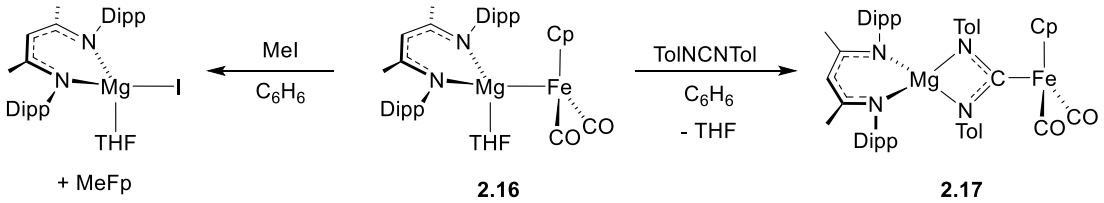

Scheme 2.4 Reactions of (^{Dipp}NacNac)MgFp(THF) (**2.16**).[4]

The reaction of [(^{Dipp}NacNac)CaI(THF)]$_2$ with KFp in THF followed by benzene extraction afforded a product of composition "(^{Dipp}NacNac)CaFp$(THF)_2$" (**2.18**), according to NMR and elemental analysis.[9] The solid state IR spectrum of **2.18** revealed two strong ν(CO) bands at 1823 and 1780 cm^{-1}, consistent with the symmetric and asymmetric stretches of a coordinated Fp anion. Compound **2.18** was not stable for long periods in non-donor solvents.[4] However, a saturated THF solution of **2.18** afforded diffraction-quality crystals of [(^{Dipp}NacNac)Ca(μ-Fp)$(THF)_2$]$_2$ (**2.19**, Scheme 2.5). Structural authentication revealed that the dimeric structure possessed no direct Ca–Fe bonds; the Fp units instead bridge between the Ca centres through Ca(μ-OC)Fe isocarbonyl interactions. The analogous reaction between [(^{Dipp}NacNac)YbI(THF)]$_2$

and KFp afforded [(^{Dipp}NacNac)Yb(μ-Fp)(THF)$_2$]$_2$ (**2.20**) which is isostructural with **2.19**.

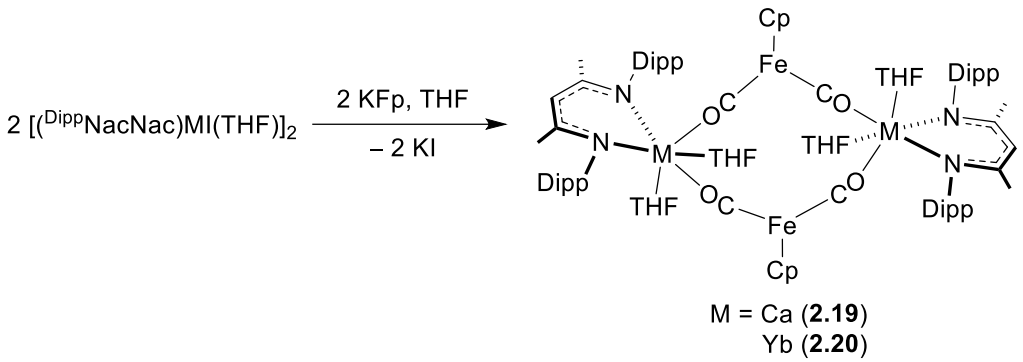

Scheme 2.5 The synthesis of isostructural complexes [(^{Dipp}NacNac)Ca(μ-Fp)(THF)$_2$]$_2$ (**2.19**) and [(^{Dipp}NacNac)Yb(μ-Fp)(THF)$_2$]$_2$ (**2.20**).[9]

2.2.3 Effects of the supporting ligand on structure and reactivity of Ae–TM bonded complexes

While the reductive cleavage of TM–TM dimers with Ae metals proved a facile method for the isolation of Ae–TM bonded complexes, the scope of reactivity is quite narrow. The introduction of ligands on the Ae metal centre broadens the scope of available compounds through variation of ligands. The use of β-diketiminate ligands led to the successful isolation of several Ae–TM bonded complexes. However, the reactivity of these complexes with small molecules was, aside from a few notable examples, rather limited. It was speculated that variation of the organic ligand at the Ae metal centre may allow for a modification of the reactivity of the final product.

Amidinate ligands, R'C(NR)$_2$ (R, R' = alkyl, aryl), are a widely studied and well characterised class of ligands in the coordination chemistry of both main group and transition metals.[68] These ligands were identified as a suitable substitute for the β-diketiminate ligand. While both of these ligand sets feature sterically demanding R groups at the N donor atoms, amidinate ligands have fewer C atoms in the ligand backbone than β-diketiminates. As a consequence, amidinates have a more acute N–M–N bite angle (typically between 63° and 65°)[69,70] compared to β-diketiminates (around 91°, based on the mean value of all β-diketiminate metal X-ray structures deposited in the CSD),[3] and so have the potential to give Ae–TM bonded complexes with a greater reactivity towards small molecules, due to a more accessible Ae–TM bond.

Although the N–M–N bite angle is fairly acute in amidinate complexes, these ligands still have the potential to provide substantial steric shielding. Bulky N-bound R groups (*e.g.* Dipp, Mes) can provide considerable steric protection for the chelated metal atom. In addition, work by Jordan *et al*. showed that the distal R' groups can also modify the steric protection offered by the ligand.[71] Several amidinate aluminium compounds, including $\{R'C(N^iPr)_2\}AlCl_2$ (R' = Me (**2.21**), ^{t}Bu (**2.22**)), were synthesised and structurally authenticated. Figure 2.8 illustrates the molecular structure of these compounds and shows select angles.

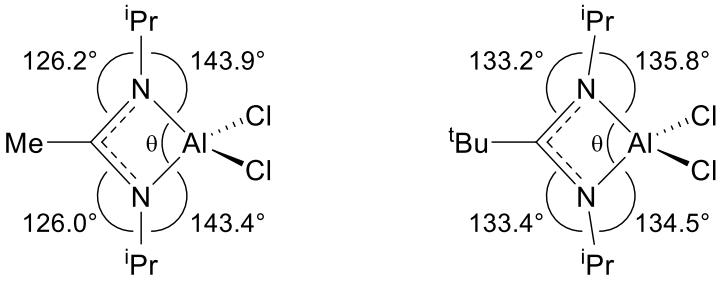

Figure 2.8 The molecular structures of $\{MeC(N^iPr)_2\}AlCl_2$ (**2.21**) and $\{^tBuC(N^iPr)_2\}AlCl_2$ (**2.22**), detailing select angles.[71]

Substitution of the distal Me group for the bulkier ^{t}Bu group results in displacement of the N-bound ^{i}Pr groups due to increased steric repulsion. Consequently, the average C–N–C(^{i}Pr) angle becomes more obtuse (from 126.1° (**2.21**) to 133.3° (**2.22**)), while the C(^{i}Pr)–N–Al angle becomes more acute (from 143.7° (**2.21**) to 135.2° (**2.22**)). There is little change in the N–Al–N bite angle (θ) between the two compounds, reducing by only 0.6° upon variation of the ligand. This demonstrates that the steric repulsion affects only the N-bound groups and not the internal ligand structure. In summation, bulkier distal groups are capable of displacing the N-bound substituents towards the chelating cavity, effectively flanking and increasing the steric protection around the metal atom.

2.3 Synthesis of Mg–TM bonded complexes supported by the N,N'-diisopropylamidinate ligand

The reactivity displayed by β-diketiminate supported Mg–TM bonded compounds is promising but has unfortunately been limited to the examples discussed earlier in this Thesis. The aim of the work in this Chapter was to synthesise new Mg–TM bonded compounds with a greater reactivity than their β-diketiminate ligated counterparts. As discussed above, amidinate ligands have been shown to be successful substitutes for β-diketiminate ligands in related areas.[72] Amidinate supported Mg–TM bonded compounds were therefore targeted as synthetic targets for this work.

Amidinate magnesium halides have been reported frequently in the scientific literature. These compounds were targeted as suitable starting point from which to access amidinate-supported Ae–TM bonded complexes *via* salt metathesis. Coles *et al.*[73] have previously reported the facile synthesis of [{MesC(NCy)$_2$}Mg(μ-Br)(OEt$_2$)]$_2$ (**2.23**, Scheme 2.6) from CyNCNCy and MesMgBr in Et$_2$O. This synthetic procedure is advantageous as it allows ready modification of the R and R' groups of R'C(NR)$_2$ by selection of appropriate carbodiimide and Grignard starting materials.

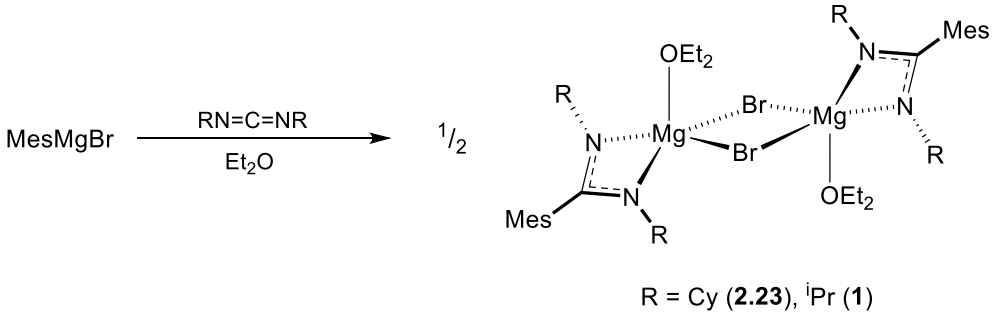

Scheme 2.6 Synthesis of amidinate-supported magnesium bromides.[73]

The new compound [{MesC(N^{i}Pr)$_2$}Mg(μ-Br)(OEt$_2$)]$_2$ (**1**, Scheme 2.6) was prepared in 88% yield from the reaction of ^{i}PrNCN^{i}Pr and MesMgBr in Et$_2$O using an analogous procedure to that of Coles *et al*. Diffraction-quality crystals of **1** were grown from a saturated Et$_2$O solution at 5 °C. The molecular structure and selected distances and angles for **1** are shown in Figure 2.9 and Table 2.1.

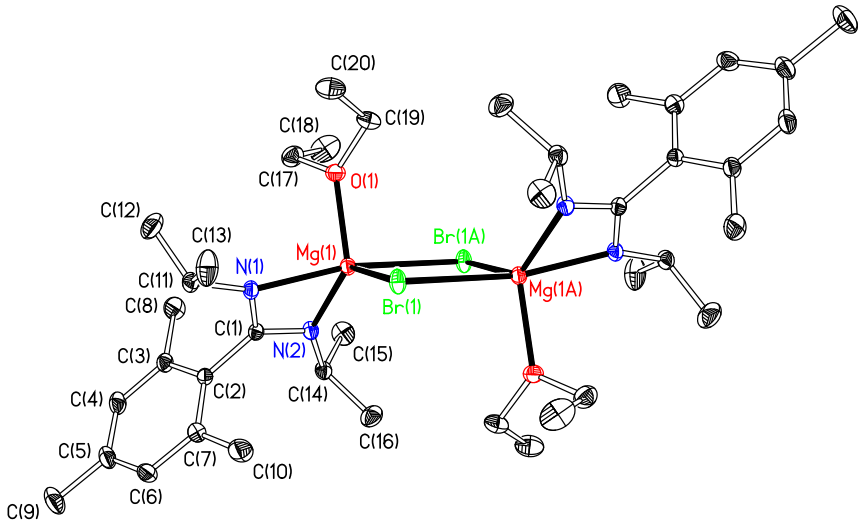

Figure 2.9 Displacement ellipsoid plot (20% probability) of $[\{MesC(N^iPr)_2\}Mg(\mu\text{-}Br)(OEt_2)]_2$ (**1**). H atoms omitted. Atoms carrying the suffix 'A' are related to their counterparts by the symmetry operator 1-x, 1-y, 1-z.

Table 2.1 Selected distances (Å) and angles (°) for $[\{MesC(N^iPr)_2\}Mg(\mu\text{-}Br)(OEt_2)]_2$ (**1**).

Mg(1)–Br(1)	2.6677(8)	Mg(1)–Br(1A)	2.5560(8)
Mg(1)–N(1)	2.1144(17)	Mg(1)–N(2)	2.0757(17)
Mg(1)–O(1)	2.0398(16)	C(1)–N(1)	1.327(3)
C(1)–N(2)	1.331(2)	C(1)–C(2)	1.501(3)
Mg(1)–Br(1)–Mg(1A)	92.64(3)	Br(1)–Mg(1)–Br(1A)	87.36(3)
Br(1)–Mg(1)–N(1)	164.69(5)	Br(1)–Mg(1)–N(2)	100.45(5)
Br(1)–Mg(1)–O(1)	91.46(5)	Br(1A)–Mg(1)–N(1)	101.55(6)
Br(1A)–Mg(1)–N(2)	130.19(6)	Br(1A)–Mg(1)–O(1)	108.33(5)
N(1)–Mg(1)–N(2)	64.29(6)	N(1)–C(1)–N(2)	114.02(17)
N(1)–Mg(1)–O(1)	97.40(7)	N(2)–Mg(1)–O(1)	120.39(7)

Compound **1** is dimeric in the solid state, bridged by two μ-Br ligands. The Mg centre is five-coordinate with a bidentate amidinate, Et_2O and two μ-Br ligands. The τ parameter, defined by Addison *et al*. (Equation 2.2), quantifies the level of geometric distortion in five-coordinate compounds by taking the difference of the two largest L–M–L angles, *A* and *B* (where *B* is the larger of the two angles).[74] In a perfect square based pyramid both *A* and *B* are 180° and τ = 0. In a perfect trigonal bipyramid the

angles are $B = 180°$ and $A = 120°$ and $\tau = 1$. In the case of **1** $\tau = 0.57$, which is 57% on the pathway of distortion between a square based pyramid and a trigonal bipyramid. Compound **1** is therefore best described as a distorted trigonal bipyramid.

$$\tau = \frac{(B - A)}{60}$$

Equation 2.2[74]

The bite-angle of the amidinate ligand (N(1)–Mg(1)–N(2) = 64.29(6)°) is in the range typically observed in amidinate metal compounds.[70] Other distances and angles are as expected and are comparable to those reported by Coles *et al*. for **2.23**.

The NMR tube-scale reaction of **1** with KFp in THF-d_8 showed quantitative conversion to a new product by ^{1}H NMR, ostensibly {MesC(N^{i}Pr)$_2$}MgFp(THF) (**2**, Scheme 2.7). The reaction was scaled up in an attempt to isolate and identify the product. However, benzene extraction of the crude reaction mixture gave a complex mixture of products, evidenced by the presence of multiple amidinate ligand environments and Fp_2 in the ^{1}H NMR spectrum, the latter being a common decomposition product in the chemistry of the $[Fp]^-$ anion.[75] Given the stability of **2.16** in THF and benzene, the decomposition of **2** was somewhat unexpected. It is possible that some combination of reduced bite angle of the ligand and the absence of steric protection from bulky N-bound aromatic substituents results in the instability of the Mg–Fe bonded species. Due to the extent of decomposition this reaction was not investigated further.

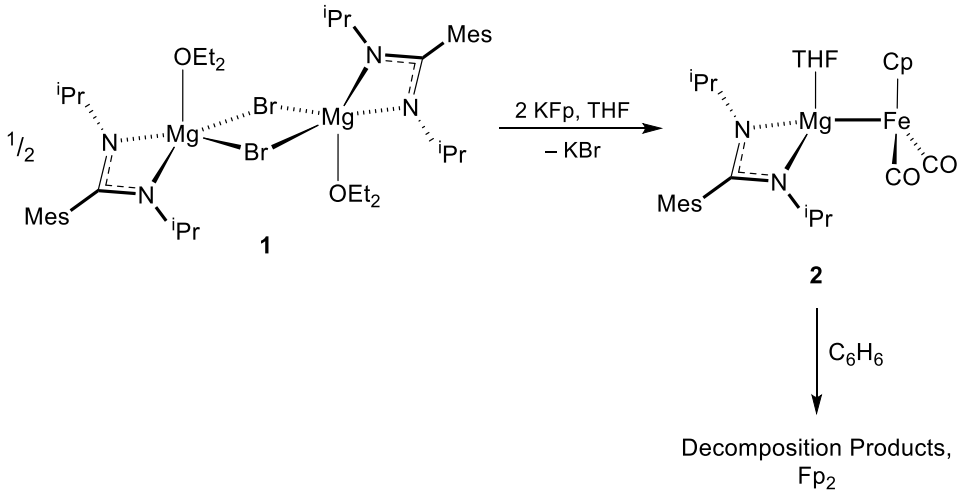

Scheme 2.7 The attempted synthesis of {MesC(N^{i}Pr)$_2$}MgFp(THF) (**2**) and its decomposition to Fp_2 and other decomposition products.

The reaction of **1** with NaRp(THF) in THF afforded {MesC(N^{i}Pr)$_2$}MgRp(THF) (**3**, Equation 2.3) in 46% isolated yield, following benzene extraction. The fact that **2** could not be isolated in this way makes the successful isolation of **3** noteworthy. As previously discussed, the 4*d* valence orbitals of Ru are less contracted than the 3*d* valence orbitals of Fe. Thus, Rp^{-} is likely to form stronger bonds than its Fe counterpart with suitable bond partners. This increased bond strength is the likely cause of the stability of **3** in non-donor solvent environments.

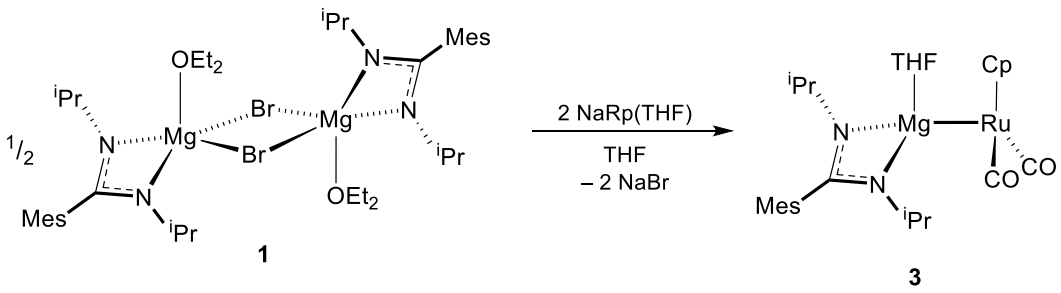

Equation 2.3

The solid state IR spectrum of **3** shows ν(CO) bands at 1950 and 1874 cm^{-1}. There are no lower frequency ν(CO) bands, indicating an absence of isocarbonyl bridging interactions. These data are consistent with a terminal Rp unit bonded to the Mg centre in a similar fashion to the Fp unit in **2.16**. The ν(CO) bands are comparable to those for {^{i}Pr$_2$NC(NCy)$_2$}Al(Cl)Rp (**2.24**, ν(CO) = 1989, 1927 cm^{-1}, CH_2Cl_2 solution)[33] and Cp*$_2$Th(I)Rp (**2.25**, ν(CO) = 2023, 1959 cm^{-1}, THF solution),[41] reported by Aldridge and Marks, respectively. The solution IR spectrum of **3** in toluene shows two ν(CO) bands at 2025 and 1972 cm^{-1}, suggesting the monomeric structure is maintained in solution.

The reaction of **1** with K[Co(CO)$_3$(PCy$_3$)](THF)$_2$ in THF gave {MesC(N^{i}Pr)$_2$}Mg{Co(CO)$_3$(PCy$_3$)}(THF) (**4**, Equation 2.4) in 58% isolated yield, following benzene extraction. Diffraction-quality crystals of **4** were grown from pentane at room temperature. The molecular structure and selected distances and angles for **4** are shown in Figure 2.10 and Table 2.2.

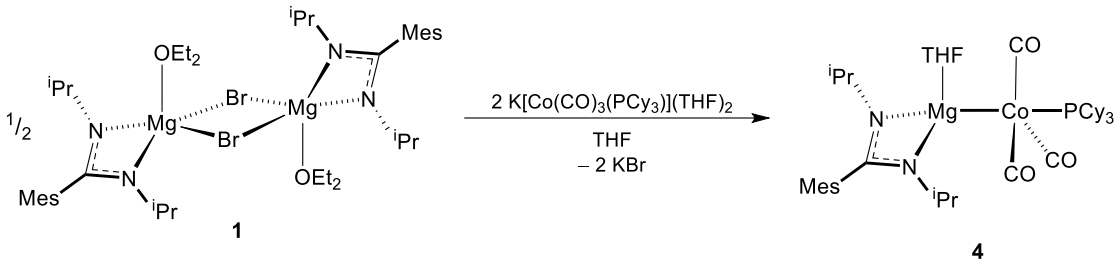

Equation 2.4

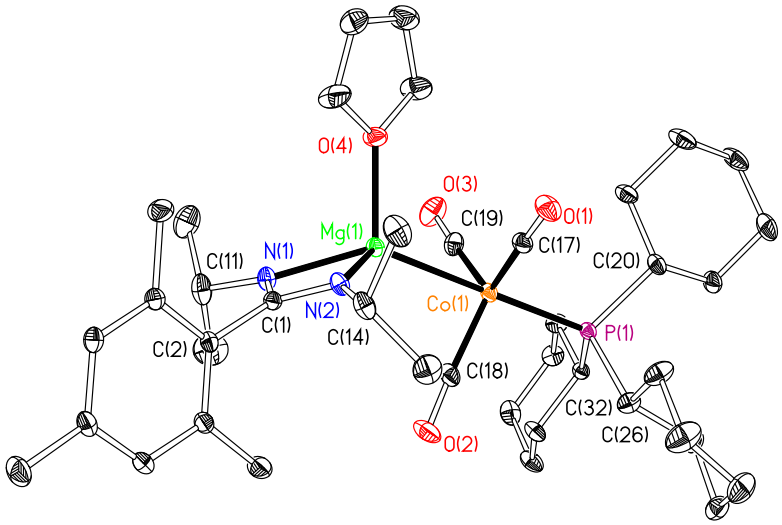

Figure 2.10 Displacement ellipsoid plot (25% probability) of {MesC(N^{i}Pr)$_2$}Mg{Co(CO)$_3$(PCy$_3$)}(THF) (**4**). H atoms omitted for clarity.

Compound **4** is a heterobimetallic species which is monomeric in the solid state. The geometry at the four-coordinate Mg centre is approximately tetrahedral with two bonds to the bidentate amidinate ligand and one to each of the THF and Co(CO)$_3$(PCy$_3$) moieties. The rigidity of the amidinate backbone prevents the possibility of an ideal tetrahedral angle (109.5°)[76] for anything but the Co–Mg–O(THF) angle. The geometry at Co is essentially trigonal bipyramidal with the three carbonyls lying in the equatorial plane and the Mg and P atoms occupying the axial positions with an essentially linear arrangement (Mg–Co–P = 174.58(2)). The molecule contains one Mg–Co bond with a distance of 2.5310(7) Å, within the sum of the respective covalent radii (2.67(8) Å).[77] This Mg–Co distance is comparable with those observed by Jonas *et al.* in **1.19** (2.480(4) Å) and **1.20** (2.565(3) Å)[78] and also with those reported by Blake and Mountford for **1.46** (2.6163(6) and 2.5427(6) Å).[5] Compound **4** represents only the fourth report of a complex containing a Mg–Co bond.[3,6]

Table 2.2 Selected distances (Å) and angles (°) for {MesC(N^{i}Pr)$_2$}Mg{Co(CO)$_3$(PCy$_3$)}(THF) (**4**).

Mg(1)–Co(1)	2.5310(7)	Mg(1)–N(1)	2.0777(18)
Mg(1)–N(2)	2.0498(17)	Mg(1)–O(4)	2.0312(16)
Co(1)–P(1)	2.2071(5)	Co(1)–C(17)	1.745(2)
Co(1)–C(18)	1.759(2)	Co(1)–C(19)	1.745(2)
C(1)–N(1)	1.332(3)	C(1)–N(2)	1.327(3)
C(1)–C(2)	1.510(3)		
Co(1)–Mg(1)–N(1)	137.70(6)	Co(1)–Mg(1)–N(2)	120.64(6)
Co(1)–Mg(1)–O(4)	109.92(5)	N(1)–Mg(1)–N(2)	65.28(7)
N(1)–Mg(1)–O(4)	106.23(7)	N(2)–Mg(1)–O(4)	108.22(7)
Mg(1)–Co(1)–P(1)	174.58(2)	Mg(1)–Co(1)–C(17)	76.45(7)
Mg(1)–Co(1)–C(18)	80.87(7)	Mg(1)–Co(1)–C(19)	80.20(7)
P(1)–Co(1)–C(17)	99.02(7)	P(1)–Co(1)–C(18)	98.62(7)
P(1)–Co(1)–C(19)	104.63(7)	C(17)–Co(1)–C(18)	115.17(10)
C(17)–Co(1)–C(19)	115.48(11)	C(18)–Co(1)–C(19)	119.07(11)
N(1)–C(1)–N(2)	113.75(17)		

The solid state IR spectrum of **4** contains three major high frequency ν(CO) bands at 1963, 1922 and 1879 cm^{-1} and no significant lower frequency ν(CO) bands, consistent with the crystallographically derived structure which contains no isocarbonyl interactions. These ν(CO) bands are similar to those reported by Blake and Mountford for terminal carbonyl ligands in **1.46** (1935 and 1861 cm^{-1}). The isocarbonyl interactions in **1.46** are reflected in a ν(CO) band at 1720 cm^{-1}, which appears at a considerably lower frequency than those observed in **4**. The solution IR spectrum of **4** in toluene is more complicated with three ν(CO) bands at 1969, 1904 and 1895 cm^{-1}, attributed to a Mg–Co bonded species, and lower frequency bands at 1839 and 1755 cm^{-1}, possibly indicative of more complex behaviour in solution.

Although **3** and **4** were synthesised successfully, the inability of **2** to tolerate non-donor solvents and its subsequent decomposition was an unfortunate outcome. The amidinate ligand affords enough steric protection to stabilise both the Mg–Ru and Mg–Co bonded compounds. However, this is not sufficient to stabilise the Mg–Fe bond. It appeared

possible that an amidinate ligand with bulkier N-bound substituents would be capable of stabilising the Mg–Fe bond in addition to the other Mg–M' bonded compounds. Given the success of ^{Dipp}NacNac in stabilising a Mg–Fe bonded complex, Dipp was the natural choice for a sterically protecting N-bound substituent.

The synthesis of an amidinate compound with N-bound Dipp substituents presents a synthetic challenge. While the carbodiimide necessary for the synthesis of **1** (^{i}PrNCN^{i}Pr) is commercially available, DippNCNDipp is not. An additional synthetic procedure is therefore required to produce this carbodiimide before the final amidinate ligand can be obtained.

2.4 Synthesis of bulky aryl carbodiimides

An established two-step procedure for the preparation of bulky aryl carbodiimides (*e.g.* RNCNR, where R = Dipp, Mes) has been published by Cowley *et al.*[79] The process begins with the synthesis of an arylthiourea (ArNC(S)NAr) from the condensation reaction between CS_2 and two equivs. of any substituted aniline ($ArNH_2$), both readily available and relatively inexpensive starting materials. The carbodiimide is then obtained *via* the oxidative desulfurisation of the thiourea with HgO (Scheme 2.8).

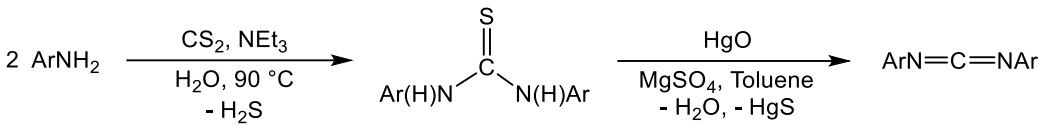

Scheme 2.8 Synthesis of arylcarbodiimides *via* oxidative desulfurisation of an thiourea intermediate with HgO.[79]

The use of HgO in this reaction was concerning due to the toxicity associated with the compound, and with Hg containing compounds in general. Conversations with a colleague who had employed this method for the synthesis of DippNCNDipp suggested that the desulfurisation step did not scale well above the sub-gram scale of the original procedure. Considering both factors, the decision was taken to seek an alternative synthesis for arylcarbodiimides.

A procedure for the oxidative desulfurisation of arylthioureas, published by Patel *et al.*, uses I_2 in the presence of Brønsted base (NEt_3) to produce the carbodiimide *via* oxidation desulfurisation.[80] This procedure uses cheap, readily available reagents and avoids the risk associated with the use of mercury and its compounds.

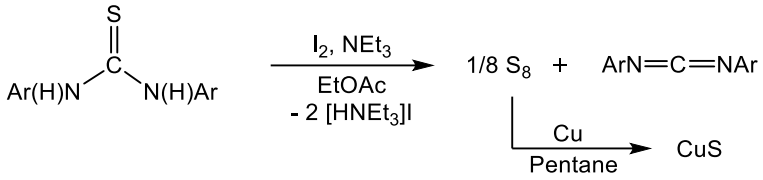

Scheme 2.9 Oxidative desulfurisation of thiourea with iodine followed by removal of residual S_8 by reaction with activated Cu.[80,81]

The elemental sulfur produced as a by-product of the iodine-mediated desulfurisation reaction must be removed from the final product. The authors report that S_8 can be separated from the product *via* silica column chromatography with hexane as the eluent. Although this method is somewhat successful, some sulfur was found to co-elute with the product when the procedure was carried out on the multi-gram scale. An envelope at *m*/*z* = 255.8 Da in the mass spectra of the carbodiimide products showed that samples obtained in this manner were contaminated with quantities of S_8.

A report by Blumer describes a method for removing elemental sulfur from hydrocarbon fractions by eluting the sulfur-contaminated sample through a column of activated copper.[81] This process was adapted to remove S_8 from large samples of reaction material. The addition of activated Cu to contaminated samples of carbodiimides in hydrocarbon solvents resulted in precipitation of insoluble CuS which was separated by eluting the solution through a silica plug. The mass spectra of carbodiimide samples obtained *via* this method were collected. The peak at *m*/*z* = 255.8 Da, which was present in the mass spectra of S_8 contaminated samples, was absent in samples treated with activated Cu, indicating that all S_8 contamination had been removed.

The described synthetic procedures were used to produce DippNCNDipp (**5**) and MesNCNMes (**6**).

2.5 Synthesis of Mg–TM bonded complexes supported by the N,N'-bis(diisopropylphenyl)amidinate ligand

[{MesC(NDipp)$_2$}Mg(μ-Br)(OEt$_2$)]$_2$ (**7**, Equation 2.5) was prepared in 67% yield from the reaction of **5** and MesMgBr in Et$_2$O. Fine, needle-like crystals were readily obtained from Et$_2$O solutions of **7**. However, no samples suitable for single crystal X-ray diffraction could be isolated due to a rapid desolvation process, which consistently destroyed the crystallinity of the sample upon handling.

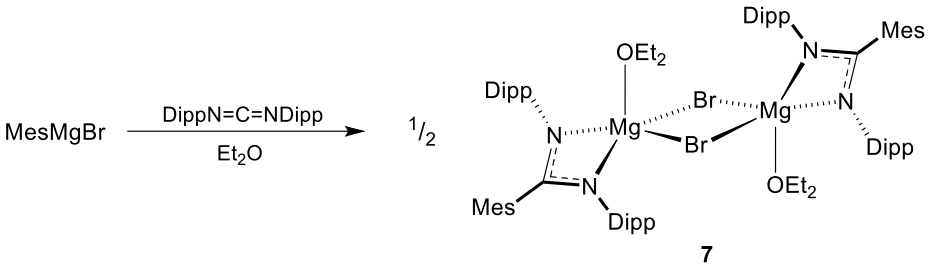

Equation 2.5

Reaction of **7** with KFp in THF followed by extraction into benzene gave {MesC(NDipp)$_2$}MgFp(THF) (**8**, Equation 2.6) as a light brown solid in 74% isolated yield. This is in stark contrast to the attempted isolation of **2**, which was unstable in non-donor solvents. Although diffraction-quality crystals of **8** could not be grown, ^{1}H and ^{13}C{^{1}H} NMR spectroscopic data are consistent with formation of the desired species. The ^{1}H NMR spectrum shows one major peak in the Cp region at 4.52 ppm with only minor quantities of the decomposition product Fp$_2$ (<5%, by integration).

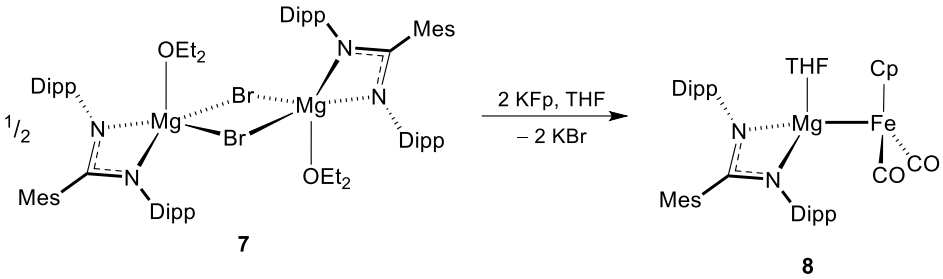

Equation 2.6

The solid state IR spectrum of **8** shows two strong ν(CO) bands at 1930 and 1866 cm^{-1}. The solution IR spectrum of **8** in toluene shows two ν(CO) bands at 2017 and 1925 cm^{-1} consistent with a non-isocarbonyl bridged species in the solution phase. For comparison, the solution IR spectrum of structurally authenticated Mg–Fe bonded **2.16** in toluene was recorded and showed two ν(CO) bands at 2017 and 1925 cm^{-1}. The similar position of the ν(CO) bands in **2.16** and **8** strongly support the latter as being Mg–Fe bonded in solution.

Reaction of **7** with NaRp(THF) in THF followed by extraction in benzene gave {MesC(NDipp)$_2$}MgRp(THF) (**9**, Equation 2.7) in 66% isolated yield. As was the case with **8**, ^{1}H and ^{13}C{^{1}H} NMR spectra were consistent with the formation of **9** as the sole product of the reaction. The ^{1}H NMR spectrum shows only one peak in the Cp region at 4.90 ppm. No diffraction-quality crystals of **9** could be grown.

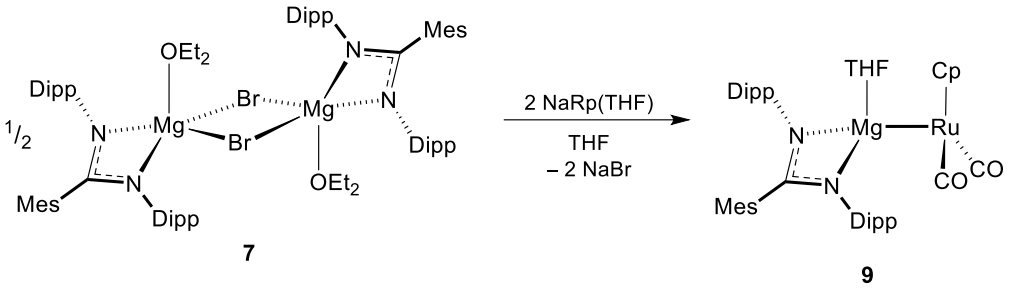

Equation 2.7

The solid state IR spectrum of **9** showed two major ν(CO) bands at 1952 and 1882 cm^{-1}. The lack of any low frequency ν(CO) bands indicates a terminal Rp unit which does not participate in isocarbonyl interactions. These ν(CO) bands are similar to those observed in **3** (1950 and 1874 cm^{-1}). The solution phase IR of **9** in toluene shows two major ν(CO) bands at 2024 and 1888 cm^{-1}, consistent with the preservation of the monomeric Mg–Ru bonded structure in solution.

Reaction of **7** with $K[Co(CO)_3(PCy_3)](THF)_2$ in THF followed by pentane extraction gave $\{MesC(NDipp)_2\}Mg\{Co(CO)_3(PCy_3)\}(THF)$ (**10**, Equation 2.8) as a grey solid in 39% isolated yield. Diffraction-quality crystals of **10** were grown from a benzene solution at room temperature. The molecular structure and selected distances and angles for **4** are shown in Figure 2.11 and Table 2.3.

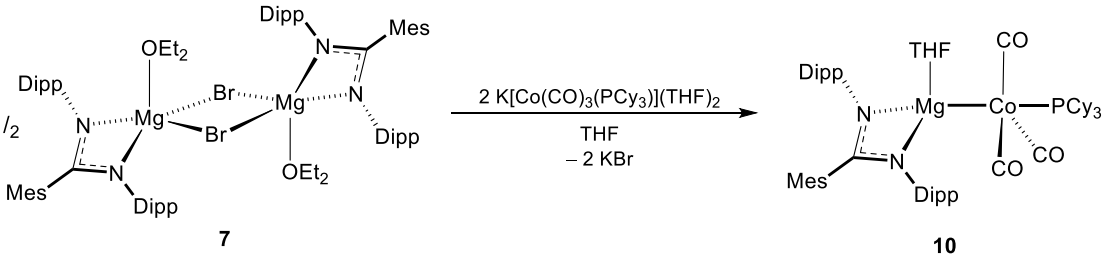

Equation 2.8

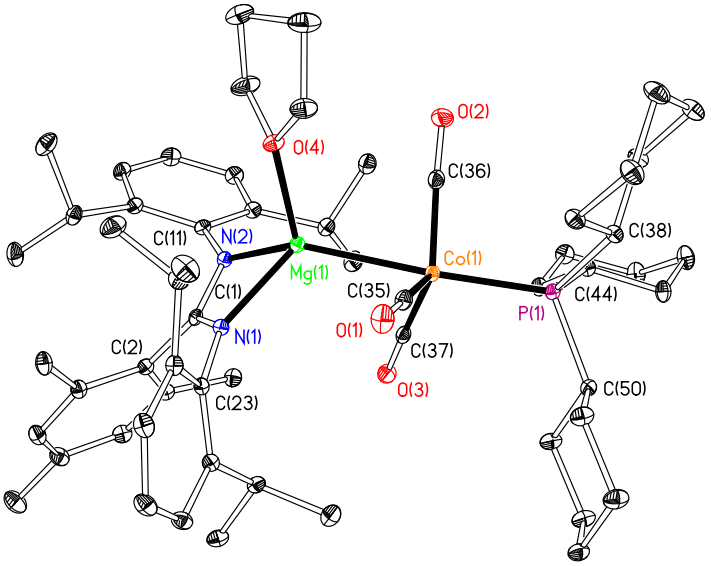

Figure 2.11 Displacement ellipsoid plot (25% probability) of {MesC(NDipp)$_2$}{MgCo(CO)$_3$(PCy$_3$)}(THF) (**10**). H atoms omitted for clarity.

Table 2.3 Selected distances (Å) and angles (°) for {MesC(NDipp)$_2$}Mg{Co(CO)$_3$(PCy$_3$)}(THF) (**10**).

Mg(1)–Co(1)	2.5193(5)	Mg(1)–N(1)	2.0590(12)
Mg(1)–N(2)	2.0983(13)	Mg(1)–O(4)	2.0317(11)
Co(1)–P(1)	2.2026(4)	Co(1)–C(35)	1.7580(16)
Co(1)–C(36)	1.7494(16)	Co(1)–C(37)	1.7605(16)
C(1)–N(1)	1.3356(17)	C(1)–N(2)	1.3531(18)
Co(1)–Mg(1)–N(1)	118.74(4)	Co(1)–Mg(1)–N(2)	134.60(4)
Co(1)–Mg(1)–O(4)	109.46(4)	N(1)–Mg(1)–N(2)	64.51(5)
N(1)–Mg(1)–O(4)	116.86(5)	N(2)–Mg(1)–O(4)	106.64(5)
Mg(1)–Co(1)–P(1)	174.780(18)	Mg(1)–Co(1)–C(35)	80.37(5)
Mg(1)–Co(1)–C(36)	80.13(5)	Mg(1)–Co(1)–C(37)	78.54(5)
P(1)–Co(1)–C(35)	104.51(5)	P(1)–Co(1)–C(36)	95.89(5)
P(1)–Co(1)–C(37)	100.97(5)	C(35)–Co(1)–C(36)	116.22(7)
C(35)–Co(1)–C(37)	112.35(7)	C(36)-Co(1)-C(37)	121.96(7)
N(1)–C(1)–N(2)	111.23(12)		

The structure of **10** is monomeric in the solid state containing a four-coordinate magnesium centre with approximately tetrahedral geometry. Surprisingly the Mg–Co distance (2.5193(5) Å) in **10** is shorter than that observed in **4** despite **10** containing bulkier N-aryl substituents on the amidinate ligand. This can be attributed to one or two different effects. First, the orientation of the Dipp groups in **10** away from the metal anion. In the case of **4** the ^{i}Pr substituents orient themselves such that the Me groups are pointing away from the distal Mes group and towards the Co centre, potentially increasing the Mg–Co distance as a result. This effect may be viewed as an extension of that reported by Jordan *et al*. for steric repulsion within sterically demanding amidinate aluminium systems.[71] In addition, the N-aryl substituted ligand in **10** gives a more electrophilic Mg centre than the N-alkyl functionalised ligand in **4**. Consistent with this, the Mg–N distances are shorter in **4** (2.0498(17) and 2.0777(18) Å) than **10** (2.0590(12) and 2.0983(13) Å), and thus the N(1)–Mg(1)–N(2) bite-angle in **10** (64.51(5)°) is slightly more acute than in **4** (65.28(7)°). For **10** ∑(P–Co–CO) = 301.37(9)°, very similar to that for **4** (302.27(12)°), indicating a significant interaction between the metal centres.

The solid state IR spectrum of **10** shows two strong ν(CO) bands at 1965 and 1873 cm^{-1}, the latter of which is quite broad and may comprise two overlapping bands. There are no ν(CO) bands at lower frequencies, indicative of a lack of isocarbonyl interactions in the solid state. These ν(CO) bands are similar to those observed in **4** (1963, 1922 and 1879 cm^{-1}). The solution IR of **10** in toluene shows only three ν(CO) bands at 1968, 1891 and 1840 cm^{-1}, consistent with preservation of the Mg–Co bond in solution.

2.6 Synthesis of Mg–TM bonded complexes supported by the N,N'-bis(trimethylphenyl)amidinate

[{MesC(NMes)$_2$}Mg(μ-Br)(OEt$_2$)]$_2$ (**11**, Equation 2.9) was prepared in 93% isolated yield from the reaction of **6** and MesMgBr in Et$_2$O. Diffraction-quality crystals of **11** were grown from an Et$_2$O solution at 5 °C. The molecular structure and selected distances and angles for **11** are shown in Figure 2.12 and Table 2.4.

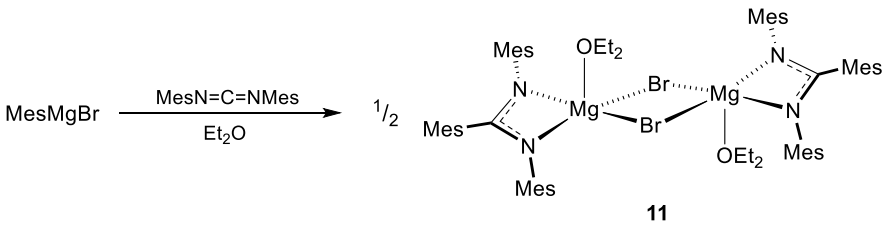

Equation 2.9

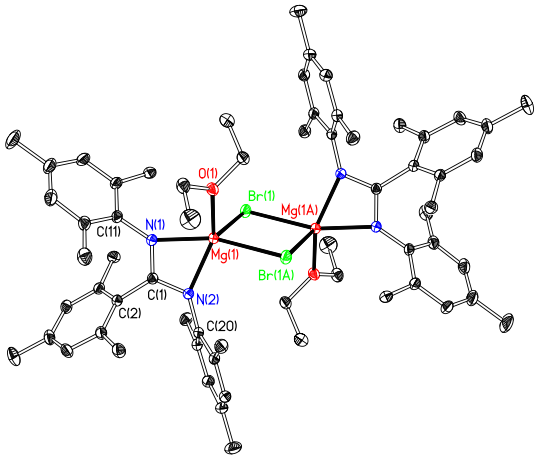

Figure 2.12 Displacement ellipsoid plot (20% probability) of [Mg{MesC(NMes)$_2$}(μ-Br)(OEt$_2$)]$_2$ (**11**). H atoms omitted for clarity. Atoms carrying the suffix 'A' are related to their counterparts by the symmetry operator 1–x, 1-y, 1-z.

Table 2.4 Selected distances (Å) and angles (°) for [{MesC(NMes)$_2$}Mg(μ-Br)(OEt$_2$)]$_2$ (**11**).

Mg(1)–Br(1)	2.5656(6)	Mg(1)–Br(1A)	2.6753(6)
Mg(1)–N(1)	2.1153(15)	Mg(1)–N(2)	2.1183(15)
Mg(1)–O(1)	2.0522(14)	C(1)–N(1)	1.341(2)
C(1)–N(2)	1.336(2)	C(1)–C(2)	1.514(2)
Mg(1)–Br(1)–Mg(1A)	90.935(17)	Br(1)–Mg(1)–Br(1A)	89.065(17)
Br(1)–Mg(1)–N(1)	112.38(5)	Br(1)–Mg(1)–N(2)	112.57(5)
Br(1)–Mg(1)–O(1)	102.32(4)	Br(1A)–Mg(1)–N(1)	157.32(5)
Br(1A)–Mg(1)–N(2)	102.41(4)	Br(1A)–Mg(1)–O(1)	88.97(4)
N(1)–Mg(1)–N(2)	63.44(6)	N(1)–C(1)–N(2)	112.52(14)
N(1)–Mg(1)–O(1)	93.30(6)	N(2)–Mg(1)–O(1)	143.24(6)

The solid state structure of **11** is analogous to that of **1**, namely a dimer bridged by two μ-Br ligands. The atoms around the five-coordinate Mg(1) centre form a distorted square-based pyramid ($\tau = 0.41$). The Br(1) atom occupies the apical position of the pyramid while the κ_2-amidinate, Et_2O group and Br(1A) atom lie in the basal plane. This geometry contrasts with that seen in **1** ($\tau = 0.57$) which, while extremely distorted, had more trigonal bipyramidal character than square pyramidal. The contrast is more pronounced with Coles' compound, **2.23** ($\tau = 0.70$), which has decisively more trigonal bipyramidal character than square pyramidal. The shift towards a square based pyramidal geometry is likely explained by the introduction of bulky N-aryl substituents. The rigidity of these groups prevents the amidinate ligand from adopting the axial/equatorial configuration seen in **1** and instead forces it to sit solely in the equatorial plane.

^{1}H NMR analysis of crystals of **11** grown from Et_2O shows one equivalent of Et_2O per ligand. However, prolonged drying of the bulk material *in vacuo* leads to partial loss of Et_2O and two distinct ligand environments when observed in C_6D_6, consistent with Et_2O coordinated and solvent free Mg amidinate environments. In contrast, the ^{1}H NMR spectrum recorded for **11** in THF-d_8 shows only one set of ligand environments consistent with a fully solvent-coordinated molecule with equivalent N-Mes environments.

The reaction of **11** with KFp in THF followed by benzene extraction gave {MesC(NMes)$_2$}MgFp(THF) (**12**, Equation 2.10) by ^{1}H NMR spectroscopy, among other minor ligand environments and Fp_2 which presumably result from the partial decomposition of **12** in the non-donor solvent environment. This result can be easily rationalised in terms of sterics; **2** was the least sterically protected species and decomposed completely in non-donors solvents, while **8** was the most sterically protected species and tolerated non-donor solvent environments with no decomposition. The intermediate steric protection afforded by the ligand of **12** partially inhibits decomposition in non-donor solvents but does not prevent it entirely. In order to avoid this decomposition process, the reaction was modified to use THF as the only solvent. This allowed isolation of **12** as the sole product in 68% isolated yield.

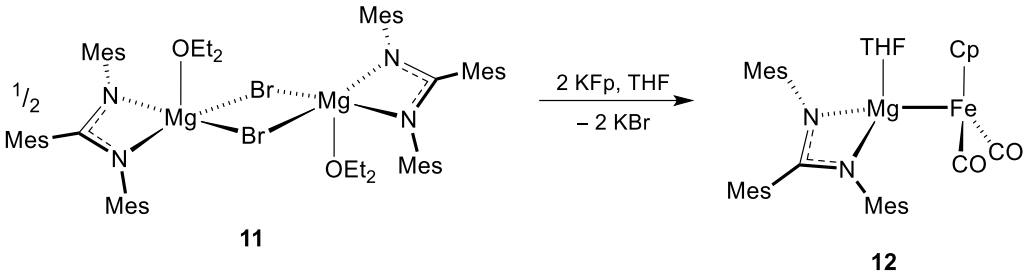

Equation 2.10

The solid state IR spectrum of **12** showed two main ν(CO) bands at 1923 and 1858 cm^{-1}, notably absent are lower frequency ν(CO) bands that would indicate the presence of isocarbonyl interactions. The solution IR spectrum of **12** in THF is more complex but nonetheless dominated by ν(CO) bands at 1921 and 1861 cm^{-1}. Reassuringly, the previously reported solution IR spectrum of Mg–Fe bonded **2.16** in THF similarly shows bands at 1926 and 1871 cm^{-1}.[4]

Reaction of **11** with NaRp(THF) in THF followed by benzene extraction gave {MesC(NMes)$_2$}MgRp(THF) (**13**, Equation 2.11) in 76% isolated yield. As was the case with **3**, no decomposition products were observed in the ^{1}H NMR spectrum of the product despite the decomposition processes associated with the Fp analogues, **2** and **12**.

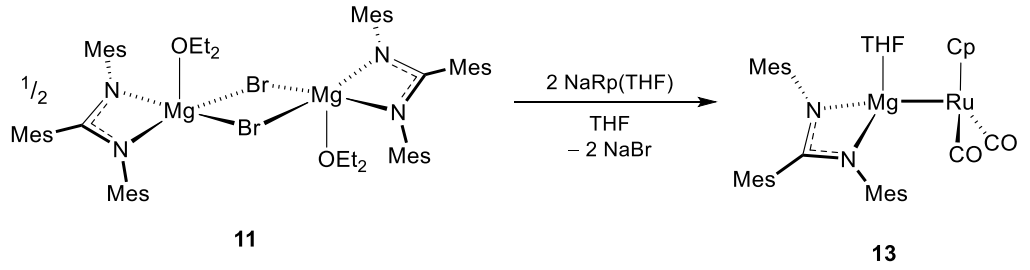

Equation 2.11

The solid state IR spectrum of **13** is complex with ν(CO) bands at 2029, 1969, 1945 and 1874 cm^{-1}. Consistent with the Mg–Rp compounds discussed previously, the lack of any low frequency ν(CO) bands indicates a terminal Rp unit with no isocarbonyl bonding interactions. The solution IR of **13** in toluene shows ν(CO) bands at 2024 and 1970 cm^{-1}, consistent with the preservation of the Mg–Ru bond in solution.

Reaction of **11** with K[Co(CO)$_3$(PCy$_3$)](THF)$_2$ in THF followed by benzene extraction gave {MesC(NMes)$_2$}Mg{Co(CO)$_3$(PCy$_3$)}(THF) (**14**, Equation 2.12) in 84% isolated

yield. Unlike the previous amidinate analogues **4** and **10**, no diffraction-quality crystals of **14** could be obtained.

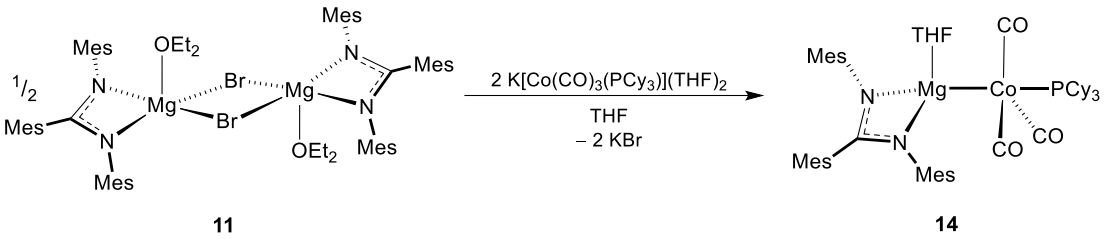

11 **14**

Equation 2.12

The solid state IR spectrum of **14** shows a large number of ν(CO) bands at 1964, 1937, 1885, 1865 and 1720 cm^{-1}. Comparison with the IR data for **10** suggests that those at 1964 and 1885 cm^{-1} are likely to be attributable to the A_1- and E-type ν(CO) stretching modes of the monomeric Mg–Co complex (assuming local approximate C_{3v} symmetry). The peaks at 1937, 1865 and 1720 cm^{-1} are likely the result of a secondary species which exhibits Mg(μ-OC)Co isocarbonyl interactions. The solution IR spectrum of **14** in toluene shows ν(CO) bands at 1970, 1910, 1890, 1836 and 1755 cm^{-1}, again consistent with two species with at least one band in the range indicating an isocarbonyl interaction. These data contrast with those of **10**, which showed no significant low frequency ν(CO) bands in solution or the solid state and was confirmed to be Mg–Co bonded by X-ray crystallography.

2.7 Reactivity studies of amidinate-supported Mg–TM bonded compounds

A principal motivation for the synthesis of amidinate supported Mg–TM bonded compounds was the potential for greater reactivity compared with the β-diketiminate supported compounds. The Mg–Fe bonded compounds **8** and **12** reacted with MeI in C_6D_6 on the NMR-tube scale to produce the known product MeFp and a product with one set of ligand environments by ^{1}H NMR, assumed to be (L)MgI(THF) in both cases. This demonstrates that both **8** and **12** act a source of the Fp^- anion, replicating the reactivity previously demonstrated by **2.16**.[4]

Each of the Mg–TM bonded compounds synthesised was screened for reactivity with TolNCNTol, ^{i}PrNCN^{i}Pr, ^{t}BuNCO, CO_2 and CS_2 on the NMR-tube scale in C_6D_6. These reactions were monitored by ^{1}H NMR and also by ^{31}P{^{1}H} NMR in the case of the {$Co(CO)_3(PCy_3)$} containing compounds. Every compound reacted with the carbodiimides in an uncontrolled fashion giving complex mixtures of products.

Reactions occurred more slowly with TolNCNTol than with ^{i}PrNCN^{i}Pr, which typically took place immediately. The ^{1}H NMR spectra typically showed several ligand environments in addition to the common decomposition products of the TM anions (Fp_2, Rp_2 and RpH, and $[Co(CO)_3(PCy_3)]_2$). In the case of the cobalt compounds, decomposition to $[Co(CO)_3(PCy_3)]_2$ was more clearly indicated in the $^{31}P\{^{1}H\}$ NMR spectrum. Reactions with ^{t}BuNCO produced a mixture of products including substantial quantities of the common decomposition products, which were identifiable by NMR. This was also the case with reactions with CO_2, which produced the TM decomposition products as the primary product alongside unidentifiable ligand-containing species.

The reaction of **12** with CS_2 in C_6D_6 was monitored by ^{1}H NMR. The reaction mixture contained two Cp environments and two sets of ligand environments. One Cp resonance corresponds to Fp_2, implying a decomposition mechanism is in operation during the reaction. One set of ligand environments should therefore correspond to the decomposition of the corresponding (L)Mg moiety. The remaining Cp and ligand environments likely belong to a possible product. Given the previous reactivity of Mg–Fe bonded **2.16**, it is likely an insertion reaction of the CS_2 into the Mg–Fe bond of **12** is responsible for this unknown product. Unfortunately, the mixture of products was inseparable and all attempts to isolate any product besides Fp_2 were unsuccessful. In order to test the hypothesis of an insertion reaction between **12** and CS_2, a parallel synthesis was devised for the predicted product, $\{MesC(NMes)_2\}Mg(S_2CFp)$ (**15**).

Angelici *et al*. have previously described the *in situ* synthesis of $Na[S_2CFp]$ (**2.26**),[82] a dithiocarboxylate anion formed from the reaction of CS_2 with NaFp in THF. The potassium anaologue was later spectroscopically characterised by Ellis *et al*.[83] This species was employed by Cutler *et al*. for the synthesis of $Cp_2Zr(Cl)S_2CFp$ (**2.27**) from Cp_2ZrCl_2 (Scheme 2.10),[84] during their investigations into insertion reactions of CE_2 (E = O, S) into Zr–Fe bonds.[84–86] Cutler *et al*. have also reported the synthesis of $Cp_2Zr(Cl)O_2CFp$ (**2.28**) through an analogous method.[85,86] They found that **2.28** could also be synthesised *via* insertion of CO_2 into the Zr–Fe bond of $Cp_2Zr(Cl)Fp$. Compound **2.27** could not be synthesised through the analogous insertion reaction with CS_2 and was only accessible *via* the stepwise synthetic process described above. Quantities of Fp_2 were present in the reaction mixture of both insertion reactions of CE_2 (E = O, S) into $Cp_2Zr(Cl)Fp$.

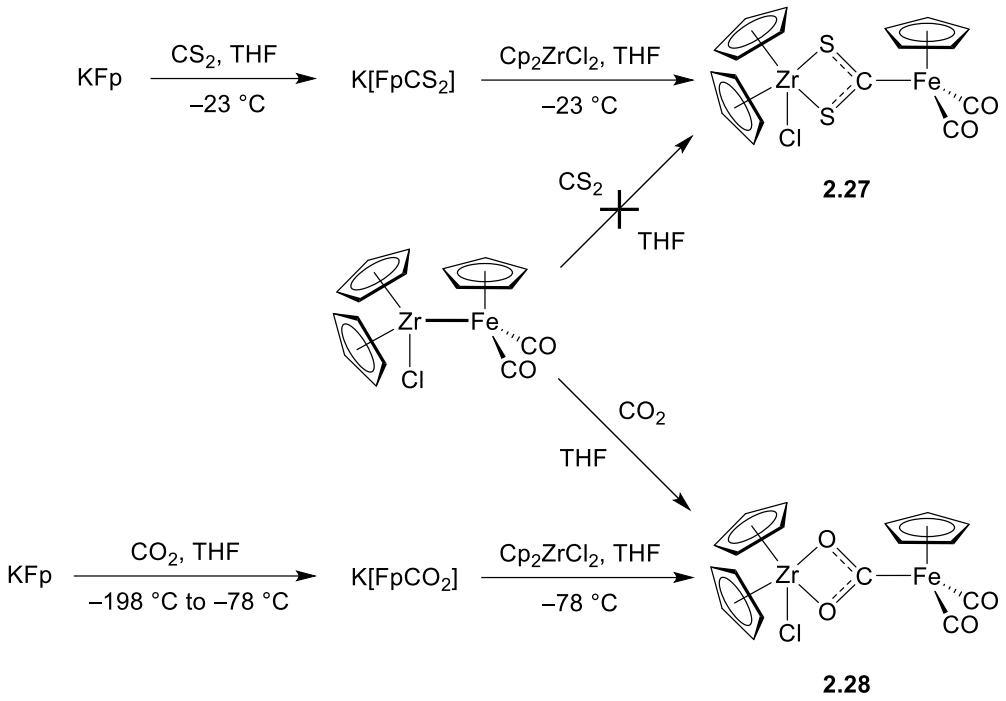

Scheme 2.10 Synthesis of a $Cp_2Zr(Cl)E_2CFp$ (E = O (**2.28**), S (**2.27**)) *via* stepwise and direct insertion reactions.[84–86]

A similar method to that of Cutler *et al*. was employed for the synthesis of **15**, the suspected product of the insertion reaction between **12** and CS_2. Reaction of CS_2 with KFp in THF formed the metallodithiocarboxlate species $K[FpCS_2]$, which was reacted *in situ* with **11** to give **15** (Scheme 2.11). The ^{1}H NMR spectrum contained only one product, the resonances of which matched perfectly to those found in the NMR-tube scale reaction of **12** with CS_2 (Figure 2.13). The quantity of Fp_2 formed from this reaction was negligible (< 2% by integration in the ^{1}H NMR spectrum of the crude reaction mixture). Attempted extraction with benzene gave the product alongside roughly 20% Fp_2 (by integration). The pure product was therefore isolated by extraction with THF at −70 °C to give **15**·2.5(THF).

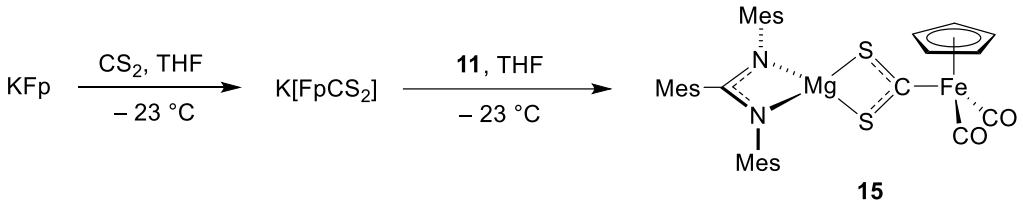

Scheme 2.11 Stepwise synthesis of $\{MesC(NMes)_2\}Mg(S_2CFp)$ (**15**).

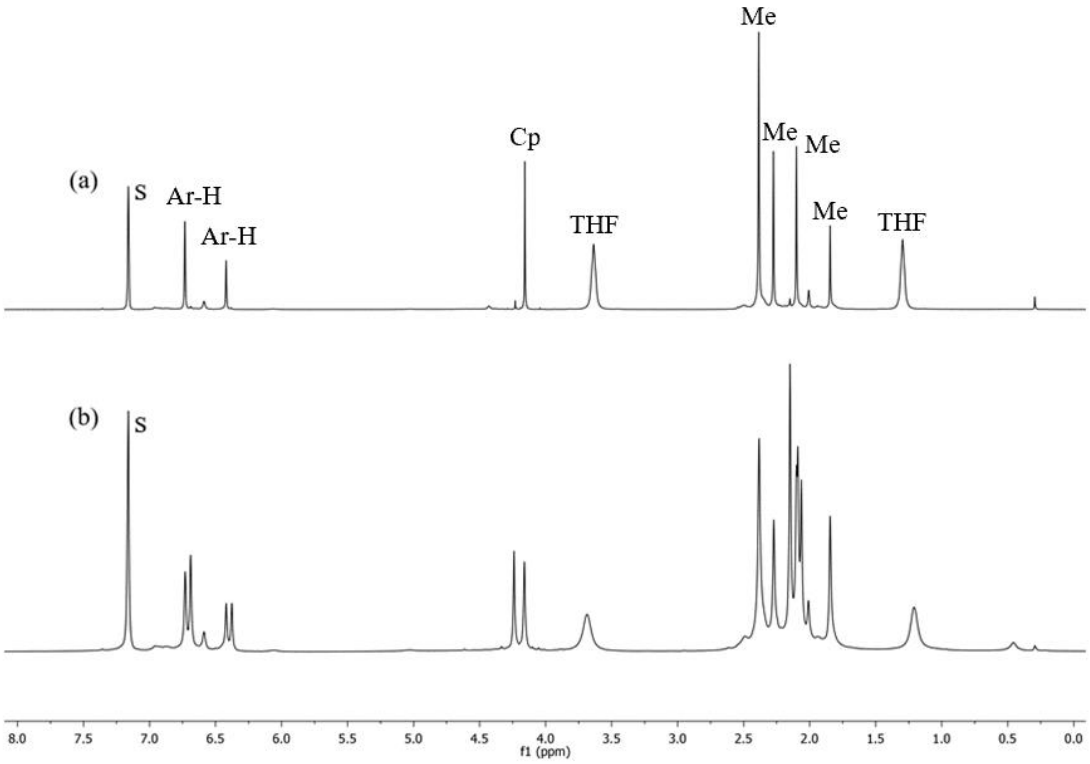

Figure 2.13 ^{1}H NMR (C_6D_6, 400.2 MHz) spectra of {MesC(NMes)$_2$}Mg(S_2CFp)·2.5(THF) (**15**, a), and the reaction of {MesC(NMes)$_2$}Mg(THF)Fp (**12**) with CS_2 (b). 's' denotes residual protio solvent.

These ^{1}H NMR spectra clearly show that the same product is formed from both reactions. Unfortunately, no crystals of **15** could be grown, and structural authentication was not possible. Nevertheless, the parallel syntheses of **15**, coupled with the precedent provided by Cutler *et al*.,[84] indicate that **15** is the likely product of these reactions.

The solid state IR spectrum of **15** shows ν(CO) bands at and 2021 and 1971 cm^{-1} indicating a terminal Fp moiety with no isocarbonyl interactions, consistent with the suggested structure. These bands appear at higher frequency than those observed for the parent compound **12** (ν(CO) 1921, 1861 cm^{-1}). This increase in ν(CO) frequency upon insertion into a Mg–Fp bond has been observed previously by Mountford *et al*. The metalloamidinate compound **2.17** has higher frequency ν(CO) bands (2010 and 1956 cm^{-1}) than the parent Mg–Fe bonded compound **2.16** (ν(CO) 1926, 1857 cm^{-1}). In both of these cases the formal oxidation state of Fe increases from Fe(0) to Fe(II) upon insertion of a substrate into the Mg–Fe bond. The decrease in electron density at the Fe(II) centre results in less back-bonding to the CO ligands and, hence, stronger CO

bonds with a higher ν(CO) stretching frequencies in both **15** and **2.17**. The ν(CO) bands of **15** are also comparable to those reported by Cutler *et* al. for **2.27** (ν(CO) 2034, 1987 cm^{-1}). The IR spectrum of **15** also shows ν(SCS) bands at 951 and 851 cm^{-1}, which are comparable to those reported by Cutler *et al*. for **2.27** (ν(SCS) 934, 851 cm^{-1}).

Given the successful identification of a sole product (albeit alongside a substantial quantity of decomposition product) from the reaction of **12** with CS_2, the remaining N-Mes amidinate Mg–TM complexes (**13** and **14**) were selected for investigation. The NMR-tube scale reaction of **13** with CS_2 in C_6D_6 showed extremely slow conversion (reaction time > 4 days) to an unknown product accompanied by decomposition to Rp_2 and RpH, evident in the Cp region of the ^1H NMR spectrum. When this reaction was repeated at 50 °C, the starting material was consumed within 24 hours. However, the formation of Rp_2 and RpH was much more pronounced. The presence of the unidentified product accompanied by decomposition products suggests that the reactions taking place are similar for the Mg–Fe and Mg–Ru compounds. The unidentified Cp-containing product of this reaction is therefore assumed to be the Ru analogue of **15**, {MesC(NMes)$_2$}Mg(S_2CRp). Due to the uncontrolled reactivity, the expense associated with the use of Ru compounds and the similar reactivity of Fp and Rp, this reaction was not investigated further. The reaction of **14** with CS_2 in C_6D_6 on the NMR-tube scale resulted in the total decomposition to $[Co(CO)_3(PCy_3)]_2$, evident by ^1H and $^{31}P\{^1H\}$ NMR. No other Co containing products were present in the reaction mixture.

It is evident from these reactivity studies that complex decomposition pathways are in operation during practically all reactions of the amidinate supported Mg–TM bonded complexes. The mechanisms of these decompositions are not well understood. However, it is not uncommon for reactions of Fp containing species to result in the formation of the homocoupled product (Fp_2) alongside the desired compound. For example, the reaction between FpI and Grignard reagents (RMgX), published by Turnbull and Li, resulted in the formation of Fp_2 and R_2 alongside the desired products, FpR.[87] The authors suggest that this result is possible *via* either a polar mechanism or through a free-radical mechanism.

The reaction of **12** with trityl chloride in C_6D_6 on the NMR-tube scale was performed and monitored by ^1H NMR (Equation 2.13). If only a simple S_N2 reaction is possible the expected products would be {MesC(NMes)$_2$}Mg(THF)Cl and Ph_3CFp (in a similar

fashion to the reaction of **12** with MeI). In fact, the products of the reaction were identified as Fp_2, Gomberg's dimer ($Ph_3CCH(C_6H_4)CPh_2$) and a product with one set of ligand environments, ostensibly {MesC(NMes)$_2$}Mg(THF)Cl. The reaction is instantaneous, so a mechanism is difficult to elucidate. Trityl chloride has been reported to act as a one-electron oxidant and has been employed in several instances for the oxidation of Ce(III) to Ce(IV).[88,89] In this case trityl chloride probably acts as a one-electron oxidant towards **12** giving {MesC(NMes)$_2$}Mg(THF)Cl, $Fp^{\bullet}$ and $Ph_3C^{\bullet}$. The Fp radical ultimately ends as a constituent of Fp_2; whether this occurs by combining with another $Fp^{\bullet}$ or by abstracting a Fp moiety directly from another molecule of **12** is unclear. The exceptional reactivity expected of Fp radicals makes both routes a possibility. $Ph_3C^{\bullet}$ are persistent radicals in solution which are unable to couple to form hexaphenylethane.[90] These radicals instead exist in equilibrium with the so-called 'Gomberg dimer' ($Ph_3CCH(C_6H_4)CPh_2$),[91] which has characteristic resonances in the ^{1}H NMR spectrum at δ = 4.92, 5.92, 6.44 and 7.07-7.30 ppm in C_6D_6.[92] This result may suggest that radical mechanisms are operative in the reactions of the Mg–TM compounds. While not conclusive this reaction provides some insight into the possible mechanisms for the formation of homocoupled TM products *e.g.* Fp_2.

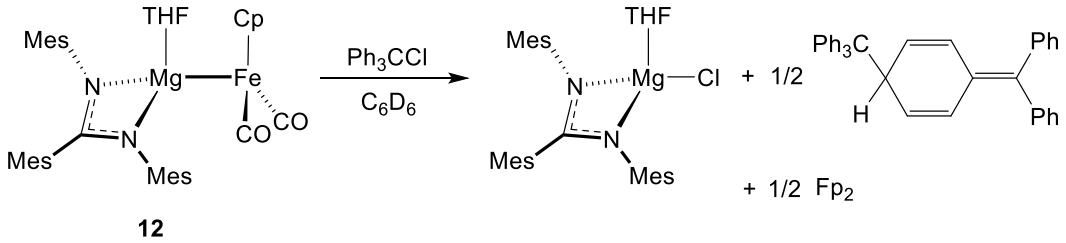

Equation 2.13

The Fp^- anion is understood to participate in radical-type reactions and single-electron transfer (SET) processes.[75] Indeed, a persistent Fe radical with a structurally similarity to Fp has been prepared and isolated by Sitzmann *et al*. $[(C_5{}^iPr_5)Fe(CO)_2]^{\bullet}$ (**2.29**) was prepared from the reduction of $(C_5{}^iPr_5)Fe(CO)_2Br$ with an equimolar quantity of potassium in THF and from the oxidation of $K[(C_5{}^iPr_5)Fe(CO)_2]$ with 1 equiv. of $Ag[BF_4]$ (Scheme 2.12).[93] The monomeric nature of **2.29** in solution was confirmed by IR and EPR spectroscopies and magnetic susceptibility measurements. However, when crystallised from petroleum ether, **2.29** was obtained as a carbonyl-bridged dimer. Clearly, the persistence of **2.29** as an Fe-based radical is a result of the sterically protecting nature of the bulky substituted cyclopentadienyl ligand. In contrast, the lack

of any sterically protecting groups would make Fp• exceptionally reactive and only detectable as a reactive intermediate. Nevertheless, the synthesis of **2.29** supports the idea of Fp• as an accessible reactive intermediate in the chemistry of Fp containing compounds.

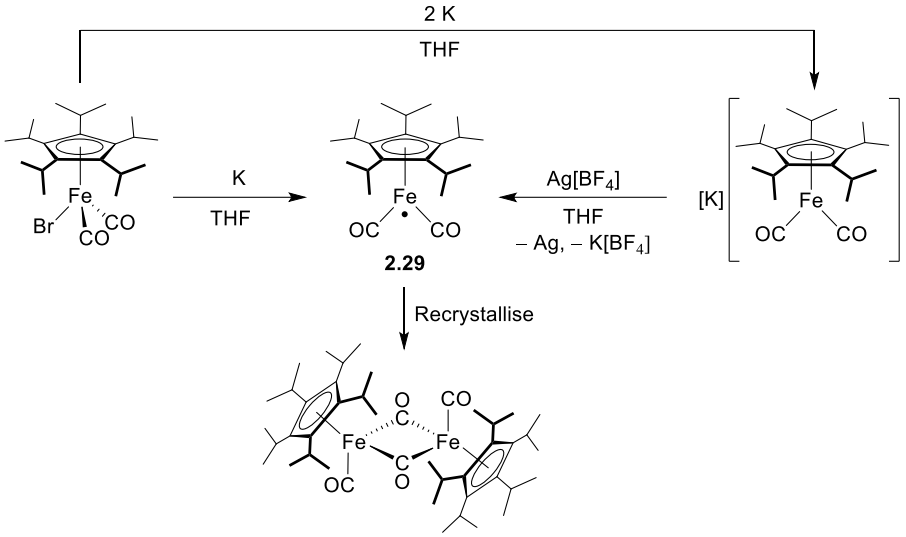

Scheme 2.12 Synthesis of a sterically protected cyclopentadienylirondicarbonyl radical.[93]

Krusic *et al*. have published spectroscopic evidence of free-radicals in the reaction between NaFp and various alkyl halides (including ^{i}PrI, ^{n}BuI, ^{sec}BuI and ^{t}BuI).[94] When performed in a mixing cell within an ESR spectrometer, these reactions produced clear resonances arising from the corresponding alkyl radicals. The authors surmise that at least one radical-based reaction is in competition with the traditional S_N2 reaction.

Beletskaya *et al*. have proposed an alternative mechanism for the homocoupling of TM carbonyl anions.[95,96] The Halogen Metal Exchange pathway (HME, Scheme 2.13) begins with attack by the TM nucleophile on the halogen of the R–X compound, forming TM–X. A further equivalent of TM nucleophile then attacks the TM–X species eliminating X^- and TM_2. This mechanism was found to be operational in reactions involving $[Re(CO)_5]^-$ with polyfluorinated vinyl halides. Evidence was provided that supports this mechanism in the analogous reaction of Fp^- with the same polyfluorinated vinyl halides, but this was described by the authors as "less than conclusive".[95] It is possible that both the HME mechanism and the radical-type mechanism are accessible in the chemistry of TM^- compounds and exist in competition with each other. The

prevalence of one mechanism over another is therefore likely the result of the particular properties of the reactants under study.

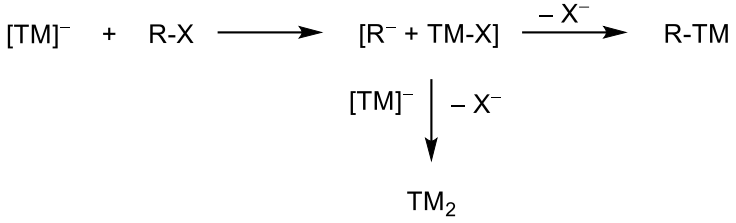

Scheme 2.13 Halogen Metal Exchange (HME) mechanism for the homocoupling of transition metal anions.[96]

The potential for amidinate ligands to allow for greater reactivity in Mg–TM bonded complexes has been clearly demonstrated. The β-diketiminate supported **2.16** was shown to be limited in its reactivity while all amidinate supported Mg–TM complexes have been shown to react with a wide range of small molecules. Unfortunately, the reactivity of these amidinate compounds is perhaps too great, giving uncontrolled reactions and substantial decomposition to homocoupled TM dimers. The issue of decomposition has been addressed *via* the consideration of two potential mechanisms. However, due to the rapid nature of these reactions and the difficulty in separating out any potential products it was difficult to perform any mechanistic studies. These reactions were therefore not studied further.

2.8 Synthesis of a Mg–Fe bonded complex supported by the N,N'-bis(diisopropylphenyl)guanidinate ligand

Part of the preliminary studies for work in this section was performed alongside a Part II student, Alicia Walker. These studies formed a Part II research project which was designed by me, based on my work, and was carried out under my direct supervision.

Guanidinate ligands, $R'_2NC(NR)_2$ (R, R' = alkyl, aryl) are structurally similar to amidinate ligands in that both are N,N'-bidentate ligands which form a 4-membered chelate with metal atoms. Donation of electron density from the additional N atom in the distal position gives guanidinate ligands subtly different electronic properties from their amidinate counterparts. The additional resonance structure available to guanidinate ligands (Figure 2.14) results in an increase in the overall Lewis basicity of the ligand which can potentially increase the strength of interaction with Lewis acidic metal centres.[97]

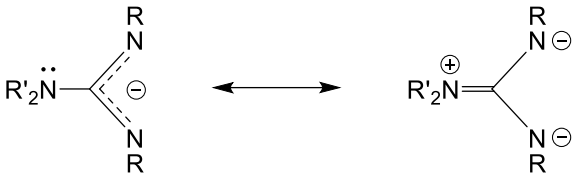

Figure 2.14 Resonance structures of guanidinate ligands.[97]

The Dipp substituent was selected as the R group for the guanidinate ligand due to the success of compounds featuring this substituent in β-diketiminate and amidinate systems. A range of guanidinate ligands have been reported with bulky R' groups,[69] these substituents offer very little steric protection for the metal centre and are typically selected for their solubilising properties. The solubilising Dipp groups remove the need for additional solubilisation, hence a simple NMe_2 group was selected for its simple NMR resonance and ease of access.

The reaction of $LiNMe_2$ with **5** in THF followed by aqueous work up and extraction into Et_2O gave $Me_2NC(NDipp)(NHDipp)$ (**16**, Equation 2.14) in 69% isolated yield. Work in our group suggested that the formation of a metal lithiate complex would be problematic for further syntheses. Isolation of the guanidine avoids the possibility of lithiate complex formation by completely removing Li from the product before further reaction. Crystals of **16** were grown from slow evaporation of a hexane solution at RT. The molecular structure and selected distances and angles for **16** are shown in Figure 2.15 and Table 2.5.

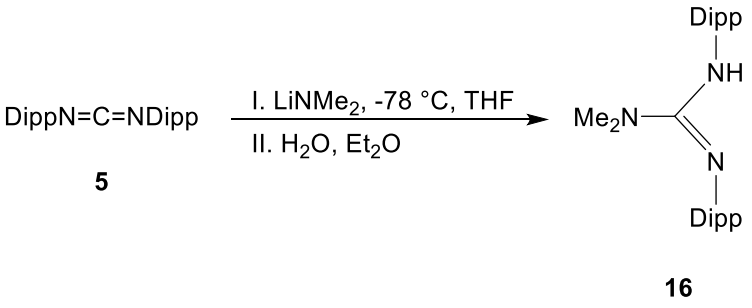

5 **16**

Equation 2.14

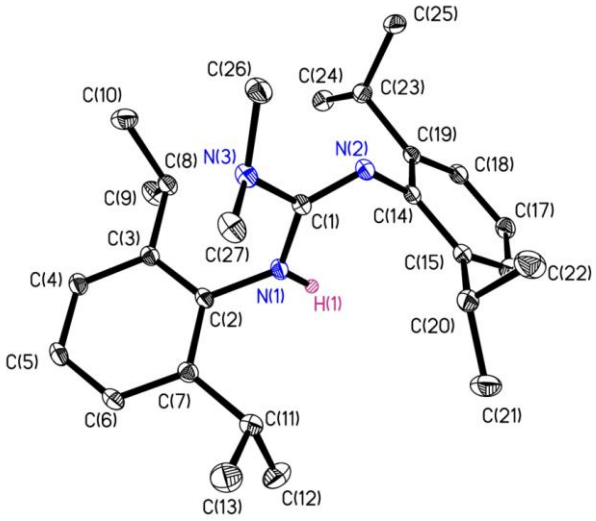

Figure 2.15 Displacement ellipsoid plot (20% probability) of $Me_2NC(NDipp)(NHDipp)$ (**16**). C-bound H atoms omitted for clarity.

Table 2.5 Selected distances (Å) and angles (°) for $Me_2NC(NDipp)(NHDipp)$ (**16**).

N(1)–H(1)	0.886(18)	N(1)–C(1)	1.3777(17)
N(2)–C(1)	1.2821(17)	N(3)–C(1)	1.4004(18)
N(1)–C(1)–N(2)	124.92(13)	N(1)–C(1)–N(3)	114.83(11)
N(2)–C(1)–N(3)	120.25(12)		

Compound **16** is monomeric in the solid state which is surprising given the potential for hydrogen bonding. This is probably a consequence of the bulky Dipp groups preventing oligomerisation. All distances and angles are within expected values and are comparable to a similar compound reported by Jones *et al*., $^{i}Pr_2NC(NDipp)(NHDipp)$ (**2.30**).[98]

Reaction of **16** with MeMgI in Et_2O gave $\{Me_2NC(NDipp)_2\}MgI(OEt_2)$ (**17**, Equation 2.15) in 95% isolated yield. Diffraction-quality crystals were obtained from a benzene solution at RT. The molecular structure and selected distances and angles for **17** are shown in Figure 2.16 and Table 2.6.

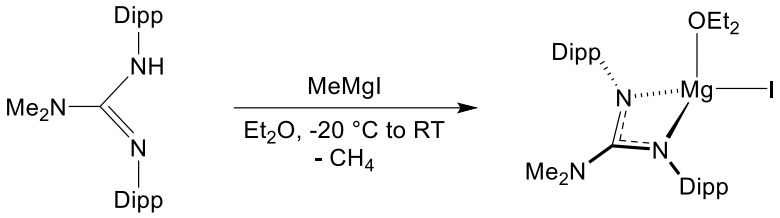

16 **17**

Equation 2.15

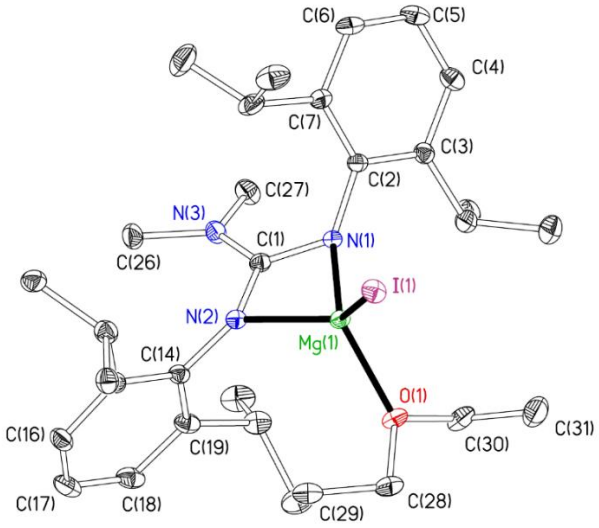

Figure 2.16 Displacement ellipsoid plot (20% probability) of $\{Me_2NC(NDipp)_2\}MgI(OEt_2)$ (**17**). H atoms omitted for clarity.

Table 2.6 Selected distances (Å) and angles (°) for $\{Me_2NC(NDipp)_2\}MgI(OEt_2)$ (**17**).

Mg(1)–I(1)	2.6500(13)	Mg(1)–N(1)	2.052(3)
Mg(1)–N(2)	2.040(3)	Mg(1)–O(1)	2.029(3)
N(1)–C(1)	1.351(5)	N(2)–C(1)	1.355(5)
N(3)–C(1)	1.355(5)		
I(1)–Mg(1)–N(1)	126.28(10)	I(1)–Mg(1)–N(2)	129.76(11)
N(1)–Mg(1)–N(2)	66.86(13)	I(1)–Mg(1)–O(1)	105.59(10)
N(1)–Mg(1)–O(1)	116.14(13)	N(2)–Mg(1)–O(1)	108.16(14)
Mg(1)–N(1)–C(1)	89.9(2)	Mg(1)–N(2)–C(1)	90.4(2)
N(1)–C(1)–N(2)	112.8(3)	N(1)–C(1)–N(3)	123.7(3)
N(2)–C(1)–N(3)	123.4(3)		

Compound **17** is monomeric in the solid state with an approximately tetrahedral Mg centre. This contrasts with the analogous compound reported by Jones *et al*., {^{i}Pr$_2$NC(NDipp)$_2$}Mg(μ-I)$_2$Mg(OEt$_2$){(NDipp)$_2$CN^{i}Pr$_2$} (**2.31**), which is dimeric in the solid state.[72] It is unclear why substitution of the distal methyl groups for isopropyl groups would lead to dimerisation of the compound. Since both compounds contain Dipp groups proximal to the metal chelating cavity this result is unlikely to be steric in nature. A clear observation is that **17** contains one coordinated Et$_2$O unit per Mg centre, while **2.31** contains only 0.5 Et$_2$O units per Mg centre. The authors report that **2.31** was dried *in vacuo* before recrystallisation from hexane; it is possible that this method results in partial removal of Et$_2$O from the compound which causes dimerisation in order to satisfy an electron-deficient metal centre. Comparable distances and angles are similar between **17** and **2.31** with the obvious exception of Mg–I bonds which are lengthened in **2.31** as a result of the bridging interactions.

The reaction of **17** with KFp in THF was unsuccessful. When performed on the NMR-tube scale in THF-d_8 no evidence of reaction could be observed. THF is a stronger Lewis base than Et$_2$O and should be expected to displace the latter, giving {Me$_2$NC(NDipp)$_2$}MgI(THF). It is possible that this complex is more inert with respect to reactions with nucleophiles such as Fp$^-$ and may explain why **17** does not react in THF.

The same reaction in benzene gave dimeric [{Me$_2$NC(NDipp)$_2$}MgFp]$_2$ (**18**, Equation 2.16). Diffraction-quality crystals of **18** were grown from a benzene solution at 5 °C. The molecular structure and selected distances and angles for **18** are shown in Figure 2.17 and Table 2.7.

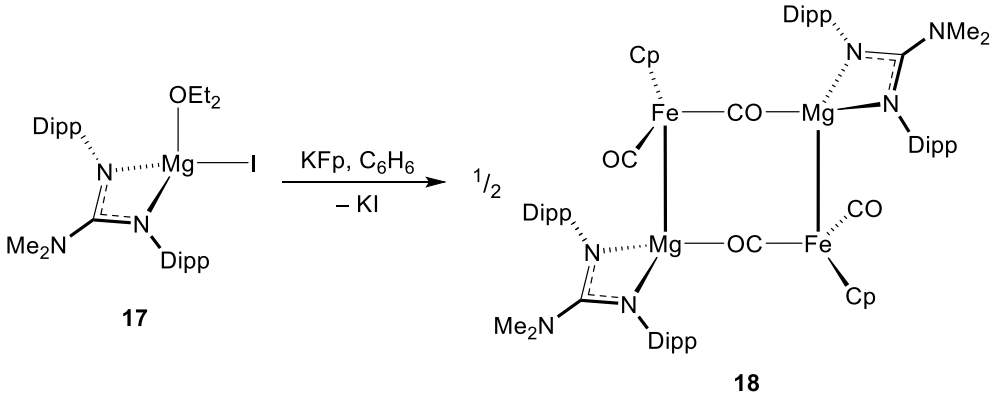

Equation 2.16

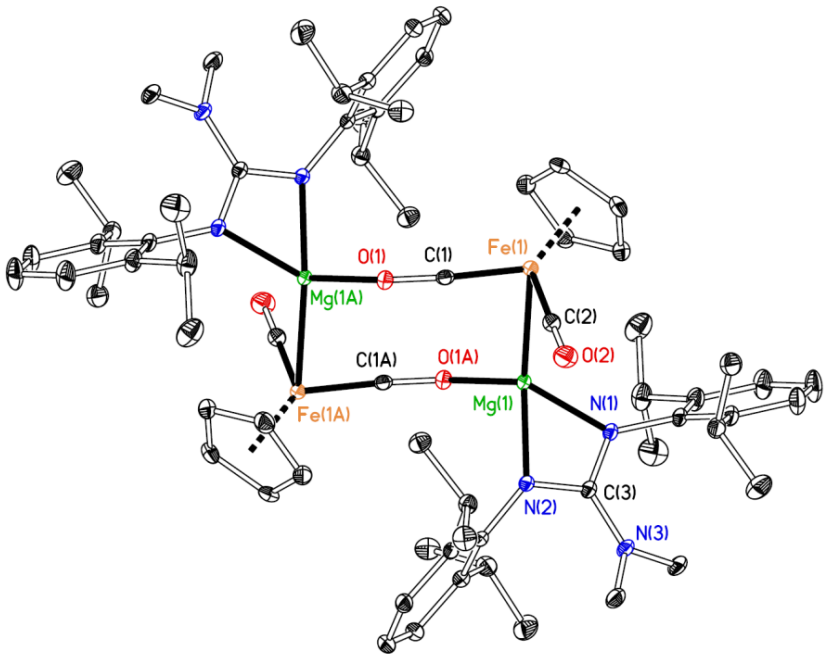

Figure 2.17 Displacement ellipsoid plot (20% probability) of [{$Me_2NC(NDipp)_2$}MgFp]$_2$ (**18**). H atoms omitted for clarity. Atoms carrying the suffix 'A' are related to their counterparts by the symmetry operator 1-x, 1-y, 1-z.

Compound **18** is dimeric in the solid state with two {$Me_2NC(NDipp)_2$}MgFp units connected by Mg(μ-OC)Fe isocarbonyl interactions forming an eight-membered ring structure. The geometry at each four-coordinate Mg is approximately tetrahedral with two bonds to the κ_2-guanidinate ligand and one bond each to an Fe atom and a μ-isocarbonyl group. The centrosymmetric ring structure contains one unique Mg–Fe bond (2.5279(4) Å), significantly shorter than the sum of the respective covalent radii (2.73(8) Å).[77] Compound **18** contains the shortest reported Mg–Fe bond to date[3] closely followed by Kays' **1.37** (2.530(3) Å).[7]

As previously observed for structures of this type,[5] the carbonyl group engaged in the isocarbonyl bridging interaction (C(1)O(1)) experiences a perturbation of its electron density compared to the terminal carbonyl group (C(2)O(2)). Consequently, the C(1)–O(1) distance (1.1919(15) Å) is lengthened compared to that in C(2)–O(2) (1.1567(18) Å). In addition, the Fe(1)–C(1) distance (1.6985(12) Å) is shortened compared to Fe(1)–C(2) (1.7469(14) Å).

Table 2.7 Selected distances (Å) and angles (°) for [{$Me_2NC(NDipp)_2$}MgFp]$_2$ (**18**).

Mg(1)–Fe(1)	2.5279(4)	Mg(1)–N(1)	2.0620(10)
Mg(1)–N(2)	2.0627(10)	Mg(1)–O(1A)	2.0552(10)
Fe(1)–C(1)	1.6985(12)	Fe(1)–C(2)	1.7469(14)
Fe(1)–$Cp_{cent(1)}$	1.436	N(1)–C(3)	1.3422(16)
N(2)–C(3)	1.3510(15)	N(3)–C(3)	1.3674(16)
C(1)–O(1)	1.1919(15)	C(2)–O(2)	1.1567(18)
Fe(1)–Mg(1)–N(1)	121.23(3)	Fe(1)–Mg(1)–N(2)	137.58(3)
Fe(1)–Mg(1)–O(1A)	108.46(3)	N(1)–Mg(1)–N(2)	66.00(4)
N(1)–Mg(1)–O(1A)	116.84(4)	N(2)–Mg(1)–O(1A)	101.70(4)
Mg(1)–Fe(1)–C(1)	84.78(4)	Mg(1)–Fe(1)–C(2)	79.54(4)
Mg(1)–Fe(1)–$Cp_{Cent(1)}$	113.43	C(1)–Fe(1)–C(2)	94.70(6)
C(1)–Fe(1)–$Cp_{Cent(1)}$	131.56	C(2)–Fe(1)–$Cp_{Cent(1)}$	131.48
Mg(1)–N(1)–C(3)	90.57(7)	Mg(1)–N(2)–C(3)	90.30(7)
N(1)–C(3)–N(2)	113.05(10)	N(1)–C(3)–N(3)	124.18(11)
N(2)–C(3)–N(3)	122.76(11)		
[a] Hinge Angle	128		

[a] Hinge angle = (Fe(1), C(1), O(1), Fe(1A), C(1A), O(1A))-(Fe(1), Mg(1), O(1A))

The effects of perturbation of electron density in carbonyl ligand is well understood. In the case of **18** the donation of electron density from O(1) to Mg(1A) results in depletion of electron density available in the C(1)O(1) group. The back-donation of electron density from Fe(1) to the carbonyl group also increases as a consequence. These synergic effects collectively increase the electron density in the C(1)–O(1) antibonding orbital and the Fe(1)–C(1) bonding orbital, resulting in lengthened and shortened interactions, respectively.

Compound **18** is unusual in that it is the first Mg–Fe bonded complex to be isolated "base-free" *i.e.* without coordinated solvent. All Mg–Fe bonded compounds reported prior to **18** featured coordinated THF in the final structure. Kays' **1.37** is the only other structurally authenticated Mg–Fe bonded structure which has been isolated base-free.[7] Both **18** and **1.37** were synthesised in non-donor solvents (benzene and toluene, respectively), while all other Mg–Fe bonded compounds have been synthesised in THF. It is possible that during the synthesis of **18** and **1.37** the coordinated solvent in the

precursor compound (Et_2O in **17** and THF in **1.34**, respectively) is displaced does not re-coordinate to the final product. This is perhaps less surprising for **17** since Et_2O is a weaker Lewis base than THF.

The internal eight-membered ring structure, comprised of alternating M–M' bonds and M(μ-OC)M' interactions, found in **18** is the same as that that observed in **1.39**, reported by Blake and Mountford.[5] This type of metal-metal bonding within an eight-membered ring structure is remarkably rare; in addition to the Mg–Fe bonded structure **1.39** Mountford *et al*. have reported Ca–Fe (**1.41**),[9] Yb-Fe (**1.42**),[9] and Mg–Co (**1.46**)[5] bonded analogues from the reduction of TM dimers with Ae amalgams. These structures were detailed in Chapter One. Several other structures have been reported which feature this structural motif. $[Pb\{Cp^*Mo(CO)_3\}_2]_2$ (**2.32**),[99] reported by Lappert *et al*. in 1987, and $[\{(DAB)B\}Al\{Fe(CO)_4\}(THF)]_2$ (**2.33**),[100] reported by Jones *et al*. in 2017, possess this ring formation within discrete molecular structures. Shore *et al*. reported two polymeric structures, $[\{(MeCN)_3YbFe(CO)_4\}_2\cdot MeCN]_\infty$ (**2.34**)[101,102] and $[(MeCN)_3YbFe(CO)_4]_\infty$ (**2.35**),[102] both of which feature analogous 8-membered ring formations within infinite polymeric structures. More recently, Kempe *et al*. reported $[(THF)_2YbRp_2]_\infty$ (**2.36**),[39] which features analogous, vertex-sharing 8-membered rings as the core structural component in polymeric chains. The molecular structures of these compounds are shown in Figure 2.18.

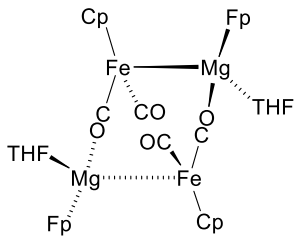

1.39

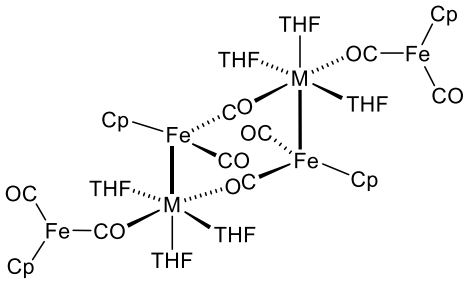

M = Ca (**1.41**) or Yb (**1.42**)

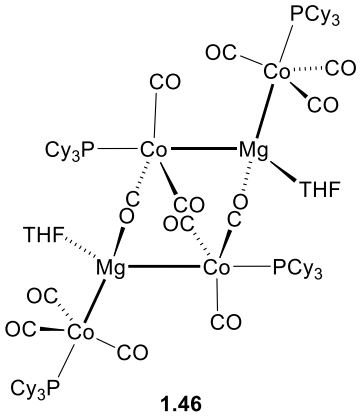

1.46

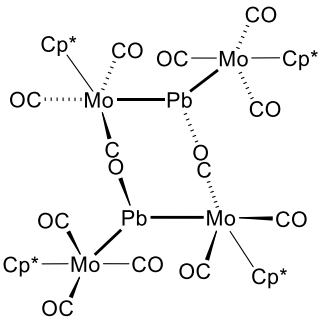

2.32

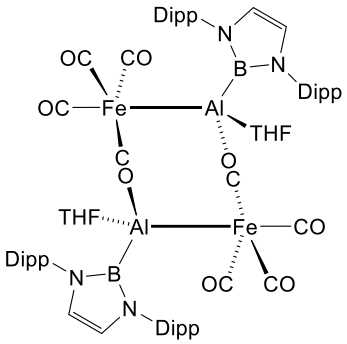

2.33

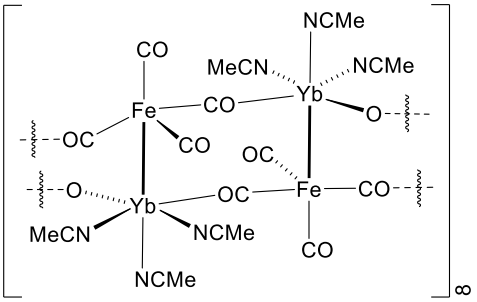

$[\{(MeCN)_3YbFe(CO)_4\}_2 \cdot MeCN]_\infty$

2.34

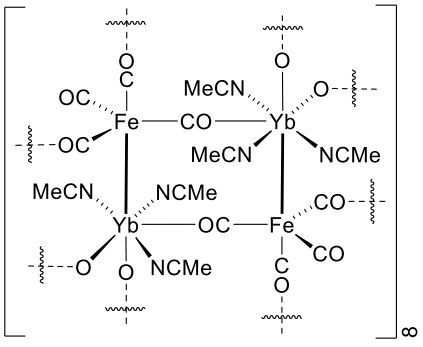

$[(MeCN)_3YbFe(CO)_4]_\infty$

2.35

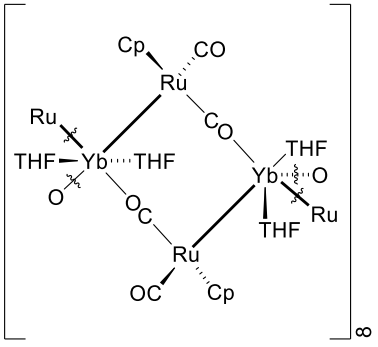

$[(THF)_2YbRp_2]_\infty$

2.36

Figure 2.18 Structurally authenticated complexes containing eight-membered ring structures comprised of M–M' and M(μ-OC)M' interactions.[5,9,39,99–102]

The centrosymmetric ring structure of **18** adopts a chair conformation where Fe(1), O(1), C(1), Fe(1A), O(1A) and C(1A) are coplanar. Mg(1) and Mg(1A) occupy positions above and below this plane. The angle between these atoms and the plane is referred to as the "hinge angle" (Figure 2.19). The hinge angle found in **18** (128°) is considerably more acute than those found in other eight-membered Ae–TM bonded rings of this type. Indeed, **18** has the second most acute hinge angle of any of these eight-membered ring structures after Jones' Al–Fe bonded structure (125°).[100]

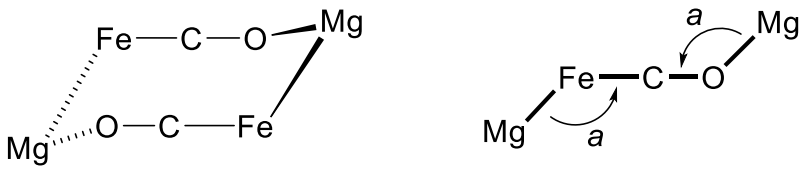

Figure 2.19 Simplified ring structure of [{$Me_2NC(NDipp)_2$}$MgFp]_2$ (**18**, left) and depiction of the hinge angle (a, right).

The solid state IR spectrum of **18** shows two main ν(CO) bands at 1944 and 1778 cm^{-1}, consistent with the structure determined by X-ray crystallography. The lower frequency band results from the weakened C≡O bond as a consequence of the bridging isocarbonyl interaction. The solution IR spectrum of **18** in toluene also shows a low frequency ν(CO) band at 1781 cm^{-1}, consistent with preservation of the isocarbonyl interaction in solution. The solution IR spectrum in THF is dominated by two major high frequency ν(CO) bands (2014 and 1946 cm^{-1}), consistent with dissociation to a monomeric structure without isocarbonyl bridging, most probably the THF adduct {$Me_2NC(NDipp)_2$}MgFp(THF) (**19**). This result is supported by diffusion NMR experiments (*vide infra*).

The dissolution of **18** in THF followed by removal of volatiles *in vacuo* afforded **18** unchanged. This result was verified by comparison of the NMR and IR spectra of the compound before and after exposure to THF. The results of the solution phase IR study of **18** suggest that the dimeric complex dissociates in THF to a monomeric species (**19**, Equation 2.17). This result suggests that exposure of hypothetical compound **19** to vacuum removes the coordinated THF to reform the dimeric **18**.

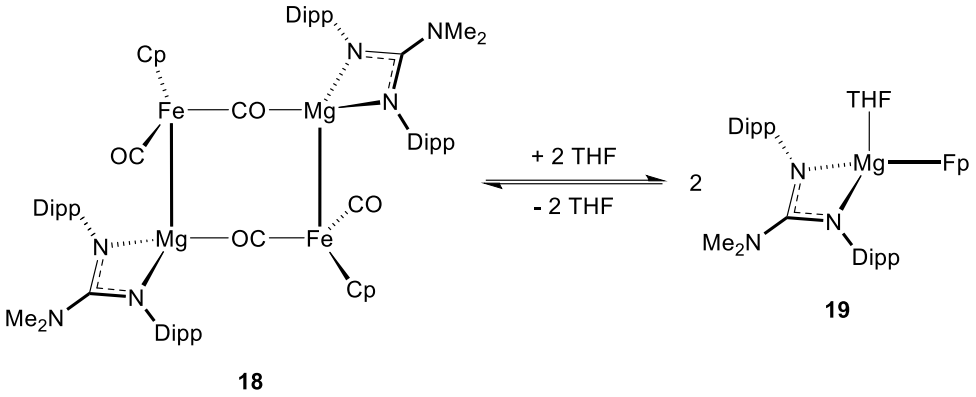

18 **19**

Equation 2.17

2.9 Reactivity of a guanidinate supported Mg–TM bonded compound

The reactivity of **18** was tested with several small molecules in C_6D_6 on the NMR-tube scale. The reaction of **18** with MeI was slow compared to amidiate complexes **8** and **12**, which were instantaneous. The reaction produced **17** and MeFp alongside Fp_2. This contrasts again with the reactivity displayed by **8** and **12**, which produced no Fp_2 upon reaction with MeI. It is possible that the dimeric nature of **18** partially arrests its reactivity and is responsible for its slower reaction times. The decomposition to Fp_2 is possibly the result of a halogen metal exchange reaction, discussed previously for the reactions of the amidinate compounds (Scheme 2.13, *vide supra*).

The reaction of **18** with TolNCNTol gave a complex mixture of products which could not be identified. Reaction with ^{i}PrNCN^{i}Pr gave Fp_2 as the only Cp-containing product and unknown ligand containing species. The same result was observed for the reaction of **18** with CO_2. The reactions of **18** with either CS_2 or TolNCO gave significant quantities of protio-ligand in the ^{1}H NMR. As a result of extensive decomposition these reactions were not investigated further.

2.10 Diffusion measurements by NMR spectroscopy

The solution phase behaviour of weakly coordinated dimeric species can be complex with the possibility of partial dissociation. The dynamic nature of these equilibria can be difficult to interrogate through standard techniques (*e.g.* 1D NMR) which typically provide only a 'freezeframe' glimpse of static structures. The dynamic solution phase behaviour of a compound can be interpreted *via* translational diffusion of the chemical species through solution over a period of time. The diffusion coefficients of chemical compounds can be determined by Pulsed Gradient Spin Echo (PGSE) NMR.

Translational diffusion results from the Brownian motion of molecules through their surrounding media. The magnitude of this effect can be approximately quantified by the diffusion coefficient (*D*), which is the rate of the root mean square of molecular displacement. Signal attenuation is achieved by applying a pulsed field gradient across the NMR sample, allowing molecular diffusion to progress in solution for a period of time and then applying the inverse field. A molecule which does not move at all will receive no signal attenuation whatsoever since the effects of the two gradient pulses cancel each other out. A molecule which diffuses away from its starting position experiences signal reduction as the two gradient pulses no longer cancel out perfectly. Smaller molecules diffuse further over time and so experience greater signal reduction than larger molecules. The diffusion coefficient is obtained by fitting this signal attenuation to the Stejskal-Tanner equation (Equation 2.18, where D is the diffusion coefficient, G is the strength of applied gradient, δ is the length of time over which the gradient is applied, Δ is the delay between gradient pulses, I_G is the signal intensity under a given gradient strength, and γ is the gyromagnetic ratio of the observed nucleus).

$$I_G = I_{G=0}\exp\left(-(\gamma\delta G)^2 D\left(\Delta - \frac{\delta}{3}\right)\right)$$

Equation 2.18[103]

The diffusion coefficient can be related to the hydrodynamic radius (r_s) of the species by the Stokes-Einstein equation (Equation 2.19, where *k* is the Boltzmann constant, T is the temperature and η is the viscosity). This equation assumes that molecules in solution move as perfect spheres.

$$\mathrm{D} = \frac{kT}{6\pi r_s \eta}$$

Equation 2.19[103]

The hydrodynamic radius obtained from the Stokes-Einstein equation can then be used to estimate the molecular volume of species in solution (referred to as the NMR volume). This volume can be compared with the molecular volume calculated from a crystallographically derived structure (if available) to ascertain whether any deviations in structure are present between the solid and solution phase.

The approximation of molecular species as perfect spheres in solution is a reasonable one, albeit inaccurate for the calculation of the true hydrodynamic radii of molecules which are not perfectly spherical. The molecular volumes calculated in this way therefore carry an inherent error and can give only qualitative information about a species' size and behaviour in solution. Although it is not possible to quote uncertainty errors for diffusion coefficients, it has been reported that hydrodynamic radii calculated by this method have an associated error of 9 – 32%.[104] Some modifications to the Stokes-Einstein equation have been proposed which account for the non-spherical nature of molecules by treating species as either oblate or prolate spheroids.[105]

Comparative studies of hydrodynamic radii (and hence molecular volumes) calculated *via* this method are capable of discerning basic structural behaviours in solution. This study aims to investigate the solution phase monomer/dimer behaviour of the analytes. This can be achieved by determining a ratio between the NMR and X-ray volumes of a species. The inherent errors associated with the diffusion measurements should therefore not be great enough to substantially impact the conclusions.

Diffusion NMR analysis was carried out to interrogate the solution phase behaviour of **8**, **10**, **14** and **18**, in addition to **2.16**, reported previously by Blake and Mountford.[4] Samples of (^{Dipp}NacNac)MgFp(THF) (**2.16**), {MesC(NDipp)$_2$}MgFp(THF) (**8**), {MesC(NDipp)$_2$}Mg{Co(CO)$_3$(PCy$_3$)}(THF) (**10**), and {MesC(NMes)$_2$}Mg{Co(CO)$_3$(PCy$_3$)}(THF) (**14)** in toluene-d_8 were prepared with a concentration of 0.005 mol L^{-1}. A sample of [{Me$_2$NC(NDipp)$_2$}MgFp]$_2$ (**18**) in toluene-d_8 was prepared with a concentration of 0.0025 mol L^{-1}. A sample of (^{Dipp}NacNac)Mg(THF)Fp (**2.16**) in THF-d_8 was prepared with a concentration of 0.02 mol L^{-1}. A sample of [{Me$_2$NC(NDipp)$_2$}MgFp]$_2$ (**18**) in THF-d_8 was prepared with a concentration of 0.01 mol L^{-1}. In each case the residual protio solvent present was used as a reference standard. Signal attenuation was monitored over 16 experiments with gradients strengths ranging from 2 – 95% of maximum. The results of this study are presented in Table 2.8.

Table 2.8 Diffusion NMR data for (^{Dipp}NacNac)MgFp(THF) (**2.16**), {MesC(NDipp)$_2$}MgFp(THF) (**8**), {MesC(NDipp)$_2$}Mg{Co(CO)$_3$(PCy$_3$)}(THF) (**10**), {MesC(NMes)$_2$}Mg{Co(CO)$_3$(PCy$_3$)}(THF) (**14**), and [{Me$_2$NC(NDipp)$_2$}MgFp]$_2$ (**18**).

Compound	Solvent	X-Ray volume (Å^3) [a]	NMR volume (Å^3) [b]	*D* (mean) × 10^{-10} (m^2 s^{-1}) [c]	*D* (Solvent) × 10^{-10} (m^2 s^{-1}) [c]
2.16	toluene-d_8	698	519	7.96	22.02
8	toluene-d_8	936*	812	6.87	17.72
10	toluene-d_8	1034	1209	6.01	21.21
14	toluene-d_8	1116*	1224	5.98	18.45
18	toluene-d_8	1239	1139	6.12	20.19
2.16	THF-d_8	698	536	9.94	27.43
18	THF-d_8	1239	663	8.84	26.76

[a] Molecular volume based on the caption formula and X-ray crystal structures measured using 1.4 Å probe radius. Volumes denoted with * are instead based on that expected for a monomeric structure using the 18 Å^3 rule. [b] Molecular volume measured by diffusion NMR spectroscopy in toluene-d_8 or THF-d_8. [c] Diffusion coefficient of the compound and the residual protio solvent in the sample under consideration (for comparison the diffusion coefficients for the protio solvents were 23.54 × 10^{-10} m^2 s^{-1} in pure toluene-d_8 and 27.0154 × 10^{-10} m^2 s^{-1} in pure THF-d_8).

The calculated NMR volumes are compared with the corresponding X-ray volumes. These X-ray volumes are calculated by interrogating the surface topology of a crystallographically derived structure (where available) with a 1.4 Å probe. This method determines the molecular surface area, from which a total molecular volume is calculated. Where no crystallographic data is available the X-ray volume was estimated using the "18 Å^3 rule", which states that each non-hydrogen atom in a molecular structure occupies roughly 18 Å^3.[106,107]

Compound **2.16** has been shown to be monomeric in the solid state and solution (toluene and THF) by X-ray diffraction and IR measurements.[4] Its structural similarities to the amidinate and guanidinate compounds reported in this Chapter make it an ideal standard reference molecule. The solution volumes of **2.16** calculated from diffusion

experiments in toluene (519 Å^3) and THF (536 Å^3) are similar to the expected molecular volume, calculated from the solid state structure (698 Å^3).

It was not possible to obtain solid state data for **8**. However, the solution volume (812 Å^3) is similar to that of a monomeric structure (936 Å^3) predicted using the 18 Å^3 rule.

The solution volume of **10** (1209 Å^3) was similar to the expected molecular volume, calculated from the solid state structure (1034 Å^3). This corresponds with the IR studies which were consistent with a monomeric structure containing no isocarbonyl interactions.

As with **8**, no solid state data could be obtained for **14**. Nevertheless, the calculated solution volume of **14** (1224 Å^3) was similar to that expected for a monomeric structure, predicted using the 18 Å^3 rule (1116 Å^3). This contrasts with the IR studies performed for **14**, which showed complex solution phase behaviour, with respect to isocarbonyl interactions. Together these results suggest that individual molecules of **14** are capable of associating with each other through weak isocarbonyl interactions but diffuse through solution as predominantly monomeric species.

Compound **18** has a calculated solution volume (1139 Å^3) similar to that of the dimeric solid state structure (1239 Å^3). This similarity in volumes suggest little, if any, dissociation in toluene solution. Diffusion NMR measurements were also made in THF-d_8. These showed a solution effective volume (663 Å^3) close to half that of the solid state (1239 Å^3), consistent with a dissociation of the dimer to monomeric units in the donor solvent environment. This observation is consistent with the IR studies of **18**, which also shows dissociation of the dimeric structure in THF.

2.11 Conclusions

The work contained in this Chapter has reported the synthesis of several amidinate supported Mg–Fe (**8** and **12**), Mg–Ru (**3**, **9** and **13**) and Mg–Co (**4**, **10** and **14**) bonded species. Crystal structures for **4** and **10** showed that these compounds contain unsupported Mg–Co bonds. IR spectroscopic data for each compound shows that a degree of direct metal-metal bonding is taking place *via* comparison with analogous data obtained from structurally authenticated compounds.

The reactivity of all amidinate supported Mg–TM compounds was explored with small molecules, including MeI, TolNCNTol, ^{i}PrNCN^{i}Pr, ^{t}BuNCO, CO_2 and CS_2. Reactions

of Mg–Fe bonded species with MeI confirmed these compounds as sources of the Fp^- anion. The reaction of **12** with CS_2 produced a product determined to be $\{MesC(NMes)_2\}Mg(S_2CFp)$ (**15**). Evidence for this compound was obtained from a parallel synthesis between $K[S_2CFp]$ and **11**. Compound **15** was determined to be the product of both reaction by comparison of NMR data. The reaction of **12** with Ph_3CCl was shown to afford Fp_2 and Gomberg's dimer, suggesting a possible radical mechanism for the reaction of Fp containing compounds.

The reactivity of Mg–TM bonded species with other small molecules was shown to lead to extensive decomposition. The possible mechanisms of these decompositions are presented with a focus towards Fp compounds.

Reaction of a $\{Me_2NC(NDipp)_2\}MgI(OEt_2)$ (**17**) with KFp gave the Mg–Fe bonded $[\{Me_2NC(NDipp)_2\}MgFp]_2$ (**18**). Compound **18** contains the shortest Mg–Fe bond to date (2.5279(4) Å) and was the first Mg–Fe bonded species to isolated without a coordinated base. The reactivity of **18** was shown to be slightly lower than that of the amidinate counterparts but still uncontrolled with respect to the formation of single products.

The solution phase behaviour of several of these compounds was investigated *via* diffusion NMR techniques. Compounds **8**, **10**, **14** and **18** were shown to behave as monomers in toluene solution while **18** was shown to retain its dimeric structure. Compound **18** was shown to undergo a reversible dissociate to a monomeric structure in THF solution.

2.12 References

1. S. T. Liddle, Ed., *Molecular Metal–Metal Bonds. Compounds, Synthesis, Properties*, Wiley-VCH, Weinheim, 2015.

2. J. Bauer, H. Braunschweig, and R. D. Dewhurst, *Chem. Rev.*, 2012, **112**, 4329–4346.

3. D. A. Fletcher, R. F. McMeeking, and D. Parkin, *J. Chem. Inf. Comput. Sci.*, 1996, **36**, 746–749.

4. M. P. Blake, N. Kaltsoyannis, and P. Mountford, *Chem. Commun.*, 2013, **49**, 3315–3317.

5. M. P. Blake, N. Kaltsoyannis, and P. Mountford, *J. Am. Chem. Soc.*, 2015, **137**,

12352–12368.

6. R. Green, A. C. Walker, M. P. Blake, and P. Mountford, *Polyhedron*, 2016, **116**, 64–75.
7. C. Birchall, G. J. Moxey, J. McMaster, A. J. Blake, W. Lewis, and D. L. Kays, *Inorg. Chim. Acta*, 2017, **458**, 97–100.
8. C. Jones, S. Aldridge, T. Gans-Eichler, and A. Stasch, *Dalton Trans.*, 2006, 5357.
9. M. P. Blake, N. Kaltsoyannis, and P. Mountford, *J. Am. Chem. Soc.*, 2011, **133**, 15358–61.
10. R. M. Campbell, L. M. Clarkson, W. Clegg, D. R. Hockless, N. L. Pickett, and N. C. Norman, *Chem. Ber.*, 1992, **125**, 55–59.
11. X. He, R. A. Bartlett, and P. P. Power, *Organometallics*, 1994, **13**, 548–552.
12. M. A. Bush and P. Woodward, *J. Chem. Soc. A*, 1967, **0**, 1833–1838.
13. P. Gusbeth and H. Vahrenkamp, *Chem. Ber.*, 1985, **118**, 1746–1757.
14. M. S. Hill, P. B. Hitchcock, and R. Pongtavornpinyo, *Dalton Trans.*, 2008, 2854.
15. P. T. Greene and R. F. Bryan, *J. Chem. Soc. A*, 1970, **0**, 1696–1702.
16. J. E. O'Connor and E. R. Corey, *Inorg. Chem.*, 1967, **6**, 968–971.
17. L. F. Dahl and Trinh-Toan, *J. Am. Chem. Soc.*, 1971, **93**, 2654–2666.
18. P. L. Arnold, J. McMaster, and S. T. Liddle, *Chem. Commun.*, 2009, **0**, 818–820.
19. J. W. van Hal, L. B. Alemany, K. H. Whitmire, Jaap W. van Hal, Lawrence B. Alemany, and K. H. Whitmire, *Inorg. Chem.*, 1997, **36**, 3152–3159.
20. J. M. Wallis, G. Müller, and H. Schmidbaur, *J. Organomet. Chem.*, 1987, **325**, 159–168.
21. R. Schiwon, R. Metzinger, C. Pfirrmann, and C. Limberg, *Zeitschrift für Naturforsch. B*, 2013, **68**.
22. T. J. Mazzacano and N. P. Mankad, *J. Am. Chem. Soc.*, 2013, **135**, 17258–17261.
23. M. E. Giuseppetti and A. R. Cutler, *Organometallics*, 1987, **6**, 970–973.
24. T. A. Shackleton and M. C. Baird, *Organometallics*, 1989, **8**, 2225–2232.

25. R. B. King, *J. Inorg. Nucl. Chem.*, 1963, **25**, 1296–1298.

26. M. L. H. Green and P. L. I. Nagy, *J. Chem. Soc.*, 1963, 189.

27. K. Inkrott, R. Goetze, and S. G. Shore, *J. Organomet. Chem.*, 1978, **154**, 337–342.

28. P. K. Sazonov, G. A. Artamkina, and I. P. Beletskaya, *Theor. Exp. Chem.*, 2011, **46**, 350–358.

29. J. S. Plotkin and S. G. Shore, *Inorg. Chem.*, 1981, **20**, 284–285.

30. F. Dulich, K.-H. Müller, A. R. Ofial, and H. Mayr, *Helv. Chim. Acta*, 2005, **88**, 1754–1768.

31. D. L. Reger, D. J. Fauth, and M. D. Dukes, *Synth. React. Inorg. Met. Chem.*, 1977, **7**, 151–155.

32. J. R. Pinkes and A. R. Cutler, *Inorg. Chem.*, 1994, **33**, 759–764.

33. I. M. Riddlestone, J. Urbano, N. Phillips, M. J. Kelly, D. Vidovic, J. I. Bates, R. Taylor, and S. Aldridge, *Dalton Trans.*, 2013, **42**, 249–258.

34. J. C. Calabrese, L. M. Clarkson, T. B. Marder, N. C. Norman, and N. J. Taylor, *J. Chem. Soc., Dalton Trans.*, 1992, 3525–3529.

35. D. Nied, E. Matern, H. Berberich, M. Neumaier, and F. Breher, *Organometallics*, 2010, **29**, 6028–6037.

36. H. Braunschweig, R. Dörfler, K. Hammond, T. Kramer, J. Mies, K. Radacki, and M. Schäfer, *Inorg. Chem.*, 2012, **51**, 1225–1227.

37. K. Toyota, Y. Wakisaka, Y. Yamamoto, and K. Akiba, *Organometallics*, 2000, **19**, 5122–5133.

38. I. Bytheway, C. S. Griffith, G. A. Koutsantonis, B. W. Skelton, and A. H. White, *Eur. J. Inorg. Chem.*, 2007, 3240–3246.

39. C. Döring, A.-M. Dietel, M. V. Butovskii, V. Bezugly, F. R. Wagner, and R. Kempe, *Chem. Eur. J.*, 2010, **16**, 10679–10683.

40. I. P. Beletskaya, A. Z. Voskoboynikov, E. B. Chuklanova, N. I. Kirillova, A. K. Shestakova, I. N. Parshina, A. I. Gusev, and G. K. I. Magomedov, *J. Am. Chem. Soc.*, 1993, **115**, 3156–3166.

41. R. S. Sternal, C. P. Brock, and T. J. Marks, *J. Am. Chem. Soc.*, 1985, **107**, 8270–8272.

42. B. M. Gardner, D. Patel, A. D. Cornish, J. McMaster, W. Lewis, A. J. Blake, and S. T. Liddle, *Chem. Eur. J.*, 2011, **17**, 11266–11273.

43. G. Jansen, M. Schubart, B. Findeis, L. H. Gade, I. J. Scowen, and M. McPartlin, *J. Am. Chem. Soc.*, 1998, **120**, 7239–7251.

44. D. Patel, F. Moro, J. McMaster, W. Lewis, A. J. Blake, and S. T. Liddle, *Angew. Chem. Int. Ed.*, 2011, **50**, 10388–10392.

45. R. A. Fischer, J. Behm, T. Priermeier, and W. Scherer, *Angew. Chem. Int. Ed.*, 1993, **32**, 746–748.

46. W. R. Robinson and D. P. Schussler, *Inorg. Chem.*, 1973, **12**, 848–854.

47. J. M. Burlitch and T. W. Theyson, *J. Chem. Soc., Dalton Trans.*, 1974, 828.

48. J. K. Stalick and J. A. Ibers, *J. Organomet. Chem.*, 1970, **22**, 203–211.

49. R. D. Ball and D. Hall, *J. Organomet. Chem.*, 1973, **52**, 293–295.

50. C. Loubser, J. L. M. Dillen, and S. Lotz, *Polyhedron*, 1991, **10**, 2535–2539.

51. J. M. Geller, J. H. Wosnick, I. S. Butler, D. F. Gilson, F. G. Morin, and F. Bélanger-Gariépy, *Can. J. Chem.*, 2002, **80**, 813–820.

52. L. F. Dahl and A. S. Foust, *J. Am. Chem. Soc.*, 1970, **92**, 7337–7341.

53. L. J. Farrugia, N. C. Norman, and P. M. Webster, *Acta Cryst. C*, 1993, **49**, 91–93.

54. F. Calderazzo, R. Poli, and G. Pelizzi, *J. Chem. Soc., Dalton Trans.*, 1984, 2535.

55. G. Etzrodt, R. B. Und, and G. Schmid, *Chem. Ber.*, 1979, **112**, 2574–2580.

56. D. Zhao, F. T. Ladipo, J. Braddock-Wilking, L. Brammer, and P. Sherwood, *Organometallics*, 1996, **15**, 1441–1445.

57. G. B. McVicker, *Inorg. Chem.*, 1975, **14**, 2087–2092.

58. V. K. Belsky, A. N. Protsky, I. V. Molodnitskaya, B. M. Bulychev, and G. L. Soloveichik, *J. Organomet. Chem.*, 1985, **293**, 69–74.

59. M. V. Butovskii, O. L. Tok, F. R. Wagner, and R. Kempe, *Angew. Chem. Int.*

Ed., 2008, **47**, 6469–6472.

60. R. Schiwon, C. Knispel, and C. Limberg, *Organometallics*, 2010, **29**, 1670–1674.

61. R. Schiwon, B. Braun, R. Metzinger, and C. Limberg, *Zeitschrift für Anorg. und Allg. Chemie*, 2016, **642**, 1198–1206.

62. M. V. Butovskii, C. Döring, V. Bezugly, F. R. Wagner, Y. Grin, and R. Kempe, *Nat. Chem.*, 2010, **2**, 741–744.

63. M. V. Butovskii, B. Oelkers, T. Bauer, J. M. Bakker, V. Bezugly, F. R. Wagner, and R. Kempe, *Chem. Eur. J.*, 2014, **20**, 2804–2811.

64. D. Patel, D. M. King, B. M. Gardner, J. McMaster, W. Lewis, A. J. Blake, and S. T. Liddle, *Chem. Commun.*, 2011, **47**, 295–297.

65. B. M. Gardner, J. McMaster, W. Lewis, and S. T. Liddle, *Chem. Commun.*, 2009, 2851.

66. M. V. Butovskii and R. Kempe, *New J. Chem.*, 2015, **39**, 7544–7558.

67. M. L. H. Green, L. Pratt, and G. Wilkinson, *J. Chem. Soc.*, 1958, 3916.

68. J. Barker and M. Kilner, *Coord. Chem. Rev.*, 1994, **133**, 219–300.

69. F. T. Edelmann, *Adv. Organomet. Chem.*, 2013, **61**, 55–374.

70. F. T. Edelmann, *Chem. Soc. Rev.*, 2012, **41**, 7657–72.

71. M. P. Coles, D. C. Swenson, R. F. Jordan, and V. G. Young, *Organometallics*, 1997, **16**, 5183–5194.

72. S. P. Green, C. Jones, and A. Stasch, *Science*, 2007, **318**, 1754–1757.

73. B. M. Day, W. Knowelden, and M. P. Coles, *Dalton Trans.*, 2012, **41**, 10930–10933.

74. A. W. Addison, T. N. Rao, J. Reedijk, J. van Rijn, and G. C. Verschoor, *J. Chem. Soc., Dalton Trans.*, 1984, 1349.

75. R. Theys, M. Dudley, and M. Hossain, *Coord. Chem. Rev.*, 2009, **253**, 180–234.

76. W. E. Brittin, *J. Chem. Educ.*, 1945, **22**, 145.

77. B. Cordero, V. Gómez, A. E. Platero-Prats, M. Revés, J. Echeverría, E.

Cremades, F. Barragán, and S. Alvarez, *Dalton Trans.*, 2008, 2832–2838.

78. K. Jonas, G. Koepe, and C. Krüger, *Angew. Chem. Int. Ed.*, 1986, **25**, 923–925.
79. M. Findlater, N. J. Hill, and A. H. Cowley, *Dalton Trans.*, 2008, 4419–4423.
80. A. R. Ali, H. Ghosh, and B. K. Patel, *Tet. Lett.*, 2010, **51**, 1019–1021.
81. M. Blumer, *Anal. Chem.*, 1957, **29**, 1039–1041.
82. L. Busetto, U. Belluco, and R. J. Angelici, *J. Organomet. Chem.*, 1969, **18**, 213–215.
83. J. E. Ellis, R. W. Fennell, and E. A. Flom, *Inorg. Chem.*, 1976, **15**, 2031–2036.
84. J. R. Pinkes, S. M. Tetrick, B. E. Landrum, and A. R. Cutler, *J. Organomet. Chem.*, 1998, **566**, 1–7.
85. J. C. Vites, B. D. Steffey, M. E. Giuseppetti-Dery, and A. R. Cutler, *Organometallics*, 1991, **10**, 2827–2834.
86. J. R. Pinkes, B. D. Steffey, J. C. Vites, and A. R. Cutler, *Organometallics*, 1994, **13**, 21–23.
87. H. Li and M. M. Turnbull, *J. Organomet. Chem.*, 1991, **419**, 245–249.
88. P. L. Arnold, Z. R. Turner, N. Kaltsoyannis, P. Pelekanaki, R. M. Bellabarba, and R. P. Tooze, *Chem. Eur. J.*, 2010, **16**, 9623–9629.
89. J. R. Robinson, P. J. Carroll, P. J. Walsh, and E. J. Schelter, *Angew. Chem. Int. Ed.*, 2012, **51**, 10159–10163.
90. M. Gomberg, *J. Am. Chem. Soc.*, 1900, **22**, 757–771.
91. H. Lankamp, W. T. Nauta, and C. MacLean, *Tet. Lett.*, 1968, **9**, 249–254.
92. A. I. Germeroth, Reactivity of Electropositive f-Block Metal N-Heterocyclic Carbene Complexes, PhD Thesis, University of Edinburgh, 2013.
93. H. Sitzmann, T. Dezember, W. Kaim, F. Baumann, D. Stalke, J. Kärcher, E. Dormann, H. Winter, C. Wachter, and M. Kelemen, *Angew. Chem. Int. Ed.*, 1996, **35**, 2872–2875.
94. P. J. Krusic, P. J. Fagan, and J. San Filippo, *J. Am. Chem. Soc.*, 1977, **99**, 250–252.

95. P. K. Sazonov, G. A. Artamkina, V. N. Khrustalev, M. Y. Antipin, and I. P. Beletskaya, *J. Organomet. Chem.*, **681**, 59–69.

96. P. K. Sazonov, V. A. Ivushkin, G. A. Artamkin, and I. P. Beletskaya, *Arkivoc*, 2003, 323.

97. P. J. Bailey and S. Pace, *Coord. Chem. Rev.*, 2001, **214**, 91–141.

98. G. Jin, C. Jones, P. C. Junk, K.-A. Lippert, R. P. Rose, and A. Stasch, *New J. Chem.*, 2009, **33**, 64–75.

99. P. B. Hitchcock, M. F. Lappert, and M. J. Michalczyk, *J. Chem. Soc., Dalton Trans.*, 1987, 2635–2642.

100. D. Dange, C. P. Sindlinger, S. Aldridge, and C. Jones, *Chem. Commun.*, 2017, **53**, 149–152.

101. H. Deng and S. G. Shore, *J. Am. Chem. Soc.*, 1991, **113**, 8538–8540.

102. H. Deng, S.-H. Chun, P. Florian, P. J. Grandinetti, and S. G. Shore, *Inorg. Chem.*, 1996, **35**, 3891–3896.

103. T. D. W. Claridge, *High-Resolution NMR Techniques in Organic Chemistry*, Elsevier, Amsterdam, 3rd Edition, 2016.

104. D. Zuccaccia and A. Macchioni, *Organometallics*, 2005, **24**, 3476–3486.

105. A. Macchioni, G. Ciancaleoni, C. Zuccaccia, and D. Zuccaccia, *Chem. Soc. Rev.*, 2008, **37**, 479–489.

106. W. Clegg, *Crystal Structure Determination*, Oxford University Press, Oxford, 1998.

107. C. J. E. Kempster and H. Lipson, *Acta Cryst. B*, 1972, **28**, 3674–3674.

Chapter Three

Synthetic study of Zn–Hg–Zn and Zn–Zn bonded complexes

3.1 Overview

This Chapter describes the attempted synthesis of Zn–Hg–Zn bonded compounds and the resulting isolation of several Zn–Zn bonded compounds. Relativistic DFT calculations are performed to compare the stability of Zn–Zn bonded compounds to their Zn–Hg–Zn bonded counterparts.

3.2 Introduction

In 2015 Blake and Mountford reported the synthesis and the single-crystal X-ray structure of $\{(^{Dipp}NacNac)Zn\}_2Hg$ (**3.1**, Equation 3.1) from the reduction of $(^{Dipp}NacNac)ZnI$ with an excess of potassium amalgam (K/Hg) in THF or hexanes.[1] This was the first published example of a complex which contained bonds between two different group 12 elements and the first example of a heterocatenate complex of the group 12 elements. The Zn–Hg distance (2.4846(3) Å) was within the sum of covalent radii, as compiled by both Alvarez (2.54(6) Å)[2] and Pyykkö (2.51 Å).[3] The Zn–Hg distance was also similar to the value obtained (2.466 Å) by linear extrapolation of the intermetallic distances between Robinson's $(^{Dipp}NacNac)_2Zn_2$ (Zn–Zn, 2.3586(7) Å)[4] and Power's $Ar^*_2Hg_2$ (Hg–Hg, 2.5738(3) Å).[5] Compound **3.1** features a linear coordination environment at Hg (Zn–Hg–Zn = 180°) and an usual T-shaped coordination geometry at both three-coordinate Zn centres (Zn–N(1,2) distances 1.9643(19) and 2.002(2) Å; Hg–Zn–N(1,2) angles 153.37(6) and 111.85(6)°). The distortion away from trigonal planar geometry at both Zn centres is attributed to attractive forces between the aryl groups of the NacNac ligands and the Hg centre. No signal could be observed in the ^{199}Hg NMR spectrum.

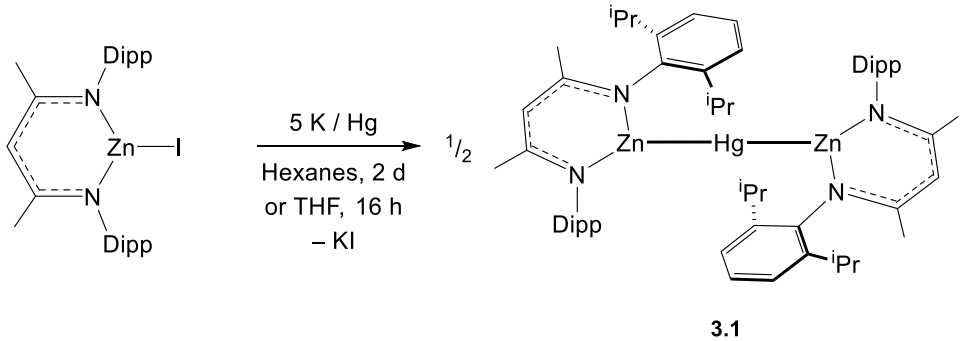

3.1

Equation 3.1[1]

Relativistic DFT calculations at the PBEPBE level of theory incorporating Grimme's D3 dispersion corrections[6,7] were performed to gain insight into the molecular and electronic structure of **3.1**.[1] Several other chemical species were modelled at this level of theory to allow their direct comparison to the model of **3.1** in order to gain a deeper comprehension of the properties of the Zn–Hg bonds. The calculated structure of **3.1** reproduced the distorted geometry observed in the solid state structure. When the same calculations were performed omitting dispersion corrections the bent geometry of the NacNac ligands was not reproduced, instead a structure was produced with a regular geometry at the Zn centres with average Hg–Zn–N angles of 132.4 and 132.9 °. This result suggests that the origin of the distorted ligand geometry arises from dispersive van der Waals interactions between the Hg atom and the aryl substituents.

Analysis of the DFT MOs of {(^{H}NacNac)Zn}$_2$Hg (a simplified model of **3.1**) showed two occupied MOs based primarily on metal centres. The HOMO possessed mainly Zn character (56% 4s and 24% 4p) and only 7% Hg (6p) character, with a computed energy of −3.50 eV. This MO arises from the bonding interaction between the Hg 6p orbital and the out-of-phase combination of the two α-SHOMOs of the Zn fragments. To compare, the HOMO of the model Zn–Zn bonded complex (^{H}NacNac)$_2$Zn$_2$ possessed 78% Zn character, with a computed energy of −4.44 eV. The HOMO−7 of {(^{H}NacNac)Zn}$_2$Hg has mainly Hg 6s character (69%) and only 12% Zn character, with a computed energy of −6.92 eV. It arises from the in-phase combination of the two α-SHOMOs with the Hg 6s orbital. For comparison, the 6s AO of Hg has a somewhat similar computed energy of −6.79 eV, indicating that the HOMO−7 of {(^{H}NacNac)Zn}$_2$Hg is not considerably stabilised compared to its primary contributing orbital.

QTAIM analysis[8] of **3.1** finds bond critical points between Zn and Hg atoms supporting the existence of Zn–Hg bonds. Various model compounds and fragments, including (^{Dipp}NacNac)Zn$^{\bullet}$, (^{Dipp}NacNac)$_2$Zn$_2$ and (^{Dipp}NacNac)ZnI, were modelled using AIM methods to facilitate their comparison with **3.1**. The atomic charge on each Zn atom in **3.1** (+0.67 au) was closer to the values found in (^{Dipp}NacNac)Zn$^{\bullet}$ (+0.58 au) and (^{Dipp}NacNac)$_2$Zn$_2$ (+0.59 au) (both formally Zn(I)) than that found in (^{Dipp}NacNac)ZnI (+0.93 au, formally Zn(II)). The atomic charge on Hg (−0.14 au) is minor, showing only 0.07 electrons per (^{Dipp}NacNac)Zn fragment are transferred upon their coordination to Hg. As a consequence of these models Blake and Mountford describe

the oxidation states of their Zn–Hg–Zn system as $[Zn(I)]_2Hg(0)$ with a small degree of charge transfer to Hg upon Zn–Hg bond formation. QTAIM analysis did not find any bond paths between any atom in the aryl groups and the μ-Hg atom, suggesting that the distorted, "T-shaped" ligand geometry arises solely as the result of dispersive, van der Waals interactions between these groups and is not the result of any covalent interaction.

The formation of **3.1** likely proceeds through the reduction of Zn(II) iodide to give a transient Zn(I) species. These Zn(I) radical species would then couple to form a dimer (in this case Robinson's Zn(I) dimer, **1.81**). However, the steric repulsion between the flanking Dipp groups of the NacNac ligands is likely to be great. Since the reduction event occurs at the interface of the organic solution and the metal amalgam the effective concentration of Hg is high in the proximity of the transient Zn(I) species. Hence, it is energetically more favourable for these Zn(I) species to pick up a Hg atom which acts as a 'spacer' between the two metal atoms than it is for the Zn(I) species to dimerise directly due to the steric repulsion between the aryl groups of the ligand. The interception of transient intermediates by Hg at a solvent/amalgam interface is well precedented in amalgam reduction chemistry.[9]

There is only one other structurally authenticated example of molecular Zn–Hg bonding. As described in Chapter One, Jones *et al*. reported the reduction of L*ZnBr (**3.2**, L* = N(Ar*)(Si^iPr_3), Ar* = $C_6H_2\{C(H)Ph_2\}_2Me$) with $[(^{Mes}NacNac)Mg]_2$ (**1.13**) to give L*ZnMg(^{Mes}NacNac) (**1.31**).[10] The extremely bulky monodentate amide ligand prevents dimerisation of the L*Zn fragments at RT, instead affording **1.31**. The dimer L*ZnZnL* (**3.3**) could be obtained by heating **1.31** with **3.2** at 70 °C for 12 h. Reaction of **1.31** with $ZnBr_2$(TMEDA) gave L*ZnZnBr(TMEDA) (**3.4**, Zn–Zn 2.3751(6) Å). Reaction of **1.31** with 0.5 equiv. of the group 12 binary halides $ZnBr_2$, CdI_2 and $HgCl_2$ gave the centrosymmetric complexes L*ZnZnZnL* (**3.5** Zn–Zn = 2.384(1) Å), L*ZnCdZnL* (**3.6** Zn–Cd = 2.487(2) Å), and L*ZnHgZnL* (**3.7** Zn–Hg = 2.476(5) Å), respectively. This set of compounds represents the first example of a homologous Zn–M–Zn series for all the (non-synthetic) group 12 metals. Compounds **3.6** and **3.7** have Zn–M bonds lengths that are identical, within experimental error, as a consequence of the lanthanide contraction. Attempts to produce a longer metal catenate *via* the reaction of **1.31** with Hg_2Cl_2 were unsuccessful, giving a mixture of products, which included

3.7. As was the case with Mountford's complex, **3.1**, no signal could be observed in the ^{199}Hg NMR spectrum of **3.7**.

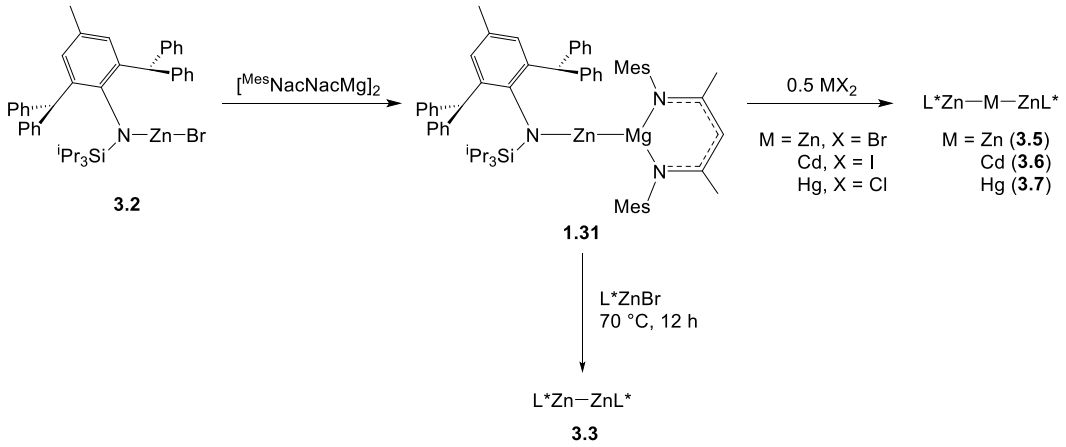

Scheme 3.1 Formation of L*ZnMg(^{Mes}NacNac) (**1.31**), its reaction at elevated temperatures to form dimeric L*ZnZnL* (**3.3**), and its reaction with group 12 halides to form L*ZnMZnL* (M = Zn (**3.5**), Cd (**3.6**), Hg (**3.7**)).[10]

The steric bulk of the ligand plays an important role in the formation of these higher order heterocatenate complexes. When Jones *et al*. employed a less sterically encumbering ligand during the reduction of L'ZnBr(THF) (**3.8**, L' = N(Ar')(SiMe$_3$), Ar' = C$_6$H$_2${C(H)Ph$_2$}$_2$^{i}Pr) with (^{Mes}NacNac)$_2$Mg$_2$ the reaction proceeded directly to L'ZnZnL' (**3.9**), even at low temperatures.[10] The authors used this methodology to produce L'CdCdL' (**3.10**) and L'HgHgL' (**3.11**) from the reduction of L'CdI and L'HgI, respectively. This is only the second reported example of a homologous series of group 12 dimers, the other being the terphenylated group 12 dimers reported by Power *et al*., discussed in Chapter One.[5]

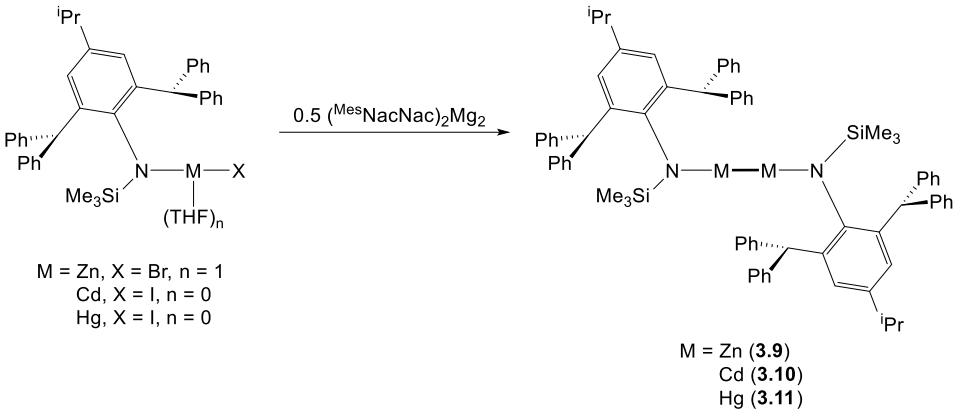

Scheme 3.2 The synthesis of L'MML' (M = Zn **3.9**, Cd **3.10**, Hg **3.11**) from the reduction of L'ZnBr(THF), L'CdI and L'HgI, respectively.[10]

To date there has been only one other published example of a molecular Group 12 trimetallic complex, reported very recently by Crimmin *et al*. During the synthesis and purification of **1.33** a small quantity of crystals was isolated which did not match those of the bulk sample. X-ray diffraction analysis showed these crystals to be {(^{Dipp}NacNac)Zn}$_2$Zn (**3.12**, Equation 3.2), containing a linear trizinc unit with a Zn–Zn bond length of 2.3908(3) Å.[11] Compound **3.12** is isostructural to **3.1**, including the bent, T-shaped geometry of the NacNac ligands.

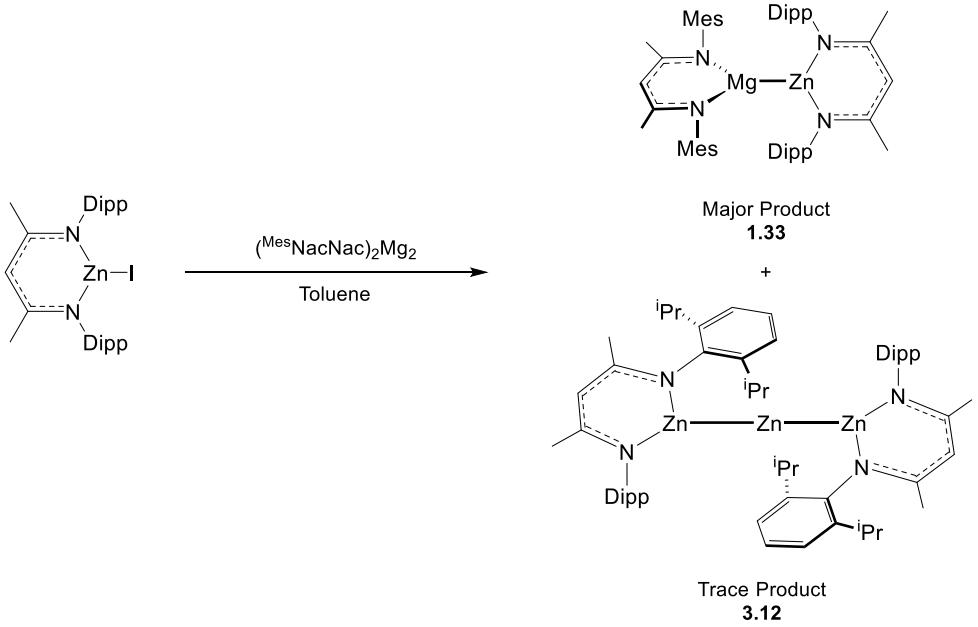

Equation 3.2[11]

Compound **3.12** was obtained in small quantities as a minor product from the synthesis of **1.33**. Compound **1.33** was shown to be unstable under the reaction conditions for its formation, decomposing to form Zn(0), among other products. It is possible that the Mg(I) dimer, previously demonstrated to participate in single-electron transfer processes,[12] reduces the Zn(II) to a transient Zn(I) species. These Zn(I) species may then pick up a Zn(0) atom from solution (present from the decomposition of **1.33**) to act as a spacer between two Zn(I) species, analogous to the formation of **3.1**. In the case of **3.1** a high effective concentration of Hg(0) is present at the reduction event. The low effective concentration of Zn(0) at the reduction event accounts for the low yield of **3.12**. The authors report that attempts to synthesise **3.12** rationally have been unsuccessful.

Clearly **3.1** and **3.12** differ only by the bridging group 12 atom. For comparative purposes independent DFT calculations for **3.12** were carried out by Mountford,[13] following the initial publication of the structural data by Crimmin *et al.*, to supplement the calculations performed for **3.1**. The relativistic DFT calculations were again performed at the PBEPBE level incorporating Grimme's D3 dispersion corrections.[6,7] The geometry optimisation of **3.12** under this regime reproduced the distorted geometry observed in the crystallographically derived structure. As was the case with **3.1**, omitting dispersion corrections during the geometry optimisation failed to reproduce the bent geometry of the NacNac ligands and gave regular geometries at the terminal Zn centres with average Zn–Zn–N angles of 132.9°.

Analysis of the DFT MOs of $\{(^{H}\text{NacNac})\text{Zn}\}_2\text{Zn}$ (the simplified model of **3.12**) showed two principle metal-based MOs. The HOMO possesses 16% μ-Zn (4p) character and 35% contribution from each terminal Zn atom (24% 4s, 11% 4p). The HOMO−5 is localised on the μ-Zn atom with 66% contribution (4s character) with 9% contribution from each terminal Zn atom. These orbitals are analogous to the HOMO and HOMO−7 found in the calculated structure of $\{(^{H}\text{NacNac})\text{Zn}\}_2\text{Hg}$ (the simplified model of **3.1**). The bonding situations in **3.1** and **3.12** can therefore be considered broadly analogous. The slightly greater μ-metal contribution in the HOMO of the Zn_3 system and the slightly greater contribution from the terminal Zn atoms in the lower energy HOMO−5 are indicative of a marginally more covalent interaction between the metal atoms in **3.12**.

QTAIM analysis reveals a slightly lower atomic charge for each terminal Zn atom in **3.12** (+0.52 au) than for the same atoms in **3.1** (+0.67 au). The μ-Zn atom carries a slightly positive atomic charge (+0.18 au) in **3.12**, compared to the slightly negative atomic charge (−0.14 au) of μ-Hg in **3.1**. The lesser Pauling electronegativity of Zn (1.65 *c.f.* 2.00 for Hg)[14,15] results in a more covalent interaction between the terminal Zn atoms and the bridging metal atom in **3.12** and, hence, less polar Zn–M–Zn bonds. The reduction in atomic charges of the terminal Zn atoms and the switch from negative to positive atomic charge for the bridging metal atom upon replacement of Hg with Zn reflect this increased covalency. The atomic charges in **3.12** are consistent with two Zn(I) moieties bridged by a μ-Zn(0) atom.

These compounds represent the only known examples of heterocatenate complexes for the group 12 elements. However, there are many known examples of homobimetallic compounds within group 12, a number of which have been discussed in Chapter One.

Following Carmona's landmark discovery of $Zn_2Cp^*_2$ (**1.79**),[16] the topic of group 12 metal–metal bonding, and particularly the study of molecular Zn(I) compounds, was approached with renewed vigour. Notably Schulz *et al*. discovered that the lability of Cp* ligands in **1.79** could be exploited to access a wide range of ligand substitution reactions.

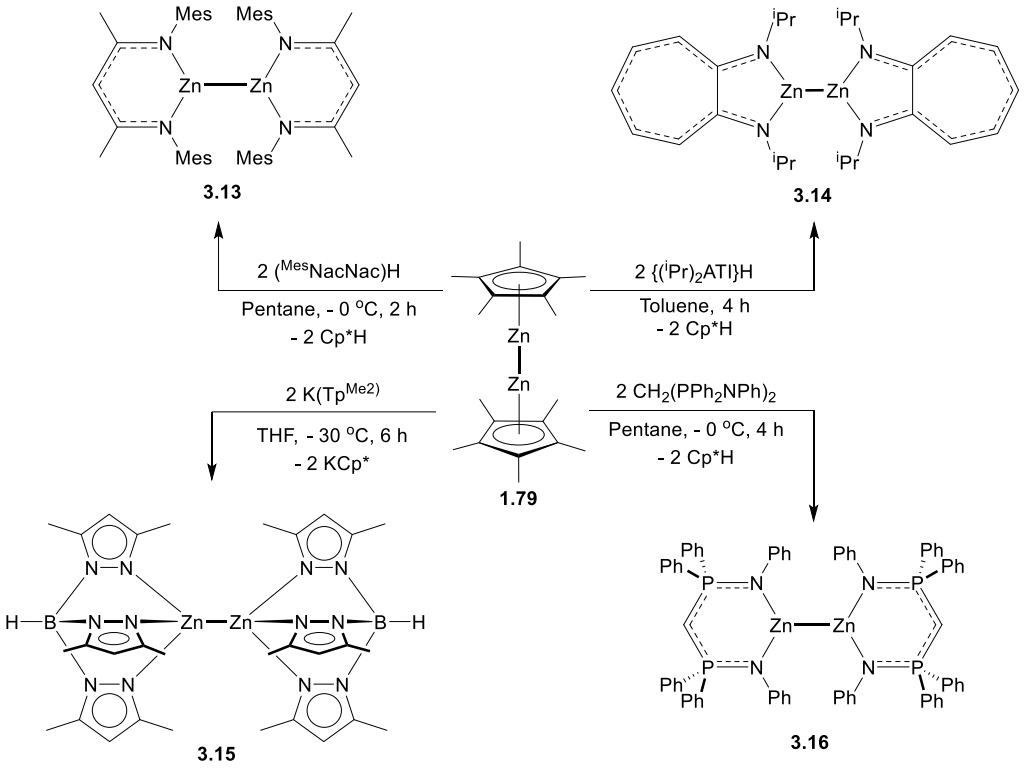

Scheme 3.3 Ligand exchange reactions of $Zn_2Cp^*_2$ (**1.79**) to afford $(^{Mes}NacNac)_2Zn_2$ (**3.13**), $\{(^iPr)_2ATI\}_2Zn_2$ (**3.14**), $(Tp^{Me2})_2Zn_2$ (**3.15**) and $\{HC(PPh_2NPh)_2\}_2Zn_2$ (**3.16**).[17–20]

When utilised as a synthon for $[Zn_2]^{2+}$, **1.79** undergoes ligand substitution with a variety of protio-ligands, such as β-diketiminates,[17] aminotropiniminates,[18] trispyrazolylborates[19] and (iminophosphorano)methanes.[20] The complexes $(^{Mes}NacNac)_2Zn_2$ (**3.13**), $\{(^iPr)_2ATI\}_2Zn_2$ (**3.14**), $(Tp^{Me2})_2Zn_2$ (**3.15**) and $\{HC(PPh_2NPh)_2\}_2Zn_2$ (**3.16**) have all been synthesised in this manner (Scheme 3.3).

Interestingly, the reaction of **1.79** with more sterically demanding (iminophosphorano)methane ligands did not produce homoleptic analogues of **3.16**. Instead, a partial ligand substitution reaction was observed to give the heteroleptic complexes {CH(PPh$_2$NR)$_2$}ZnZnCp* (R = SiMe$_3$ (**3.17**), Dipp (**3.18**); Scheme 3.4).[20] The heteroleptic variant of **3.16**, {HC(PPh$_2$NPh)$_2$}ZnZnCp* (**3.19**) was obtained *via* the equimolar reaction between **1.79** and CH$_2$(PPh$_2$NPh)$_2$. These ligand exchange reactions have been particularly successful in furthering the number of Zn(I) dimers available in the literature.

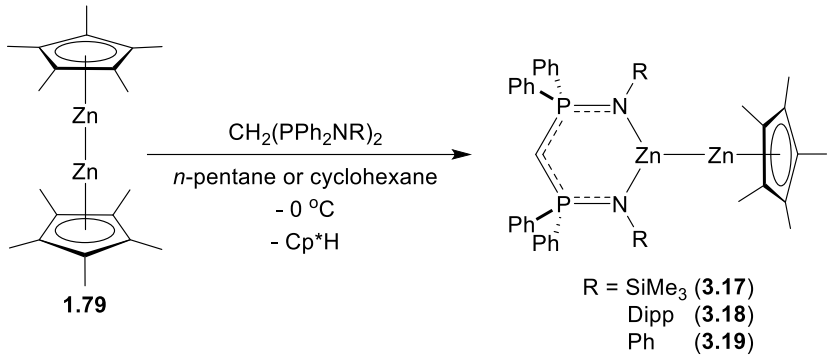

Scheme 3.4 The reaction of Zn$_2$Cp*$_2$ (**1.79**) with equimolar quantities of CH$_2$(PPh$_2$NR)$_2$ (R = SiMe$_3$, Dipp, Ph) to give heteroleptic complexes {CH(PPh$_2$NR)$_2$}ZnZnCp* (R = SiMe$_3$ (**3.17**), Dipp (**3.18**), Ph (**3.19**).[20]

3.3 Attempted syntheses of new β-diketiminate supported Zn–Hg–Zn compounds

At the time of its discovery **3.1** was the sole example of a compound containing bonds between three contiguous group 12 atoms, in addition to being the first reported compound containing direct Zn–Hg bonds.[1] The work detailed in this Chapter aims to synthesise structural analogues of **3.1** in order to ascertain the effect of ligand sterics on the stability of the Zn–Hg–Zn structure.

An early assumption was made that the steric demands of the NacNac aryl groups helped to stabilise the Zn–Hg interactions. Initial investigations were therefore directed towards varying the aryl groups of the NacNac ligand to establish how significant these groups are in stabilising the Zn–Hg–Zn structure. (^{Mes}NacNac)ZnI (**3.20**) was synthesised previously by Schulz *et al*. from the reaction of (^{Mes}NacNac)ZnMe with I$_2$.[21] Recrystallisation from THF gave **3.20**·THF. The monomeric structure consisted of a tetrahedral Zn centre coordinated to I, THF and the bidentate ^{Mes}NacNac ligand.

Alternative methods for the synthesis of (^{Ar}NacNac)MX type compounds exist and the decision was taken to follow a method used previously in our group.[1] Compound **3.20** was synthesised *via* the deprotonation of (^{Mes}NacNac)H with K[N(SiMe$_3$)$_2$] followed by reaction with ZnI_2 in THF. The crude reaction mixture was extracted into hot benzene. The ^{1}H NMR spectrum of the crude material in THF-d_8 matched that of **3.20** reported by Schulz *et al*.[21] Diffraction-quality crystals were obtained from a pentane solution of **3.20**. The unit cell parameters obtained from a cursory scan of these crystals did not match those from the structure published previously by Schulz *et al*. X-ray diffraction of these crystals showed the solid state structure to be [(^{Mes}NacNac)Zn(μ-I)]$_2$ (**19**). The molecular structure and selected distances and angles are shown in Figure 3.1 and Table 3.1.

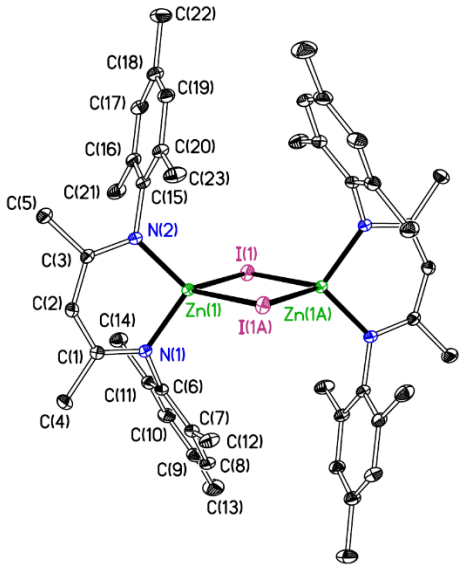

Figure 3.1 Displacement ellipsoid plot (20% probability) of [(^{Mes}NacNac)Zn(μ-I)]$_2$ (**19**). H atoms omitted for clarity. Atoms carrying the suffix "A" are related to their counterparts by the operator 1-x, 1-y, 1-z.

Table 3.1 Selected distances (Å) and angles (°) for [(^{Mes}NacNac)Zn(μ-I)]$_2$ (**19**).

Zn(1)–I(1)	2.6116(3)	Zn(1)–I(1A)	2.7102(3)
Zn(1)–N(1)	1.952(2)	Zn(1)–N(2)	1.952(2)
I(1)–Zn(1)–I(A)	99.701(10)	I(1)–Zn(1)–N(1)	112.85(6)
I(2)–Zn(1)–N(2)	121.20(6)	I(1A)–Zn(1)–N(1)	111.59(6)
I(1A)–Zn(1)–N(2)	111.11(6)	N(1)–Zn(1)–N(2)	100.74(9)

Compound **19** is the dimeric form of **3.20**. In the absence of coordinating solvent the iodide ligands act as bridging ligands to give the dimeric structure shown in Figure 3.1. All distances and angles are as expected for a compound of this type. It is interesting to note that the when crystallised from non-donor solvents, **3.20** crystallises as a dimer while (^{Dipp}NacNac)ZnI crystallises as a monomer.[1] This is presumably the result of the different steric demands of the ligands; the ^{Dipp}NacNac ligand does not allow dimerisation of the LZnI units due to the bulk of its aryl substituents.

Reduction of **3.20** with K/Hg in THF did not give the desired Zn–Hg–Zn bonded species, and instead (^{Mes}NacNac)$_2$Zn$_2$ (**3.13**) was the sole product of the reaction (Equation 3.3). This is in direct contrast with the reduction of (^{Dipp}NacNac)ZnI with K/Hg which gave **3.1** as the only product with no trace of [(^{Dipp}NacNac)Zn]$_2$ (**1.81**).

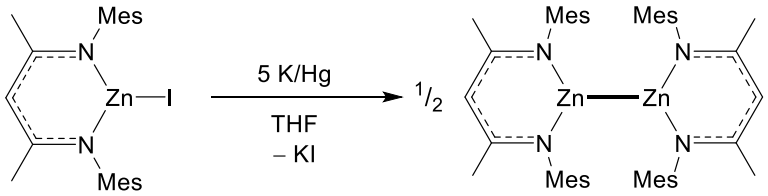

3.20 **3.13**

Equation 3.3

The results of these two reactions suggest that the steric profiles of the ligand may play a role in the stabilisation of the Zn–Hg interactions. To interrogate this possibility a NacNac ligand with an intermediate steric bulk between ^{Mes}NacNac and ^{Dipp}NacNac was targeted for synthesis. Following an analogous route to that published by Gong and Ma,[22] the condensation reaction between {Dipp(H)N}(Me)CCHC(O)Me and MesNH$_2$ in the presence of p-toluenesulfonic acid was performed in refluxing toluene under Dean-Stark conditions to afford (^{DippMes}NacNac)H (**20**, Equation 3.4).

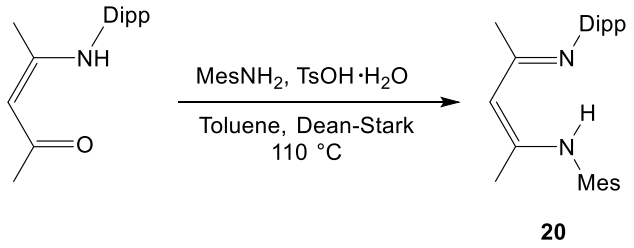

20

Equation 3.4

The reaction of **20** with K[N(SiMe$_3$)$_2$] in THF followed by the subsequent reaction with ZnI$_2$ in THF afforded (^{DippMes}NacNac)ZnI·0.75(THF) (**21**·0.75(THF), Equation 3.5). Diffraction-quality crystals were grown from the slow cooling of a hot hexane solution of **21**. X-ray diffraction showed the solid state structure to be (^{DippMes}NacNac)ZnI(THF) (**21**·THF). The molecular structure and selected distances and angles are shown in Figure 3.2 and Table 3.2.

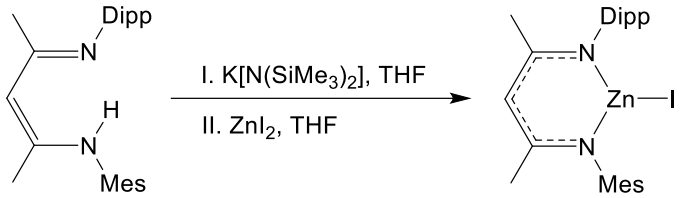

20 **21**

Equation 3.5

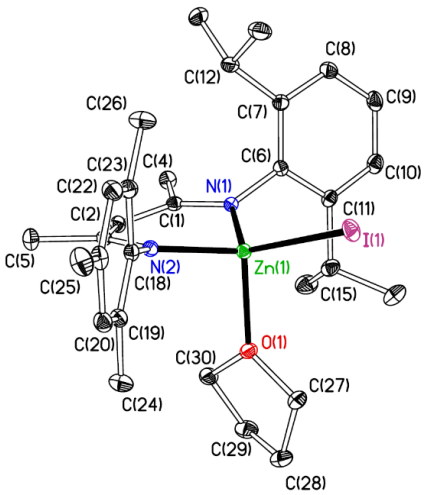

Figure 3.2 Displacement ellipsoid plot (20% probability) of (^{DippMes}NacNac)ZnI(THF) (**21**·THF). H atoms omitted for clarity.

Table 3.2 Selected distances (Å) and angles (°) for (^{DippMes}NacNac)ZnI(THF) (**21**·THF).

Zn(1)–I(1)	2.5080(3)	Zn(1)–N(1)	1.9751(17)
Zn(1)–N(2)	1.9681(16)	Zn(1)–O(1)	2.1205(15)
I(1)–Zn(1)–N(1)	119.11(5)	I(1)–Zn(1)–N(2)	127.05(5)
I(1)–Zn(1)–O(1)	105.03(4)	N(1)–Zn(1)–N(2)	98.10(7)
N(1)–Zn(1)–O(1)	105.26(6)	N(2)–Zn(1)–O(1)	99.07(7)

Compound **21** is monomeric in the solid state. The approximately tetrahedral Zn centre has bonds to I, THF and the two N atoms of the bidentate NacNac ligand. All distances and angles are within the expected ranges for a compound of this type.

Reduction of **21** with K/Hg in THF over 18 h gave a vivid orange solution not unlike that of **3.1**. The ^{1}H NMR spectrum of an aliquot taken from this solution showed complete consumption of the starting material and two distinct products (see Figure 3.4). The organic layer was isolated and volatiles removed under reduced pressure. Exposure of the crude solid to hexane caused visible decomposition of the orange material to a colourless solution with grey precipitate. The mixture was stirred in hexane until colourless (approx. 18 h) and then filtered. Diffraction-quality crystals were obtained from this hexane solution at 5 °C. X-ray diffraction showed these crystals to be (^{DippMes}NacNac)$_2$Zn$_2$ (**22**, Equation 3.6). The molecular structure and selected distances and angles are shown in Figure 3.3 and Table 3.3.

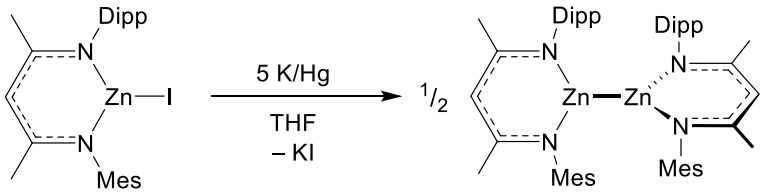

21 **22**

Equation 3.6

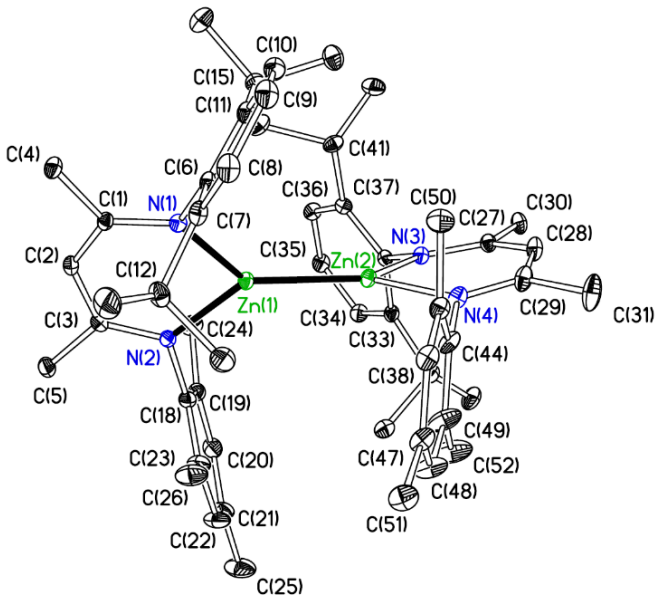

Figure 3.3 Displacement ellipsoid plot (20% probability) of (^{DippMes}NacNac)$_2$Zn$_2$ (**22**). H atoms omitted for clarity.

Table 3.3 Selected distances (Å) and angles (°) for (^{DippMes}NacNac)$_2$Zn$_2$ (**22**).

Zn(1)–Zn(2)	2.3593(4)	Zn(1)–N(1)	2.006(2)
Zn(1)–N(2)	1.996(2)	Zn(2)–N(3)	2.000(2)
Zn(2)–N(4)	1.992(2)		
Zn(2)–Zn(1)–N(1)	135.65(6)	Zn(2)–Zn(1)–N(2)	130.29(6)
N(1)–Zn(1)–N(2)	93.95(8)	Zn(1)–Zn(2)–N(3)	136.89(6)
Zn(1)–Zn(2)–N(4)	129.33(6)	N(3)–Zn(2)–N(4)	93.73(8)

Compound **22** contains Zn–Zn bonds measuring 2.3593(4) and 2.3367(3) Å (two independent molecules in the unit cell). These distances are comparable to the Zn–Zn bonds found in (^{Dipp}NacNac)$_2$Zn$_2$ (**1.81**, 2.3586(7) Å)[4] and (^{Mes}NacNac)$_2$Zn$_2$ (**3.13**, 2.3813(8) Å).[17]

It is interesting to note the vivid orange colour observed during the reduction of **21** to form **22**. This colour is also observed in the reduction of (^{Dipp}NacNac)ZnI, which affords the Zn–Hg–Zn bonded species, **3.1** (which has a vivid orange colour in solution and in the solid state). A solution aliquot taken during the reduction of **21** shows signals from two species by ^{1}H NMR, one of which corresponds to the final product, **22** (Figure 3.4). It is a feasible assumption that the orange colour arises from the unidentified species which is likely to be {(^{DippMes}NacNac)Zn}$_2$Hg (**23**), the structural analogue of **3.1**. Elimination of elemental Hg can be observed as the orange solution obtained from the reduction of **21** undergoes decolouration. This provides further evidence for the identity of **23** as a Hg-containing species.

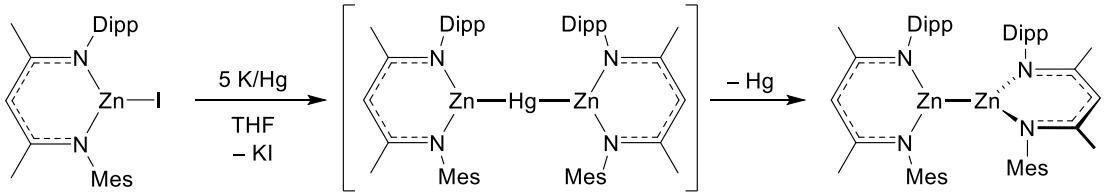

Scheme 3.5 Reduction of (^{DippMes}NacNac)ZnI (**21**) to form (^{DippMes}NacNac)$_2$Zn$_2$ (**22**) *via* a postulated Zn–Hg–Zn bonded intermediate (**23**).

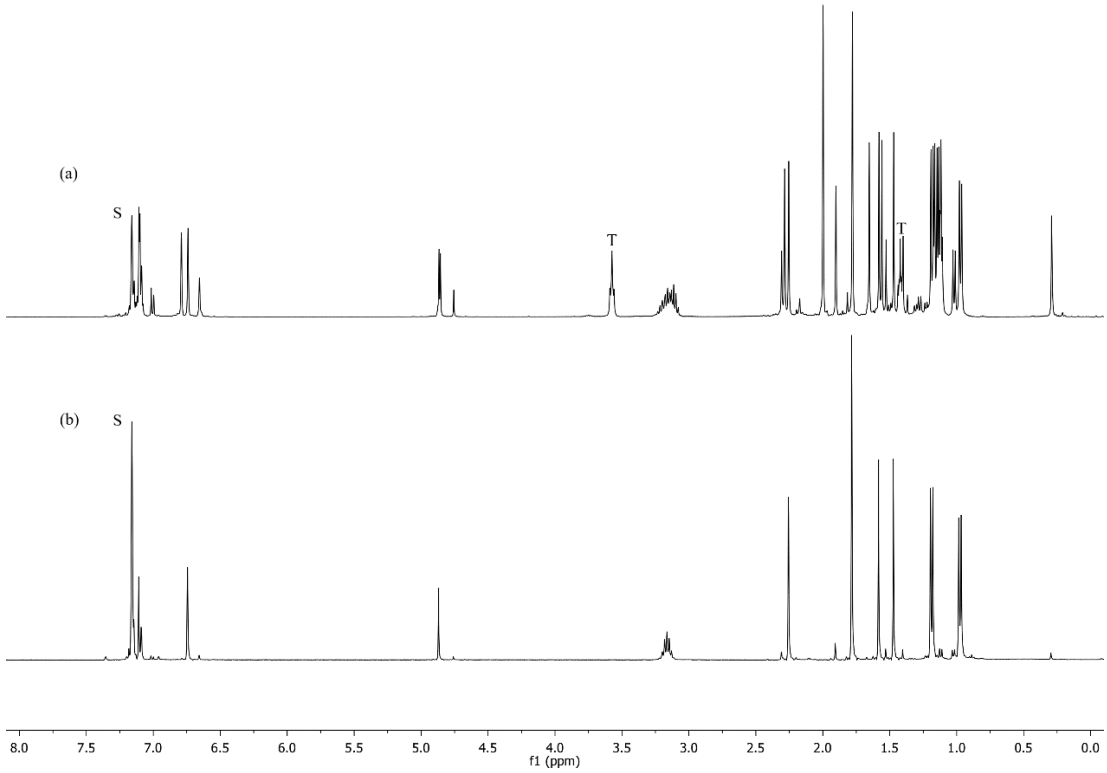

Figure 3.4 ^{1}H NMR (C_6D_6, 400.2 MHz) spectra of the reaction aliquot of the reduction of (^{DippMes}NacNac)ZnI (**21**) with K/Hg in THF (a), and a pure sample of (^{DippMes}NacNac)$_2$Zn$_2$ (**22**, b). 'S' denotes residual protio solvent, 'T' denotes residual THF.

Efforts to isolate **23** *via* fractional crystallisation were unsuccessful at both room temperature and low temperatures; the chemical species degrades to give **22** in all solvent environments tested (hexane, benzene, toluene, THF, pyridine). Compound **23** appeared to be at least somewhat stable in the solid state. It was possible to remove solvent under reduced pressure and store the solid material (a mixture of **22** and **23**) for several days before resolvation without any significant decomposition during storage. Nevertheless, it was not possible to obtain chemically pure samples of **23** in this way, since significant quantities of **22** were always produced alongside **23**. Mixing a pure sample of **22** with excess Hg did not give any **23** (as judged by ^{1}H NMR), suggesting that the conversion of **23** to **22** is an irreversible process.

These observations do not definitively prove that **23** is an intermediate in the formation of **22** however the fact that **23** appears to decompose in solution to give **22**, certainly supports this hypothesis. The ^{DippMes}NacNac ligand was envisaged as a steric hybrid between ^{Dipp}NacNac and ^{Mes}NacNac. Recall that the reduction of (^{Dipp}NacNac)ZnI with

K/Hg amalgam gave **3.1** as a stable Zn–Hg bonded species while the reduction of **3.20** under identical conditions gave only **3.13**, with no evidence of Zn–Hg bonded species present during the reaction. The intermediate steric bulk of the ^{DippMes}NacNac ligand allows the formation of **23** by imparting kinetic stability. However, it is insufficient to thermodynamically stabilise the species which decomposes to form **22** by eliminating Hg. Compound **23** is therefore best described as a long-lived transient intermediate in the formation of **22** (Scheme 3.5).

3.4 DFT study of the relative stabilities of β-diketiminate supported Zn–Hg–Zn compounds

DFT analysis was used to gain insight into the relative stabilities of the Zn–Zn bonded species and their Zn–Hg–Zn bonded counterparts. The observation that reduction of **21** affords a transient Zn–Hg–Zn bonded species (**23**) which converts to give the final Zn–Zn bonded product **22** hints at a possible mechanism for the formation of Zn–Zn bonded species. It can be inferred that Zn–Hg–Zn species are intermediates along the synthetic pathway to the formation of Zn–Zn bonded products.

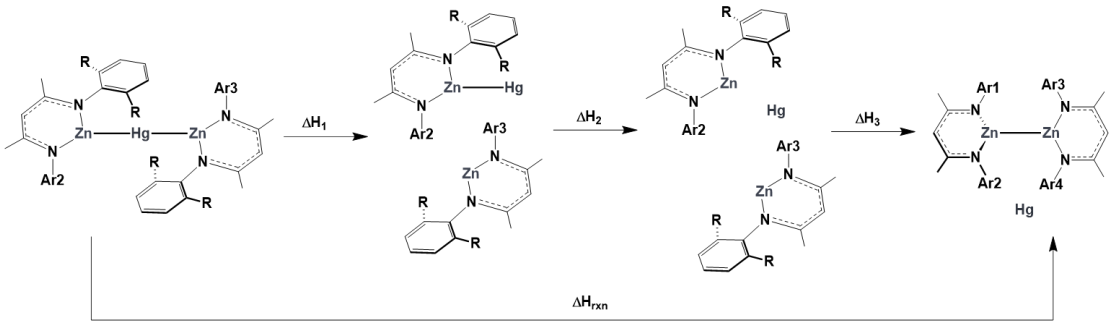

Scheme 3.6 A proposed pathway for the conversion of {(^{Ar}NacNac)Zn}$_2$Hg to (^{Ar}NacNac)$_2$Zn$_2$.

Scheme 3.6 details a hypothetical step-wise pathway for the conversion of Zn–Hg–Zn bonded intermediates to Zn–Zn bonded products. The ligand systems considered for this study were ^{Dipp}NacNac, ^{Mes}NacNac and ^{DippMes}NacNac. During the first step, one Zn–Hg bond is broken to give (^{Ar}NacNac)ZnHg and (^{Ar}NacNac)Zn fragments. The second step involves the breaking of the remaining Zn–Hg bond to give two (^{Ar}NacNac)Zn fragments and one Hg atom. The final step involves the combination of the two (^{Ar}NacNac)Zn fragments to give (^{Ar}NacNac)$_2$Zn$_2$. DFT calculations at the PBEPBE level with Grimme's D3 dispersion corrections[6,7] were employed to obtain optimised geometries for each chemical species in this scheme. The Δ*H* of each step is

given in Table 3.4. The total enthalpy change of reaction (ΔH_{rxn}) is given by the sum of ΔH of each step *i.e.* $\Delta H_{rxn} = \Delta H_1 + \Delta H_2 + \Delta H_3$. The entropy changes ($\Delta S$) associated with the various steps are assumed to be constant. The ΔH_{rxn} values provide only a qualitative assessment of the relative thermodynamic stabilities of the species.

When considering the geometry of Zn–Hg–Zn compounds, the ^{DippMes}NacNac ligand presents an additional computational challenge. As seen from the crystal structure of **3.1**, one Ar group from each ligand associates with the Hg *via* dispersive interactions. In the case of {(^{DippMes}NacNac)Zn}$_2$Hg the possible iterations are a structure with both Dipp groups associated (Dipp trans), both Mes groups associated (Mes trans) or one Dipp group and one Mes group associated (Dipp/Mes trans).

Table 3.4 Enthalpies of reaction (ΔH) for the stepwise conversion of {(^{Ar}NacNac)Zn}$_2$Hg to (^{Ar}NacNac)$_2$Zn$_2$ (Ar = Dipp, Mes or DippMes). All values in kJ/mol.

Ar Group	ΔH_{rxn}	ΔH_1	ΔH_2	ΔH_3
Dipp[1]	0.8	286.8	53.6	−339.6
Mes	−49.2	260.2	48.5	−357.9
DippMes (Dipp trans)	−34.6	269.6	51.0	−355.2
DippMes (Mes trans)	−34.4	269.8	51.0	−355.2
DippMes (Dipp/Mes trans)	−34.7	269.5	51.0	−355.2

The stepwise dissociation of **3.1** was calculated and reported previously by Blake and Mountford.[1] The remaining systems were calculated following this established procedure. In all cases both bond dissociation steps (ΔH_1 and ΔH_2) are endothermic, with ΔH_1 being substantially greater than ΔH_2. Similarly, the combination of (^{Ar}NacNac)Zn fragments (ΔH_3) is exothermic in all cases.

The first bond dissociation enthalpy (ΔH_1) of **3.1** is the most endothermic of all systems calculated, indicating a comparatively stronger Zn–Hg bond. This is likely the result of stronger dispersive interactions between Hg and the Dipp groups. Accordingly, ΔH_2 is also most endothermic for the ^{Dipp}NacNac system. The combination of (^{Ar}NacNac)Zn fragments (ΔH_3) is least exothermic for the ^{Dipp}NacNac system, likely due to some steric

repulsion between the Dipp groups on opposing ligands which slightly destabilises the product compared to its other ^{Ar}NacNac counterparts. The overall ΔH_{rxn} is very slightly endothermic for the ^{Dipp}NacNac system. This is consistent with the observation that **3.1** is the thermodynamic product for the reduction of (^{Dipp}NacNac)ZnI with K/Hg. The thermodynamic stability of **3.1** is therefore the result of comparatively strong Zn–Hg bonds giving high bond dissociation enthalpies and a reduced energetic "payback" from the recombination of the hypothetical (^{Dipp}NacNac)Zn fragments.

In contrast to the ^{Dipp}NacNac system, the overall ΔH_{rxn} is exothermic for the ^{Mes}NacNac system. This result is consistent with the observation that {(^{Mes}NacNac)Zn}$_2$Hg is not observed and that **3.13** is the only product of the reduction of **3.20** with K/Hg. Both bond dissociation steps (ΔH_1 and ΔH_2) are less endothermic than those for the ^{Dipp}NacNac system, while the recombination step (ΔH_3) is more exothermic. In each case this makes the overall ΔH_{rxn} more exothermic than the ^{Dipp}NacNac system and results in a ΔH_{rxn} that is 50 kJ/mol more exothermic in the case of the ^{Mes}NacNac system.

The ^{DippMes}NacNac system, as expected, has values between the ^{Dipp}NacNac and ^{Mes}NacNac systems. Both bond dissociation steps (ΔH_1 and ΔH_2) are more endothermic than those found in the ^{Mes}NacNac system but less endothermic than those found in the ^{Dipp}NacNac system. Interestingly the recombination step (ΔH_3) for the ^{DippMes}NacNac system only differs from that found in the ^{Mes}NacNac system by 2.7 kJ/mol, while there is a 15.6 kJ/mol difference between the ^{DippMes}NacNac and ^{Dipp}NacNac systems. If the change in values were electronic in nature a more intermediate value would be expected for the ΔH_3 of the ^{DippMes}NacNac system. The fact that the values for the ^{DippMes}NacNac and ^{Mes}NacNac systems are so similar while the same value for the ^{Dipp}NacNac system is much greater suggests that ΔH_3 is dominated by steric effects. Crucially, the overall ΔH_{rxn} is an intermediate value, between those found in the ^{Dipp}NacNac and ^{Mes}NacNac systems. This may explain the longer-lived, albeit transitory, nature of **23** before its ultimate conversion to **22**.

This study only considers the thermodynamics of the processes under investigation and does not take into account the kinetic profiles of the reactions. A simplistic kinetic regime can be constructed by considering the Zn–Zn bonded species as the product of a bimolecular reaction comprising the combination of two (^{Ar}NacNac)Zn radical fragments. Figure 3.5 presents typical kinetic profiles for a general bimolecular reaction

in which reactants (R) combine to form a product (P) *via* a transition state (TS). The transition state is an intermediate between the reactants and the product and therefore both the reactants and the product contribute to its relative energy (*E*). An exothermic reaction, in which the energy of the product is lower than that of the reactants, will therefore lower the relative energy of the transition state and will hence lower the activation barrier ($\Delta G^{\ddagger}$) of the reaction. Conversely, the transition state of endothermic reactions will have a higher energy and thus a higher $\Delta G^{\ddagger}$.

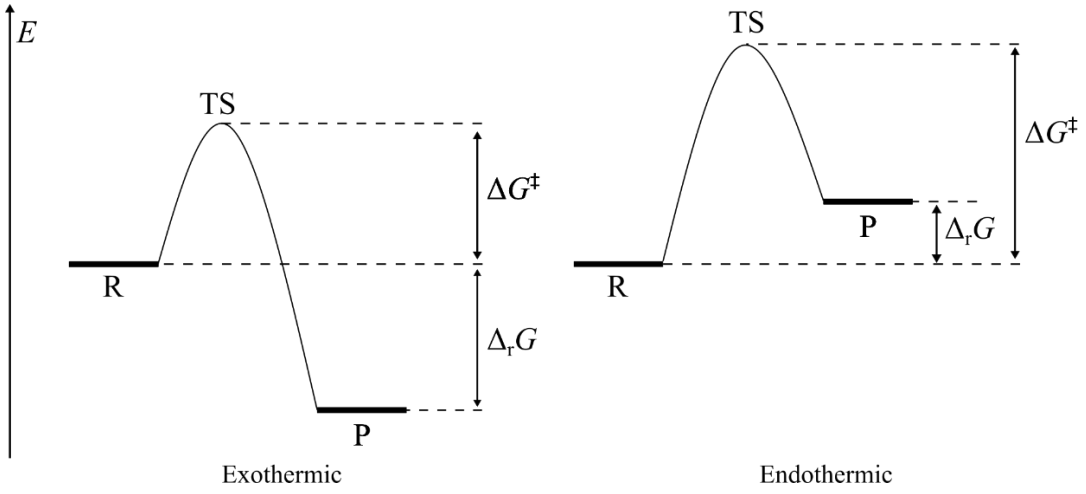

Figure 3.5 Typical kinetic profiles for the exothermic (left) and endothermic (right) reactions of reactants (R) to give a product (P) *via* a transition state (TS).

Under this regime the conversion of the Zn–Hg–Zn compound **3.1** to the Zn–Zn compound **1.81** should have the highest activation energy ($\Delta G^{\ddagger}$) due to the endothermic nature of the reaction. The fact that **1.81** could not be accessed *via* the thermal or photochemical decomposition of **3.1** in the original publication[1] would support this proposal. The conversion of {(^{Mes}NacNac)Zn}$_2$Hg to **3.13** was the most exothermic reaction of the systems examined and hence should have the lowest barrier to activation. Accordingly, no evidence of {(^{Mes}NacNac)Zn}$_2$Hg could be observed and **3.13** is the sole product of the reduction of **3.20** with K/Hg. The thermodynamic calculations demonstrate that the conversion of **23** to **22** is exothermic and has an intermediate value between the ^{Dipp}NacNac and ^{Mes}NacNac systems. As such the activation energy of this process is sufficiently high to allow **23** to exist as a long-lived intermediate but not high enough to allow for its isolation as a stable chemical species.

3.5 Attempted synthesis of a guanidinate supported Zn–Hg–Zn compound

Attempts to synthesise stable Zn–Hg–Zn bonded species with less bulky β-diketiminate ligands were unsuccessful. These results suggest that steric bulk at the forefront of the ligand (proximal to the chelating cavity) is of great importance in preventing the formation of a Zn–Zn bond between two LZn fragments (and thus promoting Zn–Hg–Zn bonding). Given the structure and stability of **3.1**, Dipp appears to be the most suitable substituent for stabilising these catenate-type interactions. As shown in Chapters One and Two, guanidinates have been successfully employed as mimics for β-diketiminate ligands in related areas.[23,24] A guanidinate ligand with N-bound Dipp substituents was therefore considered as a candidate for the stabilisation of the Zn–Hg–Zn interaction.

Attention was directed to $[Me_2NC(NDipp)_2]^-$ due to its previous success in the formation of a stable Mg–Fe bonded complex, as discussed in Chapter Two.[24] Initial attempts to synthesise the guanidinate zinc iodide in a one pot reaction between $LiNMe_2$, DippNCNDipp and ZnI_2 in THF gave $[\{Me_2NC(NDipp)_2\}ZnI_2Li(THF)_2]_2$ (**24**, Equation 3.7). Diffraction-quality crystals were grown from the slow cooling of a hot hexane solution of **24**. The molecular structure and selected distances and angles for **24** are shown in Figure 3.6 and Table 3.5.

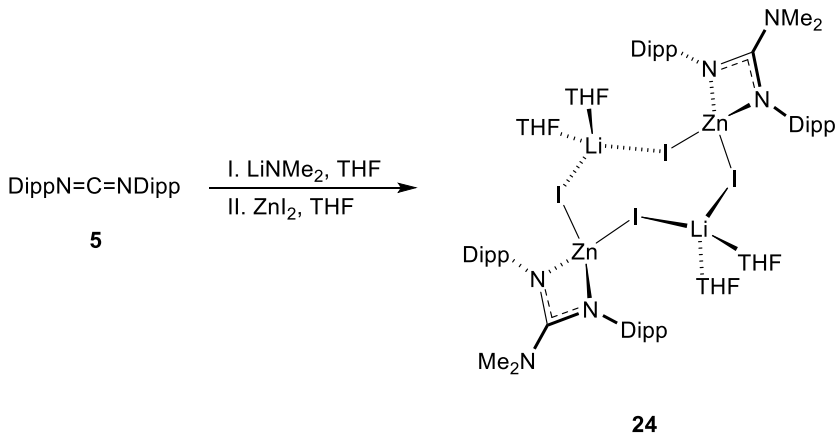

Equation 3.7

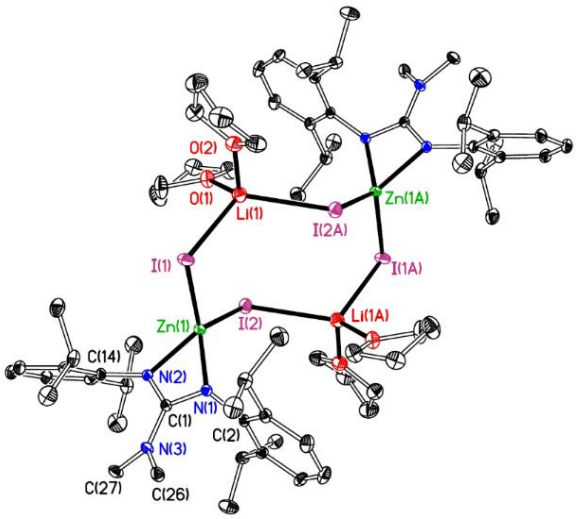

Figure 3.6 Displacement ellipsoid plot (20% probability) of [{$Me_2NC(NDipp)_2$}$ZnI_2Li(THF)_2$]$_2$ (**24**). H atoms omitted for clarity. Atoms carrying the suffix 'A' are related to their counterparts by the symmetry operator 1-x, 1-y, 1-z.

Table 3.5 Selected distances (Å) and angles (°) for [{$Me_2NC(NDipp)_2$}$ZnI_2Li(THF)_2$]$_2$ (**6**).

Zn(1)–I(1)	2.5931(4)	Zn(1)–I(2)	2.5768(4)
Zn(1)–N(1)	2.028(3)	Zn(1)–N(2)	2.063(2)
Li(1)–I(1)	2.815(6)	Li(1)–I(2A)	2.844(6)
Li(1)–O(1)	1.891(7)	Li(1)–O(2)	1.917(7)
C(1)–N(1)	1.338(4)	C(1)–N(2)	1.338(4)
C(1)–N(3)	1.368(4)		
I(1)–Zn(1)–I(2)	111.638(15)	I(1)–Zn(1)–N(1)	111.07(7)
I(1)–Zn(1)–N(2)	119.07(7)	I(2)–Zn(1)–N(1)	125.43(7)
I(2)–Zn(1)–N(2)	117.05(7)	N(1)–Zn(1)–N(2)	66.04(10)
I(1)–Li(1)–I(2A)	115.9(2)	I(1)–Li(1)–O(1)	109.0(3)
I(1)–Li(1)–O(2)	96.2(2)	I(2A)–Li(1)–O(1)	122.2(3)
I(2A)–Li(1)–O(2)	101.7(3)	O(1)–Li(1)–O(2)	107.7(3)
Zn(1)–I(1)–Li(1)	99.00(13)	Zn(1)–I(2)–Li(1A)	119.59(13)
Zn(1)–N(1)–C(1)	91.26(18)	Zn(1)–N(2)–C(1)	89.74(18)
N(1)–C(1)–N(2)	112.9(3)	N(1)–C(1)–N(3)	122.7(3)
N(2)–C(1)–N(3)	124.4(3)		

Compound **24** is the lithiate complex of the desired guanidinate zinc iodide. Unlike typical lithiate compounds, **24** forms a dimeric complex with an eight-membered $Zn_2I_4Li_2$ ring structure. The coordination environments at the Zn and Li centres are both approximately tetrahedral. Distances and angles are as expected for a compound of this type. Attempts to eliminate LiI and obtain the monomeric guanidinate zinc iodide by heating **24** in toluene-d_8 (100 °C) were unsuccessful.

Deprotonation of $Me_2NC(NDipp)NHDipp$ (**16**) with $K[N(SiMe_3)_2]$ in THF followed by reaction with ZnI_2 gave $[\{Me_2NC(NDipp)_2\}Zn(\mu\text{-}I)]_2$ (**25**, Equation 3.8). Diffraction-quality crystals were grown from the slow cooling of a hot hexane solution of **25**. The molecular structure and selected distances and angles for **25** are shown in Figure 3.7 and Table 3.6.

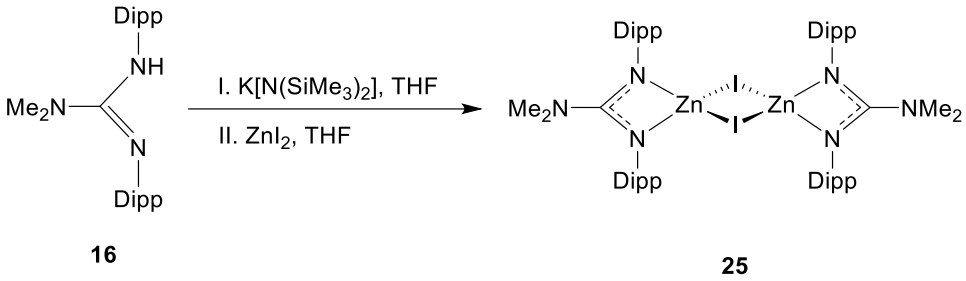

Equation 3.8

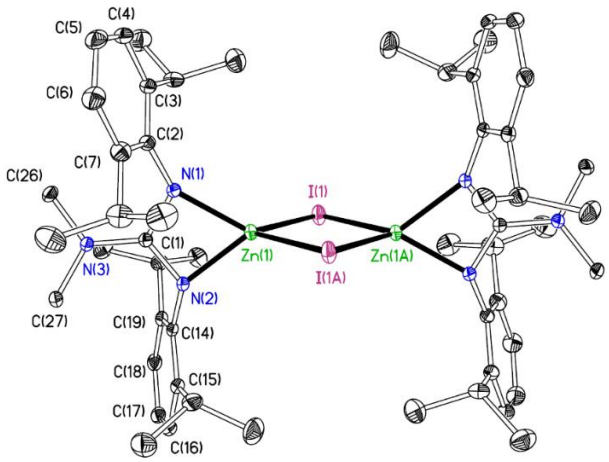

Figure 3.7 Displacement ellipsoid plot (20% probability) of $[\{Me_2NC(NDipp)_2\}Zn(\mu\text{-}I)]_2$ (**25**). H atoms omitted for clarity. Atoms carrying the suffix 'A' are related to their counterparts by the symmetry operator ½-x, 3/2-y, 1-z.

Table 3.6 Selected distances (Å) and angles (°) for [{$Me_2NC(NDipp)_2$}Zn(μ-I)]$_2$ (**25**).

Zn(1)–I(1)	2.6375(4)	Zn(1)–I(1A)	2.6124(3)
Zn(1)–N(1)	2.0111(19)	Zn(1)–N(2)	2.0019(18)
C(1)–N(1)	1.350(3)	C(1)–N(2)	1.344(3)
C(1)–N(3)	1.353(3)		
I(1)–Zn(1)–I(1A)	100.712(11)	I(1)–Zn(1)–N(1)	124.08(6)
I(1)–Zn(1)–N(2)	117.60(6)	I(1A)–Zn(1)–N(1)	123.86(6)
I(1A)–Zn(1)–N(2)	122.04(6)	N(1)–Zn(1)–N(2)	67.66(7)
Zn(1)–I(1)–Zn(1A)	79.288(11)	Zn(1)–N(1)–C(1)	89.85(13)
Zn(1)–N(2)–C(1)	90.43(13)	N(1)–C(1)–N(2)	112.05(19)
N(1)–C(1)–N(3)	123.75(19)	N(2)–C(1)–N(3)	124.21(19)

Compound **25** has a dimeric structure consisting of two LZnI units linked by two μ-I interactions. The coordination environment at the Zn atoms is approximately tetrahedral. Distances and angles are as expected for a compound of this type.

Treatment of **25** with K/Hg in THF gave the homoleptic compound {$Me_2NC(NDipp)_2$}$_2$Zn (**26**, Equation 3.9) *via* a disproportionation reaction. Diffraction-quality crystals were grown *via* concentration of the reaction solution. The molecular structure and selected distances and angles for **26** are shown in Figure 3.8 and Table 3.7.

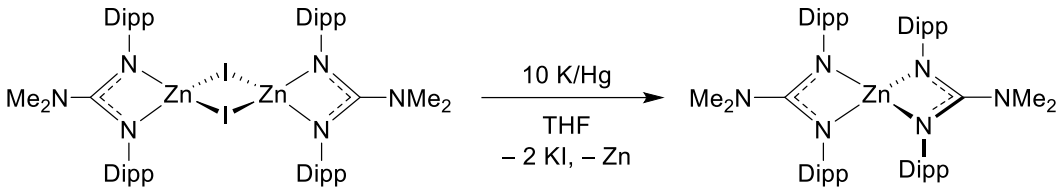

25 **26**

Equation 3.9

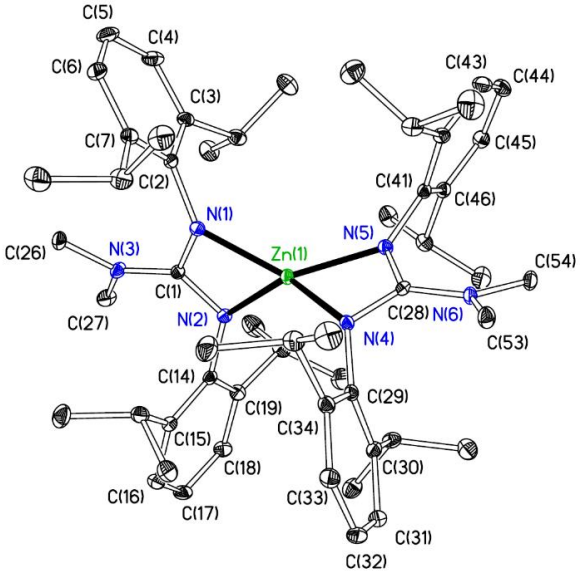

Figure 3.8 Displacement ellipsoid plot (20% probability) of $\{Me_2NC(NDipp)_2\}_2Zn$ (**26**). H atoms omitted for clarity.

Table 3.7 Selected distances (Å) and angles (°) for $\{Me_2NC(NDipp)_2\}_2Zn$ (**26**).

Zn(1)–N(1)	2.016(2)	Zn(1)–N(2)	2.040(2)
Zn(1)–N(4)	2.021(2)	Zn(1)–N(5)	2.024(2)
C(1)–N(1)	1.357(3)	C(1)–N(2)	1.343(3)
C(1)–N(3)	1.358(3)	C(28)–N(4)	1.346(3)
C(28)–N(5)	1.345(3)	C(28)–N(6)	1.362(3)
N(1)–Zn(1)–N(2)	67.21(8)	N(1)–Zn(1)–N(4)	135.74(9)
N(1)–Zn(1)–N(5)	134.97(9)	N(2)–Zn(1)–N(4)	131.08(8)
N(2)–Zn(1)–N(5)	134.30(9)	N(4)–Zn(1)–N(5)	66.83(8)
N(1)–C(1)–N(2)	112.5(2)	N(1)–C(1)–N(3)	123.3(2)
N(2)–C(1)–N(3)	124.3(2)	Zn(1)–N(1)–C(1)	90.45(15)
Zn(1)–N(2)–C(1)	89.85(15)	N(4)–C(28)–N(5)	111.8(2)
N(4)–C(28)–N(6)	123.4(2)	N(5)–C(28)–N(6)	124.8(2)
Zn(1)–N(4)–C(28)	90.72(15)	Zn(1)–N(5)–C(28)	90.65(15)

Compound **26** is a homoleptic compound possessing two guanidinate ligands coordinated to a central Zn atom. The geometry around the Zn centre is approximately tetrahedral. All distances and angles are as expected for a compound of this type.[25]

The single crystal from which the X-ray diffraction pattern was collected was dissolved in C_6D_6. The ^{1}H NMR spectrum of this crystal matched that collected from an aliquot of the reaction mixture, demonstrating that **26** is the only major product of the reaction, in addition to the by-products, KI and elemental Zn.

Guanidinate zinc compounds were targeted for this investigation due to their ability to act as substitutes for β-diketiminate ligands. Although this methodology has been successful in other areas,[23,24] the presence of the distal N-donor in the guanidine structure gives guanidinate complexes electronic properties distinct from those of their β-diketiminate counterparts. As a result, the guanidinate zinc compound **25** is insufficiently robust to tolerate the reducing environment of the K/Hg amalgam and instead undergoes a disproportionation reaction.

3.6 Conclusions

This Chapter detailed the investigation of Zn–Hg–Zn bonded compounds. An introduction to the first Zn–Hg bonded compound, {(^{Dipp}NacNac)Zn}$_2$Hg (**3.1**), along with other notable examples in the area of Gp12–Gp12 bonding were presented. A DFT study of the isostructural compounds {(^{Dipp}NacNac)Zn}$_2$Hg and {(^{Dipp}NacNac)Zn}$_2$Zn showed that the trizinc system possesses more covalent Zn–Gp12–Zn interactions.

The reduction of (^{Mes}NacNac)ZnI with K/Hg did not produce {(^{Mes}NacNac)Zn}$_2$Hg, as expected. Instead, (^{Mes}NacNac)$_2$Zn$_2$ (**3.13**), previously reported by Schulz *et al*.,[17] was the sole product of this reaction.

The ligand ^{DippMes}NacNac was sought as a steric intermediate between ^{Dipp}NacNac and ^{Mes}NacNac. ^{DippMes}NacNacH (**20**) was obtained *via* the condensation reaction between {Dipp(H)N}(Me)CCHC(O)Me and MesNH$_2$ under Dean-Stark conditions. The ligand was installed onto Zn using previously reported methods[1] to give (^{DippMes}NacNac)ZnI (**21**).

Reduction of **21** with K/Hg amalgam in THF gave a mixture of two products, (^{DippMes}NacNac)$_2$Zn$_2$ (**22**) and {(^{DippMes}NacNac)Zn}$_2$Hg (**23**), the latter of which converted in solution to give **22** as the sole thermodynamic product of the reaction. Compound **23** is therefore assumed to be a reactive intermediate on the synthetic pathway to **22**.

A DFT analysis was performed for the stepwise dissociation of {(^{Ar}NacNac)Zn}$_2$Hg to give (^{Ar}NacNac)$_2$Zn$_2$ and Hg (Ar = Dipp, Mes, DippMes). This study found that this

process was overall endothermic for the conversion of **3.1** to (^{Dipp}NacNac)$_2$Zn$_2$. This result supports the observation that **3.1** is stable and is the thermodynamic product of the reduction of (^{Dipp}NacNac)ZnI with K/Hg. Conversely, the conversion of the hypothetical {(^{Mes}NacNac)Zn}$_2$Hg to (^{Mes}NacNac)$_2$Zn$_2$ (**3.13**) was found to be overall exothermic, consistent with the observation that **3.13** is the sole product of the reduction of (^{Mes}NacNac)ZnI with K/Hg. The study found the conversion of **23** to **22** to be overall exothermic with values intermediate between the ^{Dipp}NacNac and ^{Mes}NacNac examples, possibly explaining the long-lived nature of **23** as a reactive intermediate in the synthesis of **22**. The study found that the ΔH for combination of (^{Ar}NacNac)Zn fragments was very similar for Ar = Mes and DippMes while ΔH for Dipp was much less exothermic. This difference is likely to arise from the sterics of ligands and supports the original hypothesis of this Chapter that the ligand sterics have a substantial impact on the stability of Zn–Hg–Zn bonded compounds.

The guanidinate compound [{Me$_2$NC(NDipp)$_2$}Zn(μ-I)]$_2$ (**25**) was synthesised. Reduction of **25** with K/Hg in THF gave the homoleptic compound {Me$_2$NC(NDipp)$_2$}$_2$Zn (**26**) as the sole product of the reaction. No evidence of any Zn–Hg or Zn–Zn bonded compounds was observed.

3.7 References

1. M. P. Blake, N. Kaltsoyannis, and P. Mountford, *Chem. Commun.*, 2015, **51**, 5743–5746.
2. B. Cordero, V. Gómez, A. E. Platero-Prats, M. Revés, J. Echeverría, E. Cremades, F. Barragán, and S. Alvarez, *Dalton Trans.*, 2008, 2832–2838.
3. P. Pyykkö and M. Atsumi, *Chem. Eur. J.*, 2009, **15**, 186–197.
4. Y. Wang, B. Quillian, P. Wei, H. Wang, X. Yang, Y. Xie, R. B. King, P. v. R. Schleyer, H. F. Schaefer, and G. H. Robinson, *J. Am. Chem. Soc.*, 2005, **127**, 11944–11945.
5. Z. Zhu, M. Brynda, R. J. Wright, R. C. Fischer, W. A. Merrill, E. Rivard, R. Wolf, J. C. Fettinger, M. M. Olmstead, and P. P. Power, *J. Am. Chem. Soc.*, 2007, **129**, 10847–10857.
6. S. Grimme, *J. Comput. Chem.*, 2006, **27**, 1787–1799.
7. S. Grimme, S. Ehrlich, and L. Goerigk, *J. Comput. Chem.*, 2011, **32**, 1456–1465.

8. R. F. W. Bader, *Atoms in Molecules: A Quantum Theory*, Oxford University Press, Oxford, 1990.

9. M. L. H. Green, P. C. Konidaris, and P. Mountford, *J. Chem. Soc., Dalton Trans.*, 1994, 2851–2859.

10. J. Hicks, E. J. Underhill, C. E. Kefalidis, L. Maron, and C. Jones, *Angew. Chem. Int. Ed.*, 2015, **54**, 10000–10004.

11. C. Bakewell, B. J. Ward, A. J. P. White, and M. R. Crimmin, *Chem. Sci.*, 2018, **9**, 2348–2356.

12. S. J. Bonyhady, S. P. Green, C. Jones, S. Nembenna, and A. Stasch, *Angew. Chem. Int. Ed.*, 2009, **48**, 2973–2977.

13. P. Mountford, *Personal Communication*.

14. D. R. Lide, Ed., *CRC Handbook of Chemistry and Physics, 84th Edition*, Boca Raton, Florida, 2003.

15. L. Pauling, *The Nature of the Chemical Bond, Third Edition*, Cornell University Press, Ithaca, New York, 1960.

16. I. Resa, E. Carmona, E. Gutierrez-Puebla, and A. Monge, *Science*, 2004, **305**, 1136–1138.

17. S. Schulz, D. Schuchmann, U. Westphal, and M. Bolte, *Organometallics*, 2009, **28**, 1590–1592.

18. H. P. Nayek, A. Lühl, S. Schulz, R. Köppe, and P. W. Roesky, *Chem. Eur. J.*, 2011, **17**, 1773–1777.

19. S. Gondzik, D. Bläser, C. Wölper, and S. Schulz, *Chem. Eur. J.*, 2010, **16**, 13599–13602.

20. S. Schulz, S. Gondzik, D. Schuchmann, U. Westphal, L. Dobrzycki, R. Boese, and S. Harder, *Chem. Commun.*, 2010, **46**, 7757.

21. S. Schulz, T. Eisenmann, U. Westphal, S. Schmidt, and U. Flörke, *Z. Anorg. Allg. Chem.*, 2009, **635**, 216–220.

22. S. Gong and H. Ma, *Dalton Trans.*, 2008, 3345.

23. A. Sidiropoulos, C. Jones, A. Stasch, S. Klein, and G. Frenking, *Angew. Chem.*

Int. Ed., 2009, **48**, 9701–9704.

24. R. Green, A. C. Walker, M. P. Blake, and P. Mountford, *Polyhedron*, 2016, **116**, 64–75.

25. D. A. Fletcher, R. F. McMeeking, and D. Parkin, *J. Chem. Inf. Comput. Sci.*, 1996, **36**, 746–749.

Chapter Four

Reactivity study of $\{(^{Dipp}NacNac)Zn\}_2Hg$

4.1 Overview

This Chapter describes the reactivity of the heterocatenate complex {(^{Dipp}NacNac)Zn}$_2$Hg with various small-molecule reagents, including silyl halides, phenyl azide, carbon disulfide, isocyanates, peroxides and azobenzene.

4.2 Introduction

Chapter Three describes the synthesis of {(^{Dipp}NacNac)Zn}$_2$Hg (**3.1**) and its assignment as a [Zn(I)]$_2$Hg(0) species, supported by DFT and QTAIM analysis.[1] With the exception of **3.1**, the study of the reactivity of zinc in the +1 oxidation state has been limited to that of Zn(I)–Zn(I) dimers.

During the report of the synthesis of the first Zn(I) complex, $Zn_2Cp^*_2$ (**1.79**), Carmona *et al*. also reported the first reaction of a Zn(I) species. Compound **1.79** reacts with the isocyanide, CNXyl, producing the half-sandwich iminoacyl species Cp*Zn{C(NXyl)C$_5$Me$_5$} (**4.1**) and Zn(0) *via* a disproportionation reaction (Equation 4.1).[2]

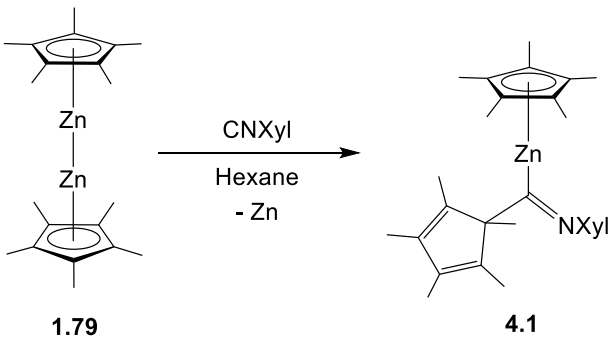

1.79 **4.1**

Equation 4.1[2]

Further studies have shown **1.79** to be a particularly labile species. Indeed, this landmark discovery of the first Zn(I) complex has stimulated much research concerning its unique reactivity. Fischer *et al*. have published several reactions between **1.79** and various oxidising agents.[3] The reaction of **1.79** with Brookhart's Acid, [H(OEt$_2$)$_2$][BAr$^F_4$], gives the double sandwich complex, [$Zn_4Cp^*_3$(Et$_2$O)$_2$][BAr$^F_4$] (**4.2**, Scheme 4.1) *via* protolytic cleavage of a Cp* moiety. The solid state structure of **4.2** has two Zn–Zn bonds measuring 2.310(1) and 2.307(1) Å; similar in length to that observed in **1.79** (2.305(3) Å).[2] Reaction of **1.79** with the aprotic oxidising agent

$[FeCp_2][BAr^F_4]$ in diethyl ether gave $[Cp^*Zn_2(OEt_2)_3][BAr^F_4]$ (**4.3**, Scheme 4.1) *via* oxidative cleavage of one Cp* group. X-ray analysis of crystals of **4.3** showed a lengthened Zn–Zn bond of 2.324(2) Å, compared with that of **1.79**.

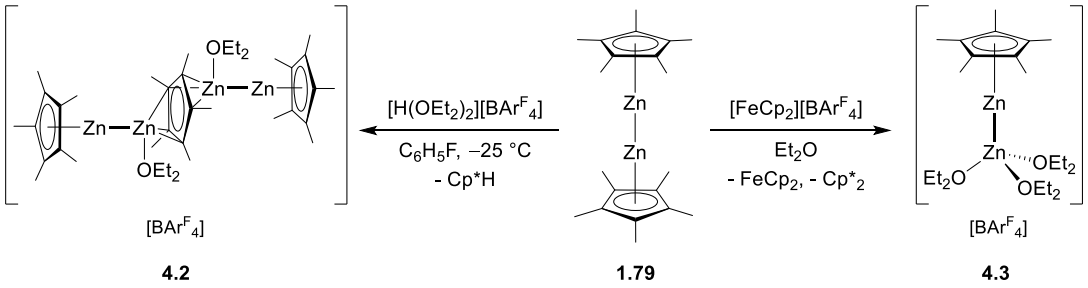

Scheme 4.1 Oxidative cleavage reactions of **1.79**.[3]

Schulz *et al*. have reported the reaction of **1.79** with the Lewis base DMAP (4-dimethylaminopyridine) to give $Cp^*ZnZn(DMAP)_2Cp^*$ (**4.4**, Equation 4.2).[4] X-ray crystal analysis of **4.4** shows two DMAP units coordinating to one Zn atom in a germinal coordination mode. The Cp* ligand of this base-coordinated Zn atom has slipped from the η^5 to the η^1 coordination mode in order to maintain a stable 18 valence electron state in accordance with the "18-electron rule".[5] With the additional ZnCp* unit, the geometry around the base-coordinated Zn atom is approximately tetrahedral. The Zn–Zn distance of 2.418(1) Å is significantly lengthened compared to that found in **1.79**.

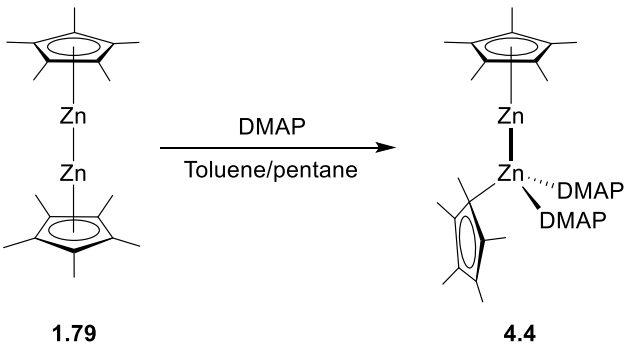

Equation 4.2[4]

In a later report, Schulz *et al*. show that **4.4** reacts with $[H(OEt_2)_2][Al\{OC(CF_3)_3\}_4]$ to give $[Zn_2(DMAP)_6][Al\{OC(CF_3)_3\}_4]_2$ (**4.5**, Equation 4.3),[6] the first isolated example of a base-stabilised $[Zn_2]^{2+}$ dication. X-ray analysis of **4.5** shows a Zn–Zn bond length of 2.419(1) Å, identical within error to the parent compound, **4.4** (2.418(1) Å).

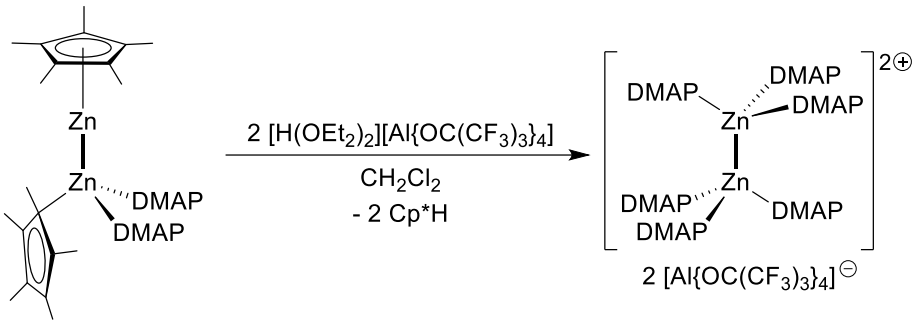

4.4 **4.5**

Equation 4.3[6]

Fischer *et al*. have demonstrated that **1.79** undergoes reactions with a variety of main group and transition metals. The reaction of **1.79** with $[Ga_2Cp^*][BAr^F_4]$ gave $[Zn_2(GaCp^*)_6][BAr^F_4]_2$ (**4.6**, Scheme 4.2).[7] The solid state structure contained a $[Zn_2]^{2+}$ core with a Zn(I)–Zn(I) distance of 2.411(1) Å, which is elongated slightly compared to **1.79** and is likely the result of substitution of Cp* ligands for the more electrophilic Cp*Ga moieties. Zn and Ga are neighbours in the periodic table and it is therefore difficult to unambiguously assign atomic identities for the solid state structure of **4.6** due to their similar X-ray scattering properties. The atomic absorption spectrum of **4.6** supported the structural assignment with a Zn/Ga ratio of 2.0:5.7. The RT ^{1}H NMR spectrum of **4.6** showed only a single resonance attributable to the Cp* methyl protons, suggesting rapid interconversion between the bridged structure of **4.6** and an unbridged intermediate (Scheme 4.2). The ^{1}H NMR spectrum at −90 °C contained two broadened singlets with an integral ratio of 5:1. The solid state structure of **4.6** contains four terminal and two bridging Cp*Ga moieties, giving an expected integral ratio of 2:1. The authors attribute the deviation in the expected Cp* integral ratio to the existence of a second isomer in solution, which contains all-terminal Cp*Ga ligands. This is a reasonable assumption given that such a structure is a possible intermediate in the fluxional process which interconverts the terminal and bridging Cp*Ga ligands.

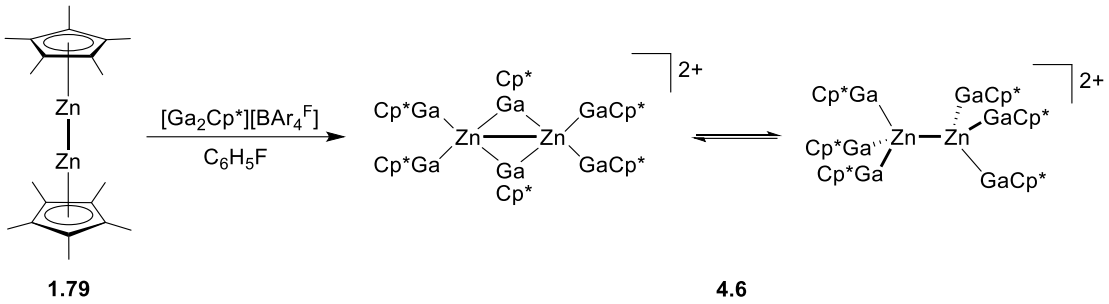

1.79 **4.6**

Scheme 4.2 Reaction of **1.79** with $[Ga_2Cp^*][BAr^F_4]$ to afford $[Zn_2(GaCp^*)_6][BAr^F_4]$ (**4.6**), which exists in fast exchange between bridged and unbridged forms.[7] Counteranions are omitted for clarity.

Fischer *et al*. also demonstrated that **1.79** reacts with $Pd(GaCp^*)_4$ to afford $Pd(GaCp^*)_2(ZnCp^*)_2(ZnZnCp^*)_2$ (**4.7**) and $Pd(ZnCp^*)_4(ZnZnCp^*)_4$ (**4.8**) (Scheme 4.3).[8] The ligands in **4.7** are arranged about Pd in an approximately octahedral coordination environment while the coordination environment of **4.8** is best described as a distorted trigonal dodecahedron. Although the Cp*Zn ligands in **4.7** and **4.8** arise from **1.79**, these cyclopentadienyl Zn(I) ligands are not solely related to the chemistry of that compound and have been observed to result from the reduction of $ZnCp_2$ with a wide variety of transition metal compounds.[9] Crucially, both **4.7** and **4.8** contain the first example of the monovalent Cp*ZnZn ligand. Although some consideration is given to the mechanisms which result in the formation of **4.7** and **4.8**, no conclusive processes are specified by the authors. Cp*Zn moieties are likely to be the result of homolysis at the Zn–Zn bond of **1.79**. The authors note that a stoichiometric quantity of Cp^*_2Zn is present for each Cp*ZnZn unit formed. This suggests that a disproportionative mechanism is in operation, where $Cp^*_2Zn^I_2$ produces $Cp^*Zn^IZn^0$ and $Cp^*_2Zn^{II}$. The authors suggest that this process may take place *via* Cp* transfer reactions between **1.79** and low coordinate Cp*Zn containing intermediates. This outcome was also observed for all Pt analogues in the reaction between **1.79** and $Pt(GaCp^*)_4$.

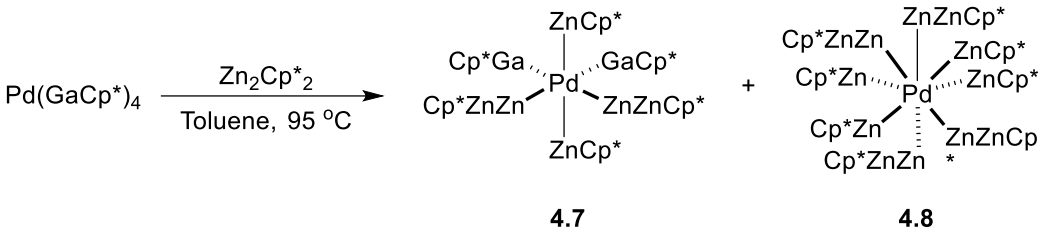

4.7 **4.8**

Scheme 4.3 Reaction of **1.79** with $Pd(GaCp^*)_4$ to give $Pd(GaCp^*)_2(ZnCp^*)_2(ZnZnCp^*)_2$ (**4.7**) and $Pd(ZnCp^*)_4(ZnZnCp^*)_4$ (**4.8**).[8]

Fischer *et al*. have demonstrated that similar homolytic cleavage reactions of the Zn–Zn moiety of **1.79** can be achieved with other transition metal elements. Reaction of **1.79** with $M(cod)_2$ (M = Ni, Pt; cod = 1,5-cyclooctadiene) or $PdMe_2(TMEDA)$ gives $Cp^*M(ZnCp^*)_3$ (M = Ni (**4.9**), Pt (**4.10**), Pd (**4.11**)).[10] Following Zn–Zn bond cleavage three Cp*Zn moieties are trapped by the transition metal centre while Cp* transfer from Zn to M results in a redox process whereby the metal is formally oxidised from M(0) to M(I) and Zn is reduced, eliminating from the reaction mixture as metallic Zn(0). The reaction of $PdMe_2(TMEDA)$ with **1.79** was somewhat more complicated, producing several other products, however **4.11** was isolated *via* extraction, recrystallisation and manual crystal separation. The authors note that if an excess (8 equiv.) of **1.79** is used in the production of either **4.9** or **4.10**, the formation of $M(ZnCp^*)_4(ZnZnCp^*)_4$ (M = Ni, Pt) is observed, which resemble **4.8** (*vide supra*).

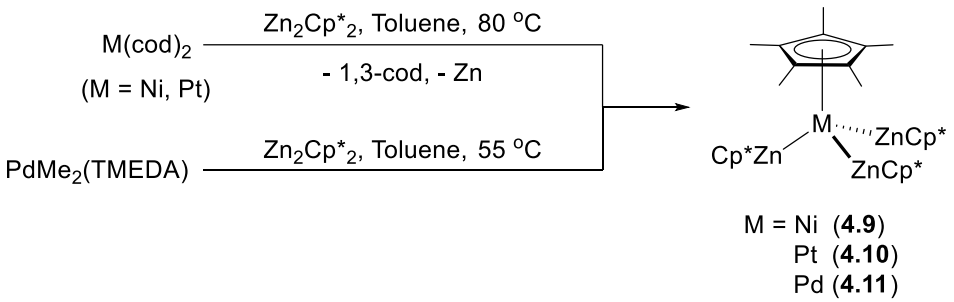

Scheme 4.4 Reaction of **1.79** with group 10 complexes to afford $Cp^*M(ZnCp^*)_3$ (M = Ni (**4.9**), Pt (**4.10**), Pd (**4.11**)).[10]

More recently Fischer and co-workers have utilised **1.79** to produce exotic metallacycles. The reaction between **1.79** and *in situ* generated $[ZnCp^*]^+$ or CuCp* produces $[Zn_3Cp^*_3][BAr^F_4]$ (**4.12**) and $Zn_2CuCp^*_3$ (**4.13**), respectively (Scheme 4.5).[11] These 3 membered triangular metallacycles are isolobal with the trihydrogen ion, $[H_3]^+$, and are stabilised by σ-aromaticity, which manifests as a three-centre two-electron

bond. Both complexes are extremely reactive, particularly **4.12**, which cannot be redissolved without extensive decomposition to $Zn_2Cp^*_2$, $ZnCp^*_2$ and BAr^F_3, among other products. Mass spectrometric analysis of **4.13** failed to reveal a mass ion peak, but instead revealed the presence $[Zn_4Cu_3Cp^*_5]^+$, $[Zn_4Cu_2Cp^*_6]^+$, and $[Zn_3CuCp^*_3]^+$, suggesting the potential of **4.13** as a synthon for higher nuclearity metal clusters. The authors suggest that complexes such as these will become useful for the "bottom-up" synthesis of metallic clusters and alloys in the future, referring to **4.13** as "embryonic brass".

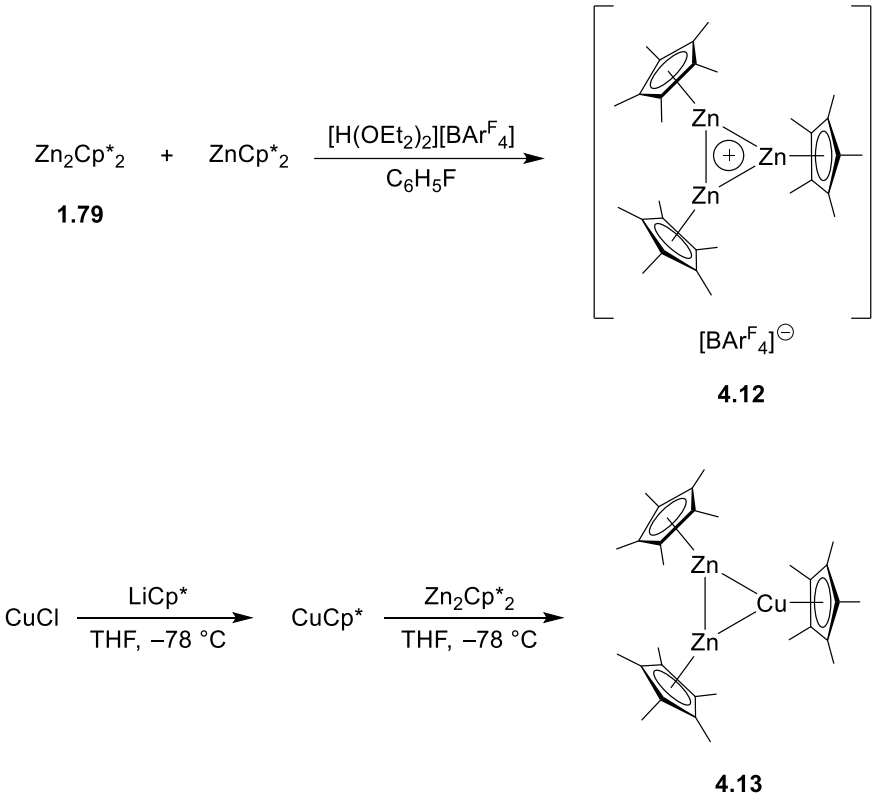

Scheme 4.5 Formation of Zn containing metallacycles from **1.79**.[11]

Fischer *et al*. have published further results which advance their goal of bottom-up, atom-precise syntheses for organometallic metal clusters using **1.79** as a starting point. Reaction of **1.79**, $[FeCp_2][BAr^F_4]$ and $ZnMe_2$ in 12:2:1 molar ratio gives the organometallic cluster complex $[Zn_{10}Cp^*_6Me][BAr^F_4]$ (**4.14**).[12] This compound was found to be stable only below −10 °C in polar, aprotic, non-coordinating solvents such as C_6H_5F and CH_2Cl_2. The authors note that the extreme lability of **4.14** should allow further transformations to other organometallic cluster complexes. Indeed, dissolution of **4.14** in THF caused abstraction of $[MeZn(THF)_3][BAr^F_4]$ giving the neutral cluster complex $Zn_9Cp^*_6$ (**4.15**), while reaction with the softer ligand ^{t}BuNC gave

$[Zn_8Cp^*_5(^tBuNC)_3][BAr^F_4]$ (**4.16**). This research demonstrates that controlled fragmentation of labile organozinc clusters such as **4.14** can furnish a variety of atom-precise products based upon the choice of coordinating ligands.

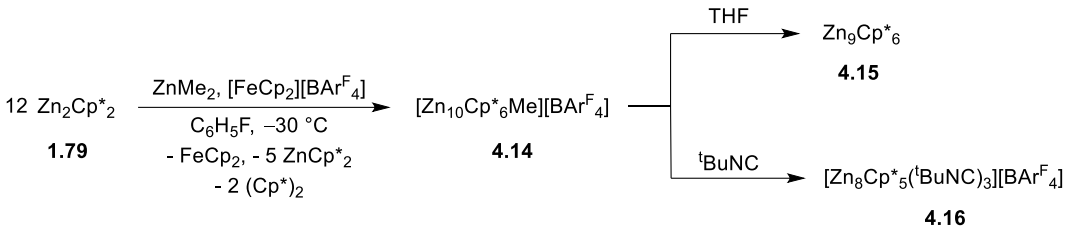

Scheme 4.6 Formation of Zn_{10} cluster **4.14** and its controlled destruction with Lewis bases to afford atom precise organozinc clusters.[12]

Roesky *et al*. have shown that **1.79** reacts with SO_2 to give $Zn_4(O_2SCp^*)_6O$ (**4.17**, Equation 4.4) in moderate yield.[13] Complex **4.17** presumably arises from the insertion of SO_2 into the Zn–C bonds and the reductive abstraction of an oxo moiety, although the authors state that other processes cannot be ruled out. The reductive cleavage of SO_2 into SO and O^{2-} is generally disfavoured due to the instability of SO. The isolation of **4.17** therefore demonstrates the strong reducing capability of Zn(I) species.

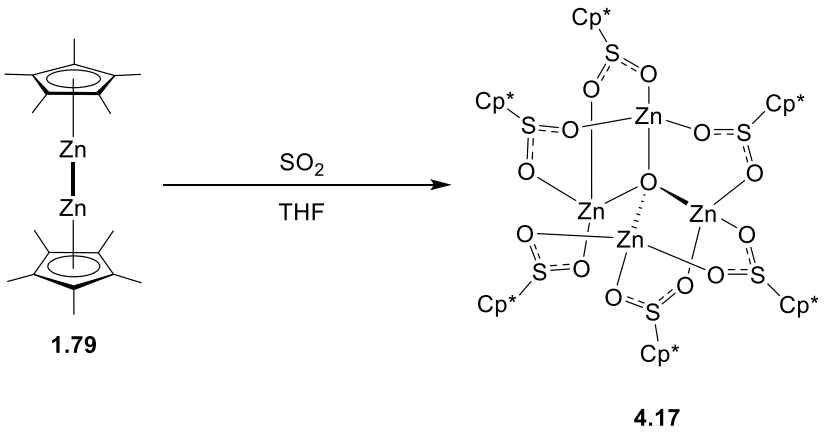

Equation 4.4[13]

Since developing a facile synthesis for $(^{Mes}NacNac)_2Zn_2$ (**3.13**) from **1.79** (see Chapter Three) Schulz and co-workers have been working to further the known reactivity of such Zn(I) compounds. In 2014, they demonstrated the reaction of **3.13** with several chalcogenide reagents (Scheme 4.7). Reaction of **3.13** with PhSeSePh gave $[(^{Mes}NacNac)Zn(\mu\text{-}SePh)]_2$ (**4.18**),[14] wherein each Zn(I) centre acts as a one electron reductant resulting in reductive cleavage of the Se–Se bond. Structural authentication

of the crystalline product by X-ray diffraction shows two Zn(II) units in an approximately tetrahedral geometry bridged by two phenyl selenide ligands. The reaction of **3.13** with PhTeTePh proceeded in an analogous fashion. Although crystals of the product could not be obtained its identity was assumed to be [(^{Mes}NacNac)Zn(μ-TePh)]$_2$ (**4.19**). Reaction of **4.19** with O_2 furnished a crude product from which single crystals could be obtained after recrystallisation. X-ray analysis of these crystals determined the product to be [(^{Mes}NacNac)Zn(μ-O_2TePh)]$_2$ (**4.20**). The reaction of **4.19** with O_2 is therefore assumed to involve the oxidation of Te(II) to Te(IV), affording the corresponding metallated phenyltellurinic acid.

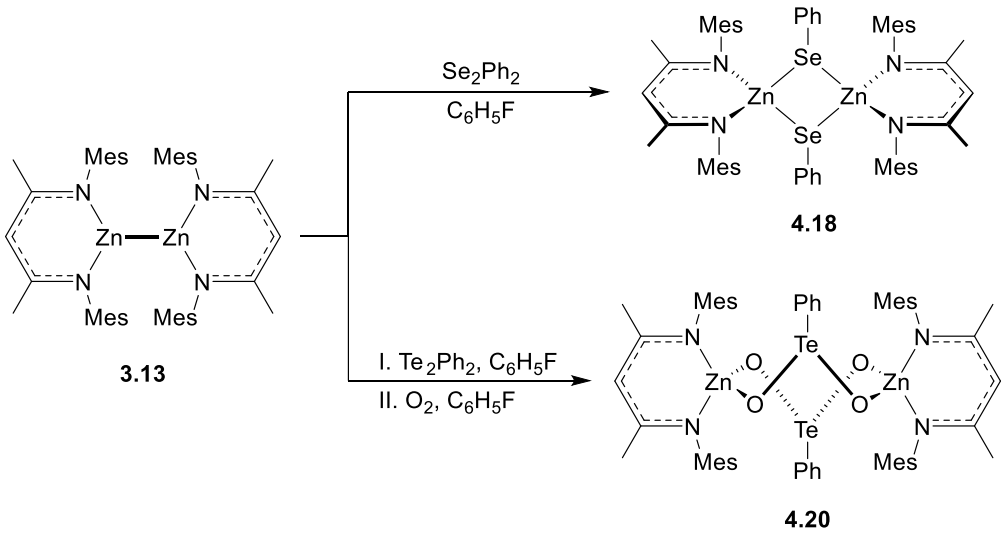

Scheme 4.7 Reaction of **3.13** with phenyl chalcogenide dimers.[14]

Schulz *et al*. have also reported the reaction of **3.13** with various group 14 azides (Scheme 4.8). Complex **3.13** reacts with Me_3MN_3 (M = Si, Sn) to afford the dimeric zinc azido complex, [(^{Mes}NacNac)Zn(μ-N_3)]$_2$ (**4.21,** Scheme 4.8), and the corresponding Me_6M_2 disilane or distannane compound.[15] Reaction with PhN_3 gave the hexazene complex (^{Mes}NacNac)Zn(μ-1,6-Ph_2N_6)Zn(^{Mes}NacNac) (**4.22**, Scheme 4.8). X-ray crystallographic analysis shows a molecular structure in which two PhN_3 molecules have become reductively coupled to form a Ph_2N_6 unit which acts as a bridging ligand between the two (^{Mes}NacNac)Zn moieties. The analogous reaction of **3.13** with $DippN_3$ proceeded in a similar fashion. However, no crystals suitable for X-ray diffraction were obtained. Nevertheless, the product of this reaction gave a similar IR spectrum to that of **4.22** and so it is expected that it will possess the analogous hexazene moiety. In a later publication Schulz *et al*. reported that the reaction of (^{Dipp}NacNac)$_2$Zn$_2$ (**1.81**) also

reacts with PhN_3 to produce (^{Dipp}NacNac)Zn(μ-1,6-Ph_2N_6)Zn(^{Dipp}NacNac) (**4.23**, Scheme 4.8).[16] The authors further demonstrated that the hexazene moiety could be transmetallated; reaction of either **4.22** or **4.23** with $ZnMe_2$ gave the complex MeZn(μ-1,6-Ph_2N_6)ZnMe,[16,17] which could be isolated as single crystals of Me(py)Zn(μ-1,6-Ph_2N_6)Zn(py)Me (**4.24**) upon addition of pyridine to the base-free complex.

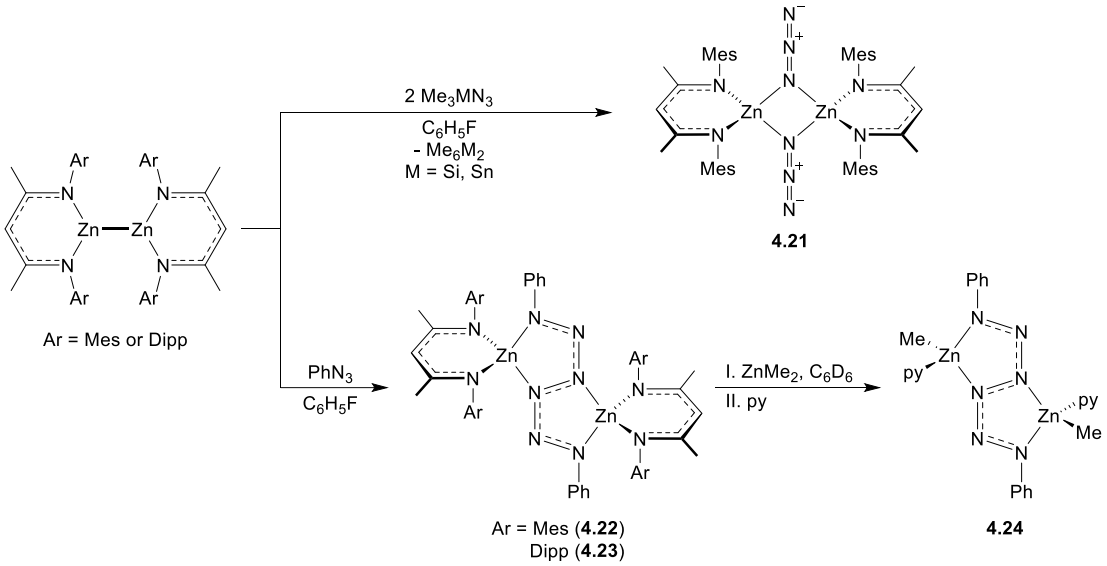

Scheme 4.8 Reactivity of β-diketiminate Zn(I) dimers with group 14 azides.[15,16]

In 2009 Fedushkin and co-workers reported the reaction of $[Zn(Dipp\text{-}BIAN)]_2$ (**1.88**) with 2 equiv. of phenylacetylene to give the phenylacetylide bridged complex $[(Dipp\text{-}BIAN)Zn(\mu\text{-}CCPh)]_2$ (**4.25**, Equation 4.5).[18] During this reaction each phenylacetylene molecule is reduced by an electron transfer from Zn(I) to give the acetylide moiety, Zn(II) and 0.5 equiv. of H_2.

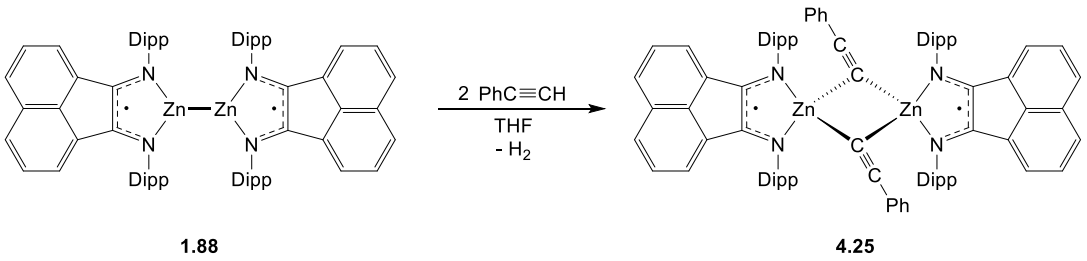

Equation 4.5[18]

Following this, Wu *et al*. reported the analogous reaction between the neutral α-diimine Zn(I) complex, ^{Me}LZnZn^{Me}L (**1.94**), and 2 equiv. of phenylacetylene to produce [^{Me}LZn(μ-CCPh)]$_2$ (**4.26,** Scheme 4.9).[19] Reaction of **1.94** with 4 equiv. of phenylacetylene gave the monomeric complex ^{Me}LZn(CCPh)$_2$ (**4.27**), in which the both

the Zn(I) centres and the ligands have undergone oxidation. Finally, Wu *et al*. reported that the anionic α-diimine Zn(I) complex, [^{Me}LZnZn^{Me}L][K(15-Crown-5)$_2$]$_2$ (**1.92**), also reacts with 4 equiv. of phenylacetylene to give [Zn(CCPh)$_4$][K(15-Crown-5)$_2$]$_2$ (**4.28**) with elimination of H_2, ^{Me}L and metallic Zn.

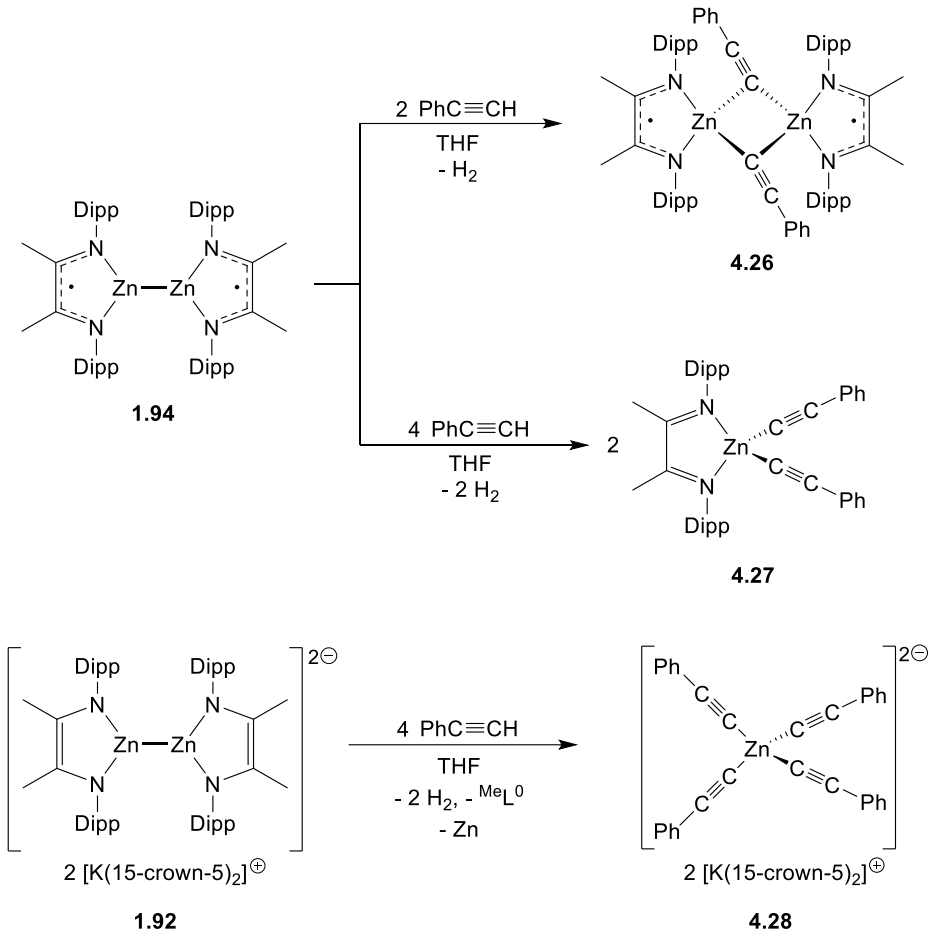

Scheme 4.9 Reactions of α-diimine Zn(I) dimers with phenyl acetylene.[19]

In most cases, the ligands of β-diketiminato Zn(I) dimers have been innocent during the reactions which take place at the Zn(I) centres. However, Schulz *et al*. have also observed cases in which these ligands participate in reactions. The reaction of **3.13** with S_8 gives (^{Mes}NacNacS)$_2$Zn (**4.29**, Equation 4.6)[20] in which nucleophilic attack at the γ-carbon of the β-diketiminato ligand results in sulfurisation of the ligand backbone to give the new thio-β-ketiminato ligated Zn species. Compound **4.29** could also be synthesised *via* the reaction of **4.19** or (^{Mes}NacNac)ZnMe with S_8.

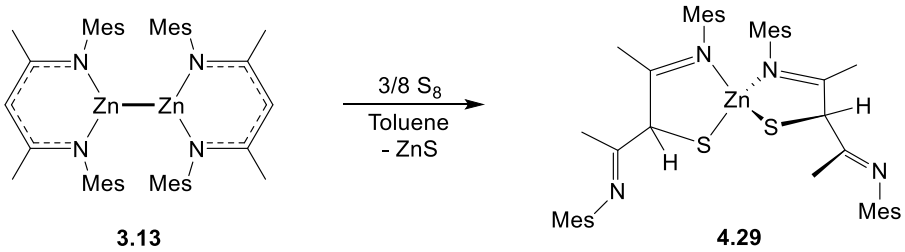

Equation 4.6[20]

After their discovery of **3.1**, Blake and Mountford performed extensive DFT and QTAIM analysis which concluded that the Zn–Hg–Zn complex should be described as a $[Zn(I)]_2Hg(0)$ system. To test whether the complex behaved as a source of Zn(I) *in vitro* the authors performed several chemical tests with simple small molecules.[1] The reaction between **3.1** and I_2 afforded the precursor halide complex (^{Dipp}NacNac)ZnI. Reaction of **3.1** with 1 equiv. of FpI gave (^{Dipp}NacNac)ZnI and (^{Dipp}NacNac)ZnFp; the latter product was synthesised independently through the reaction of KFp and (^{Dipp}NacNac)ZnI for verification. Reaction of **3.1** with 2 equiv. of FpI gave primarily (^{Dipp}NacNac)ZnI and the known species $HgFp_2$.[21] Reaction of **3.1** with Fp_2 afforded (^{Dipp}NacNac)ZnFp among other unknown products.

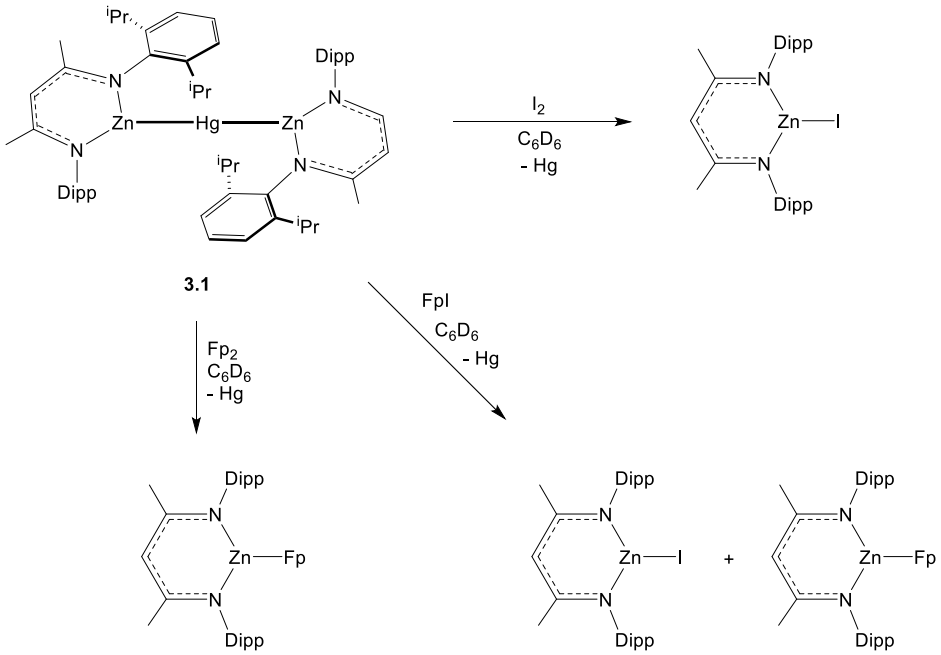

Scheme 4.10 Reactions of **3.1** with I_2, FpI and Fp_2.[1]

The work in this Chapter seeks to expand the reactivity of the Zn–Hg–Zn bonded **3.1** with unsaturated organic substrates. The substrates selected for this work are azides, heterocumulenes (*e.g.* CS_2, isocyanates), peroxides, and azobenzene.

4.3 Reactions of {(^{Dipp}NacNac)Zn}$_2$Hg with silyl halides

A simple test of reactivity for metal-metal complexes within our group has been reaction of the metal-metal bonded complex with simple alkyl halides, such as methyl iodide.[1,22] In the case of **3.1**, the risk of a reaction producing highly toxic alkyl mercury complexes, *e.g*. $HgMe_2$, was deemed too great. Hence, the decision was taken to study the reactivity of **3.1** with silyl halides with the knowledge that the potential Hg containing products would present a significantly reduced risk.

Reaction of **3.1** with 2 equiv. of Me_3SiI in C_6D_6 over 24 h on the NMR tube-scale gave (^{Dipp}NacNac)ZnI by ^{1}H NMR. Precipitation of a grey solid was observed in the NMR tube which is attributed to elimination of Hg from the parent compound. $Hg(SiMe_3)_2$, which appears as a singlet at $\delta = 0.20$ ppm,[23] was not observed in the ^{1}H NMR spectrum of the reaction mixture, nor was Si_2Me_6 ($\delta = 0.04$ ppm).[15] A singlet peak was observed at $\delta = 0.12$ ppm which was attributed to HMDSO,[24] formed by the scavenging of adventitious O_2 by trimethylsilyl radicals.

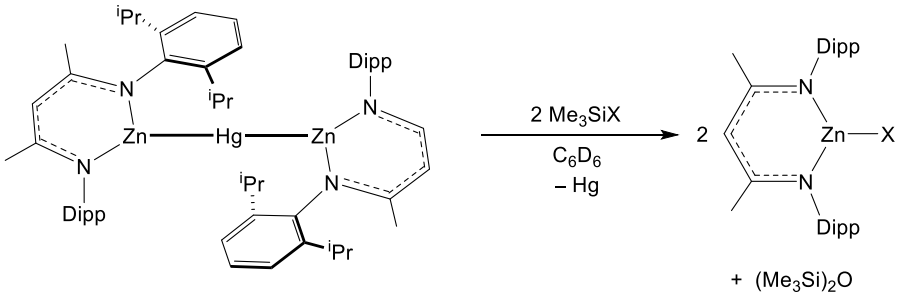

Equation 4.7

The reaction of **3.1** with 2 equiv. of either Me_3SiCl or Me_3SiBr gave similar results. The precipitation of Hg in the NMR tube was observed in each case. A singlet peak in each ^{1}H NMR spectrum, located at $\delta = 0.12$ ppm, was observed to grow in over the course of each reaction. In the case of reaction with Me_3SiCl, peaks can be observed that are consistent with the previously reported compound (^{Dipp}NacNac)ZnCl,[25] along with a considerable quantity of protio-ligand. The ^{1}H NMR spectrum of (^{Dipp}NacNac)ZnBr has not been reported in C_6D_6 and so the product of the reaction of **3.1** with Me_3SiBr cannot be directly referenced to a known set of chemical shifts. Nevertheless, having observed the outcomes of the previous two reactions it can be reasonably assumed that the product of this reaction is (^{Dipp}NacNac)ZnBr. Indeed, there

is one major set of peaks in the ^{1}H NMR spectrum which can be attributed to this expected product. Peaks corresponding to a small quantity of protio-ligand can be observed alongside the major products.

The reactions observed for **3.1** thus far can be broadly described as two one-electron reductions, in which each Zn(I) unit is oxidised to Zn(II). Each reagent employed thus far has possessed a single bond at the reaction site and so each reduction has resulted in bond cleavage within the reagent. In order to test the extent of its reduction capability, the reactions of **3.1** with a range of multiply bonded small molecules was investigated.

4.4 Reaction of {(^{Dipp}NacNac)Zn}$_2$Hg with phenyl azide

The synthesis of **4.22** and **4.23** from the reaction of (^{Ar}NacNac)$_2$Zn$_2$ (Ar = Mes (**3.13**), Dipp (**1.81**)) with PhN_3 (*vide supra*) is driven by the oxidation of two Zn(I) centres which reductively couple two azide units to form the central hexazene moiety.[16,17] Since **3.1** has been shown to behave as a Zn(I) complex it was hypothesised that a similar reaction would take place. The product of this reaction would be expected to be **4.23**, formed from the coordination of two (^{Dipp}NacNac)Zn units to a diphenylhexazene moiety following the elimination of Hg.

The NMR-tube scale reaction of **3.1** with two equivalents of PhN_3 in C_6D_6 gave a ^{1}H NMR spectrum which contained resonances assigned to **4.23** amongst a complex mixture of other products (Equation 4.8). When this reaction was performed in the presence of a known quantity of 1,4-dimethoxybenzene (acting as an internal reference standard) the spectral yield of **4.23** was determined to be below 10% by integration. Despite this low yield the presence of **4.23** in the reaction mixture suggests that **3.1** can behave in a similar manner to Zn–Zn bonded species.

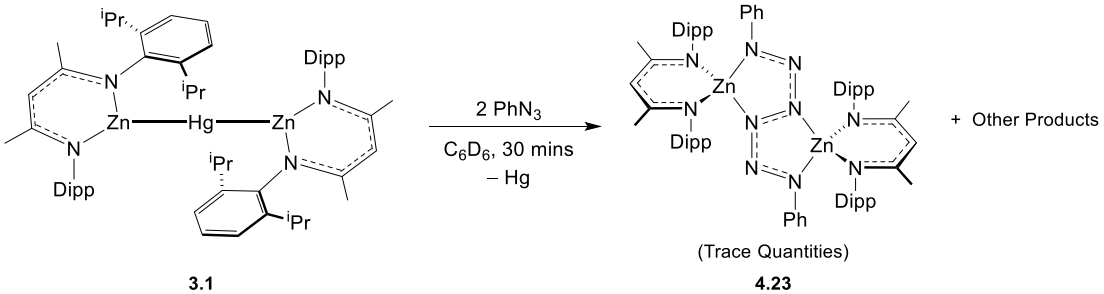

3.1 **4.23**

Equation 4.8

4.5 Reaction of {(^{Dipp}NacNac)Zn}$_2$Hg with carbon disulfide

Reaction of **3.1** with 2 equiv. of CS_2 gave the bimetallic complex (^{Dipp}NacNac)Zn(μ-CS_2)Zn(^{Dipp}NacNac) (**27**) as a pale yellow solid in 82% yield. Diffraction-quality crystals of **27**·2(C_6H_{14}) were grown from a concentrated hexane solution at 5 °C. The molecular structure and selected distances and angles are shown in Figure 4.1 and Table 4.1. Elemental analysis of these crystals returned a CHN content that was low in C for the determined chemical composition of the crystals (**27**·2(C_6H_{14})) but high in C for solvent-free **27**. This suggests that the crystalline sample submitted for analysis had undergone partial loss of the hexanes of crystallisation before the elemental analysis could be performed. The CHN content obtained is consistent with a loss of roughly 80% of the hexane of crystallisation.

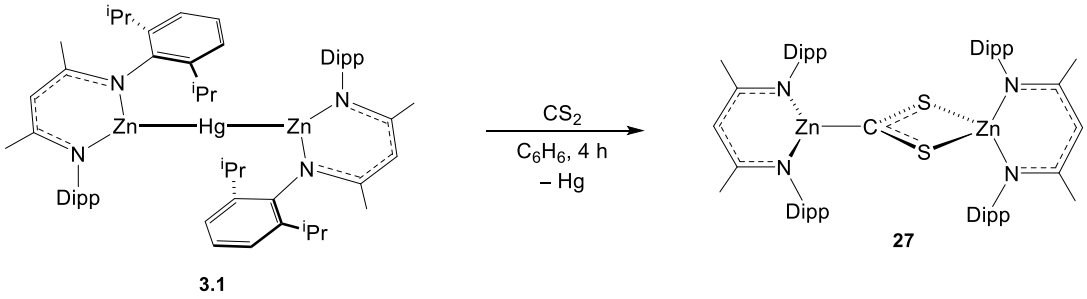

Equation 4.9

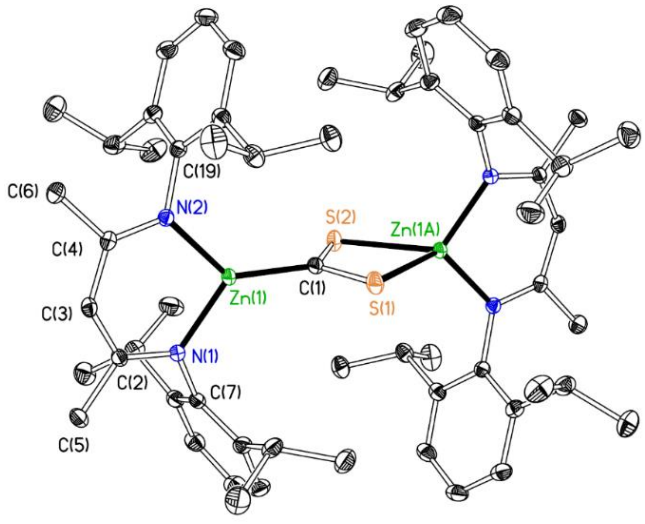

Figure 4.1 Displacement ellipsoid plot (20% probability) of (^{Dipp}NacNac)Zn(μ-CS_2)Zn(^{Dipp}NacNac) (**27**). H atoms omitted for clarity. Atoms carrying the suffix "A" are related to their counterparts by the operator 1-x, 1-y, 1-z.

Table 4.1 Selected distances (Å) and angles (°) for (^{Dipp}NacNac)Zn(μ-CS_2)Zn(^{Dipp}NacNac) (**27**).

Zn(1)–C(1)	1.904(2)	Zn(1)–N(1)	1.9464(8)
Zn(1)–N(2)	1.9454(8)	Zn(1A)–S(1)	2.3892(6)
Zn(1A)–S(2)	2.4584(6)	C(1)–S(1)	1.690(2)
C(1)–S(2)	1.683(2)		
N(1)–Zn(1)–N(2)	100.49(3)	N(1)–Zn(1)–C(1)	128.67(8)
N(2)–Zn(1)–C(1)	130.75(6)	S(1)–C(1)–S(2)	118.82(12)
S(1)–Zn(1A)–S(2)	73.569(18)	S(1)–Zn(1A)–N(1A)	123.04(3)
S(1)–Zn(1A)–N(2A)	122.41(3)	S(2)–Zn(1A)–N(1A)	117.73(3)
S(2)–Zn(1A)–N(2A)	119.72(3)		

Compound **27** is a bimetallic complex with two ^{Dipp}NacNacZn moieties bridged by a reduced CS_2 unit. The three-coordinate Zn(1) is coordinated to one bidentate NacNac ligand and the carbon atom of carbon disulfide, giving a trigonal planar geometry. The four-coordinate Zn(1A) is coordinated to one bidentate NacNac ligand and the two sulfur atoms of carbon disulfide in a bidentate bonding mode, giving it an approximately tetrahedral geometry. The CS_2 unit in the crystal structure of **27** is disordered across an inversion centre which relates the two ^{Dipp}NacNacZn units by symmetry. The structural effects of the different coordination environments of each Zn atom could not therefore be interrogated by crystallography as the X-ray structure gives an average of the two environments.

The ^{1}H and ^{13}C NMR spectra of **27** show two distinct sets of ligand peaks, consistent with the chemical inequivalence of the two (^{Dipp}NacNac)Zn units. The ^{13}C NMR spectrum also contains an unusually high chemical shift at δ = 319 ppm, attributable to the μ-CS_2 moiety. The chemical shift of the $^{13}CS_2$ unit is similar to that found in **15** (δ = 330, C_6D_6) and Cutler's **2.27** (δ = 324, $CDCl_3$). The infrared spectrum shows $\nu(CS_2)$ stretching frequencies of 942 and 859 cm^{-1} for the CS_2 unit.

DFT calculations at the PBEPBE level with Grimme's D3 dispersion corrections[26,27] were performed starting from crystallographically obtained atomic coordinates. The DFT model of **27** reproduces the crystallographically observed structure after geometric optimisation (Figure 4.2). The effect of the different coordination environments on the

Zn atoms can be seen in DFT optimised structure. The calculated Zn–N bond lengths at the three-coordinate Zn are 1.95 Å, while the calculated Zn–N bond lengths at the four-coordinate Zn are 1.98 Å.

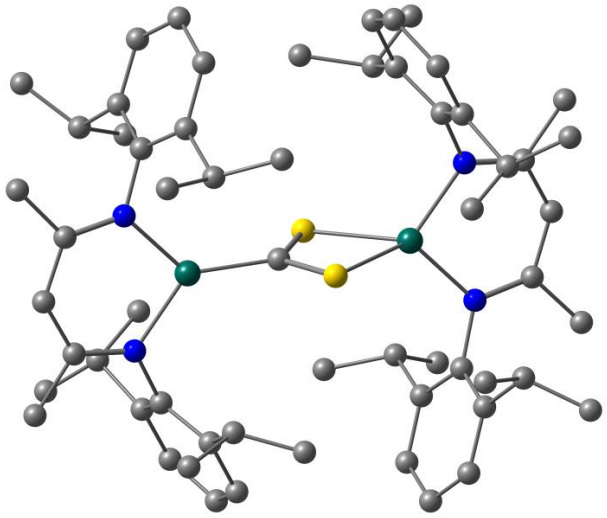

Figure 4.2 DFT optimised structure of (^{Dipp}NacNac)Zn(μ-CS_2)Zn(^{Dipp}NacNac) (**27**).

QTAIM analysis[28] performed for **27** shows *Q*(CS_2) (the sum of the atomic charges within the CS_2 unit) to be −0.96 au. QTAIM analysis previously performed on the reference compound ^{Dipp}NacNacZnI (see Chapter Three) shows an atomic charge of −0.43 au for iodide (formally in the −1 oxidation state).[1] Comparison with this value shows that the CS_2 unit has been fully reduced and can therefore be formally represented as $(CS_2)^{2-}$. Upon reaction the atomic charge of each Zn atom changes from +0.67 au (in **3.1**)[1] to +1.01 au (avg, **27**), consistent with oxidation from Zn(I) to Zn(II).

Compound **27** is the final product of the reaction of **3.1**, even in the presence of excess CS_2. Compound **27** could not be prompted to react further, even after heating with 10 equiv. of CS_2 in C_6D_6 at 70 °C for 18 h.

Although many dithiocarboxylate complexes are known in Zn chemistry,[29] **27** represents the first instance of a CS_2 unit bound to Zn atoms at both the C and S positions. Clearly, dithiocarboxylate (RCS_2^-) and dithiocarbamate ($R_2NCS_2^-$) ligands are nothing new in the field of coordination chemistry and many metal complexes exist which feature ligands of this type. Significantly rarer however are the metallodithiocarboxylate complexes (*e.g.* M–CS_2–M') in which the CS_2 unit is coordinated to metal atoms at both the C and S atoms.[29]

The first of these was reported in 1975 by Angelici, Clardy *et al.*[30] $[Cl(Ph_3P)_2Pt(\mu\text{-}CS_2)Pt(PPh_3)_2][BF_4]$ (**4.30**) was formed by allowing a solution of $[(Ph_3P)_2Pt(Cl)(CS)][BF_4]$ in a 1:1 mixture of CH_2Cl_2/hexane to stand in air for 1 day. Compound **4.30** formed as a yellow crystalline solid and was structurally authenticated by X-ray diffraction studies. The C–S distances of 1.709(21) and 1.692(20) Å found in **4.30** are comparable with those found in **27**.

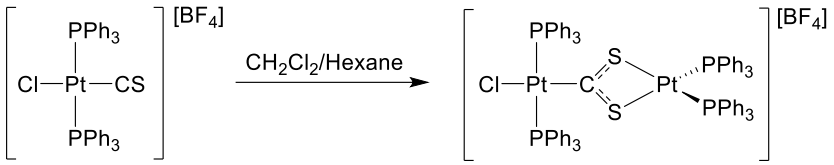

4.30

Equation 4.10[30]

Metallodithiocarboxylate complexes formed by insertion of CS_2 directly into metal-metal bonds began to be reported shortly following **4.30**. In 1981 Grundy *et al*. reported the synthesis and structural characterisation of $Pt_2Cl_2(\mu\text{-}CS_2)(\mu\text{-}DPPM)_2$ (**4.31**, Equation 4.11, DPPM = diphenylphosphinomethane), formed from reaction of $Pt_2Cl_2(\mu\text{-}DPPM)_2$ with CS_2.[31] Unlike **27** the $\mu\text{-}CS_2$ moiety in **4.31** bridges through the C atom and only one S atom. Reports of structurally authenticated compounds[32–35] published in the decades following this initial discovery suggest that this bonding mode is not particularly unusual.

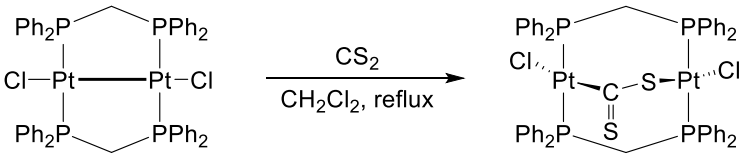

4.31

Equation 4.11[31]

Metal-metal bonds between main group elements are rarer than those between transition metal elements[29] and therefore examples of CS_2 insertion into main group metal-metal bonds are rarer as a consequence. Nevertheless, reactivity of this type was reported by Uhl *et al*. in 1993.[36] The Al–Al bonded complex $[Al\{CH(SiMe_3)_2\}_2]_2$ was shown to react in neat CS_2 to afford $\{(Me_3Si)_2CH\}_2Al(\mu\text{-}S)Al\{CH(SiMe_3)_2\}_2$ (**4.32**) and $\{(Me_3Si)_2CH\}_2Al(\mu\text{-}CS_2)Al\{CH(SiMe_3)_2\}_2$ (**4.33**), in 65% and 15% yields,

respectively (Equation 4.12). These products were structurally authenticated following recrystallisation.

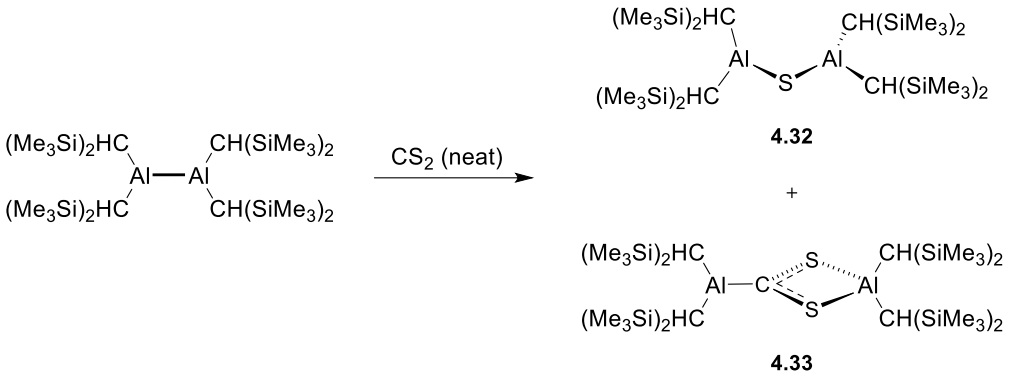

Equation 4.12[36]

It is notable that two products are formed during this reaction; the CS_2 insertion product **4.33** and the sulfide bridged product **4.32**, the product of a two-electron reductive cleavage of CS_2. This contrasts with the formation of **27**, which is the sole product of the reaction between **3.1** and CS_2. It is likely that the electron donating alkyl ligands of the dialane make the species more reducing than **3.1**, while the NacNac ligands of **3.1** allow for redistribution of electron density away from the Zn centre, which diminish its reducing capability. The overall greater reducing power of the Al species on CS_2 therefore results in an additional reductive cleavage reaction to afford the sulfide-bridged species, in addition to the CS_2-bridged species which is analogous to the sole product of the reaction between **3.1** and CS_2.

The C–S bond distances of 1.65(1), 1.67(1), 1.68(1) and 1.70(1) Å found in **4.33** (two independent molecules in the asymmetric unit) are comparable to those found in **27** (1.683(2) and 1.690(2) Å). The ^{13}C NMR spectrum of **4.33** showed $\delta = 240$ ppm for the CS_2 unit, almost 80 ppm less than that found in **27**. This value is consistent with a more shielded C atom and therefore greater electron density within the CS_2 unit. The IR spectrum of **4.33** shows a CS_2 stretching frequency ($\nu(CS_2)$) of 1045 cm^{-1}, over 100 cm^{-1} greater than that found in **27**.

4.6 Reactions of {(^{Dipp}NacNac)Zn}$_2$Hg with isocyanates

Complex **3.1** reacts with 2 equiv. of ArNCO (Ar = Ph or Tol) to give (^{Dipp}NacNac)Zn{OC(NPh)$_2$}Zn(^{Dipp}NacNac) (**28**, 88% yield) and (^{Dipp}NacNac)Zn{OC(NTol)$_2$}Zn(^{Dipp}NacNac) (**29**, 51% yield), respectively. Diffraction-quality crystals of **28** and **29** were grown from concentrated hexane solutions at 5 °C. The molecular structure and selected distances and angles for **28** are shown in Figure 4.3 and Table 4.2. The corresponding data for **29** are shown in Figure 4.4 and Table 4.3.

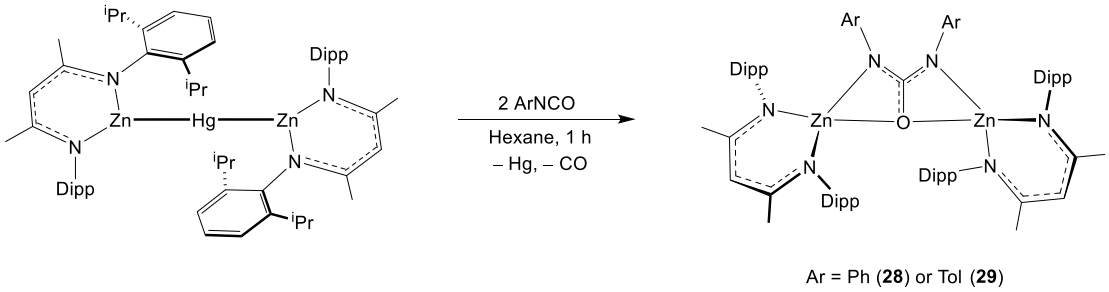

Equation 4.13

Compound **28** is a bimetallic complex with two (^{Dipp}NacNac)Zn unit bridged by a doubly deprotonated ureato moiety, with the O atom and one N atom coordinating each Zn unit. Each four-coordinate Zn atom is best described as having a distorted tetrahedral coordination environment. The Zn–O–Zn interaction is almost linear at 173.17(15)°.

Compound **29** shares similar structural features with its counterpart **28**. The coordination environment of the Zn atoms is again of distorted tetrahedral geometry with a near linear Zn–O–Zn interaction at 172.89(7)°.

DFT calculations at the PBEPBE level with Grimme's D3 dispersion corrections[26,27] were performed for **28** and **29** starting from crystallographically obtained atomic coordinates. The DFT models of **28** and **29** reproduce the crystallographically observed structure after geometric optimisation. QTAIM analysis of **28** found a Q{OC(NPh)$_2$} value of −1.26 au, corresponding to a dianionic ligand (*c.f.* Q(CS$_2$) = −0.96 au for (CS$_2$)$^{2-}$ in **27**). This value is consistent with a doubly deprotonated ureato species and is slightly more negative than that of the [μ-CS$_2$]$^{2-}$ ligand found in **27** due to the more electronegative N and O atoms.

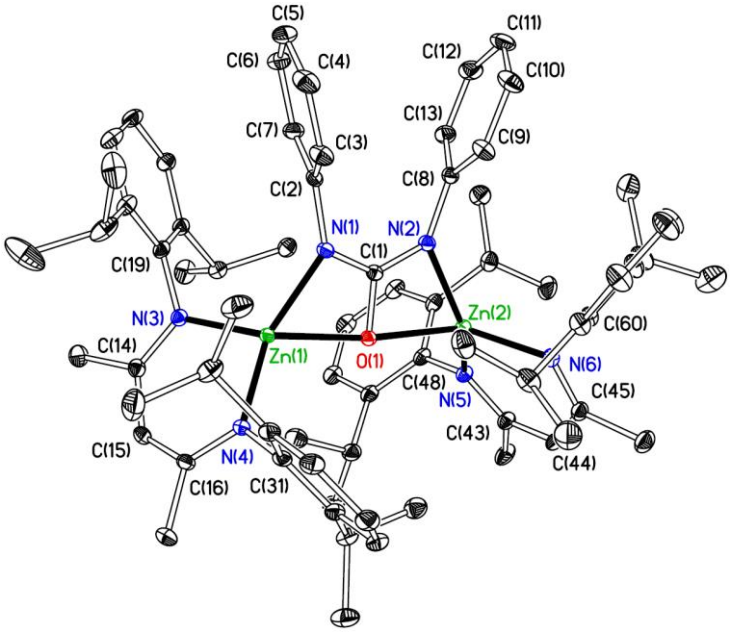

Figure 4.3 Displacement ellipsoid plot (20% probability) of (^{Dipp}NacNac)Zn{OC(NPh)$_2$}Zn(^{Dipp}NacNac) (**28**). H atoms omitted for clarity.

Table 4.2 Selected distances (Å) and angles (°) for (^{Dipp}NacNac)Zn{OC(NPh)$_2$}Zn(^{Dipp}NacNac) (**28**).

Zn(1)–O(1)	2.1832(10)	Zn(1)–N(1)	1.9803(11)
Zn(1)–N(3)	1.9782(12)	Zn(1)–N(4)	1.9579(12)
Zn(2)–O(1)	2.1570(10)	Zn(2)–N(2)	1.9738(12)
Zn(2)–N(5)	1.9521(12)	Zn(2)–N(6)	1.9721(12)
C(1)–O(1)	1.3209(17)	C(1)–N(1)	1.3323(18)
C(1)–N(2)	1.3367(18)		
O(1)–Zn(1)–N(1)	64.09(4)	O(1)–Zn(1)–N(3)	126.40(4)
O(1)–Zn(1)–N(4)	111.85(4)	N(1)–Zn(1)–N(3)	113.22(5)
N(1)–Zn(1)–N(4)	144.23(5)	N(3)–Zn(1)–N(4)	97.63(5)
O(1)–Zn(2)–N(2)	64.65(4)	O(1)–Zn(2)–N(5)	113.98(5)
O(1)–Zn(2)–N(6)	122.48(4)	N(2)–Zn(2)–N(5)	139.81(5)
N(2)–Zn(2)–N(6)	115.11(5)	N(5)–Zn(2)–N(6)	99.37(5)
O(1)–C(1)–N(1)	113.26(12)	O(1)–C(1)–N(2)	112.85(12)
N(1)–C(1)–N(2)	133.89(13)	Zn(1)–O(1)–Zn(2)	173.17(5)

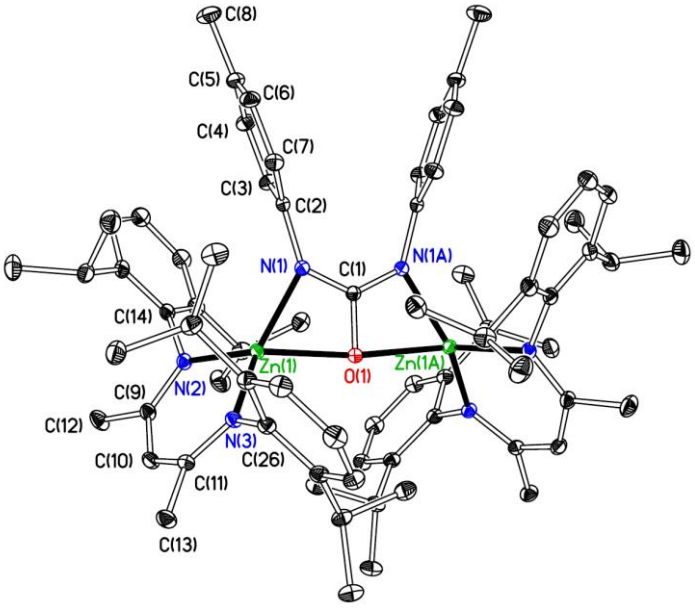

Figure 4.4 Displacement ellipsoid plot (20% probability) of (^{Dipp}NacNac)Zn{OC(NTol)$_2$}Zn(^{Dipp}NacNac) (**29**). H atoms omitted for clarity. Atoms carrying the suffix "A" are related to their counterparts by the operator 1-x, 1+y, 3/2-z.

Table 4.3 Selected distances (Å) and angles (°) for (^{Dipp}NacNac)Zn{OC(NTol)$_2$}Zn(^{Dipp}NacNac) (**29**).

Zn(1)–O(1)	2.1868(2)	Zn(1)–N(1)	1.9875(12)
Zn(1)–N(2)	1.9789(13)	Zn(1)–N(3)	1.9622(12)
C(1)–O(1)	1.323(3)	C(1)–N(1)	1.3370(15)
O(1)–Zn(1)–N(1)	64.17(5)	O(1)–Zn(1)–N(2)	123.53(4)
O(1)–Zn(1)–N(3)	113.88(5)	N(1)–Zn(1)–N(2)	115.29(5)
N(1)–Zn(1)–N(3)	140.94(5)	N(2)–Zn(1)–N(3)	98.25(5)
O(1)–C(1)–N(1)	113.45(10)	N(1)–C(1)–N(1A)	133.1(2)
Zn(1)–O(1)–Zn(1A)	172.89(7)		

Compounds **28** and **29** exhibit full delocalisation within the ureato ligand. Several complexes have been synthesised and structurally authenticated which possess bridging ureato moieties that do not exhibit this delocalisation. These complexes, {Fe(CO)$_3$}$_2${OC(NPh)$_2$}[37] (**4.34**), (Cp*Co)$_2${OC(NPh)$_2$}[38] (**4.35**) and {Mo(NPh)(S$_2$CNEt$_2$)}$_2$(μ-NPh){PhNC(O)NPh}[39] (**4.36**), instead feature ureato ligands which bridge between the transition metal units solely through the lone pairs of

the N atoms (Figure 4.5). In these structures the C=O and C–N bonds are entirely localised. The C–O and C–N bond lengths for the ureato unit of these complexes are summarised in Table 4.4, along with those for **28** and **29**. Complexes **28** and **29** exhibit significantly longer C–O bonds and significantly shorter C–N bonds as a result of this delocalisation. The C–O bands appear below 1600 cm^{-1} in the IR spectra of **28** and **29** as a consequence of the decreased CO bond order which gives a weaker C–O bond with a decreased stretching frequency.

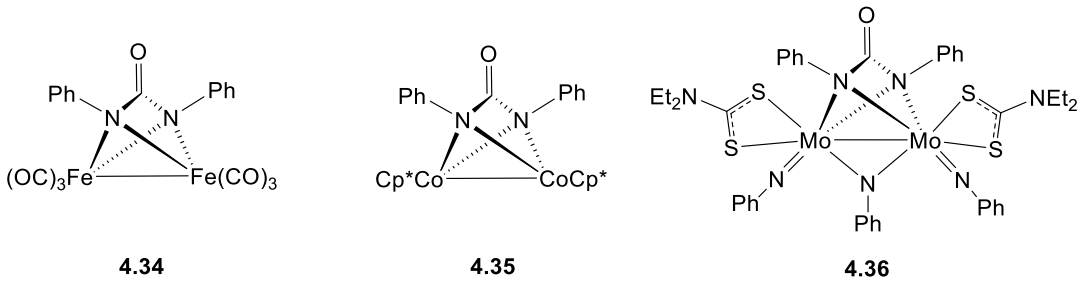

Figure 4.5 Complexes featuring an alternative coordination mode for bridging ureato ligands.[37–39]

Table 4.4 C–O and C–N bond lengths (Å) for selected bridged dimetalloureate complexes.[37–39]

Compound	C–O	C–N	C–N
28	1.3209(17)	1.3323(18)	1.3367(18)
29	1.323(3)	1.3370(15)	1.3370(15)
4.34	1.200	1.410	1.410
4.35	1.217(8)	1.396(7)	1.413(7)
4.36	1.211(20)	1.386(22)	1.420(20)

The reactions which form **28** and **29** are quite rapid. Discolouration of the orange solution of **3.1** is seen immediately upon addition of the isocyanate. Insight into the mechanism by which **28** and **29** are formed is therefore difficult to obtain. At present, it is thought that 1 equiv. of the isocyanate is reduced by electron transfer from both Zn(I) centres, eliminating CO to yield a reactive nitrene intermediate which reacts with a second isocyanate to form the ureato complex **28**. When performed on the NMR tube-scale no evidence for CO could be observed in the $^{13}C\{^{1}H\}$ spectrum. The gaseous

nature of CO and the low natural abundance of the NMR active isotope ^{13}C will make any evolved CO difficult to detect in a standard NMR experiment. The lack of observable CO is therefore unsurprising. The hydrolysis reaction of **28** with H_2O on the NMR tube-scale produced signals attributable to N,N'-diphenylurea in the ^{1}H NMR spectrum.

The reactivity of **3.1** towards alkyl isocyanates was also investigated. No reaction between **3.1** and ^{t}BuNCO was observed under the same conditions, or upon heating at 60 °C for several hours. ^{t}Bu is a strongly electron donating substituent, unlike both Ph and Tol. The presence of this additional electron density on the isocyanate may account for its lack of reactivity with the reducing Zn(I) centres.

Prior to the synthesis of compounds **28** and **29** there were only 2 reported examples of bridging ureato complexes which exhibit this particular bonding mode. The first of these was reported by Floriani in 1979 while investigating the reactivity of $Cp_2Ti(CO)_2$ (**4.37**) with heterocumulenes.[40] Reaction of 3 equiv. of **4.37** with 4 equiv. of PhNCO gave $(Cp_2Ti)_3\{OC(NPh)_2\}_2$ (**4.38**). The trimetallic complex features two Cp_2Ti units chelated by the two N atoms of a ureato moiety. The O of each ureato species bridges to an additional Cp_2Ti unit (Scheme 4.11).

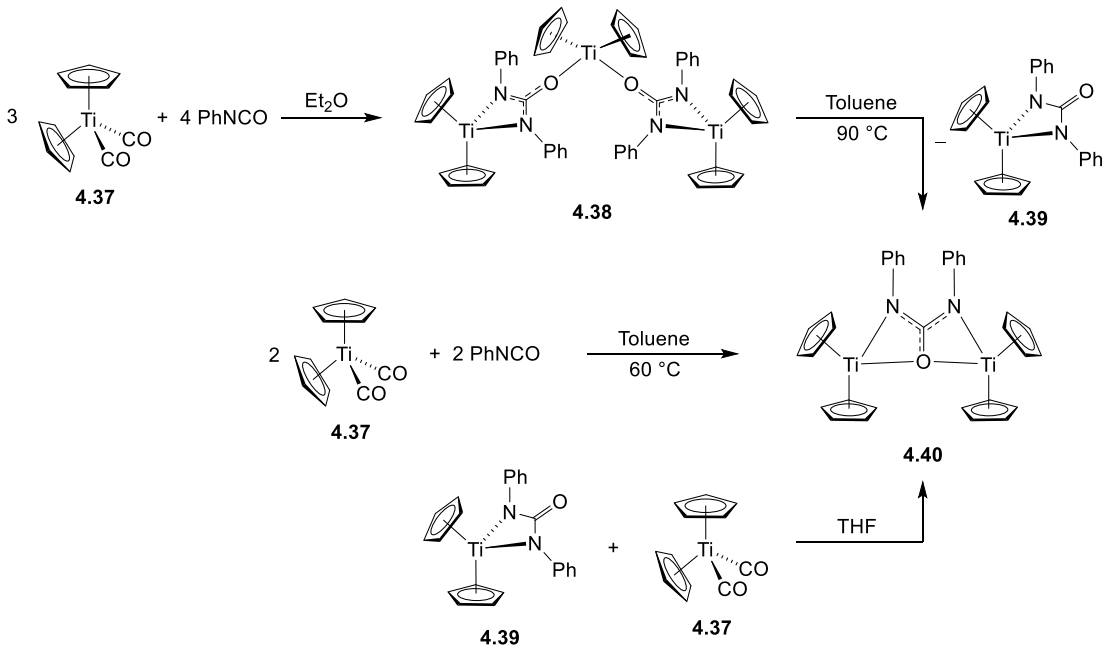

Scheme 4.11 Synthesis of various Ti-metallated ureate complexes.[40]

When **4.38** was heated in toluene, crystals of $Cp_2Ti\{OC(NPh)_2\}$ (**4.39**) were formed. Complex **4.39** features a diphenylureato ligand bonded to the Cp_2Ti unit through both N atoms in a bidentate bonding mode. When the supernatant was isolated from the crystals of **4.39** and cooled, crystals of $(Cp_2Ti)_2\{OC(NPh)_2\}$ (**4.40**) were formed. Complex **4.40** is comparable to **28** and **29** in that the diphenylurato ligand bonds to two Ti centres through the O atom and one N atom per metal. Reaction of **4.37** with **4.39** (isolated from the previous reaction) also led to formation of **4.40**. Perhaps most crucially, **4.40** could also be formed *via* the equimolar reaction of **4.37** and PhNCO in toluene at 60 °C. The formation of **4.40** from the addition of isocyanate to **4.37** is directly comparable to the formation of **28** and **29**.

As seen for complexes **28** and **29**, significant lengthening of the C–O bond (1.334(6) Å) and significant shortening of the C–N bonds (1.314(10) and 1.323(8) Å) is indicative of a fully delocalised ureate moiety within **4.40**.

More recently, Jones *et al*. published an example of a complex featuring a similar bridging ureato species which was synthesised in two-step procedure beginning from a Mg(I) dimer. $(^{Dipp}NacNac)_2Mg_2$ (**1.10**) was oxidised with N_2O to give $\{(^{Dipp}NacNac)Mg\}(O)\{Mg(^{Dipp}NacNac)\}$, which was reacted with CyNCNCy to afford $\{(^{Dipp}NacNac)Mg\}\{OC(NCy)_2\}\{Mg(^{Dipp}NacNac)\}$ (**4.41**, Scheme 4.12).[41] Compound **4.41** demonstrates the same electronic delocalisation seen in other bridging ureato compounds of this type and in fact possesses the longest C–O bond (1.372(2) Å) and shortest C–N bonds (1.3282(14) Å) of all known bridging ureato compounds. This is likely a consequence of the more electron donating cyclohexyl groups increasing the overall electron density of the ureato ligand.

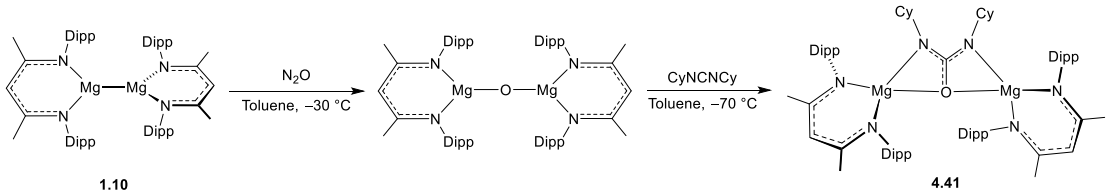

Scheme 4.12 Sequential two-step synthesis of **4.41** from a Mg(I) dimer.[41]

Compounds **28**, **29**, **4.40** and **4.41** are the only reported examples to date of a ureato ligand bonding to two metal atoms in this fashion. Additionally, Jones *et al*. have reported a similar reaction in which **1.10** reacts with 2 equiv. of ^{t}BuNCO to give $(^{Dipp}NacNac)Mg(\mu\text{-}O_2C_2N_2{}^{t}Bu_2)Mg(^{Dipp}NacNac)$ (**4.42**, Equation 4.14). The oxamide

ligand forms from the reductive coupling of two units of isocyanate, forming a new C–C bond. The ligand binds one Mg atom through one N atom and one O atom and the other Mg atom through both O atoms. This result contrasts with the formation of **28** and **29** in which 1 equiv. of CO is eliminated to give the ureato species from 2 equiv. of isocyanate.

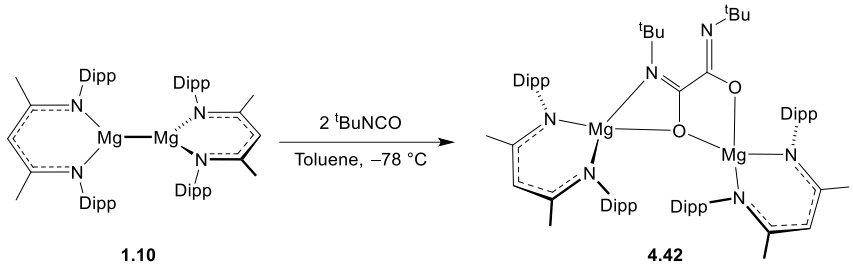

1.10 **4.42**

Equation 4.14[42]

4.7 Reaction of {(DippNacNac)Zn}$_2$Hg with peroxides

Exposure of **3.1** to ^{t}BuOO^{t}Bu in C_6D_6 on the NMR-tube scale did not give any reaction at RT. The reaction was not attempted at higher temperatures due to the instability of organic peroxides towards heat.

In the case of isocyanates (*vide supra*) **3.1** only reacted with arylisocyanates (PhNCO and TolNCO), while exposure to an alkylisocyanate (^{t}BuNCO) gave no reaction. It is possible that this reactivity also applies to peroxides and **3.1** would be reactive towards a diarylperoxide. Unfortunately, the instability of arylperoxides under general laboratory conditions prohibits their availability as useful synthetic reagents.[43] As such reactivity studies with peroxides were not pursued further.

4.8 Reaction of {(DippNacNac)Zn}$_2$Hg with azobenzene

Compound **3.1** reacts with 1 equiv. of azobenzene at RT in C_6H_6 to give {(^{Dipp}NacNac)Zn}(μ-PhNNPh){Zn(^{Dipp}NacNac)} (**30**). The reaction proceeds relatively slowly, over 18 h. The elimination of Hg was observed alongside a slow colour change from the initial orange of **3.1** to a pale green solution. The ^{1}H NMR spectrum of the crude material showed a single species with many ligand peaks, indicating either a high degree of asymmetry within the product or extensive steric congestion within the molecule. When the reaction was repeated with an excess of azobenzene only 1 equiv. was consumed (referenced against 1 equiv. of 1,4-dimethoxybenzene as an internal standard), giving a ^{1}H NMR spectrum consistent with

the same product and residual azobenzene. Several attempts were made to recrystallise the crude product from hexane, benzene, and toluene however no crystals which produced an NMR spectrum consistent with that of the crude material were obtained.

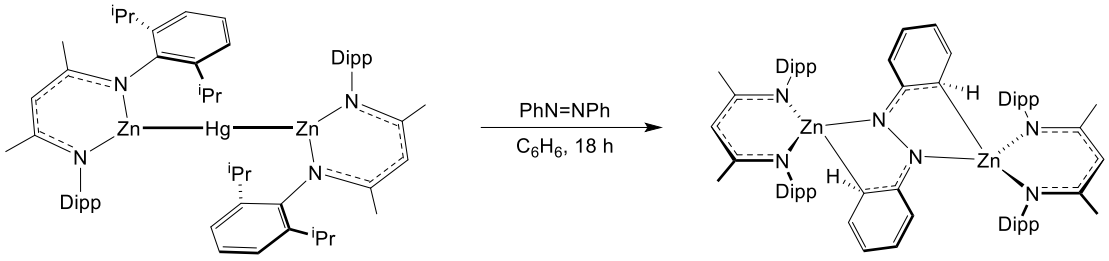

3.1 **30**

Equation 4.15

Given the reactivity displayed by **3.1** thus far the reaction is expected to involve transfer of 2 electrons to the azobenzene unit to give a hydrazinato moiety which will bridge between two Zn(II) centres. The expected product **30** is shown in Equation 4.15. Indeed, the Mg analogue of this species, {(^{Dipp}NacNac)Mg}(μ-PhNNPh){Mg(^{Dipp}NacNac)} (**4.43**, Equation 4.16) has been prepared and structurally characterised by Jones *et al*. in a similar fashion *via* the reaction of (^{Dipp}NacNac)$_2$Mg$_2$ (**1.10**) with azobenzene.[42]

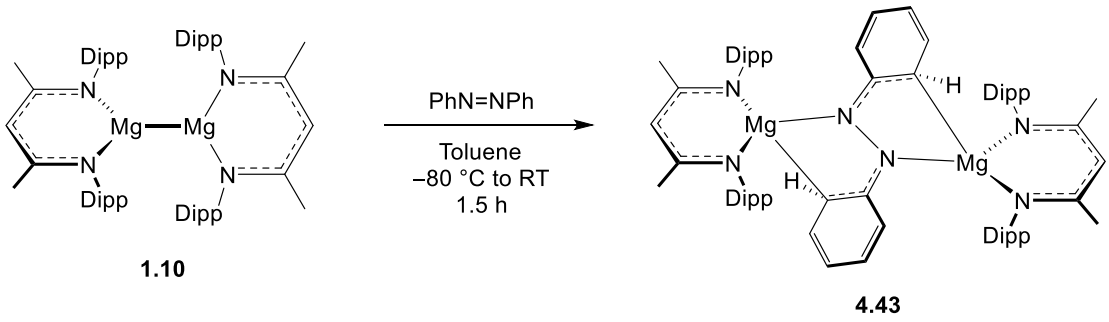

1.10 **4.43**

Equation 4.16[42]

Compound **4.43** features two Mg(II) centres bridged by the reduced hydrazinato unit. Interestingly, each Mg(II) atom also participates in orthometallation with the ortho carbon of the opposite phenyl ring of the hydrazinato unit. This coordination mode results in loss of aromaticity within the aryl rings and results in a particularly downfield shift of the ortho proton, at δ = 5.68 ppm. These ortho protons deviate from the phenyl plane by a mean value of 0.39 Å as a result of this loss of aromaticity. Also of note is the particularly downfield CH<u>Me</u>$_2$ shift at δ = 0.31 ppm.

It is expected that the reaction of **3.1** with azobenzene will give a similar product to **4.43**, namely {(^{Dipp}NacNac)Zn}(μ-PhNNPh){Zn(^{Dipp}NacNac)} (**30**). Elemental analysis gave CHN contents that are consistent with this proposed formula. Similar to those observed by Jones *et al*. in **4.43**, exceptionally downfield shifts are observed in the ^{1}H NMR spectrum of **30** which are attributable to ortho aryl protons (δ = 5.37 ppm) and isopropyl methyl groups (δ = 0.05 ppm).

Relativistic DFT calculations at the PBEPBE level incorporating Grimme's D3 dispersion corrections[26,27] in conjunction with QTAIM analyses were used to gain insight into the assumed structure of **30**. The input structure did not include the Zn···C$_{ortho}$ interactions. However, they independently arose during the geometry optimisation. This manifests as a distortion in the geometry of the hydrazinato unit leading to short Zn···C$_{ortho}$ distances. Additionally, the H atoms of coordinating *ortho* carbons deviate from the phenyl planes by a mean value of 0.32 Å. Both of these features were observed by Jones *et al*. in the solid state structure of their Mg analogue, **4.43**. The N–N bond length of 1.403 Å obtained from the DFT optimised structure of **30** is indicative of a N–N single bond and is comparable to that found by Jones *et al*. in the analogous **4.43** (1.424(2) Å).[42]

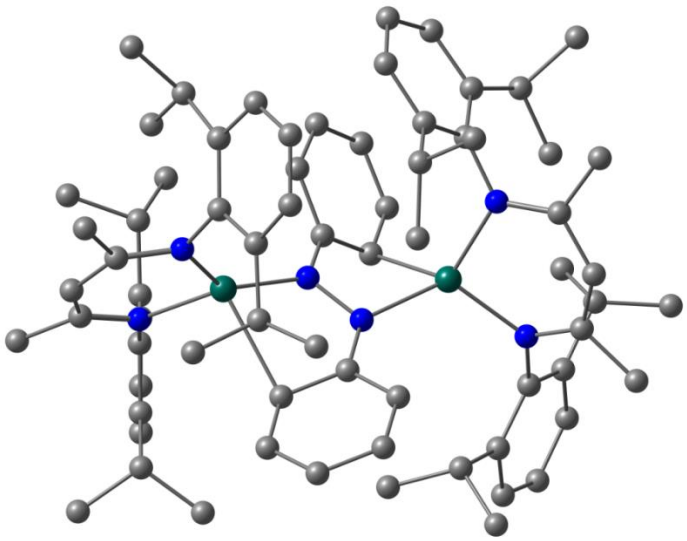

Figure 4.6 DFT optimised structure of (^{Dipp}NacNac)Zn(μ-PhNNPh)Zn(^{Dipp}NacNac) (**30**).

QTAIM analysis of **30** further supports the existence of Zn···C$_{ortho}$ interactions by finding bond paths between each Zn, C$_{ortho}$ pair. Compound **30** forms from the

two-electron reduction of azobenzene. Accordingly, the QTAIM analysis of **30** finds a *Q*(PhNNPh) value of −1.067 au, consistent with reduction of azobenzene to the singly-bonded $(PhNNPh)^{2-}$ moiety.

As a reference DFT and QTAIM calculations were also performed for **4.43**, using Jones' crystallographically obtained atomic coordinates as a starting point. The DFT optimised structure reproduced the crystallographically observed geometry and QTAIM calculations also show the existence of bond paths between each Mg, C_{ortho} pair. The selected QTAIM data for **30** and **4.43** at the respective M–C_{ortho} bond critical points are listed in Table 4.5.

Table 4.5 Selected QTAIM data (atomic units) for {(^{Dipp}NacNac)Zn}(μ-PhNNPh){Zn(^{Dipp}NacNac)} (**30**) and {(^{Dipp}NacNac)Mg}(μ-PhNNPh){Mg(^{Dipp}NacNac)} (**4.43**). Values for ρ (electron density), $\nabla^2\rho$ (electron density Laplacian), H (energy density) were obtained at the bond critical point. δ(A–B) is the delocalisation index for the stated pair of atoms.

Compound	A, B Pair	ρ	$\nabla^2\rho$	H	δ(A–B)	Q(A)	Q(B)
30	Zn, C_{ortho}	0.042	+0.100	−0.007	0.244	1.098	−0.160
4.43	Mg, C_{ortho}	0.020	+0.080	+0.002	0.068	1.692	−0.215

During the attempted crystallisation of **30** crystals were obtained of (^{Dipp}NacNac)Zn{N(Ph)N(H)Ph} (**31**) from a hexane solution. The molecular structure and selected distances and angles for **31** are shown in Figure 4.7 and Table 4.6. Complex **31** is probably formed as the result of partial hydrolysis of **30** by adventitious H_2O present in the recrystallisation solution. The N–N distance of 1.4159(16) Å is similar to that found in the DFT optimised structure of **30** (1.403 Å) and that found by Jones *et al*. in **4.43** (1.424(2) Å).[42] This distance is consistent with a N–N single bond, indicating that the previously double bonded azobenzene has been reduced during the reaction.

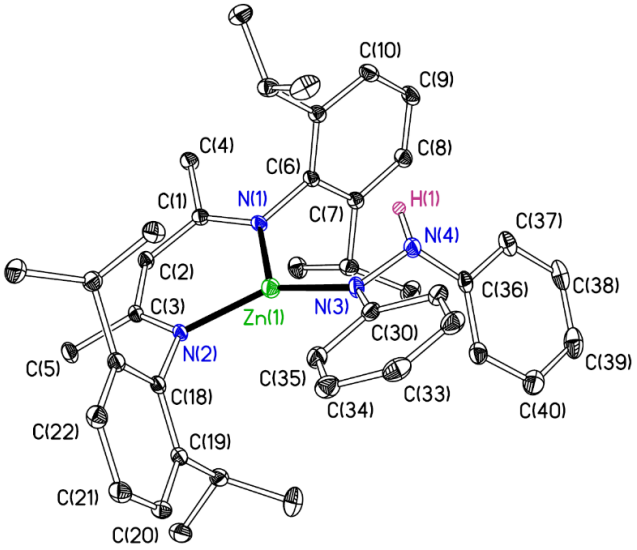

Figure 4.7 Displacement ellipsoid plot (20% probability) of (^{Dipp}NacNac)Zn{N(Ph)N(H)Ph} (**31**). C-bound H atoms omitted for clarity.

Table 4.6 Selected distances (Å) and angles (°) for (^{Dipp}NacNac)Zn{N(Ph)N(H)Ph} (**31**).

Zn(1)–N(1)	1.9533(11)	Zn(1)–N(2)	1.9311(11)
Zn(1)–N(3)	1.8897(11)	N(3)–N(4)	1.4159(16)
N(1)–Zn(1)–N(2)	99.93(5)	N(1)–Zn(1)–N(2)	119.64(5)
N(2)–Zn(1)–N(3)	140.24(5)	Zn(1)–N(3)–N(4)	117.06(9)
Zn(1)–N(3)–C(30)	128.46(9)	N(4)–N(3)–C(30)	113.46(11)
N(3)–N(4)–H(1)	114.8(16)	N(3)–N(4)–C(36)	119.79(12)
C(36)–N(4)–H(1)	114.4(16)		

The NMR tube-scale hydrolysis reaction of **30** with H_2O produces N,N'-diphenylhydrazine by ^{1}H NMR. This indicates that, prior to hydrolysis, **30** likely contains a N–N single bonded moiety which is formed from the two-electron reduction of azobenzene.

4.9 Conclusions

Following on from the previously reported reactivity of {(^{Dipp}NacNac)Zn}$_2$Hg (**3.1**) with I_2, FpI and Fp_2, the reactivity of **3.1** with a wide range of substrates was presented. The NMR tube-scale reaction of **3.1** with Me_3SiX (X = Cl, I) produced the known products (^{Dipp}NacNac)ZnCl and (^{Dipp}NacNac)ZnI, respectively, in addition to elemental

Hg. Reaction of **3.1** with Me_3SiBr produced a product with one set of ligand environments which is assumed to be (^{Dipp}NacNac)ZnBr, in addition to elemental Hg.

The reaction of **3.1** with phenyl azide on the NMR tube-scale gave a complex mixture of products. One of these products was identified as (^{Dipp}NacNac)Zn(μ-1,6-Ph_2N_6)Zn(^{Dipp}NacNac) (**4.23**). When performed in the presence of an internal standard the yield of **4.23** was determined to be below 10%. This result contrasts with that of Schulz *et al*. who showed that reaction of (^{Dipp}NacNac)$_2Zn_2$ (**1.81**) with phenyl azide quantitatively formed **4.23**.

The reaction of **3.1** with CS_2 gave (^{Dipp}NacNac)Zn(μ-CS_2)Zn(^{Dipp}NacNac) (**27**) containing a fully reduced $[CS_2]^{2-}$ moiety bridging between Zn atoms. Structural authentication of **27** was unable to differentiate the different coordination environments of the Zn atoms due to the disorder of the μ-CS_2 unit over a crystallographic inversion centre. A DFT optimised structure was calculated from the crystallographically obtained atomic coordinates which allowed the different Zn–N bond distances to be interrogated. QTAIM analysis of **27** shows that the μ-CS_2 unit has been reduced to $[CS_2]^{2-}$.

The reaction of **3.1** with PhNCO and TolNCO gave (^{Dipp}NacNac)Zn{OC(NPh)$_2$}Zn(^{Dipp}NacNac) (**28**) and (^{Dipp}NacNac)Zn{OC(NTol)$_2$}Zn(^{Dipp}NacNac) (**29**), respectively. These compounds are rare examples of a fully delocalised ureato ligand bridging between two metal centres through the N and O atoms. DFT and QTAIM analyses support these observations, finding that both ureato units act as dianionic ligands.

The reaction of **3.1** with azobenzene gave {(^{Dipp}NacNac)Zn}(μ-PhNNPh){Zn(^{Dipp}NacNac)} (**30**). Elemental analysis, DFT and QTAIM data were consistent with the proposed formula for **30**. Compound **30** is the Zn analogue of {(^{Dipp}NacNac)Mg}(μ-PhNNPh){Mg(^{Dipp}NacNac)} (**4.43**), reported previously by Jones *et al*.[42] Although no crystal structure of **30** could be obtained, the compound shares many features with **4.43**. Both compounds feature remarkably downfield isopropyl methyl and *ortho* phenyl proton chemical shifts in the ^{1}H NMR, due to the orthometallation of the phenyl groups of the hydrazinato unit. This orthometallation results in the dearomatisation of each phenyl group and in the case of **30**, results in a complicated NMR spectrum due to the particular asymmetry of the compound. DFT

analysis of **30** supports the proposed structure, finding that the orthometallation of the phenyl groups arises independently during geometry optimisation. QTAIM analysis finds bond paths between both Zn, C_{ortho} pairs. QTAIM analysis was also performed for **4.43** and finds similar values between the Zn and Mg analogues with slight differences arising from the greater electronegativity of Zn compared to Mg.[44,45] Attempted crystallisation of **30** gave (^{Dipp}NacNac)Zn{N(Ph)N(H)Ph} (**31**), a partially hydrolysed structure derived from **30**. Compound **31** possesses a N–N distance consistent with a singly bonded species. The full hydrolysis of **30** with H_2O yields the singly bonded N,N'-diphenylhydrazine.

4.10 References

1. M. P. Blake, N. Kaltsoyannis, and P. Mountford, *Chem. Commun.*, 2015, **51**, 5743–5746.
2. I. Resa, E. Carmona, E. Gutierrez-Puebla, and A. Monge, *Science*, 2004, **305**, 1136–1138.
3. K. Freitag, H. Banh, C. Ganesamoorthy, C. Gemel, R. W. Seidel, and R. A. Fischer, *Dalton Trans.*, 2013, **42**, 10540.
4. D. Schuchmann, U. Westphal, S. Schulz, U. Flörke, D. Bläser, and R. Boese, *Angew. Chem. Int. Ed.*, 2009, **48**, 807–810.
5. C. A. Tolman, *Chem. Soc. Rev.*, 1972, **1**, 337.
6. S. Schulz, D. Schuchmann, I. Krossing, D. Himmel, D. Bläser, and R. Boese, *Angew. Chem. Int. Ed.*, 2009, **48**, 5748–5751.
7. K. Freitag, H. Banh, C. Gemel, P. Jerabek, R. W. Seidel, G. Frenking, and R. A. Fischer, *Inorg. Chem.*, 2015, **54**, 352–358.
8. T. Bollermann, K. Freitag, C. Gemel, R. W. Seidel, M. von Hopffgarten, G. Frenking, and R. A. Fischer, *Angew. Chem. Int. Ed.*, 2011, **50**, 772–776.
9. T. Bollermann, C. Gemel, and R. A. Fischer, *Coord. Chem. Rev.*, 2012, **256**, 537–555.
10. T. Bollermann, K. Freitag, C. Gemel, R. W. Seidel, and R. A. Fischer, *Organometallics*, 2011, **30**, 4123–4127.
11. K. Freitag, C. Gemel, P. Jerabek, I. M. Oppel, R. W. Seidel, G. Frenking, H.

Banh, K. Dilchert, and R. A. Fischer, *Angew. Chem. Int. Ed.*, 2015, **54**, 4370–4374.

12. H. Banh, K. Dilchert, C. Schulz, C. Gemel, R. W. Seidel, R. Gautier, S. Kahlal, J.-Y. Saillard, and R. A. Fischer, *Angew. Chem. Int. Ed.*, 2016, **55**, 3285–3289.

13. R. P. Kelly, N. Kazeminejad, C. A. Lamsfus, L. Maron, and P. W. Roesky, *Chem. Commun.*, 2016, **52**, 13090–13093.

14. S. Gondzik, S. Schulz, D. Bläser, and C. Wölper, *Chem. Commun.*, 2014, **50**, 1189–1191.

15. S. Gondzik, S. Schulz, D. Bläser, C. Wölper, R. Haack, and G. Jansen, *Chem. Commun.*, 2014, **50**, 927–929.

16. C. Stienen, S. Gondzik, A. Gehlhaar, R. Haack, C. Wölper, G. Jansen, and S. Schulz, *Organometallics*, 2016, **35**, 1022–1029.

17. S. Gondzik, C. Wölper, R. Haack, G. Jansen, and S. Schulz, *Dalton Trans.*, 2015, **44**, 15703–15711.

18. I. L. Fedushkin, O. V. Eremenko, A. A. Skatova, A. V. Piskunov, G. K. Fukin, S. Y. Ketkov, E. Irran, and H. Schumann, *Organometallics*, 2009, **28**, 3863–3868.

19. J. Gao, S. Li, Y. Zhao, B. Wu, and X.-J. Yang, *Organometallics*, 2012, **31**, 2978–2985.

20. S. Gondzik, D. Bläser, C. Wölper, and S. Schulz, *J. Organomet. Chem.*, 2015, **783**, 92–95.

21. R. B. King, *J. Inorg. Nucl. Chem.*, 1963, **25**, 1296–1298.

22. M. P. Blake, N. Kaltsoyannis, and P. Mountford, *Chem. Commun.*, 2013, **49**, 3315–3317.

23. N. L. Pickett, O. Just, D. G. VanDerveer, and W. S. Rees, *Acta Cryst. C*, 2000, **56**, 412–413.

24. G. R. Fulmer, A. J. M. Miller, N. H. Sherden, H. E. Gottlieb, A. Nudelman, B. M. Stoltz, J. E. Bercaw, and K. I. Goldberg, *Organometallics*, 2010, **29**, 2176–2179.

25. J. Prust, H. Hohmeister, A. Stasch, H. W. Roesky, J. Magull, E. Alexopoulos, I. Usón, H.-G. Schmidt, and M. Noltemeyer, *Eur. J. Inorg. Chem.*, 2002, 2156–2162.

26. S. Grimme, *J. Comput. Chem.*, 2006, **27**, 1787–1799.

27. S. Grimme, S. Ehrlich, and L. Goerigk, *J. Comput. Chem.*, 2011, **32**, 1456–1465.

28. R. F. W. Bader, *Atoms in Molecules: A Quantum Theory*, Oxford University Press, Oxford, 1990.

29. D. A. Fletcher, R. F. McMeeking, and D. Parkin, *J. Chem. Inf. Comput. Sci.*, 1996, **36**, 746–749.

30. J. M. Lisy, E. D. Dobrzynski, R. J. Angelici, and J. Clardy, *J. Am. Chem. Soc.*, 1975, **97**, 656–657.

31. T. S. Cameron, P. A. Gardner, and K. R. Grundy, *J. Organomet. Chem.*, 1981, **212**.

32. H.-F. Klein, J. Montag, U. Zucha, U. Flörke, and H.-J. Haupt, *Inorg. Chim. Acta*, 1990, **177**, 35–42.

33. C. B. Pamplin, S. J. Rettig, B. O. Patrick, and B. R. James, *Inorg. Chem.*, 2011, **50**, 8094–8105.

34. C. M. Palit, D. J. Graham, C.-H. Chen, B. M. Foxman, and O. V. Ozerov, *Chem. Commun.*, 2014, **50**, 12840–12842.

35. I. Kulai, O. Brusylovets, N. Saffon, Z. Voitenko, S. Mazières, and M. Destarac, *Fr. Ukr. J. Chem.*, 2015, **3**, 53–59.

36. W. Uhl, A. Vester, and W. Hiller, *J. Organomet. Chem.*, 1993, **443**, 9–17.

37. J. A. J. Jarvis, B. E. Job, B. T. Kilbourn, R. H. B. Mais, P. G. Owston, and P. F. Todd, *Chem. Commun.*, 1967, 1149–1150.

38. C. P. Casey, R. A. Widenhoefer, and R. K. Hayashi, *Inorg. Chem.*, 1995, **34**, 1138–1144.

39. T. A. Coffey, G. D. Forster, and G. Hogarth, *J. Chem. Soc., Dalton Trans.*, 1995, 2337.

40. G. Fachinetti, C. Biran, C. Floriani, A. C. Villa, and C. Guastini, *J. Chem. Soc.,*

Dalton Trans., 1979, 792–800.

41. R. Lalrempuia, A. Stasch, and C. Jones, *Chem. Sci.*, 2013, **4**, 4383–4388.

42. S. J. Bonyhady, S. P. Green, C. Jones, S. Nembenna, and A. Stasch, *Angew. Chem. Int. Ed.*, 2009, **48**, 2973–2977.

43. M. Klussmann, *Chem. Eur. J.*, 2018, **24**, 4480–4496.

44. D. R. Lide, Ed., *CRC Handbook of Chemistry and Physics, 84th Edition*, Boca Raton, Florida, 2003.

45. L. Pauling, *The Nature of the Chemical Bond, Third Edition*, Cornell University Press, Ithaca, New York, 1960.

Chapter Five

Experimental details and characterising data

5.1 General methods and instrumentation

All manipulations were carried out using standard Schlenk line or dry-box techniques under an atmosphere of argon or dinitrogen. Solvents were degassed by sparging with dinitrogen and dried by passing through a column of the appropriate drying agent (diethyl ether, benzene, pentane and hexanes).[1] Alternatively, solvents were predried over activated 4 Å molecular sieves and refluxed over sodium (toluene), potassium (THF) or NaK alloy (diethyl ether) and distilled. Deuterated solvents were dried over sodium (toluene-d_8) or potassium (C_6D_6 and THF-d_8), distilled under reduced pressure and stored under argon in Teflon valve ampoules. NMR samples were prepared under dinitrogen in 5 mm Wilmad 507-PP tubes fitted with J. Young Teflon valves. ^{1}H, ^{13}C{^{1}H} and ^{31}P{^{1}H} spectra were recorded on a Bruker Avance III 400, a Bruker Avance III 500 or a Bruker Avance 500 spectrometer equipped with a ^{13}C cryoprobe at ambient temperature. ^{1}H and ^{13}C{^{1}H} spectra are referenced internally to residual protio-solvent (^{1}H) or solvent (^{13}C) resonances and are reported relative to tetramethylsilane (δ = 0 ppm). ^{31}P{^{1}H} spectra were referenced externally to an 85% H_3PO_4 solution. Assignments were confirmed as necessary with the use of two-dimensional ^{1}H–^{1}H and ^{13}C–^{1}H NMR correlation experiments. Chemical shifts are quoted in δ (ppm) and coupling constants in Hz. Diffusion NMR spectroscopic studies were performed on a Bruker Avance III 500 spectrometer. IR spectra were recorded on a Thermo Scientific Nicolet iS5 FTIR spectrometer and samples prepared in a dry-box as Nujol mulls between NaCl plates or as a solution (THF or toluene) in a NaCl cell. The data are quoted in wavenumbers (cm^{-1}). Mass spectra were recorded by the mass spectrometry service of Oxford University's Department of Chemistry. Elemental analyses were carried out by the Elemental Analysis Service at London Metropolitan University.

5.2 X-ray data collection and processing parameters

Crystals were mounted on glass fibres using perfluoropolyether oil and cooled rapidly in a stream of cold N_2 using an Oxford Cryosystems Cryostream unit. Diffraction data were measured using an Enraf-Nonius KappaCCD diffractometer or Agilent Technologies Supernova diffractometer using Mo-Kα or Cu-Kα, respectively. As appropriate, absorption and decay corrections were applied to the data and equivalent

reflections merged.[2,3] All structures were solved by the author using SIR92[4] or Superflip,[5] and further refinements and all other crystallographic calculations were performed using the CRYSTALS program suite.[6] Other details of the structure solution and refinements are given in the CD Appendix.

5.3 Computational details

Gradient corrected density functional theory calculations were carried out using the PBE functional,[7,8] as implemented in the Gaussian 09 Rev D.01 (G09) quantum chemistry code.[9] The cc-pVDZ basis set of Dunning *et al.* was used for all atoms, except Hg and I. For Hg a relativistic pseudopotential plus (8s7p6d2f)/[6s5p3d2f] valence contraction was employed.[10] For I a relativistic pseudopotential plus (4s5p)/[2s3p] valence contraction was employed.[11] The ultrafine grid was employed and the SCF convergence criterion set to 10^{-6} in all cases. For geometry optimisations, the default convergence criteria were used or decreased maxstep specified where convergence could not otherwise be achieved. All frequency calculations were performed at optimised geometries. For optimisations where the geometry was unconstrained, no imaginary frequencies were observed.

Bond dissociation enthalpies were calculated from frequency calculations in G09 at optimised geometries (SCF total energies modified with zero point energies and thermal corrections to 298.15 K). Molecular orbital contributions were calculated in G09 using Mulliken population analysis.

Atoms-in-molecules analyses were performed with the AIMALL program (Version 14.04.17),[12] using wavefunction or formatted checkpoint files from G09 as input. Electron densities, Laplacians and energy densities were all calculated at bond critical points. Partial atomic charges and bond delocalisation indices were also calculated.

5.4 Diffusion NMR details

Samples of (^{Dipp}NacNac)MgFp(THF) (**2.16**), {MesC(NDipp)$_2$}MgFp(THF) (**8**), {MesC(NDipp)$_2$}Mg{Co(CO)$_3$(PCy$_3$)}(THF) (**10**), and {MesC(NMes)$_2$}Mg{Co(CO)$_3$(PCy$_3$)}(THF) (**14**) in toluene-d_8 were prepared with a concentration of 0.005 mol L^{-1}. A sample of [{Me$_2$NC(NDipp)$_2$}MgFp]$_2$ (**18**) in toluene-d_8 was prepared with a concentration of 0.0025 mol L^{-1}. A sample of (^{Dipp}NacNac)Mg(THF)Fp (**2.16**) in THF-d_8 was prepared with a concentration of 0.02

mol L^{-1}. A sample of [{$Me_2NC(NDipp)_2$}MgFp]$_2$ (**18**) in THF-d_8 was prepared with a concentration of 0.01 mol L^{-1}.

Diffusion NMR spectra were collected on a Bruker Avance III 500 spectrometer equipped with a $^1H/^{19}F–^{107}Ag$ BBO probe regulated at 298 K with an air flow of 400 L h^{-1}. Samples were equilibrated in the probe for at least 30 min prior to data collection. The bipolar LED stimulated echo sequence[13] was used with a diffusion time (Δ) of 300 ms and gradient pulses (δ) as listed in Table 5.1 (applied as sine-bell shaped bipolar pairs).

Table 5.1 Gradient pulse durations (δ) for diffusion NMR measurements of (^{Dipp}NacNac)MgFp(THF) (**2.16**), {MesC(NDipp)$_2$}MgFp(THF) (**8**), {MesC(NDipp)$_2$}Mg{Co(CO)$_3$(PCy$_3$)}(THF) (**10**), {MesC(NMes)$_2$}Mg{Co(CO)$_3$(PCy$_3$)}(THF) (**14**), and [{$Me_2NC(NDipp)_2$}MgFp]$_2$ (**18**).

Compound	Solvent	δ (μs)
2.16	Tol-d_8	600
8	Tol-d_8	660
10	Tol-d_8	650
14	Tol-d_8	685
18	Tol-d_8	650
2.16	THF-d_8	540
18	THF-d_8	550

Signal attenuation was monitored over 16 experiments with gradients strengths ranging from 2–95% of maximum (50.0 G cm^{-1}). Signal decays were fitted to the Stejskal-Tanner equation using the Bruker *T_1/T_2 Relaxation* module within TOPSPIN 3.2.[14] For all samples the residual toluene or THF solvent signal was used as an internal reference signal to monitor for possible viscosity differences between sample preparations.

Diffusion coefficients D were used to calculate hydrodynamic radii r_s according to the Stokes-Einstein equation assuming solvent viscosity to be that of the pure (protio) solvents toluene (0.560 mPa·s at 298 K) and THF (0.456 mPa·s at 298 K),

respectively.[15] Effective molecule volumes were then derived from these radii as spherical volumes. Molecular volumes derived from crystal structures were determined using Accelrys Discovery Studio Visualizer 4.1.0[16] based on a solvent accessible surface area determined using a 1.4 Å probe.

5.5 Literature preparations

Metals, starting materials and reagents were purchased from Sigma Aldrich, Strem Chemicals or Alfa Aesar and either used as received or purified according to standard procedures. Hg was filtered, washed with $HCl_{(aq)}$, distilled water, acetone then dried under reduced pressure. KFp,[17] NaRp(THF),[18] $K[Co(CO)_3(PCy_3)](THF)_2$,[19] DippN(H)C(S)N(H)Dipp,[20] MesN(H)C(S)N(H)Mes,[20] activated Cu,[21] {Dipp(H)N}(Me)CCHC(O)Me,[22] $\{(^{Dipp}NacNac)Zn\}_2Hg$,[23] and PhN_3[24] were synthesised according to published procedures.

5.6 Experimental details and characterising data for Chapter Two

$[\{MesC(N^iPr)_2\}Mg(\mu\text{-}Br)(OEt_2)]_2$ (1). To a stirring solution of MesMgBr in Et_2O (60.0 mL, 0.5 M, 30.0 mmol) was added ^{i}PrNCN^{i}Pr (4.50 mL, 29.0 mmol) dropwise. The solution was stirred for 18 h at RT to give a white precipitate. The solid was isolated by filtration then washed with cold Et_2O (2 x 20 mL, −78 °C) before drying *in vacuo* to afford **1** as a white solid. Yield: 10.8 g (88%). Diffraction-quality crystals of **1** were grown from an Et_2O solution at 5 °C. ^{1}H NMR (C_6D_6, 400.2 MHz): δ 6.82 (4 H, s, C_6H_2), 3.73 (8 H, quart, ^3J = 7.0 Hz, OCH_2), 3.24 (4 H, sept, ^3J = 5.9 Hz, C<u>H</u>Me$_2$), 2.38 (12 H, s, *o*-C_6H_2<u>Me</u>$_3$), 2.16 (6 H, s, *p*-C_6H_2<u>Me</u>$_3$), 1.27 (24 H, d, ^3J = 5.9 Hz, CH<u>Me</u>$_2$), 1.17 (12 H, t, ^3J = 7.0 Hz, OCH_2<u>Me</u>). ^{13}C{^{1}H} NMR (C_6D_6, 100.6 MHz): δ 173.9 (CN_2), 136.8 (*p*-C_6H_2), 134.5 (*o*-C_6H_2), 133.6 (*i*-C_6H_2), 128.4 (*m*-C_6H_2), 65.5 (OCH_2), 47.2 (<u>C</u>HMe$_2$), 26.9 (CH<u>Me</u>$_2$), 21.2 (*p*-C_6H_2<u>Me</u>$_3$), 20.5 (*o*-C_6H_2<u>Me</u>$_3$), 14.5 (OCH_2<u>Me</u>). IR (NaCl plates, Nujol mull, cm^{-1}): 1355 (m), 1340 (m), 1233 (m), 1181 (m), 1166 (m), 1119 (m), 1090 (m), 1051 (m), 998 (m), 902 (w), 860 (m), 836 (w), 824 (w), 783 (m), 767 (m), 693 (w). EI-MS *m/z* = 499 (95%) $[\{MesC(N^iPr)_2\}Mg\{(N^iPr)_2C(C_6H_2Me_2)\}]^+$. It was not possible to obtain a satisfactory elemental analysis for **1**.

$\{MesC(N^iPr)_2\}MgRp(THF)$ (3). To $[Mg\{MesC(N^iPr)_2\}(Br)(OEt_2)]_2$ (**1**, 250 mg, 0.30 mmol) and NaRp(THF) (190 mg, 0.59 mmol) was added THF (20 mL). The solution was stirred for 18 h before removal of volatiles under reduced pressure. The dark brown solid was extracted with benzene (3 x 5 mL) and volatiles removed under reduced

pressure. The residue was washed with pentane (3 x 5 mL) at −78 °C and dried *in vacuo* to afford **3** as a light red-brown solid. Yield: 0.15 g (46%). ^{1}H NMR (C_6D_6, 400.2 MHz, 293 K): δ 6.80 (2 H, s, C_6H_2), 5.11 (5 H, s, Cp), 3.90 (4 H, s, OCH_2), 3.08 (2 H, sept, ^{3}J = 6.2 Hz, C<u>H</u>Me$_2$), 2.39 (6 H, s, *o*-C_6H_2<u>Me</u>$_3$), 2.16 (3 H, s, *p*-C_6H_2<u>Me</u>$_3$), 1.31 (4 H, s, OCH_2C<u>H</u>$_2$), 1.06 (12 H, br s, CH<u>Me</u>$_2$). ^{13}C{^{1}H} NMR (C_6D_6, 100.6 MHz, 293 K): δ 209.2 (CO), 173.3 (CN_2), 137.1 (*p*-C_6H_2), 134.2 (*o*-C_6H_2), 132.9 (*i*-C_6H_2), 128.6 (*m*-C_6H_2), 82.2 (Cp), 69.5 (OCH_2), 46.5 (<u>C</u>HMe$_2$), 27.2 (CH<u>Me</u>$_2$), 25.3 (OCH_2<u>C</u>H_2), 21.1 (*p*-C_6H_2<u>Me</u>$_3$), 20.5 (*o*-C_6H_2<u>Me</u>$_3$). IR (NaCl plates, Nujol mull, cm^{-1}): 3881 (w), 3794 (w), 3731 (w), 2030 (s), 1970 (sh), 1950 (s), 1874 (s), 1611 (m), 1356 (m), 1333 (m), 1315 (m), 1240 (m), 1178 (m), 1165 (m), 1144 (m), 1119 (m), 1018 (m), 990 (w), 921 (w), 872 (m), 852 (m), 790 (m), 766 (m), 729 (m), 693 (m), 677 (m). IR (NaCl cell, toluene, *ν*(CO), cm^{-1}): 2025 (s), 1971 (m), 1916 (w), 1884 (w). EI-MS *m/z* = 231 (100%) [$Me_2C_6H_3C(N^iPr)_2$]$^+$ Anal. found (calcd for $C_{27}H_{38}MgN_2O_3Ru$): C, 57.34 (57.50); H, 6.84 (6.79); N, 5.17 (4.97)%.

{MesC(N^{i}Pr)$_2$}Mg{Co(CO)$_3$(PCy$_3$)}(THF) (4). To [{MesC(N^{i}Pr)$_2$}Mg(μ-Br)(OEt$_2$)]$_2$ (**1**, 400 mg, 0.472 mmol) and K[Co(CO)$_3$(PCy$_3$)](THF)$_2$ (572 mg, 0.944 mmol) was added THF (20 mL). The brown solution was stirred for 3 h before removal of volatiles under reduced pressure. The dark brown solid was extracted with benzene (3 x 5 mL) and volatiles removed under reduced pressure. The residue was washed with cold pentane (10 mL, −78 °C) and dried *in vacuo* to afford **4** as a grey-brown solid. Diffraction quality crystals of **4** were grown from pentane at RT. Yield: 418 mg (58%). ^{1}H NMR (C_6D_6, 400.2 MHz): δ 6.79 (2 H, s, C_6H_2), 4.13 (4 H, s, OCH_2), 3.19 (2 H, br sept, ^{3}J = 5.3 Hz, C<u>H</u>Me$_2$), 2.43 (6 H, s, *o*-C_6H_2<u>Me</u>$_3$), 2.15 (3 H, s, *p*-C_6H_2<u>Me</u>$_3$), 2.04 (3 H, m, 1-C_6H_{11}), 1.79 (6 H, m, 4-C_6H_{11}), 1.64 (12 H, m, 2,6-C_6H_{11}), 1.35 (4 H, s, OCH_2C<u>H</u>$_2$), 1.24 (24 H, d & m overlapping, ^{3}J = 5.3 Hz, CH<u>Me</u>$_2$ & 3,5-C_6H_{11}). ^{13}C{^{1}H} NMR (C_6D_6, 100.6 MHz): δ 210.2 (s, CO), 173.9 (s, CN_2), 136.9 (s, *p*-C_6H_2), 134.6 (s, *o*-C_6H_2), 133.0 (s, *i*-C_6H_2), 128.5 (s, *m*-C_6H_2), 70.0 (s, OCH_2), 46.8 (s, <u>C</u>HMe$_2$), 37.6 (d, ^{1}J = 16.8 Hz, 1-C_6H_{11}), 30.5 (s, 2,6-C_6H_{11}), 28.2 (d, ^{3}J = 10.2 Hz, 3,5-C_6H_{11}), 27.0 (m, overlapping CH<u>Me</u>$_2$ & 4-C_6H_{11}), 25.3 (s, OCH_2<u>C</u>H_2), 21.2 (s, *p*-C_6H_2<u>Me</u>$_3$), 20.6 (s, *o*-C_6H_2<u>Me</u>$_3$). ^{31}P{^{1}H} (C_6D_6, 162.0 MHz): δ 70.0 (s). IR (NaCl plates, Nujol mull, cm^{-1}): 3818 (w), 3438 (w), 1963 (m), 1922 (m), 1879 (s), 1864 (s), 1821 (m), 1756 (w), 1611 (w), 1582 (w), 1335 (m), 1240 (w), 1168 (w), 1143 (w), 1110 (m), 917 (w), 876 (w) 853 (m), 766 (w). IR (NaCl cell, toluene, *ν*(CO), cm^{-1}): 2038 (w), 1969 (m),

1904 (s), 1895 (s), 1839 (m). It was not possible to obtain a satisfactory elemental analysis for **4.**

DippNCNDipp (5). To a stirring solution of DippN(H)C(S)N(H)Dipp (7.93 g, 20.0 mmol) and NEt_3 (5.58 mL, 40.0 mmol) in ethyl acetate (100 mL) was added I_2 (5.58 g, 22.0 mmol) in portions over 30 min. The mixture was stirred for 2 h at RT then filtered to give a brown solution. Volatiles were removed under reduced pressure to give a brown solid. The solid was extracted with pentane (4 x 50 mL), filtered through a silica plug and the resultant brown solution added to activated Cu (3.00 g, 48.0 mmol). The mixture was stirred for 16 h at RT to give a black suspension. The suspension was filtered through silica to give a colourless solution. Volatiles were removed under reduced pressure and the resultant solid was dried *in vacuo* to afford **5** as a colourless crystalline solid. Yield: 4.74 g (65%). The ^{1}H NMR spectrum was consistent with that reported by Cowley *et al*.[20]

MesNCNMes (6). To a stirring solution of MesN(H)C(S)N(H)Mes (12.5 g, 40.0 mmol) and NEt_3 (11.2 mL, 80.0 mmol) in ethyl acetate (300 mL) was added I_2 (10.2 g, 40.0 mmol) in portions over 30 min. The mixture was stirred for 2 h at RT then filtered to give a brown solution. Volatiles were removed under reduced pressure to give a brown solid. The solid was extracted with pentane (4 x 50 mL), filtered through a silica plug and the resultant brown solution added to activated Cu (6.10 g, 96.0 mmol). The mixture was stirred for 16 h at RT to give a black suspension. The suspension was filtered through silica to give a colourless solution. Volatiles were removed under reduced pressure and the resultant solid was dried *in vacuo* to afford **6** as a colourless crystalline solid. Yield: 6.97 g (63%). The ^{1}H NMR spectrum was consistent with that reported by Cowley *et al*.[20]

[{MesC(NDipp)$_2$}Mg(μ-Br)(OEt$_2$)]$_2$ (7). To a stirring solution of MesMgBr in Et_2O (43.0 mL, 0.3 M, 12.9 mmol) was added a solution of DippNCNDipp (**5**, 4.50 g, 12.4 mmol) in Et_2O (30 mL) dropwise. The solution was stirred for 18 h to give a white precipitate. The solid was isolated by filtration and washed with cold Et_2O (2 x 50 mL, −78 °C) before drying *in vacuo* to afford (**7**) as a white solid. Yield: 5.05 g (67%). ^{1}H NMR (C_6D_6, 400.2 MHz): δ 7.02 (12 H, br s, overlapping *m*-C_6H_3 & *p*-C_6H_3), 6.34 (4 H, s, C_6H_2), 3.60 (8 H, s, OCH_2), 3.33 (8 H, br s, C<u>H</u>Me_2), 2.04 (12 H, s, *o*-C_6H_2<u>Me_3</u>), 1.81 (6 H, s, *p*-C_6H_2<u>Me_3</u>), 1.38 (24 H, s, CH<u>Me_2</u>), 1.07 (24 H, s, CH<u>Me_2</u>), 0.91 (12 H, s, OCH_2<u>Me</u>). ^{13}C{^{1}H} NMR (C_6D_6, 100.6 MHz): δ 175.0 (CN_2), 142.9 (*o*-C_6H_3), 141.7

(*o*-C_6H_3), 141.2 (*i*-C_6H_3), 137.9 (*p*-C_6H_2), 137.0 (*o*-C_6H_2), 130.5 (*i*-C_6H_2), 129.6 (*m*-C_6H_2), 124.1 (*p*-C_6H_3), 123.6 (*m*-C_6H_3), 123.4 (*m*-C_6H_3), 65.7 (OCH_2), 28.8 ($\underline{C}HMe_2$), 27.0 ($CH\underline{Me}_2$), 22.1 ($CH\underline{Me}_2$), 21.6 (*o*-$C_6H_2\underline{Me}_3$), 20.6 (*p*-$C_6H_2\underline{Me}_3$), 13.6 ($OCH_2\underline{Me}$). IR (NaCl plates, Nujol mull, cm^{-1}): 1437 (s), 1412 (sh), 1392 (s), 1319 (m), 1231 (w), 1189 (w), 1177 (m), 1051 (m), 996 (m), 967 (m), 949 (w), 936 (w), 889 (w), 853 (m), 834 (w), 779 (m), 762 (m), 754 (m), 672 (w), 659 (w). Anal. found (calcd for $C_{76}H_{110}Mg_2Br_2N_4O_2$): C, 68.92 (69.15); H, 8.52 (8.40); N, 4.28 (4.24)%.

{MesC(NDipp)$_2$}MgFp(THF) (8). To a stirring solution of [{MesC(NDipp)$_2$}Mg(μ-Br)(OEt$_2$)]$_2$ (**7**, 1.00 g, 0.76 mmol) in THF (10 mL) was added a solution of KFp (326 mg, 1.51 mmol) in THF (10 mL) dropwise. The reaction mixture was stirred for 2 h before removal of volatiles under reduced pressure. The dark brown solid was extracted with benzene (2 x 10 mL) and volatiles removed under reduced pressure. The solid was triturated with pentane (5 mL) before removal of volatiles under reduced pressure and drying *in vacuo* to afford **8** as a light brown solid. Yield: 0.89 g (74%). ^{1}H NMR (C_6D_6, 400.2 MHz): δ 7.01 (6 H, br s, overlapping *m*-C_6H_3 & *p*-C_6H_3), 6.36 (2 H, s, C_6H_2), 4.51 (5 H, s, Cp), 4.00 (4 H, s, OCH_2), 2.96 (2 H, br s, $C\underline{H}Me_2$), 2.12 (3 H, s, *o*-$C_6H_2\underline{Me}_3$), 1.96 (3 H, s, *o*-$C_6H_2\underline{Me}_3$), 1.87 (3 H, s, *p*-$C_6H_2\underline{Me}_3$), 1.50 (12 H, br s, $CH\underline{Me}_2$), 1.26 (4 H, s, $OCH_2C\underline{H}_2$). ^{13}C{^{1}H} NMR (C_6D_6, 100.6 MHz): δ 221.7 (CO), 173.6 (CN_2), 142.4 (*o*-C_6H_3), 137.8 (*o*-C_6H_2), 137.7 (*p*-C_6H_2), 137.3 (*o*-C_6H_2), 131.2 (*i*-C_6H_2), 130.0 (*m*-C_6H_2), 129.8 (*m*-C_6H_2), 128.6 (*i*-$C_6H_3{}^iPr_2$), 124.0 (*m*-C_6H_3), 123.8 (*p*-C_6H_3), 123.6 (*m*-C_6H_3), 78.7 (Cp), 71.0 ($O\underline{C}H_2CH_2$), 28.9 ($\underline{C}HMe_2$), 27.0 ($CH\underline{Me}_2$), 25.2 ($OCH_2\underline{C}H_2$), 23.6 ($CH\underline{Me}_2$), 22.8 (*o*-$C_6H_2\underline{Me}_3$), 20.6 (*p*-$C_6H_2\underline{Me}_3$). IR (NaCl plates, Nujol mull, cm^{-1}): 2020 (m), 2003 (m), 1961 (sh), 1930 (s), 1866 (s), 1791 (sh), 1609 (m), 1567 (m), 1433 (s), 1412 (s), 1311 (m), 1228 (m), 1178 (m), 1078 (m), 1052 (m), 962 (w), 945 (w), 934 (w), 872 (m), 861 (m), 852 (m), 815 (m), 800 (m), 779 (m), 760 (s), 698 (w), 664 (m). IR (NaCl cell, toluene, *ν*(CO), cm^{-1}): 2017 (s), 1925 (m). It was not possible to obtain a satisfactory elemental analysis for **8**.

{MesC(NDipp)$_2$}MgRp(THF) (9). To [{MesC(NDipp)$_2$}Mg(Br)(OEt$_2$)]$_2$ (**7**, 500 mg, 0.38 mmol) and NaRp(THF) (240 g, 0.76 mmol) was added THF (20 mL). The solution was stirred for 18 h before removal of volatiles under reduced pressure. The brown solid was extracted with benzene (3 x 5 mL) and volatiles removed under reduced pressure. The residue was washed with pentane (3 x 5 mL) at −78 °C and dried *in vacuo* to afford **9** as a red-brown solid. Yield: 0.40 g (66%). ^{1}H NMR (C_6D_6, 400.2 MHz, 298

K): δ 7.01 (6 H, br s, overlapping *m*-C_6H_3 & *p*-C_6H_3), 6.36 (2 H, s, C_6H_2), 4.90 (5 H, s, Cp), 3.96 (4 H, s, OCH_2), 3.69 (2 H, br s, C<u>H</u>Me_2) 2.98 (2 H, br s, C<u>H</u>Me_2), 2.16 (3 H, s, *o*-C_6H_2<u>Me_3</u>), 1.99 (3 H, s, *o*-C_6H_2<u>Me_3</u>), 1.84 (3 H, s, *p*-C_6H_2<u>Me_3</u>), 1.42 (24 H, br s, CH<u>Me_2</u>), 1.28 (4 H, s, OCH_2C<u>H_2</u>). $^{13}C\{^1H\}$ NMR (C_6D_6, 100.6 MHz, 293 K): δ 209.4 (CO), 173.2 (CN_2), 142.5 (*o*-C_6H_3), 137.9 (*o*-C_6H_2), 137.7 (*p*-C_6H_2), 137.3 (*o*-C_6H_2), 131.4 (*i*-C_6H_2), 130.1 (*m*-C_6H_2), 129.8 (*m*-C_6H_2), 128.6 (*i*-C_6H_3), 123.7 (*m*-C_6H_3), 123.6 (*p*-C_6H_3), 82.4 (Cp), 70.8 (OC<u>H_2</u>CH_2), 28.9 (<u>C</u>HMe_2), 26.8 (CH<u>Me_2</u>), 25.2 (OCH_2<u>C</u>H_2), 23.6 (CH<u>Me_2</u>), 22.6 (*o*-C_6H_2<u>Me_3</u>), 20.6 (*p*-C_6H_2<u>Me_3</u>). IR (NaCl plates, Nujol mull, cm^{-1}): 3810 (w), 2030 (m), 1970 (m), 1952 (s), 1882 (s), 1857 (sh), 1609 (m), 1586 (w), 1566 (w), 1433 (s), 1411 (s), 1312 (m), 1254 (m), 1228 (m), 1180 (m), 1161 (w), 1147 (w), 1079 (m), 1053 (m), 963 (w), 945 (w), 936 (w), 922 (w), 890 (w), 873 (m), 862 (m), 830 (w), 788 (m), 779 (m), 759 (m), 698 (w), 677 (w). IR (NaCl cell, toluene, *ν*(CO), cm^{-1}): 2024 (s), 1969 (m), 1888 (s). EI-MS *m/z* = 439 (20%) $[MesC(NDipp)NC_6H_4{}^iPr]^+$. Anal. found (calcd for $C_{45}H_{58}MgN_2O_3Ru$): C, 67.37 (67.53); H, 7.53 (7.30); N, 3.59 (3.50)%.

{MesC(NDipp)$_2$}Mg{Co(CO)$_3$(PCy$_3$)}(THF) (10). To [{MesC(NDipp)$_2$}Mg(μ-Br)(OEt$_2$)]$_2$ (**7**, 500 mg, 0.379 mmol) and K[Co(CO)$_3$(PCy$_3$)](THF)$_2$ (460 mg, 0.757 mmol) was added THF (20 mL). The brown solution was stirred for 18 h before removal of volatiles under reduced pressure. The grey solid was extracted with pentane (3 x 10 mL) and volatiles removed under reduced pressure. Drying *in vacuo* afforded **14** as a grey solid. Yield: 298 mg (39%). ^1H NMR (C_6D_6, 400.2 MHz): δ 7.03 (6 H, br s, overlapping *m*-C_6H_3 & *p*-C_6H_3), 6.40 (1 H, s, *m*-C_6H_2), 6.36 (1 H, s, *m*-C_6H_2), 4.16 (4 H, s, OCH_2), 3.42 (4 H, br s, C<u>H</u>Me_2) 2.38 (3 H, s, *o*-C_6H_2<u>Me_3</u>), 2.02 (3 H, m, 1-C_6H_{11}), 1.95 (3 H, s, *o*-C_6H_2<u>Me_3</u>), 1.83 (3 H, s, *p*-C_6H_2<u>Me_3</u>), 1.78 (6 H, m, 4-C_6H_{11}), 1.62 (12 H, m, 2,6-C_6H_{11}), 1.51 (12 H, s, CH<u>Me_2</u>), 1.35 (s, 4 H, OCH_2C<u>H_2</u>), 1.26 (12 H, s, CH<u>Me_2</u>), 1.21 (12 H, m, 3,5-C_6H_{11}). $^{13}C\{^1H\}$ NMR (C_6D_6, 100.6 MHz): δ 209.4 (s, CO), 174.7 (s, CN_2), 143.3 (s, *o*-C_6H_3), 142.5 (s, *o*-C_6H_3), 138.3 (s, *o*-C_6H_2), 137.6 (s, *o*-C_6H_2), 137.5 (s, *p*-C_6H_2), 131.0 (s, *i*-C_6H_2), 130.0 (s, *m*-C_6H_2), 129.3 (s, *m*-C_6H_2), 127.9 (s, *i*-C_6H_3), 123.9 (s, *p*-C_6H_3), 123.7 (s, *m*-C_6H_3), 123.6 (s, *m*-C_6H_3), 71.0 (s, OCH_2), 37.7 (d, ^1J = 17.3 Hz, 1-C_6H_{11}), 30.3 (s, 2,6-C_6H_{11}), 28.9 (s, CH<u>Me_2</u>), 28.5 (s, <u>C</u>HMe_2) 28.1 (d, ^3J = 10.3 Hz, 3,5-C_6H_{11}), 26.9 (s, 4-C_6H_{11}), 25.0 (OCH_2<u>C</u>H_2), 23.8 (*o*-C_6H_2<u>Me_3</u>), 22.7 (*o*-C_6H_2<u>Me_3</u>), 20.6 (*p*-C_6H_2<u>Me_3</u>). $^{31}P\{^1H\}$ (C_6D_6, 162.0 MHz): δ 68.6 (s). IR (NaCl plates, Nujol mull, cm^{-1}): 3827 (w), 3747 (w), 2040 (w), 1965 (s),

1873 (s), 1612 (m), 1586 (w), 1569 (w), 1433 (s), 1413 (m), 1316 (m), 1230 (w), 1198 (w), 1174 (m), 1079 (m), 1041 (m), 963 (w), 947 (w), 935 (w), 916 (w), 875 (m), 851 (m), 777 (m), 758 (m), 700 (w), 659 (w), 585 (m), 562 (m). IR (NaCl cell, toluene, ν(CO), cm^{-1}): 1968 (m), 1891 (s), 1840 (w). Anal. found (calcd for $C_{59}H_{86}CoMgN_2O_4P$): C, 70.54 (70.75); H, 8.50 (8.66); N, 2.88 (2.80)%.

[{MesC(NMes)$_2$}Mg(μ-Br)(OEt$_2$)]$_2$ (11). To a stirring solution of MesMgBr in Et_2O (43.0 mL, 0.3 M, 12.9 mmol) was added a solution of MesNCNMes (**6**, 3.48 g, 12.5 mmol) in Et_2O (30 mL) dropwise. The solution was stirred for 18 h to give a white precipitate. The solid was isolated by filtration and washed with cold Et_2O (2 x 20 mL, −78 °C) before drying *in vacuo* to afford **11** as a white solid. Yield: 6.66 g (93%). ^{1}H NMR (THF-d_8, 400.2 MHz): δ 6.54 (8 H, s, N-C_6H_2), 6.42 (4 H, s, C-C_6H_2), 3.38 (8 H, quart, ^3J = 7.0 Hz, OCH_2), 2.18 (24 H, s, N-(*o*-$C_6H_2\underline{Me}_3$)), 2.09 (12 H, s, C-(*o*-$C_6H_2\underline{Me}_3$)), 2.06 (12 H, s, N-(*p*-$C_6H_2\underline{Me}_3$)), 2.02 (6 H, s, C-(*p*-$C_6H_2\underline{Me}_3$)), 1.11 (12 H, t, ^3J = 7.0 Hz, $OCH_2\underline{Me}$). ^{13}C{^{1}H} NMR (C_6D_6, 100.6 MHz): δ 173.5 (CN_2), 144.9 (N-(*o*-C_6H_2)), 137.9 (C-(*o*-C_6H_2)), 137.7 (C-(*p*-C_6H_2)), 134.7 (C-(*i*-C_6H_2)), 132.8 (N-(*i*-C_6H_2)), 130.7 (N-(*p*-C_6H_2)), 129.5 (N-(*m*-C_6H_2)), 129.3 (C-(*m*-C_6H_2)), 66.5 (OCH_2), 23.3 (C-(*o*-$C_6H_2\underline{Me}_3$)), 21.3 (N-(*o*-$C_6H_2\underline{Me}_3$)), 21.0 (C-(*p*-$C_6H_2\underline{Me}_3$)), 20.9 (N-(*p*-$C_6H_2\underline{Me}_3$)), 15.8 ($OCH_2\underline{Me}$). IR (NaCl plates, Nujol mull, cm^{-1}): 1733 (w), 1396 (s), 1205 (m), 1181 (w), 1148 (m), 1086 (m), 1048 (m), 968 (w), 936 (w), 919 (w), 909 (w), 853 (s), 834 (w), 787 (m), 749 (w), 740 (w), 659 (w). It was not possible to obtain a satisfactory elemental analysis for **11**.

{MesC(NMes)$_2$}MgFp(THF) (12). To a stirring solution of [{MesC(NMes)$_2$}Mg(μ-Br)(OEt$_2$)]$_2$ (**11**, 300 mg, 0.260 mmol) in THF (15 mL) was added a solution of KFp (113 mg, 0.520 mmol) in THF (10 mL) dropwise. The reaction mixture was stirred for 3 h before removal of volatiles under reduced pressure. The dark brown solid was extracted with THF (2 x 10 mL) and filtered before removal of volatiles under reduced pressure. The solid was triturated with pentane before removal of volatiles under reduced pressure and drying *in vacuo* to afford **12** as a light brown solid. Yield: 236 mg (68%). ^{1}H NMR (THF-d_8, 400.2 MHz): δ 6.61 (4 H, s, N-C_6H_2), 6.52 (2 H, s, C-C_6H_2), 4.40 (5 H, s, Cp), 2.10 (6 H, s, C-(*o*-$C_6H_2\underline{Me}_3$)), 2.09 (15 H, s, N-(*o*-$C_6H_2\underline{Me}_3$) & C-(*p*-$C_6H_2\underline{Me}_3$)), 1.98 (6 H, s, N-(*p*-$C_6H_2\underline{Me}_3$)). ^{13}C{^{1}H} NMR (C_6D_6, 100.6 MHz): δ 223.1 (CO), 172.1 (CN_2), 143.9 (N-(*o*-C_6H_2)), 138.6 (C-(*p*-C_6H_2)), 137.8 (C-(*o*-C_6H_2)), 134.0 (C-(*i*-C_6H_2)), 131.4 (N-(*i*-C_6H_2)), 131.0 (N-(*p*-C_6H_2)), 130.0 (N-(*m*-C_6H_2)), 129.7

(C-(*m*-C_6H_2)), 78.8 (Cp), 22.2 (N-(*p*-$C_6H_2\underline{Me}_3$)), 21.0 (C-(*o*-$C_6H_2\underline{Me}_3$)), 20.8 (N-(*o*-$C_6H_2\underline{Me}_3$) & C-(*p*-$C_6H_2\underline{Me}_3$)). IR (NaCl plates, Nujol mull, cm^{-1}): 2019 (m), 1961 (sh), 1923 (s), 1858 (s), 1790 (sh), 1678 (w), 1610 (m), 1168 (w), 1147 (w), 969 (m), 955 (w), 935 (w), 920 (m), 852 (s), 676 (m), 634 (m), 606 (m), 592 (m). IR (NaCl cell, THF *v*(CO), cm^{-1}): 2013 (s), 1992 (sh), 1950 (sh), 1921 (s), 1879 (sh), 1861 (s). It was not possible to obtain a satisfactory elemental analysis for **12**.

{MesC(NMes)$_2$}MgRp(THF) (13). To a stirring solution of [{MesC(NMes)$_2$}Mg(μ-Br)(OEt$_2$)]$_2$ (**11**, 500 mg, 0.44 mmol) in THF (10 mL) was added a solution of NaRp(THF) (0.28 g, 0.87 mmol) in THF (10 mL) dropwise. The reaction mixture was stirred for 2 h before removal of volatiles under reduced pressure. The brown residue was extracted with benzene (2 x 10 mL), volatiles were removed under reduced pressure and the solid dried *in vacuo* to afford **13** as a brown solid. Yield: 0.47 g (76%). ^{1}H NMR (C_6D_6, 499.9 MHz, 348 K): δ 6.72 (4 H, s, N-C_6H_2), 6.45 (2 H, s, C-C_6H_2), 4.93 (5 H, s, Cp), 3.82 (4 H, s, OCH_2), 2.27 (12 H, s, N-(*o*-$C_6H_2\underline{Me}_3$), 2.14 (6 H, s, C-(*o*-$C_6H_2\underline{Me}_3$), 2.10 (6 H, s, N-(*p*-$C_6H_2\underline{Me}_3$), 1.90 (3 H, s, C-(*p*-$C_6H_2\underline{Me}_3$), 1.30 (4 H, s, $OCH_2C\underline{H}_2$). ^{13}C{^{1}H} NMR (C_6D_6, 125.7 MHz, 348 K): δ 209.3 (CO), 171.7 (CN_2), 143.4 (N-(*o*-C_6H_2)), 138.3 (C-(*p*-C_6H_2)), 137.3 (C-(*i*-C_6H_2)), 133.6 (C-(*o*-C_6H_2)), 131.7 (N-(*p*-C_6H_2)), 130.0 (N-(*i*-C_6H_2)), 130.0 (N-(*m*-C_6H_2)), 129.2 (C-(*m*-C_6H_2)), 82.2 (Cp) 70.1 (OCH_2), 25.3 ($OCH_2\underline{C}H_2$), 21.9 (C-(*o*-$C_6H_2\underline{Me}_3$)), 20.8 (C-(*p*-$C_6H_2\underline{Me}_3$)), 20.7 (N-(*p*-$C_6H_2\underline{Me}_3$)), 20.6 (N-(*o*-$C_6H_2\underline{Me}_3$)). IR (NaCl plates, Nujol mull, cm^{-1}): 3794 (w) 2029 (s), 1969 (s) 1946 (s), 1876 (s), 1625 (s), 1610 (s), 1568 (s), 1421 (s), 1395 (s), 1300 (m), 1207 (s), 1179 (m), 1167 (m), 1148 (m), 1104 (m), 970 (m), 956 (w), 935 (w), 920 (m), 871 (m), 825 (s), 755 (w), 746 (m), 736 (m), 676 (m). IR (NaCl cell, toluene, *v*(CO), cm^{-1}): 2025 (s), 1970 (m), 1920 (w), 1884 (m). EI-MS *m/z* = 398 (80%) [MesC(NMes)NHMes]$^+$. Anal. found (calcd for $C_{39}H_{46}MgN_2O_3Ru$): C, 65.36 (65.41); H, 6.45 (6.47); N, 3.81 (3.91)%.

{MesC(NMes)$_2$}Mg{Co(CO)$_3$(PCy$_3$)}(THF) (14). To a stirring solution of [{MesC(NMes)$_2$}Mg(μ-Br)(OEt$_2$)]$_2$ (**11**, 500 mg, 0.434 mmol) in THF (10 mL) was added a solution of K[Co(CO)$_3$(PCy$_3$)](THF)$_2$ (527 mg, 0.868 mmol) in THF (10 mL) dropwise. The reaction mixture was stirred for 2 h before removal of volatiles under reduced pressure. The brown residue was extracted with benzene (2 x 10 mL), volatiles were removed under reduced pressure and the solid dried *in vacuo* to afford **14** as a pale brown solid. Yield: 668 mg (84%). ^{1}H NMR (C_6D_6, 400.2 MHz): δ 6.71 (4 H, s,

N-C_6H_2), 6.42 (2 H, s, C-C_6H_2), 3.98 (4 H, s, OCH_2), 2.46 (12 H, s, N-(*o*-$C_6H_2\underline{Me}_3$), 2.26 (6 H, s, C-(*o*-$C_6H_2\underline{Me}_3$), 2.15 (12 H, br s, 2,6-C_6H_{11}), 2.06 (6 H, s, N-(*p*-$C_6H_2\underline{Me}_3$), 2.01 (3 H, br s, 1-C_6H_{11}), 1.86 (3 H, s, C-(*p*-$C_6H_2\underline{Me}_3$), 1.77 (12 H, br s, 3,5-C_6H_{11}), 1.62 (12 H, br s, 4-C_6H_{11}), 1.32 (4 H, br s, $OCH_2C\underline{H}_2$). $^{13}C\{^1H\}$ NMR (C_6D_6, 100.6 MHz): δ 211.1 (s, CO), 172.7 (CN_2), 143.3 (s, N-(*o*-C_6H_2)), 138.0 (s, C-(*p*-C_6H_2)), 137.3 (s, C-(*i*-C_6H_2)), 133.4 (s, C-(*o*-C_6H_2)), 131.5 (s, N-(*p*-C_6H_2)), 130.8 (s, N-(*i*-C_6H_2)), 129.9 (s, N-(*m*-C_6H_2)), 129.3 (s, C-(*m*-C_6H_2)), 70.0 (s, OCH_2), 37.5 (d, ^1J = 16.6 Hz, 1-C_6H_{11}), 30.4 (s, 2,6-C_6H_{11}), 28.2 (d, ^3J = 10.2 Hz, 3,5-C_6H_{11}), 27.0 (s, 4-C_6H_{11}), 25.3 (s, $OCH_2\underline{C}H_2$), 22.0 (s, C-(*o*-$C_6H_2\underline{Me}_3$)), 20.8 (s, C-(*p*-$C_6H_2\underline{Me}_3$)), 20.7 (s, N-(*p*-$C_6H_2\underline{Me}_3$)), 20.5 (s, N-(*o*-$C_6H_2\underline{Me}_3$)). $^{31}P\{^1H\}$ (C_6D_6, 162.0 MHz): δ 70.0 (s). IR (NaCl plates, Nujol mull, cm^{-1}): 2040 (w), 1964 (sh), 1937 (s), 1885 (sh), 1865 (s), 1784 (w), 1720 (s), 1569 (w), 1425 (s), 1396 (s), 1207 (m), 1172 (w), 1148 (w), 972 (w), 919 (w), 886 (m), 851 (s), 818 (w), 741 (m), 675 (w). IR (NaCl cell, toluene, *ν*(CO), cm^{-1}): 1970 (m), 1910 (m), 1890 (m), 1836 (m), 1755 (m). Anal. found (calcd for $C_{53}H_{73}CoMgN_2O_4P$): C, 69.53 (69.39); H, 8.18 (8.13); N, 2.99 (3.05)%.

NMR tube-scale reaction of {MesC(NDipp)$_2$}MgFp(THF) (8) with MeI. To a solution of {MesC(NDipp)$_2$}MgFp(THF) (**8**, 50 mg, 64.5 μmol) in C_6D_6 (0.5 mL) was added MeI (4 μL, 64.5 μmol). The ^1H NMR spectrum recorded after 30 min showed quantitative formation of FpMe by comparison with literature values.[25,26]

NMR tube-scale reaction of {MesC(NMes)$_2$}MgFp(THF) (12) with MeI. To a solution of {MesC(NMes)$_2$}MgFp(THF) (**12**, 43 mg, 64.5 μmol) in C_6D_6 (0.5 mL) was added MeI (4 μL, 64.5 μmol). The ^1H NMR spectrum recorded after 30 min showed quantitative formation of FpMe by comparison with literature values.[25,26]

General procedure for NMR tube-scale reactions of (L)Mg–TM compounds with solid or liquid reagents. To a solution of (L)Mg–TM (**3**, **4**, **8**, **9**, **10**, **12**, **13** or **14**, 1 equiv.) in C_6D_6 (0.5 mL) was added either TolNCNTol, ^{i}PrNCN^{i}Pr, ^{t}BuNCO or CS_2 (1 equiv.). The reactions were monitored by ^1H and $^{31}P\{^1H\}$ NMR (where appropriate).

General procedure for NMR tube-scale reactions of (L)Mg–TM compounds with CO$_2$. A solution of (L)Mg–TM (**12**, **13** or **14**) in C_6D_6 (0.5 mL) was prepared in a J. Young NMR tube. The headspace of the tube was evacuated with three freeze-pump-thaw cycles followed by the introduction of an overpressure of CO_2. The reactions were monitored by ^1H and $^{31}P\{^1H\}$ NMR (where appropriate).

{MesC(NMes)$_2$}Mg(S$_2$CFp)·2.5(THF) (15·2.5(THF)). To a stirring solution of KFp (55 mg, 0.25 mmol) in THF (5 mL) was added CS_2 dropwise at −23 °C. The temperature of the mixture was maintained for 20 mins with stirring before the dropwise addition of [{MesC(NMes)$_2$}Mg(μ-Br)(OEt$_2$)]$_2$ (**11**, 143 mg. 0.13 mmol). The brown solution was allowed to warm to RT then stirred for a further 60 mins at RT before removal of volatiles under reduced pressure. The brown solid was extracted with cold THF (−70 °C, 10 mL). Volatiles were removed under reduced pressure and the resultant brown solid dried *in vacuo* to afford **15·2.5(THF)**. Yield: 269 mg (63%). ^{1}H NMR (C_6D_6, 499.9 MHz): 6.73 (4 H, s, N-C_6H_2), 6.42 (2 H, s, C-C_6H_2), 4.16 (5 H, s, Cp), 3.64 (10 H, s, OCH_2), 2.39 (12 H, s, N-(*o*-$C_6H_2\underline{Me}_3$), 2.27 (6 H, s, C-(*o*-$C_6H_2\underline{Me}_3$), 2.10 (6 H, s, N-(*p*-$C_6H_2\underline{Me}_3$), 1.85 (3 H, s, C-(*p*-$C_6H_2\underline{Me}_3$), 1.30 (10 H, s, $OCH_2C\underline{H}_2$). ^{13}C{^{1}H} NMR (C_6D_6, 125.7 MHz): 330.0 (CS_2), 214.8 (CO), 172.2 (CN_2), 144.3 (N-(*o*-C_6H_2)), 137.6 (C-(*p*-C_6H_2)), 138.6 (C-(*o*-C_6H_2)), 137.2 (C-(*i*-C_6H_2)), 134.1 (N-(*i*-C_6H_2)), 130.3 (N-(*p*-C_6H_2)), 129.6 (N-(*m*-C_6H_2)), 129.3 (C-(*m*-C_6H_2)), 88.1 (Cp), 68.5 (OCH_2), 25.6 ($OCH_2\underline{C}H_2$), 22.4 (C-(*o*-$C_6H_2\underline{Me}_3$)), 20.9 (N-(*o*-$C_6H_2\underline{Me}_3$)), 20.8 (C-(*p*-$C_6H_2\underline{Me}_3$) & N-(*p*-$C_6H_2\underline{Me}_3$)). IR (NaCl plates, Nujol mull, cm^{-1}): 2020 (s, ν(CO)), 1971 (s, ν(CO)), 1626 (w), 1610 (w), 1206 (w), 951 (m, ν(SCS)), 919 (w), 880 (w), 851 (m, ν(SCS)), 828 (w), 794 (m), 628 (w), 588 (w). It was not possible to obtain a satisfactory elemental analysis for **15**.

NMR tube-scale reaction of {MesC(NMes)$_2$}MgFp(THF) (12) with Ph$_3$CCl. To a solution of {MesC(NMes)$_2$}MgFp(THF) (**12**, 10.0 mg, 14.9 μmol) in C_6D_6 (0.3 mL) was added a solution of Ph_3CCl (4.2 mg, 14.9 μmol) in C_6D_6 (0.2 mL). The reaction was monitored by ^{1}H NMR. The spectrum was consistent with conversion to {MesC(NMes)$_2$}MgCl(THF), Fp_2 and $Ph_3CCH(C_6H_4)CPh_2$. The chemical shifts of $Ph_3CCH(C_6H_4)CPh_2$ in C_6D_6 were verified by comparison with a previously reported example.[27]

Me$_2$NC(NDipp)(NHDipp) (16). To a stirring solution of $LiNMe_2$ (0.561 g, 11.00 mmol) in THF (10 mL) was added DippNCNDipp (**5**, 4.00 g, 11.00 mmol) over 5 min in THF (10 mL) at −78 °C. The colourless solution was allowed to warm to RT then stirred for a further 2 h at RT, quenched with deionised water (10 mL) and extracted into Et_2O (3 x 10 mL). Volatiles were removed under reduced pressure and the resultant white solid dried *in vacuo* to afford **16**. Yield: 4.13 g (92%). Diffraction-quality crystals were grown from a hexane solution at RT. ^{1}H NMR (C_6D_6, 400.2 MHz): δ 7.26 (2 H,

app. d, ^{3}J = 8.0 Hz, *p*-C_6H_3), 7.00 (4 H, d, ^{3}J = 7.0 Hz, *m*-C_6H_3), 5.25 (1 H, s, NH), 3.45 (2 H, br m, C<u>H</u>Me_2), 3.28 (2 H, br m, C<u>H</u>Me_2), 2.48 (6 H, s, NMe_2), 1.23 (24 H, d, ^{3}J = 6.9 Hz, CH<u>Me_2</u>). $^{13}C\{^{1}H\}$ NMR (C_6D_6, 101.6 MHz): δ 151.3 (<u>C</u>NMe_2), 145.0 (*i*-C_6H_3), 140.1 (*o*-C_6H_3), 124.1 (*m*-C_6H_3), 123.5 (*p*-C_6H_3), 39.5 (NMe_2), 29.0 (<u>C</u>HMe_2), 28.8 (<u>C</u>HMe_2), 25.0 (CH<u>Me_2</u>), 24.7 (CH<u>Me_2</u>), 23.4 (CH<u>Me_2</u>), 22.5 (CH<u>Me_2</u>). EI-HRMS: m/z found (calc. for $C_{27}H_{41}N_3$, $[Me_2NC(NDipp)(NHDipp)]^+$) 407.3303 (407.3300). IR (NaCl plates, Nujol mull, cm^{-1}): 3391 (w, ν(NH)), 1625 (s), 1260 (s), 1019 (m), 761 (w). Anal. found (calcd. for $C_{27}H_{41}N_3$): C, 79.46 (79.55); H, 10.30 (10.14); N, 10.25 (10.31)%.

{Me_2NC(NDipp)$_2$}MgI(OEt_2) (17). To a stirring solution of MeMgI in Et_2O (11.64 mL, 0.4 M, 4.91 mmol) was added a solution of $Me_2NC(NDipp)(NHDipp)$ (**16**, 2.00 g, 4.91 mmol) in Et_2O (10 mL) dropwise at −20 °C. The colourless solution was allowed to warm to RT and stirred for a further 2 h. The volatiles were removed under reduced pressure to give a white solid, which was washed with hexane (3 x 5 mL) and dried *in vacuo* to afford **17** as a white solid. Yield: 2.94 g (95%). Diffraction-quality crystals were grown from an Et_2O solution at RT. ^{1}H NMR (C_6D_6, 400.2 MHz): δ 7.20 (2 H, br m, *p*-C_6H_3), 7.14 (4 H, br m, *m*-C_6H_3), 3.71 (4 H, sept, ^{3}J = 6.8 Hz, C<u>H</u>Me_2), 3.34 (4 H, q, ^{3}J = 7.0 Hz, OCH_2), 2.14 (6 H, s, NMe_2), 1.38 (12 H, d, ^{3}J = 6.8 Hz, CH<u>Me_2</u>), 1.31 (12 H, d, ^{3}J = 6.8 Hz, CH<u>Me_2</u>), 0.93 (6 H, t, ^{3}J = 7.0 Hz, OCH_2<u>Me</u>). $^{13}C\{^{1}H\}$ NMR (C_6D_6, 101.6 MHz): δ 167.0 (<u>C</u>NMe_2), 143.4 (*i*-C_6H_3), 142.9 (*o*-C_6H_3), 123.8 (*m*-C_6H_3), 123.6 (*p*-C_6H_3), 66.9 (OCH_2), 39.6 (NMe_2), 27.9 (<u>C</u>HMe_2), 26.2 (CH<u>Me_2</u>), 23.7 (CH<u>Me_2</u>), 14.1 (OCH_2<u>Me</u>). IR (NaCl plates, Nujol mull, cm^{-1}): 1522 (s), 1315 (m), 1250 (m), 1203 (m), 1100 (m), 1042 (s), 934 (w), 835 (w), 904 (m), 835 (w), 771 (s). Anal. found (calcd. for $C_{31}H_{50}IMgN_3O$): C, 58.79 (58.92); H, 7.89 (7.98); N, 6.52 (6.65)%.

[{Me_2NC(NDipp)$_2$}MgFp]$_2$ (18). To a stirring suspension of KFp (171 mg, 0.791 mmol) in C_6H_6 (10 mL) was added a solution of {$Me_2NC(NDipp)_2$}MgI(Et_2O) (**17**, 500 mg, 0.791 mmol) in C_6H_6 (10 mL) dropwise at RT. The mixture was stirred for 1 h at RT then filtered. Volatiles were removed from the filtrate under reduced pressure to give a red solid, which was washed with cold hexane (3 x 5 mL, −78 °C) and dried *in vacuo* to afford **18** as a yellow solid. Yield: 308 mg (64%). Diffraction-quality crystals were grown from a benzene solution at 5 °C. ^{1}H NMR (C_6D_6, 400.2 MHz): δ 7.10 (4 H, br m, *p*-C_6H_3), 6.81 (8 H, br m, *m*-C_6H_3), 4.15 (10 H, s, Cp), 3.64 (8 H, br s, C<u>H</u>Me_2),

2.12 (12 H, s, NMe_2), 1.35 (24 H, d, ^3J = 7.1 Hz, $CHMe_2$), 1.25 (24 H, d, ^3J = 7.1 Hz, $CHMe_2$). $^{13}C\{^1H\}$ NMR (C_6D_6, 101.6 MHz): δ 166.0 ($CNMe_2$), 144.0 (*i*-C_6H_3), 142.6 (*o*-C_6H_3), 123.8 (*m*-C_6H_3), 123.5 (*p*-C_6H_3), 80.5 (Cp), 39.5 (NMe_2), 28.1 ($CHMe_2$), 25.7 ($CHMe_2$), 23.7 ($CHMe_2$), (δ (CO) not observed). IR (NaCl plates, Nujol mull, cm^{-1}): 2020 (m), 1962 (s), 1944 (s), 1778 (s), 1626 (m), 1410 (w), 1018 (m), 800 (m), 770 (w). IR (NaCl cell, toluene, ν(CO), cm^{-1}): 2016 (s), 1921 (m), 1781 (m). IR (NaCl cell, THF, ν(CO), cm^{-1}): 2014 (s), 1946 (m). Anal. found (calcd. for $C_{68}H_{90}Fe_2Mg_2N_6O_4$): C, 66.89 (67.18); H, 7.34 (7.46); N, 6.91 (6.76)%.

NMR tube-scale reaction of [{Me_2NC(NDipp)$_2$}MgFp]$_2$ (18) with MeI. To a solution of [{Me_2NC(NDipp)$_2$}MgFp]$_2$ (**18**, 30 mg, 23.0 μmol) in C_6D_6 (0.5 mL) was added MeI (2.9 μL, 23.0 μmol). The ^1H NMR spectrum recorded after 30 min showed partial conversion of the starting material. The formation of FpMe was confirmed by comparison with literature values,[25,26] alongside the formation of Fp_2. Additional NMR spectra showed further conversion of the starting material albeit with concomitant formation of Fp_2.

General procedure for NMR tube-scale reactions of [{Me_2NC(NDipp)$_2$}MgFp]$_2$ (18) with solid or liquid reagents. To a solution of [{Me_2NC(NDipp)$_2$}MgFp]$_2$ (**18**, 1 equiv.) in C_6D_6 (0.5 mL) was added either TolNCNTol, ^{i}PrNCN^{i}Pr, TolNCO or CS_2 (2 equiv.). The reactions were monitored by ^1H NMR.

5.7 Experimental details and characterising data for Chapter Three

Reduction of (^{Mes}NacNac)ZnI with potassium amalgam. To a stirring K amalgam (0.37 g, 9.50 mmol K; 15 mL Hg) was added a solution of (^{Mes}NacNac)ZnI (**3.20**, 1.50 g, 1.90 mmol) in THF (20 mL). The solution was stirred over the amalgam for 16 h. The pale green solution was filtered away from the amalgam and volatiles removed to give an off-white solid which was extracted with hexane (3 x 25 mL). Storage of the solution at –30 °C gave colourless crystals of (^{Mes}NacNac)$_2$Zn$_2$ (206 mg). Reduction of the volume of the supernatant solution by half and storage at –30 °C afforded a second crop of crystals (239 mg). Total yield: 445 mg (59%). ^1H NMR analysis was consistent with literature values for [(^{Mes}NacNac)Zn]$_2$.[28]

(^{DippMes}NacNac)H (20). To a stirring solution of {Dipp(H)N}(Me)CCHC(O)Me (5.00 g, 19.28 mmol) and 2,4,6-trimethylaniline (2.61 g, 19.28 mmol) in toluene (100 mL) was added *para*-toluenesulfonic acid monohydrate (2.61 g, 19.28 mmol). The reaction

vessel was fitted with a Dean–Stark apparatus and the reaction mixture heated to reflux for 24 h. The reaction mixture was cooled and the solvent removed *in vacuo* to give a yellow solid. The solid was stirred with Na_2CO_3 (4.09 g, 38.56 mmol), Et_2O (50 mL) and distilled water (50 mL). After complete dissolution the aqueous phase was separated and extracted with Et_2O (2 x 25 mL). The combined organic phases were washed with brine and dried over $MgSO_4$. The solvent was removed *in vacuo* to give an orange oil which promptly crystallised. The solid was washed with cold MeOH (4 x 10 mL, −78 °C) to give **20** as a colourless crystalline solid. Yield: 4.77 g (66%). ^{1}H NMR (C_6D_6, 400.2 MHz): δ 12.56 (1 H, s, NH), 7.17 (1 H, s, *p*-C_6H_3), 7.16 (m overlapping with solvent, *m*-C_6H_3), 6.83 (2 H, s, C_6H_2), 4.90 (1 H, s, NC(Me)C<u>H</u>), 3.26 (2 H, sept., ^3J = 6.9 Hz, C<u>H</u>Me_2), 2.22 (6 H, s, *o*-C_6H_2<u>Me_3</u>), 2.21 (3 H, s, *p*-C_6H_2<u>Me_3</u>), 1.69 (3 H, s, (Dipp)NC<u>Me</u>), 1.63 (3 H, s, (Mes)NC<u>Me</u>)), 1.24 (6 H, d, ^3J = 6.9 Hz, CH<u>Me_2</u>), 1.17 (6 H, d, ^3J = 6.9 Hz, CH<u>Me_2</u>). ^{13}C{^{1}H} NMR (C_6D_6, 100.6 MHz): δ 162.2 (<u>C</u>N(Dipp)), 160.5 (<u>C</u>N(Mes)), 142.3 (*i*-C_6H_3), 141.9 (*o*-C_6H_2), 140.7 (*i*-C_6H_2), 134.2 (*p*-C_6H_2), 132.7 (*o*-C_6H_3), 129.1 (*m*-C_6H_2), 125.4 (*p*-C_6H_3), 123.5 (*m*-C_6H_3), 94.3 (NC(Me)<u>C</u>H), 28.8 (<u>C</u>HMe_2), 24.4 (CH<u>Me_2</u>), 23.0 (CH<u>Me_2</u>), 21.0 (*p*-C_6H_2<u>Me_3</u>), 20.9 ((Dipp)NC<u>Me</u>), 20.2 ((Mes)NC<u>Me</u>), 18.4 (*o*-C_6H_2<u>Me_3</u>). IR (NaCl plates, Nujol mull, cm^{-1}): 1857 (w), 1789 (w), 1756 (w), 1725 (w), 1556 (m), 1310 (m), 1276 (m), 1178 (m), 1148 (m), 957 (w), 934 (m), 852 (s), 793 (s), 754 (s), 692 (m). ESI$^+$-HRMS: *m/z* = 377.2954 (calcd. For $[C_{26}H_{37}N_2]^+$ *m/z* = 377.2951). Anal. found (calcd for $C_{26}H_{36}N_2$): C, 82.83 (82.93); H, 9.77 (9.64); N, 7.37 (7.44)%.

(^{DippMes}NacNac)ZnI·0.75(THF) (21·0.75(THF)). To a stirring solution of (^{DippMes}NacNac)H (**20**, 2.76 g, 7.32 mmol) in THF (10 mL) was added KN($SiMe_3$)$_2$ (1.53 g, 7.69 mmol) in THF (10 mL). The solution was stirred at RT for 2 h then added dropwise to a solution of ZnI_2 (2.34 g, 7.32 mmol) in THF (10 mL). The suspension was stirred for 18 h at RT. Volatiles were removed under reduced pressure to give an off-white solid, which was extracted with hot benzene (2 x 50 mL) to give a pale yellow solution. Volatiles were removed under reduced pressure to give an off-white solid. The solid was washed with pentane (2 x 30 mL) and dried *in vacuo* to afford **21·0.75(THF)** as an off-white solid. Yield: 3.64 g (80%). Diffraction-quality crystals were grown from the slow cooling of a hot hexane solution of (^{DippMes}NacNac)ZnI(THF). ^{1}H NMR (C_6D_6, 400.2 MHz): δ 7.19 (1 H, m, *p*-C_6H_3), 7.16 (m overlapping with solvent, *m*-C_6H_3), 6.85 (2 H, s, C_6H_2), 4.92 (1 H, s, NC(Me)C<u>H</u>), 3.63 (3 H, m, OC<u>H_2</u>CH_2), 3.25 (2 H, sept., ^3J

= 6.8 Hz, C<u>H</u>Me$_2$), 2.20 (6 H, s, *o*-C$_6$H$_2$<u>Me</u>$_3$), 2.18 (3 H, s, *p*-C$_6$H$_2$<u>Me</u>$_3$), 1.70 (3 H, s, (Dipp)NC<u>Me</u>), 1.62 (3 H, s, (Mes)NC<u>Me</u>)), 1.37 (6 H, d, ^3J = 6.8 Hz, CH<u>Me</u>$_2$), 1.36 (3 H, m, OCH$_2$C<u>H</u>$_2$), 1.20 (6 H, d, ^3J = 6.8 Hz, CH<u>Me</u>$_2$). ^{13}C{^{1}H} NMR (C$_6$D$_6$, 100.6 MHz): δ 169.2 (<u>C</u>N(Dipp)), 168.7 (<u>C</u>N(Mes)), 144.0 (*i*-C$_6$H$_2$), 143.6 (*i*-C$_6$H$_3$), 142.4 (*o*-C$_6$H$_2$), 134.4 (*p*-C$_6$H$_2$), 131.4 (*o*-C$_6$H$_3$), 129.7 (*m*-C$_6$H$_2$), 126.6 (*p*-C$_6$H$_3$), 124.1 (*m*-C$_6$H$_3$), 95.7 (NC(Me)<u>C</u>H), 69.2 (O<u>C</u>H$_2$), 28.4 (<u>C</u>HMe$_2$), 25.6 (OCH$_2$<u>C</u>H$_2$), 25.2 (CH<u>Me</u>$_2$), 24.0 (CH<u>Me</u>$_2$), 24.0 ((Dipp)NC<u>Me</u>), 23.2 ((Mes)NC<u>Me</u>), 21.0 (*p*-C$_6$H$_2$<u>Me</u>$_3$), 18.9 (*o*-C$_6$H$_2$<u>Me</u>$_3$). IR (NaCl plates, Nujol mull, cm^{-1}): 1548 (m), 1515 (m), 1442 (s), 1398 (s), 1321 (m), 1216 (m), 1185 (m), 1151 (m), 1100 (m), 1054 (sh), 1028 (m), 934 (w), 914 (w), 870 (m), 857 (m), 799 (m), 761 (m), 743 (m). Anal. found (calcd for C$_{29}$H$_{41}$N$_2$O$_{0.75}$ZnI): C, 55.85 (56.00); H, 6.47 (6.64); N, 4.35 (4.50)%.

(^{DippMes}NacNac)$_2$Zn$_2$ (22). To a stirring K amalgam (0.16 g, 3.95 mmol K; 10 mL Hg) was added a solution of (^{DippMes}NacNac)ZnI·0.75(THF) (**21**, 500 mg, 0.79 mmol) in THF (15 mL). The mixture was stirred for 18 h. The orange solution was filtered away from the amalgam and the amalgam washed with THF (5 mL). Volatiles were removed and the crude material was dissolved in hexane (30 mL). The hexane solution was stirred for 18 h, over which time it converted to a colourless solution with suspended Hg. The colourless solution was filtered, volatiles were removed under reduced pressure and the solid was dried *in vacuo* to afford **22** as a white powder. Yield: 215 mg (54 %). Diffraction-quality crystals were grown from a saturated hexane solution at 5 °C. ^{1}H NMR (C$_6$D$_6$, 400.2 MHz): δ 7.16 (m overlapping with solvent, *p*-C$_6$H$_3$), 7.10 (4 H, m, *m*-C$_6$H$_3$), 6.74 (2 H, s, C$_6$H$_2$), 4.87 (2 H, s, NC(Me)C<u>H</u>), 3.16 (4 H, sept., ^3J = 6.8 Hz, C<u>H</u>Me$_2$), 2.26 (6 H, s, *p*-C$_6$H$_2$<u>Me</u>$_3$), 1.78 (12 H, s, *o*-C$_6$H$_2$<u>Me</u>$_3$), 1.58 (6 H, s, (Dipp)NC<u>Me</u>)), 1.47 (6 H, s, (Mes)NC<u>Me</u>)), 1.19 (12 H, d, ^3J = 6.8 Hz, CH<u>Me</u>$_2$), 0.98 (12 H, d, ^3J = 6.8 Hz, CH<u>Me</u>$_2$). ^{13}C{^{1}H} NMR (C$_6$D$_6$, 100.6 MHz): δ 166.0 (<u>C</u>NDipp), 165.1 (<u>C</u>NMes), 146.7 (*i*-C$_6$H$_3$), 146.5 (*i*-C$_6$H$_2$), 142.1 (*o*-C$_6$H$_3$), 132.8 (*p*-C$_6$H$_2$), 131.4 (*o*-C$_6$H$_2$), 129.3 (*m*-C$_6$H$_2$), 125.5 (*p*-C$_6$H$_3$), 123.9 (*m*-C$_6$H$_3$), 96.4 (NC(Me)<u>C</u>H), 28.2 (<u>C</u>HMe$_2$), 25.0 (CH<u>Me</u>$_2$), 24.2 ((Dipp)NC<u>Me</u>), 23.8 (CH<u>Me</u>$_2$), 23.0 ((Mes)NC<u>Me</u>), 21.1 (*p*-C$_6$H$_2$<u>Me</u>$_3$), 18.8 (*o*-C$_6$H$_2$<u>Me</u>$_3$). IR (NaCl plates, Nujol mull, cm^{-1}): 1608 (w), 1548 (s), 1521 (s), 1320 (s), 1214 (m), 1184 (s), 1150 (m), 1110 (m), 1100 (m), 1055 (m), 961 (w), 933 (m), 854 (m), 827 (w), 796 (s), 746 (m), 632 (w). Anal. found (calcd for C$_{52}$H$_{70}$N$_4$Zn$_2$): C, 70.63 (70.82); H, 8.16 (8.00); N, 6.21 (6.35)%.

In-situ ^{1}H NMR data for {(^{DippMes}NacNac)Zn}$_2$Hg (23). An aliquot of the reaction solution was taken during the reduction of (^{DippMes}NacNac)ZnI (**21**) with K/Hg in THF (*vide supra*). Volatiles were removed and the crude solid dissolved in C_6D_6. The ^{1}H NMR spectrum revealed that all starting material had been consumed and the reaction mixture contained chemical shifts from two products. The chemical shifts of (^{DippMes}NacNac)$_2$Zn$_2$ (**22**) were discounted from the spectrum leaving chemical shifts attributed to **{**(^{DippMes}NacNac)Zn}$_2$Hg (**23**). ^{1}H NMR (C_6D_6, 400.2 MHz): δ 7.16 (m overlapping with solvent, *p*-C_6H_3), 7.11 (4 H, m, *m*-C_6H_3), 6.79 (2 H, s, C_6H_2), 4.86 (2 H, s, NC(Me)C<u>H</u>), 3.11 (4 H, sept., C<u>H</u>Me$_2$), 2.28 (6 H, s, *p*-C_6H_2<u>Me</u>$_3$), 2.00 (12 H, s, *o*-C_6H_2<u>Me</u>$_3$), 1.65 (6 H, s, (Dipp)NC<u>Me</u>)), 1.56 (6 H, s, (Mes)NC<u>Me</u>)), 1.16 (12 H, d, CH<u>Me</u>$_2$), 1.13 (12 H, d, CH<u>Me</u>$_2$).

NMR tube-scale reaction of (^{DippMes}NacNac)$_2$Zn$_2$ (22) with Hg. To a solution of [(^{DippMes}NacNac)Zn]$_2$ (**22**, 20.0 mg, 22.7 μmol) in C_6D_6 (0.5 mL) was added Hg (91 mg, 453.7 μmol, 20 equiv.). The NMR tube was placed in an ultrasonic bath for 6 hours. ^{1}H NMR showed that no reaction had taken place and all signals in the NMR spectrum belonged to the starting material.

[{Me$_2$NC(NDipp)$_2$}Zn(μ-I)$_2$Li(THF)$_2$]$_2$ (24). A solution of DippNCNDipp (**5**, 2.27 g, 6.27 mmol) in THF (10 mL) was added to a stirring solution of LiNMe$_2$ (0.32 g, 6.27 mmol) in THF (10 mL). The solution was stirred for 1 h then added dropwise to a solution of ZnI$_2$ (2.00 g, 6.27 mmol) in THF (10 mL). The solution was stirred for 16 h. Volatiles were removed under reduced pressure to give a white solid, which was extracted with benzene (2 x 40 mL) to give a colourless solution. Volatiles were removed under reduced pressure to give **24** as a white solid. Yield: 4.935 g (90%). Diffraction-quality crystals were grown from the slow cooling of a hexane solution of **24**. ^{1}H NMR (C_6D_6, 400.2 MHz): δ 7.20 (4 H, d, ^3J = 7.7 Hz, *m*-C_6H_3), 7.09 (2 H, t, ^3J = 7.7 Hz, *p*-C_6H_3), 4.11 (4 H, sept., ^3J = 6.7 Hz, C<u>H</u>Me$_2$), 3.45 (8 H, m, OCH$_2$), 2.25 (6 H, s, NMe$_2$), 1.60 (12 H, d, ^3J = 6.7 Hz, CH<u>Me</u>$_2$), 1.38 (12 H, d, ^3J = 6.7 Hz, CH<u>Me</u>$_2$), 1.24 (8 H, m, OCH$_2$C<u>H</u>$_2$). ^{13}C{^{1}H} NMR (C_6D_6, 100.6 MHz): δ 164.9 (CN_3), 144.1 (*o*-C_6H_3), 143.4 (*i*-C_6H_3), 123.7 (*p*-C_6H_3), 123.6 (*m*-C_6H_3), 68.8 (OCH$_2$), 39.5 (NMe$_2$), 28.1 (<u>C</u>HMe$_2$), 27.6 (CH<u>Me</u>$_2$), 25.3 (OCH$_2$<u>C</u>H$_2$), 23.6 (CH<u>Me</u>$_2$). ^{7}Li NMR (C_6D_6, 155.5 MHz): δ −0.34. IR (NaCl plates, Nujol mull, cm^{-1}): 2176 (m), 1904 (w), 1845 (w), 1790 (w), 1626 (w), 1531 (s), 1359 (s), 1319 (s), 1250 (m), 1231 (m), 1204 (m), 1179 (m),

1100 (m), 1042 (s), 956 (w), 936 (m), 918 (m), 887 (m), 771 (m), 684 (w), 667 (w). It was not possible to obtain a satisfactory elemental analysis for **24**.

Attempted elimination of LiI from [{Me$_2$NC(NDipp)$_2$}Zn(μ-I)$_2$Li(THF)$_2$]$_2$ (24) on the NMR tube-scale. A solution of [{Me$_2$NC(NDipp)$_2$}Zn(μ-I)$_2$Li(THF)$_2$]$_2$ (**24**, 15 mg, 9.0 μmol) in toluene-d_8 (0.5 mL) was heated to 100 °C in an oil bath for 6 h. A ^{1}H NMR spectrum recorded after this time showed that no reaction had taken place and all signals in the NMR spectrum belonged to the starting material.

[{Me$_2$NC(NDipp)$_2$}Zn(μ-I)]$_2$ (25). To a solution of Me$_2$NC(NDipp)(NHDipp) (**16**, 2.20 g, 5.40 mmol) in THF (10 mL) was added KN(SiMe$_3$)$_2$ (1.13 g, 5.67 mmol) in THF (10 mL). The solution was stirred for 2 h then added to a solution of ZnI$_2$ (1.72 g, 5.40 mmol) in THF (10 mL). The suspension was stirred for 18 h. Volatiles were removed under reduced pressure to give an off-white solid, which was extracted with hot benzene (2 x 50 mL) to give a pale yellow solution. Volatiles were removed under reduced pressure to give an off-white solid. The solid was washed with pentane (2 x 30 mL) and dried *in vacuo* to give **25** as a white solid. Yield: 2.47 g (76%). Diffraction-quality crystals were grown from the slow cooling of a hexane solution of **25**. ^{1}H NMR (C$_6$D$_6$, 400.2 MHz): δ 7.07 (6 H, m, overlapping *m*-C$_6$H$_3$ & *p*-C$_6$H$_3$), 3.69 (4 H, sept., ^3J = 6.7 Hz, C<u>H</u>Me$_2$), 2.04 (6 H, s, NMe$_2$), 1.26 (12 H, d, ^3J = 6.7 Hz, CH<u>Me</u>$_2$), (12 H, d, ^3J = 6.7 Hz, CH<u>Me</u>$_2$). ^{13}C{^{1}H} NMR (C$_6$D$_6$, 100.6 MHz): δ 166.1 (CN$_3$), 143.9 (*o*-C$_6$H$_3$), 141.9 (*i*-C$_6$H$_3$), 124.5 (*p*-C$_6$H$_3$), 123.7 (*m*-C$_6$H$_3$), 39.2 (NMe$_2$), 28.2 (<u>C</u>HMe$_2$), 26.8 (CH<u>Me</u>$_2$), 23.2 (CH<u>Me</u>$_2$). Anal. found (calcd for C$_{54}$H$_{80}$N$_6$Zn$_2$I$_2$): C, 53.98 (54.15); H, 6.67 (6.73); N, 6.92 (7.02)%.

{Me$_2$NC(NDipp)$_2$}$_2$Zn (26). To a stirring potassium amalgam (0.16 g, 4.15 mmol K; 10 mL Hg) was added a solution of [{Me$_2$NC(NDipp)$_2$}Zn(μ-I)]$_2$ (**25**, 0.50 g, 0.42 mmol) in THF (10 mL). The mixture was stirred for 16 h. The colourless solution was filtered away from the amalgam. Volatiles were removed from the solution to give a white solid which was extracted with hexane (3 x 15 mL). The volume of the filtrate was reduced to afford diffraction-quality crystals of **26**. Yield: 90 mg (24%). ^{1}H NMR (C$_6$D$_6$, 400.2 MHz): δ 7.14 (4 H, d, ^3J = 7.6 Hz, *m*-C$_6$H$_3$), 7.04 (4 H, t, ^3J = 7.6 Hz, *p*-C$_6$H$_3$), 6.93 (4 H, d, ^3J = 7.6 Hz, *m*-C$_6$H$_3$), 4.13 (4 H, sept., ^3J = 6.8 Hz, C<u>H</u>Me$_2$), 3.30 (4 H, sept., ^3J = 6.8 Hz, C<u>H</u>Me$_2$), 2.02 (12 H, s, NMe$_2$), 1.56 (12 H, d, ^3J = 6.8 Hz, CH<u>Me</u>$_2$), 1.39 (12 H, d, ^3J = 6.8 Hz, CH<u>Me</u>$_2$), 1.10 (12 H, d, ^3J = 6.8 Hz, CH<u>Me</u>$_2$), 0.56 (12 H, d, ^3J = 6.8 Hz, CH<u>Me</u>$_2$). ^{13}C{^{1}H} NMR (C$_6$D$_6$, 100.6 MHz): δ 167.5 (CN$_3$),

144.2 (*o*-C_6H_3), 143.6 (*i*-C_6H_3), 142.9 (*o*-C_6H_3), 124.0 (*p*-C_6H_3), 123.8 (*m*-C_6H_3), 123.7 (*m*-C_6H_3), 39.9 (NMe_2), 28.1 ($\underline{C}HMe_2$), 27.7 ($\underline{C}HMe_2$), 24.9 ($CH\underline{Me}_2$), 24.9 ($CH\underline{Me}_2$), 23.9 ($CH\underline{Me}_2$), 23.7 ($CH\underline{Me}_2$). IR (NaCl plates, Nujol mull, cm^{-1}): 1626 (w), 1524 (s), 1359 (m), 1246 (s), 1199 (s), 1175 (m), 1061 (m), 1042 (m), 959 (w), 933 (m), 851 (w), 772 (s), 683 (w), 667 (w). Anal. found (calcd for $C_{54}H_{80}N_6Zn$): C, 73.61 (73.82); H, 9.23 (9.18); N, 9.42 (9.56)%.

5.8 Experimental details and characterising data for Chapter Four

NMR tube-scale reaction of {(^{Dipp}NacNac)Zn}$_2$Hg (3.1) with Me_3SiI. To a solution of {(^{Dipp}NacNac)Zn}$_2$Hg (**3.1**, 15 mg, 12.6 μmol) in C_6D_6 (0.5 mL) was added Me_3SiI (3.7 μL, 5.2 mg, 25.7 μmol). ^{1}H NMR spectra were recorded after 30 mins, 2 h and 24 h. These spectra showed complete conversion to (^{Dipp}NacNac)ZnI. The chemical shifts of (^{Dipp}NacNac)ZnI in C_6D_6 were verified by comparison with a previously reported example.[23]

NMR tube-scale reaction of {(^{Dipp}NacNac)Zn}$_2$Hg (3.1) with Me_3SiCl. To a solution of {(^{Dipp}NacNac)Zn}$_2$Hg (**3.1**, 20 mg, 17.1 μmol) in C_6D_6 (0.5 mL) was added Me_3SiCl (4.4 μL, 3.8 mg, 34.3 μmol). ^{1}H NMR spectra were recorded after 30 mins and 24 h. These spectra showed conversion to (^{Dipp}NacNac)ZnCl alongside significant quantities of protio-ligand. The chemical shifts of (^{Dipp}NacNac)ZnCl in C_6D_6 were verified by comparison with a previously reported example.[29]

NMR tube-scale reaction of {(^{Dipp}NacNac)Zn}$_2$Hg (3.1) with Me_3SiBr. To a solution of {(^{Dipp}NacNac)Zn}$_2$Hg (**3.1**, 15 mg, 12.6 μmol) in C_6D_6 (0.5 mL) was added Me_3SiBr (3.4 μL, 3.9 mg, 25.7 μmol). ^{1}H NMR spectra were recorded after 30 mins and 20 h. These spectra showed complete conversion to a product with one set of ligand environments, assumed to be (^{Dipp}NacNac)ZnBr by analogy with reactions with other silyl halides.

NMR tube-scale reaction of {(^{Dipp}NacNac)Zn}$_2$Hg (3.1) with PhN_3. A solution of {(^{Dipp}NacNac)Zn}$_2$Hg (**3.1**, 22 mg, 18.9 μmol) in C_6D_6 (0.5 mL) was made up with 1,4-$(MeO)_2C_6H_4$ (2.6 mg, 18.9 μmol) as an internal standard. To this solution was added PhN_3 (4.5 mg, 37.8 μmol). A ^{1}H NMR spectrum recorded after 2 h showed complete consumption of the starting material. Among several unidentifiable products was identified (^{Dipp}NacNac)Zn(μ-1,6-Ph_2N_6)Zn(^{Dipp}NacNac) in < 10% yield. The chemical

shifts of (^{Dipp}NacNac)Zn(μ-1,6-Ph_2N_6)Zn(^{Dipp}NacNac) were verified by comparison with a previously reported example.[30]

{(^{Dipp}NacNac)Zn}(μ-CS_2){Zn(^{Dipp}NacNac)} (27). To a solution of {(^{Dipp}NacNac)Zn}$_2$Hg (400 mg, 0.34 mmol) in benzene (20 ml) was added CS_2 (41.2 μL, 52 mg, 0.69 mmol). The solution was stirred for 4 h. The orange solution was filtered away from the precipitated Hg and volatiles removed under reduced pressure. The resulting solid was dried *in vacuo* to give **27** as a yellow powder. Yield: (294 mg, 82%). Diffraction-quality crystals of **27**·C_6H_{14} were grown from a saturated hexane solution at 5 °C. ^{1}H NMR (C_6D_6, 500.3 MHz): δ 7.15 (s overlapping with solvent, *p*-C_6H_3), 7.14 (2 H, br s, *p*-C_6H_3), 7.08 & 7.06 (8 H, overlapping d, ^3J = 10.39 & 10.49 Hz, *m*-C_6H_3), 4.92 (1 H, s, NC(Me)C<u>H</u>) , 4.82 (1 H, s, NC(Me)C<u>H</u>), 3.25 (4 H, sept, ^3J = 6.8 Hz, C<u>H</u>Me_2), 3.01 (4 H, sept, ^3J = 6.8 Hz, C<u>H</u>Me_2), 1.68 (6 H, s, Me), 1.64 (6 H, s, Me), 1.16 & 1.14 (24 H, overlapping d, ^3J = 6.8 & 6.8 Hz, CH<u>Me</u>$_2$) 1.12 (12 H, d, ^3J = 6.8 Hz, CH<u>Me</u>$_2$), 1.10 (12 H, d, ^3J = 6.8 Hz, CH<u>Me</u>$_2$). ^{13}C{^{1}H} NMR (C_6D_6, 125.8 MHz): δ 319.1 (<u>C</u>S_2), 168.7 (CN), 167.6 (CN), 144.4 (*i*-C_6H_3), 143.6 (*i*-C_6H_3), 142.6 (*o*-C_6H_3), 141.5 (*o*-C_6H_3), 126.3 (*p*-C_6H_3), 125.5 (*p*-C_6H_3), 123.9 (*m*-C_6H_3), 123.9 (*m*-C_6H_3), 95.6 (NC(Me)<u>C</u>H), 94.3 (NC(Me)<u>C</u>H), 28.7 (<u>C</u>HMe_2), 28.4 (<u>C</u>HMe_2), 25.0 (CH<u>Me</u>$_2$), 25.0 (CH<u>Me</u>$_2$), 24.6 (CH<u>Me</u>$_2$), 23.9 (CH<u>Me</u>$_2$), 23.6 (Me), 23.3 (Me). IR (NaCl plates, Nujol mull, cm^{-1}): 1552 (m), 1524 (s), 1371 (s), 1179 (w), 1055 (w), 942 (m), 918 (w), 859 (w), 793 (m), 755 (m). Anal. found (calcd for $C_{59}H_{82}N_4S_2Zn_2$·0.4(C_6H_{14})): C, 68.49 (68.50); H, 8.46 (8.20); N, 5.07 (5.20)%.

NMR tube-scale reaction of {(^{Dipp}NacNac)Zn}(μ-CS_2){Zn(^{Dipp}NacNac)} (27) with CS_2. To a solution of {(^{Dipp}NacNac)Zn}(μ-CS_2){Zn(^{Dipp}NacNac)} (**27**, 10 mg, 9.6 μmol) in C_6D_6 (0.5 mL) was added CS_2 (6.0 μL, 7.6 mg, 96.0 μmol). The NMR tube was heated at 70 °C for 18 h. The ^{1}H NMR spectrum recorded after heating showed no reaction had taken place.

{(^{Dipp}NacNac)Zn}{μ-CO(NPh)$_2$}{Zn(^{Dipp}NacNac)} (28). To a solution of {(^{Dipp}NacNac)Zn}$_2$Hg (300 mg, 0.26 mmol) in hexane (20 ml) was added PhNCO (55.9 μL, 61 mg, 0.52 mmol). The solution was stirred for 3 h. The colourless solution was filtered away from the precipitated Hg and volatiles removed under reduced pressure. The resulting solid was dried *in vacuo* to give **28** as a white powder. Yield: 268 mg (88%). Diffraction-quality crystals of **28** were grown from a saturated hexane solution at 5 °C. ^{1}H NMR (C_6D_6, 500.3 MHz): δ 7.30 - 6.89 (12 H, m, *m*-C_6H_3 &

p-C_6H_3), 6.44 (4 H, m, *m*-C_6H_5), 6.40 (2 H, m, *p*-C_6H_5), 5.78 (4 H, m, *o*-C_6H_5), 4.83 (2 H, s, NC(Me)C<u>H</u>), 3.44 (4 H, br sept., C<u>H</u>Me_2), 3.22 (4 H, br sept., C<u>H</u>Me_2), 1.61 (12 H, s, Me), 1.51 – 0.37 (48 H, br m, CH<u>Me</u>$_2$). $^{13}C\{^1H\}$ NMR (C_6D_6, 125.8 MHz): δ 169.3 (CN), 164.1 (OCN_2), 144.8 (*i*-C_6H_5), 143.9 (*i*-C_6H_3), 142.1 (*o*-C_6H_3), 127.1 (*m*-C_6H_5), 126.8 (*o*-C_6H_5), 126.0 (*p*-C_6H_3), 123.9 (*m*-C_6H_3), 121.9 (*p*-C_6H_5), 95.4 (NC(Me)<u>C</u>H), 28.1 (<u>C</u>HMe_2), 24.1 (Me), 24.1 (CH<u>Me</u>$_2$). IR (NaCl plates, Nujol mull, cm^{-1}): 1550 (w), 1522 (m), 1496 (w), 1401 (m), 1317 (m), 1179 (w), 937 (w), 759 (w), 702 (w), 693 (w). Anal. found (calcd for $C_{71}H_{92}N_6OZn_2$): C, 72.27 (72.50); H, 7.71 (7.88); N, 7.12 (7.14)%.

{(^{Dipp}NacNac)Zn}{μ-CO(NTol)$_2$}{Zn(^{Dipp}NacNac)} (29). To a solution of {(^{Dipp}NacNac)Zn}$_2$Hg (400 mg, 0.34 mmol) in hexane (20 ml) was added TolNCO (86.5 μL, 91 mg, 0.69 mmol). The solution was stirred for 3 h. The colourless solution was filtered away from the precipitated Hg and volatiles removed under reduced pressure. The resulting solid was dried *in vacuo* to give **29** as a white powder. Yield: 209 mg (51%). Diffraction-quality crystals of **29** were grown from a saturated hexane solution at 5 °C. ^1H NMR (C_6D_6, 500.3 MHz): δ 7.25 (4 H, m, *m*-C_6H_3), 7.15 – 6.74 (8 H, m, *p*-C_6H_3), 6.25 (4 H, d, ^3J = 8.2 Hz, *m*-C_6H_4), 5.62 (4 H, br s, *o*-C_6H_4), 4.83 (2 H, s, NC(Me)C<u>H</u>), 3.47 (4 H, sept., C<u>H</u>Me_2), 3.26 (4 H, br sept., C<u>H</u>Me_2), 1.91 (6 H, s, C_6H_4<u>Me</u>), 1.62 (12 H, s, Me), 1.54 – 0.94 (48 H, br m, CH<u>Me</u>$_2$). $^{13}C\{^1H\}$ NMR (C_6D_6, 125.8 MHz): δ 169.3 (CN), 164.5 (OCN_2), 144.0 (*i*-C_6H_3), 142.4 (*i*-C_6H_4), 142.2 (*o*-C_6H_3), 130.4 (*p*-C_6H_4), 127.5 (*m*-C_6H_4), 126.7 (*o*-C_6H_4), 126.1 (*p*-C_6H_3), 123.9 (*m*-C_6H_3), 95.4 (NC(Me)<u>C</u>H), 28.2 (<u>C</u>HMe_2), 24.3 (Me), 24.1 (CH<u>Me</u>$_2$), 20.7 (C_6H_4<u>Me</u>). IR (NaCl plates, Nujol mull, cm^{-1}): 1596 (w), 1548 (m), 1514 (m), 1318 (m), 1234 (m), 1180 (m), 1056 (m), 937 (m), 913 (w), 897 (w), 858 (m), 823 (m), 797 (m), 759 (m), 749 (m), 706 (w), 635 (m). Anal. found (calcd for $C_{73}H_{96}N_6OZn_2$): C, 72.88 (72.80); H, 7.96 (8.03); N, 6.87 (6.98)%.

NMR tube-scale hydrolysis of {(^{Dipp}NacNac)Zn}{μ-CO(NPh)$_2$}{Zn(^{Dipp}NacNac)} (28). To a solution of {(^{Dipp}NacNac)Zn}{μ-CO(NPh)$_2$}{Zn(^{Dipp}NacNac)} (**28**, 10 mg, 8.5 μmol) in C_6D_6 (0.5 mL) was added H_2O (0.1 mL, 100.0 mg, 5.6 mmol). A ^1H NMR spectrum recorded after 10 mins showed complete consumption of the starting material. The chemical shifts of PhN(H)C(O)N(H)Ph were identified in the reaction mixture by comparison with an independent sample of PhN(H)C(O)N(H)Ph in C_6D_6.

NMR tube-scale reaction of {(^{Dipp}NacNac)Zn}$_2$Hg (3.1) with ^{t}BuNCO. To a solution of {(^{Dipp}NacNac)Zn}$_2$Hg (**3.1**, 20 mg, 17.1 μmol) in C_6D_6 (0.5 mL) was added ^{t}BuNCO (4.0 μL, 3.4 mg, 34.3 μmol). ^{1}H NMR spectra recorded after 30 mins and 72 h showed no reaction between the two reactants. The NMR tube was heated at 60 °C for 72 h. The ^{1}H NMR spectrum recorded after heating showed no reaction had taken place.

NMR tube-scale reaction of {(^{Dipp}NacNac)Zn}$_2$Hg (3.1) with ^{t}BuOO^{t}Bu. To a solution of {(^{Dipp}NacNac)Zn}$_2$Hg (**3.1**, 15 mg, 12.9 μmol) in C_6D_6 (0.5 mL) was added ^{t}BuOO^{t}Bu (2.4 μL, 1.9 mg, 12.9 μmol). ^{1}H NMR spectra recorded after 30 mins and 18 h showed no reaction had taken place.

{(^{Dipp}NacNac)Zn}(μ-PhNNPh){Zn(^{Dipp}NacNac)} (30). To {(^{Dipp}NacNac)Zn}$_2$Hg (400 mg, 0.34 mmol) and PhNNPh (63 mg, 0.34 mmol) was added benzene (20 mL) to give an orange solution. The reaction mixture was stirred for 20 h to give a green solution with precipitated Hg. The solution was filtered, volatiles removed under reduced pressure and the solid dried *in vacuo* to give **30** as a pale yellow/green solid. Yield: 265 mg (67%). ^{1}H NMR (C_6D_6, 500.3 MHz): δ 7.20 (4 H, s, *m*-C_6H_3), 7.16 (s overlapping with solvent, *p*-C_6H_3), 7.01 (2 H, t, *J* = 7.8 Hz, *p*-C_6H_3), 6.91 (2 H, t, *J* = 7.8 Hz, *m*-C_6H_3), 6.80 (2 H, t, *J* = 7.8 Hz, *m*-C_6H_3), 6.75 (2 H, t, *J* = 7.5 Hz, *m*-C_6H_5), 6.22 (2 H, t, *J* = 7.5 Hz, *p*-C_6H_5), 6.14 (2 H, t, *J* = 7.5 Hz, *m*-C_6H_5), 5.97 (2 H, d, *J* = 7.5 Hz, *o*-C_6H_5), 5.37 (2 H, d, *J* = 7.5 Hz, *o*-C_6H_5), 4.94 (2 H, s, NC(Me)C<u>H</u>), 3.62 (2 H, sept, *J* = 7.0 Hz, C<u>H</u>Me$_2$), 3.38 (2 H, sept, *J* = 6.8 Hz, C<u>H</u>Me$_2$), 3.27 (2 H, sept, *J* = 6.7 Hz, C<u>H</u>Me$_2$), 2.70 (2 H, sept, *J* = 6.7 Hz, C<u>H</u>Me$_2$), 1.72 (6 H, s, Me), 1.66 (6 H, d, *J* = 7.0 Hz, CH<u>Me</u>$_2$), 1.57 (6 H, s, Me), 1.53 (6 H, d, *J* = 6.8 Hz, CH<u>Me</u>$_2$), 1.41 (6 H, d, *J* = 7.0 Hz, CH<u>Me</u>$_2$), 1.21 (6 H, d, *J* = 6.8 Hz, CH<u>Me</u>$_2$), 1.17 (6 H, d, *J* = 6.7 Hz, CH<u>Me</u>$_2$), 1.05 (6 H, d, *J* = 6.7 Hz, CH<u>Me</u>$_2$), 1.03 (6 H, d, *J* = 6.7 Hz, CH<u>Me</u>$_2$), 0.05 (6 H, d, *J* = 6.7 Hz, CH<u>Me</u>$_2$). ^{13}C{^{1}H} NMR (C_6D_6, 125.8 MHz): δ 170.5 (CN), 169.6 (CN), 157.0 (*i*-C_6H_5), 144.9 (*i*-C_6H_3), 144.5 (*i*-C_6H_3), 143.0 (*o*-C_6H_3), 142.8 (*o*-C_6H_3), 142.6 (*o*-C_6H_3), 140.5 (*o*-C_6H_3), 129.9 (*m*-C_6H_5), 128.6 (*p*-C_6H_3), 128.0 (*m*-C_6H_5), 126.6 (*p*-C_6H_3), 126.4 (*m*-C_6H_3), 125.1 (*m*-C_6H_3), 124.5 (*m*-C_6H_3), 123.0 (*m*-C_6H_3), 112.4 (*o*-C_6H_5), 112.1 (*p*-C_6H_5), 110.87 (*o*-C_6H_5), 96.7 (NC(Me)<u>C</u>H), 30.6 (<u>C</u>HMe$_2$), 29.1 (<u>C</u>HMe$_2$), 28.4 (<u>C</u>HMe$_2$), 27.7 (<u>C</u>HMe$_2$), 25.8 (<u>C</u>HMe$_2$), 25.6 (<u>C</u>HMe$_2$), 24.9 (<u>C</u>HMe$_2$), 24.8 (<u>C</u>HMe$_2$), 24.4 (Me), 24.1 (<u>C</u>HMe$_2$), 24.0 (<u>C</u>HMe$_2$), 24.0 (Me), 23.6 (<u>C</u>HMe$_2$), 23.3 (<u>C</u>HMe$_2$). IR (NaCl plates, Nujol mull, cm^{-1}): 1584 (m), 1525 (s), 1316 (s), 1294 (m), 1174 (s), 1055 (w), 985 (w), 936 (m), 879 (w), 864 (w), 795 (m), 774

(w), 760 (m), 750 (m), 989 (m), 675 (w). Anal. found (calcd for $C_{70}H_{92}N_6Zn_2$): C, 72.92 (73.22); H, 7.85 (8.08); N, 7.20 (7.32)%.

Crystallisation of (^{Dipp}NacNac)ZnN(Ph)N(H)Ph (31). During an attempted recrystallisation of **30** from hexane, crystals were obtained which were identified as **31** by analysis of single-crystal X-ray diffraction data.

NMR tube-scale hydrolysis of {(^{Dipp}NacNac)Zn}(μ-PhNNPh){Zn(^{Dipp}NacNac)} (30). To a solution of {(^{Dipp}NacNac)Zn}(μ-PhNNPh){Zn(^{Dipp}NacNac)} (**30**, 15 mg, 13.1 μmol) in C_6D_6 (0.5 mL) was added H_2O (0.1 mL, 100.0 mg, 5.6 mmol). A ^{1}H NMR spectrum recorded after 10 mins showed complete consumption of the starting material and quantitative formation of PhN(H)N(H)Ph. The chemical shifts of PhN(H)N(H)Ph were identified in the reaction mixture by comparison with an independent sample in C_6D_6.

5.9 References

1. A. B. Pangborn, M. A. Giardello, R. H. Grubbs, R. K. Rosen, and F. J. Timmers, *Organometallics*, 1996, **15**, 1518–1520.
2. Z. Otwinowski and W. Minor, *Processing of X-ray diffraction data collected in oscillation mode*, Academic Press, New York, 1997.
3. *CrysAlisPro (2011)*, Agilent Technologies, Oxford.
4. A. Altomare, G. Cascarano, C. Giacovazzo, A. Guagliardi, M. C. Burla, G. Polidori, and M. Camalli, *J. Appl. Crystallogr.*, 1994, **27**, 435–435.
5. L. Palatinus and G. Chapuis, *J. Appl. Crystallogr.*, 2007, **40**, 786–790.
6. P. W. Betteridge, J. R. Carruthers, R. I. Cooper, K. Prout, and D. J. Watkin, *J. Appl. Crystallogr.*, 2003, **36**, 1487–1487.
7. J. P. Perdew, K. Burke, and M. Ernzerhof, *Phys. Rev. Lett.*, 1996, **77**, 3865–3868.
8. J. P. Perdew, K. Burke, and M. Ernzerhof, *Phys. Rev. Lett.*, 1997, **78**, 1396–1396.
9. M. J. Frisch, G. W. Trucks, H. B. Schlegel, G. E. Scuseria, M. A. Robb, J. R. Cheeseman, G. Scalmani, V. Barone, B. Mennucci, G. A. Petersson, H. Nakatsuji, M. Caricato, X. Li, H. P. Hratchian, A. F. Izmaylov, J. Bloino, G. Zheng, J. L. Sonnenberg, M. Hada, M. Ehara, K. Toyota, R. Fukuda, J. Hasegawa, M. Ishida, T. Nakajima, Y. Honda, O. Kitao, H. Nakai, T. Vreven, J.

A. Montgomery Jr., J. E. Peralta, F. Ogliaro, M. J. Bearpark, J. Heyd, E. N. Brothers, K. N. Kudin, V. N. Staroverov, R. Kobayashi, J. Normand, K. Raghavachari, A. P. Rendell, J. C. Burant, S. S. Iyengar, J. Tomasi, M. Cossi, N. Rega, N. J. Millam, M. Klene, J. E. Knox, J. B. Cross, V. Bakken, C. Adamo, J. Jaramillo, R. Gomperts, R. E. Stratmann, O. Yazyev, A. J. Austin, R. Cammi, C. Pomelli, J. W. Ochterski, R. L. Martin, K. Morokuma, V. G. Zakrzewski, G. A. Voth, P. Salvador, J. J. Dannenberg, S. Dapprich, A. D. Daniels, Ö. Farkas, J. B. Foresman, J. V. Ortiz, J. Cioslowski, and D. J. Fox, *Gaussian 09, Revision D.01*, Gaussian Inc., (2009) Wallingford, CT, USA.

10. D. Andrae, U. Häußermann, M. Dolg, H. Stoll, and H. Preuß, *Theor. Chim. Acta*, 1990, **77**, 123–141.

11. A. Bergner, M. Dolg, W. Küchle, H. Stoll, and H. Preuß, *Mol. Phys.*, 1993, **80**, 1431–1441.

12. T. A. Keith, *AIMALL (Version 14.11.23)*, TK Gristmill Software, (2014) Overland Park, KS, USA.

13. D. H. Wu, A. D. Chen, and C. S. Johnson, *J. Magn. Reson., Ser. A*, 1995, **115**, 260–264.

14. *TopSpin 3.2*, (2006) Bruker BioSpin GmbH, Rheinstetten, Germany.

15. D. R. Lide, Ed., *CRC Handbook of Chemistry and Physics, 84th Edition*, Boca Raton, Florida, 2003.

16. Dassault Systèmes BIOVIA, *Accelrys Discovery Studio Visualizer (Version 4.1.0)*, Dassault Systèmes BIOVIA, (2014) San Diego, CA, USA.

17. J. S. Plotkin and S. G. Shore, *Inorg. Chem.*, 1981, **20**, 284–285.

18. J. C. Vites, B. D. Steffey, M. E. Giuseppetti-Dery, and A. R. Cutler, *Organometallics*, 1991, **10**, 2827–2834.

19. M. P. Blake, N. Kaltsoyannis, and P. Mountford, *J. Am. Chem. Soc.*, 2015, **137**, 12352–12368.

20. M. Findlater, N. J. Hill, and A. H. Cowley, *Dalton Trans.*, 2008, 4419–4423.

21. M. Blumer, *Anal. Chem.*, 1957, **29**, 1039–1041.

22. A. P. Dove, V. C. Gibson, E. L. Marshall, A. J. P. White, and D. J. Williams,

Dalton Trans., 2004, 570–578.

23. M. P. Blake, N. Kaltsoyannis, and P. Mountford, *Chem. Commun.*, 2015, **51**, 5743–5746.

24. K. Barral, A. D. Moorhouse, and J. E. Moses, *Org. Lett.*, 2007, **9**, 1809–1811.

25. H. Li and M. M. Turnbull, *J. Organomet. Chem.*, 1991, **419**, 245–249.

26. M. P. Blake, N. Kaltsoyannis, and P. Mountford, *Chem. Commun.*, 2013, **49**, 3315–3317.

27. A. I. Germeroth, Reactivity of Electropositive f-Block Metal N-Heterocyclic Carbene Complexes, PhD Thesis, University of Edinburgh, 2013.

28. S. Schulz, D. Schuchmann, U. Westphal, and M. Bolte, *Organometallics*, 2009, **28**, 1590–1592.

29. J. Prust, H. Hohmeister, A. Stasch, H. W. Roesky, J. Magull, E. Alexopoulos, I. Usón, H.-G. Schmidt, and M. Noltemeyer, *Eur. J. Inorg. Chem.*, 2002, 2156–2162.

30. C. Stienen, S. Gondzik, A. Gehlhaar, R. Haack, C. Wölper, G. Jansen, and S. Schulz, *Organometallics*, 2016, **35**, 1022–1029.